



REFERENCE ONLY

UNIVERSITY OF LONDON THESIS

Degree	Year	Name of Author
MPhil	2005	ADAMOPOULOS, I.

COPYRIGHT

This is a thesis accepted for a Higher Degree of the University of London. It is an unpublished typescript and the copyright is held by the author. All persons consulting the thesis must read and abide by the Copyright Declaration below.

COPYRIGHT DECLARATION

I recognise that the copyright of the above-described thesis rests with the author and that no quotation from it or information derived from it may be published without the prior written consent of the author.

LOANS

Theses may not be lent to individuals, but the Senate House Library may lend a copy to approved libraries within the United Kingdom, for consultation solely on the premises of those libraries. Application should be made to: Inter-Library Loans, Senate House Library, Senate House, Malet Street, London WC1E 7HU.

REPRODUCTION

University of London theses may not be reproduced without explicit written permission from the Senate House Library. Enquiries should be addressed to the Theses Section of the Library. Regulations concerning reproduction vary according to the date of acceptance of the thesis and are listed below as guidelines.

- A. Before 1962. Permission granted only upon the prior written consent of the author. (The Senate House Library will provide addresses where possible).
- B. 1962 - 1974. In many cases the author has agreed to permit copying upon completion of a Copyright Declaration.
- C. 1975 - 1988. Most theses may be copied upon completion of a Copyright Declaration.
- D. 1989 onwards. Most theses may be copied.

This thesis comes within category D.

This copy has been deposited in the Library of UCL

This copy has been deposited in the Senate House Library, Senate House, Malet Street, London WC1E 7HU.

Interface Micromotion in Cementless Hip Prostheses

Mohammed Rafiq bin Abdul Kadir

Thesis submitted to the University of London in conformity with the requirements of
the degree of Doctor of Philosophy and for the Diploma of Imperial College

Biomechanics Section
Imperial College London
United Kingdom

May 2005

UMI Number: U592164

All rights reserved

INFORMATION TO ALL USERS

The quality of this reproduction is dependent upon the quality of the copy submitted.

In the unlikely event that the author did not send a complete manuscript and there are missing pages, these will be noted. Also, if material had to be removed, a note will indicate the deletion.



UMI U592164

Published by ProQuest LLC 2013. Copyright in the Dissertation held by the Author.
Microform Edition © ProQuest LLC.

All rights reserved. This work is protected against
unauthorized copying under Title 17, United States Code.



ProQuest LLC
789 East Eisenhower Parkway
P.O. Box 1346
Ann Arbor, MI 48106-1346

Abstract

The most commonly reported failure modes of cementless hip stems are loosening and thigh pain; both are attributed to the relative motion at the bone-implant interface due to failure to achieve sufficient primary fixation. The main aim of the current study is to investigate, using Finite Element Analysis, various factors that could affect micromotion and could compromise the stability of cementless femoral stems. We propose a novel technique for predicting hip stem instability to analyse these problems.

The designs of cementless hip stems are crucial to its success. We first categorize them into three major types based on the overall geometry and they are all found to be stable under physiological loadings. 'Isoelastic' stems are found to increase interface micromotion, but if tight fit is achieved distally, the stem would still be stable. Having shorter stems for primary arthroplasty is beneficial if revision surgery is required, but these produce larger relative motion. The results from this study show that if sufficient cortical contact is achieved distally, stability is not impaired. Two types of hip stems' fixation are also compared; the proximal fixation design is found to be less stable than the distal fixation design, but stability can be improved with the use of proximal macrofeatures.

The strength of primary fixation also depends on surgical parameters; imprecise surgical procedures can cause interfacial gaps, implant undersizing and implant malalignment. The FE results show that undersizing should be avoided because it increases micromotion and instability, especially in stems with cylindrical design. Hip stems with varus malalignment are found to be relatively stable compared to the normally aligned undersized stem. Interfacial gaps due to surgical error are not found to impair the stem's fixation as long as maximum press-fit is achieved.

Successful implant fixation also depends on the quality of the bone. Bone with skeletal diseases of osteoporosis and osteoarthritis are analysed and compared with the results from a normal healthy bone. The hip stem in the osteoporotic bone is found to have the largest micromotion and is the most unstable, especially during stair-climbing activity.

Acknowledgements:

I would like to thank my supervisor Dr. Ulrich Hansen for all his help and guidance during the past three years, and the Government of Malaysia for their scholarship. I would also like to thank Prof. Andrew Amis for his insight into how my work could be made more interesting. I am also grateful to Mr. Duncan Lucas for his thoughts on the applicability and clinical relevance of my studies. I wish to acknowledge Centerpulse Orthopaedics for the collaboration work, and Stryker Howmedica Osteonics and DePuy for allowing me to use the CAD models of their cementless hip stems. I wish to extend my deepest gratitude to my mother and my late father who have been extremely supportive of my decision to do a PhD overseas. And to my beloved wife Marwati and lovely daughter Ainul Mardhiah – thank you for understanding my long-term absence and thank you for providing consistent support, patience and love. I would like to thank my fabulous colleagues for their friendship and assistance, particularly Andrew Hopkins, Charalampos Bitsakos, Bal Sanghera and Hippolite Amadi. And to my wonderful friends, Suhaib Fahmy, Mustafa Ahsan, Sherif Yusuf, Ishthiaq Akbar, Saiful Azhar and Tarek Zerrouki – thank you all for your friendship, encouragement and prayers. Finally, thanks are due to my juniors – Helmi, Faizal, Firdaus, Aiman, Lutfi, Azlan, Ammir, Hanafi, Azzrul, Hassan, Marwan, Khairul, Fadhli, Halim and Izree – who have helped cheer me up during times of difficulty.

Khas untukmu,

Ibu dan Ayah.

Table of Contents

ABSTRACT.....	2
ACKNOWLEDGEMENTS:.....	3
TABLE OF CONTENTS	5
LIST OF FIGURES.....	9
LIST OF TABLES.....	18
CHAPTER 1 INTRODUCTION AND LITERATURE REVIEW	20
1.1 THE HUMAN SKELETAL SYSTEM.....	22
1.1.1 Bone Tissue.....	23
1.1.2 The Human Joints	25
1.1.3 Muscle-Bone Interactions	28
1.2 THE ANATOMY AND PHYSIOLOGY OF THE HIP JOINT.....	29
1.2.1 Femoral morphology classification.....	33
1.2.2 Muscles of the Femur.....	35
1.3 HIP JOINT DISEASES AND SKELETAL DISORDERS	38
1.4 HIP ARTHROPLASTY	40
1.4.1 Types of hip implant	43
1.5 ACHIEVING PRIMARY STABILITY IN CEMENTLESS STEMS	47
1.5.1 The use of Finite Element Analysis in Orthopaedic Biomechanics.....	55
1.6 AIMS AND OBJECTIVES.....	56
1.7 STRUCTURE OF THE THESIS	57
CHAPTER 2 FINITE ELEMENT MODEL CONSTRUCTION..	60
2.1 PRE-PROCESSING	62
2.1.1 Creating a 3D model of the femur.....	62
2.1.2 3D models of hip stems.....	64
2.1.3 Aligning the stems in 3D.....	69
2.1.4 Creating bone-implant contact	71

2.2	MODELLING OF CONTACT	73
2.3	DEFINING MATERIAL PROPERTIES	75
2.4	BOUNDARY CONDITIONS OF THE MODEL	76
2.5	MICROMOTION SUBROUTINE	78
2.6	CONVERGENCE STUDY.....	81
2.6.1	Mesh convergence.....	81
2.6.2	Load Increment	86
2.7	VERIFICATION OF CONTACT AND MICROMOTION ALGORITHM	88
2.7.1	Rohlmann’s model	88
2.7.2	Results.....	90
2.7.3	The effect of location for micromotion measurement.....	92
2.8	CONCLUSION.....	95
CHAPTER 3 EXPERIMENTAL VALIDATION.....		97
3.1	EXPERIMENTAL WORK ON MICROMOTION	98
3.2	FINITE ELEMENT WORK ON MICROMOTION	108
3.3	MICROMOTION EXPERIMENT: MATERIALS AND METHODS.....	115
3.3.1	Experimental Results	124
3.4	FE MODELS OF THE EXPERIMENT	127
3.4.1	Results	129
3.5	DISCUSSION.....	130
3.6	CONCLUSION.....	133
CHAPTER 4 PARAMETERS AFFECTING FINITE ELEMENT PREDICTIONS.		134
4.1	THE EFFECT OF COEFFICIENT OF FRICTION	136
4.1.1	Methods and Results	139
4.1.2	Discussion	142
4.2	THE EFFECT OF INTERFERENCE FIT	144
4.2.1	Methods and Results	145
4.2.2	Discussion	149
4.3	THE EFFECT OF CYCLIC LOADING ON MICROMOTION.....	150
4.3.1	Methods and Results	152
4.3.2	Discussion	158
4.4	THE EFFECT OF MUSCLE LOADS ON MICROMOTION.....	160

4.4.1	Materials and Methods	162
4.4.2	Results	168
4.4.3	Discussion	174
4.5	THE EFFECT OF BONE MATERIAL PROPERTIES ON MICROMOTION	176
4.5.1	Methods and Results	177
4.5.2	Discussion	181
4.6	CONCLUSION.....	182
CHAPTER 5	THE EFFECT OF HIP STEM DESIGNS ON	
INTERFACE MICROMOTION	184	
5.1	THE GLOBAL GEOMETRY.....	197
5.1.1	Methods & Results	205
5.1.2	Discussion	211
5.2	MATERIAL STIFFNESS EFFECTS.....	216
5.2.1	Methods & Results	218
5.2.2	Discussion	222
5.3	THE EFFECT OF STEM LENGTH ON MICROMOTION.....	225
5.3.1	Methods & Results	227
5.3.2	Discussion	230
5.4	PROXIMAL VS DISTAL FIXATION DESIGNS.	232
5.4.1	Methods & Results	234
5.4.2	Discussion	239
5.5	PROXIMAL MACROFEATURES.....	242
5.5.1	Methods.....	243
5.5.2	Results	246
5.5.3	Discussion	258
5.6	CONCLUSION.....	261
CHAPTER 6	SURGICAL & PATHOLOGICAL PARAMETERS	
AFFECTING MICROMOTION	263	
6.1	THE EFFECT OF INTERFACIAL GAPS ON MICROMOTION.....	265
6.1.1	1st Method.....	267
6.1.2	Results	273
6.1.3	2 nd Method.....	274
6.1.4	Results	277

6.1.5	Discussion	280
6.2	THE EFFECT OF UNDERSIZING AND MALALIGNMENT ON MICROMOTION	286
6.2.1	Methods.....	289
6.2.2	Results.....	291
6.2.3	Discussion	295
6.3	THE EFFECT OF BONE DISEASES ON MICROMOTION	298
6.3.1	Methods.....	299
6.3.2	Results.....	301
6.3.3	Discussion	307
6.4	CONCLUSION.....	309
CHAPTER 7	SUMMARY, CONCLUSIONS AND FURTHER	
WORK.....		311
APPENDIX 1.....		321
APPENDIX 2.....		323
APPENDIX 3.....		327
APPENDIX 4.....		329
REFERENCES		332

List of figures

<i>Figure 1.1: A picture of compact bone tissue (taken from www.bioedonline.org, Baylor College of Medicine).</i>	24
<i>Figure 1.2: Pictures showing typical cancellous bone structures from the lumbar spine (left) and the femoral head (right) (Pictures taken from Hildebrand et al. 1999).</i>	24
<i>Figure 1.3: A picture of the posterior half of a proximal femur showing aligned trabeculae. The numbers represent the major groups of bone trabeculae. (Picture taken from McMinn & Hutchings 1990).</i>	25
<i>Figure 1.4: Synovial joints in the human body. Images adapted from Purves et al., “Life: The Science of Biology”, 6th edition, by Sinauer Associates.</i>	26
<i>Figure 1.5: The hip bone showing three parts – the ilium, the ischium and the pubis (picture taken from the Gray’s Anatomy).</i>	30
<i>Figure 1.6: Figure showing the acetabulum (picture taken from the Gray’s Anatomy).</i>	31
<i>Figure 1.7: The anterior and posterior side of a right femur. (Picture taken from the Gray’s Anatomy).</i>	33
<i>Figure 1.8: Pictures showing the morphology of internal proximal femur, from left to right, type A, B and C (picture taken from Berend et al. 2004).</i>	34
<i>Figure 1.9: Diagrammatic representation of the canal flare index (picture taken from Noble et al. 1988).</i>	35
<i>Figure 1.10: Three types of pure movement of the hip. Images adapted from (Nordin & Frankel 1980).</i>	36
<i>Figure 1.11: Major components of a hip joint (left) and major components of a THA (right). (Picture taken from www.aori.org).</i>	41
<i>Figure 2.12: 2D slice from a VHP dataset, showing segmentation of the right femur.</i>	63
<i>Figure 2.13: 3D model construction with triangular surface mesh of the right femur from Computed Tomography (CT) images using Amira software.</i>	63
<i>Figure 2.14: CAD models of the AML stems at different sizes (first 4 stems) received from the manufacturer, and the solid tetrahedral mesh created (right).</i>	65

Figure 2.15: The original CAD drawing with highlighted section for remeshing (left), and after remeshing (centre). The inset pictures show the extra elements created (top) and after manual repair (bottom)......67

Figure 2.16: The original CAD drawing of an Alloclassic Hip Stem (left) received from the manufacturer and the completed triangular surface mesh.67

Figure 2.17: The ABG hip stem in the original IGES format surface meshed in MARC (left) and the completed model after repairing the surface boundaries in Magics (right).68

Figure 2.18: Hip stems used in the study – the AML, the ABG, the Alloclassic and the CLS – aligned inside the VHP femur model......71

Figure 2.19: The placement of the box model to make a cut for the ante-version angle at the neck (left), the femur model with ante-version cut (middle) and the “after-reamed” femur model (right).72

Figure 2.20: Coordinate system used in all analyses (taken from “Hip 98” CD).77

Figure 2.21: Pictures showing no interface gaps (left) and with interfacial gaps with thickness of 500µm (right).80

Figure 2.22: The eight-noded hexahedral (left) and the four-noded tetrahedral (right). Higher order hexahedrals and tetrahedrals have an extra node (midside node) on each edge......82

Figure 2.23: The tetrahedral elements of the implant with increasing mesh densities.83

Figure 2.24: Graph of micromotion along the axis of the stem for different mesh densities......84

Figure 2.25: Micromotion results at increasing tetrahedral mesh densities (left to right)......85

Figure 2.26: Contour plot of micromotion for load step of 1, 5 and 10 increments....87

Figure 2.27: The micromotion distribution with 1 increment, 5 and 10 increments. ..87

Figure 2.28: A diagrammatic sketch of a longitudinal section of Rohlmann’s model and the finite element model.89

Figure 2.29: Contour plot showing relative micromotion of 5µm when the prosthetic stem (with the coating) was displaced longitudinally by 4µm and rotationally by 3µm......90

<i>Figure 2.30: Results of the Rohlmann's model using the micromotion algorithm (left) and the published result by Rohlmann et. al. (right).</i>	91
<i>Figure 2.31: Graph of relative motion along the lateral and medial side of the cylindrical prosthesis.</i>	91
<i>Figure 2.32: Contour plot of micromotion for the bending moment load of 20Nm. (Left – interface micromotion, right – micromotion relative to the periosteal surface)</i>	94
<i>Figure 2.33: Graph of micromotion along the stem on the lateral and medial side under bending moment for the interface micromotion and micromotion relative to the periosteal surface.</i>	94
<i>Figure 3.34: Diagram showing the main components of an LVDT.</i>	116
<i>Figure 3.35: Calibration of the LVDT used in the experiment to measure relative motion</i>	117
<i>Figure 3.36: Graph of volt vs displacement for calibration of the LVDT.</i>	118
<i>Figure 3.37: The jig used to drill holes on the implant and bone.</i>	120
<i>Figure 3.38: Location of the two $\phi 2\text{mm}$ steel pins for micromotion measurement.</i> ..	121
<i>Figure 3.39: The implant loaded in compression using the Instron machine.</i>	123
<i>Figure 3.40: Example of Load-crosshead displacement curve from the experiment, specimen 2.</i>	124
<i>Figure 3.41: Relative motion results from the experiment.</i>	126
<i>Figure 3.42: Alignment of the intact bone to the implanted bone (left) and alignment of the Alloclassic hip stem to the implanted bone (right).</i>	128
<i>Figure 3.43: Contour plots of micromotion for the Alloclassic hip stem under axial load of 2kN.</i>	129
<i>Figure 3.44: Graph showing the experimental range of values for the proximal and distal region after 50 cycles compared to the FE results.</i>	130
<i>Figure 4.45: Contour plots of micromotion with friction coefficient of 0.2, 0.4, 0.6, 0.8 and 1.0 (left to right). The model with friction coefficient of 0.01 is not included as the micromotion went beyond the range of the scale.</i>	140
<i>Figure 4.46: The effects of the coefficient of friction on micromotion along the anterior surface of the AML stem (proximal to distal).</i>	140
<i>Figure 4.47: Average micromotion along the anterior surface of the AML stem as a function of coefficient of friction.</i>	141

<i>Figure 4.48: Diagram showing the implant (subscript s) and the femur (subscript f) for estimating the maximum interference fit.</i>	146
<i>Figure 4.49: Contour plots of micromotion for the AML stem without an interference fit (left), with interference fit of 0.050mm (centre) and 0.100mm (right).</i>	148
<i>Figure 4.50: Micromotion along the posterior side of the three AML implants from proximal to distal.</i>	148
<i>Figure 4.51: The progression of total micromotion (elastic + permanent) for up to 10 cycles.</i>	153
<i>Figure 4.52: The progression of permanent micromotion for up to 10 cycles.</i>	154
<i>Figure 4.53: The progression of elastic micromotion for up to 10 cycles.</i>	155
<i>Figure 4.54: The graph of an average micromotion along the AML stem for 10 cycles to show total micromotion, permanent micromotion and reversible micromotion.</i>	156
<i>Figure 4.55: Total, Permanent and Reversible micromotion for the first cycle (first three stems) and the tenth cycle (last three stems).</i>	157
<i>Figure 4.56: The graph of average micromotion along the AML stem with an interference fit of 100μm for up to 10 cycles.</i>	158
<i>Figure 4.57: Identification of muscle paths from the VHP dataset (top). The magnitude and direction of the muscle forces and joint contact force for the three phases of the gait cycle (bottom). Solid lines are for heel strike, short-dots are for mid-stance and long-dots are for toe-off. (Picture taken from Fisher 1999)</i>	165
<i>Figure 4.58: Location of the muscles attachment used by Duda together with maximum loading configurations during walking and stair climbing (Taken from Hip CD 98).</i>	167
<i>Figure 4.59: Contour plots of micromotion for the three phases of the gait cycle with (top) and without (bottom) muscle loads.</i>	169
<i>Figure 4.60: Contour plots of micromotion for walking and stair climbing with muscle loads and without muscle loads using Duda' loadcases.</i>	170
<i>Figure 4.61: Deflection of the AML implant during walking and stair-climbing using Duda's loadcases for both with and without muscle loads.</i>	172
<i>Figure 4.62: Implants deformation between with (top set) and without (bottom set) muscle forces for the three phases of the gait cycle.</i>	173

<i>Figure 4.63: Contour plots of micromotion with decreasing stiffness values using Fishers's walking (top) and Duda's stair-climbing loads (bottom).</i>	179
<i>Figure 4.64: Graph showing the increase in surface area unfeasible for bone ingrowth vs the percentage of stiffness reduction.</i>	180
<i>Figure 5.65: Femoral components with straight cylindrical design (the pictures are not resized to scale).</i>	200
<i>Figure 5.66: Femoral components with tapered design (the pictures are not resized to scale).</i>	201
<i>Figure 5.67: Femoral components with anatomic design (the pictures are not resized to scale).</i>	202
<i>Figure 5.68: Pictures of the AML, the Alloclassic and the ABG, taken from the manufacturer's website.</i>	206
<i>Figure 5.69: Contour plots of micromotion for the cylindrical (left), the tapered (middle) and the anatomical (right) using Fisher's gait loading (top) and Duda's stair-climbing loads (bottom) after the 1st iteration.</i>	208
<i>Figure 5.70: Contour plots of micromotion for the cylindrical (left), the tapered (middle) and the anatomical (right) using Fisher's gait loading (top) and Duda's stair-climbing loads (bottom) after simulated interfacial bone loss.</i>	209
<i>Figure 5.71: Percentage area of predicted bone ingrowth for the cylindrical, the tapered and the anatomical stem designs using Fisher's gait (G) and Duda's stair-climbing (S) loads.</i>	210
<i>Figure 5.72: Micromotion results for the AML stem made of CoCr (left), TiAl (middle) and Composite (right) after 1st iteration.</i>	219
<i>Figure 5.73: Micromotion results for the AML stem made of CoCr (left), TiAl (middle) and Composite (right) after final iteration.</i>	219
<i>Figure 5.74: Progression of surface area (grey colour) unfeasible for bone growth for the composite stem (iteration 1 to 5).</i>	220
<i>Figure 5.75: The reduction in surface area with less than 50μm for the CoCr, TiAl and Composite stems.</i>	221
<i>Figure 5.76: Micromotion results for the AML at various stem length for the 1st iteration.</i>	228

Figure 5.77: Micromotion results for the AML at various stem length for the final iteration. The fourth model was not included as the surface was surrounded with micromotion in excess of the chosen threshold limit.228

Figure 5.78: The reduction in surface area with less than 50µm of micromotion for the standard, medium and short stems.229

Figure 5.79: The distal fixation design (left) and the proximal fixation design showing enlargement in medio-lateral and antero-posterior directions (right).234

Figure 5.80: Contour plots of micromotion for a distal fixation and a proximal fixation design using Fisher's gait cycle (top) and Duda's stairclimbing (bottom) after 1st iteration. Posterior side on the left, anterior side on the right.235

Figure 5.81: Contour plots of micromotion for a distal fixation and a proximal fixation design using Fisher's gait cycle (top) and Duda's stairclimbing (bottom) after final iteration. Posterior side on the left, anterior side on the right.236

Figure 5.82: Progression of surface area (grey colour) unfeasible for bone growth for the proximal fixation stem (iteration 1 & 2) for the walking load (left two) and stair-climbing load (right two).237

Figure 5.83: The reduction in surface area with less than 50µm of micromotion for the distal and proximal fixation designs using Fisher's gait cycle and Duda's stair-climbing loads.238

Figure 5.84: Types of macrofeature studied. From left to right, top to bottom – blank, fins, medial ridges, vertical grooves, 45^o grooves, horizontal grooves and 135^o grooves. These resemble the most common types of macrofeatures.244

Figure 5.85: The blank ABG as control and the actual ABG stem with semi-circular indentation feature.245

Figure 5.86: Contour plots of micromotion for the blank CLS, the ridged CLS, the finned CLS and the grooved CLS at various angles using Duda's stair-climbing loads after the 1st iteration.249

Figure 5.87: Contour plots of micromotion for the blank CLS, the ridged CLS, the finned CLS and the grooved CLS at various angles using Fisher's gait cycle loads after the 1st iteration.250

Figure 5.88: Progression of surface area unfeasible for bone ingrowth (grey area) for the blank CLS under simulated stair-climbing loads (iteration 1 to 5).251

Figure 5.89: Progression of surface area unfeasible for bone ingrowth (grey area) for the blank CLS under simulated walking loads (iteration 1 and 2).251

Figure 5.90: Progression of surface area unfeasible for bone ingrowth (grey area) for the ridged CLS under simulated stair-climbing loads (iteration 1 to 3).252

Figure 5.91: Progression of surface area unfeasible for bone ingrowth (grey area) for the ridged CLS under simulated walking loads (iteration 1 to 4).252

Figure 5.92: Progression of surface area unfeasible for bone ingrowth (grey area) for the 45⁰ grooved CLS under simulated stair-climbing loads (iteration 1 to 3). .253

Figure 5.93: Progression of surface area unfeasible for bone ingrowth (grey area) for the 45⁰ grooved CLS under simulated walking loads (iteration 1 and 2).253

Figure 5.94: Progression of surface area unfeasible for bone ingrowth (grey area) for the vertically grooved CLS under simulated stair-climbing loads (iteration 1 to 3).254

Figure 5.95: Progression of surface area unfeasible for bone ingrowth (grey area) for the vertically grooved CLS under simulated walking loads (iteration 1 and 2).254

Figure 5.96 : Percentage of surface area feasible for bone ingrowth for the blank, finned, grooved and ridged CLS under simulated stair-climbing loads.255

Figure 5.97: Percentage of surface area feasible for bone ingrowth for the blank, finned, grooved and ridged CLS under simulated walking loads.256

Figure 5.98: Contour plot of micromotion for the ABG with and without proximal indentation macrofeatures. Results for Fisher’s gait (top) and Duda’s stairclimbing (bottom).257

Figure 6.99: Normal CT and PQCT from two different cadavers with Alloclassic hip implant showing interfacial gaps on the posterior side.268

Figure 6.100: The original CAD drawing from the manufacturer (left), the created surface-meshed model (centre) and model constructed from CT images (right).269

Figure 6.101: The Alloclassic hip stem on a CT slice of an implanted femur, showing the artefacts at the interface (strong white mark) that translate into high stiffness at the interface using the Carter & Hayes density-stiffness relationship.269

Figure 6.102: The three sets of CT data – Intact bone (left), after reaming (middle) and after implantation (right).270

Figure 6.103: Pictures showing the aligned Alloclassic and gaps at the interface...271

Figure 6.104: Pictures showing interfacial gaps on the anterior and posterior side of the stem (left). The interfacial gaps turned into elements (right).272

Figure 6.105: Micromotion results using Fisher's loadcase (left) and Duda's loadcase (right). Each set contains the micromotion result for without gaps (left) and with gaps (right).273

Figure 6.106: Three cases of the ABG stem analysed – without interfacial gaps (left), distal gap (centre) and distal & lateral-proximal gap (right).275

Figure 6.107: Three cases of the AML stem analysed – without interfacial gaps (left), with gaps in the proximal $\frac{1}{3}$ (middle) and with gaps in the proximal $\frac{1}{2}$ (right).276

Figure 6.108: Micromotion results using Fisher's gait cycle forces for the ABG stem with distal gap (middle) and distal + lateral proximal gap (right) compared with a perfect fit model (left). Top pictures are results without interference fit, bottom pictures are results with an interference fit of 0.1mm.278

Figure 6.109: Micromotion results using Duda's stair-climbing forces for the ABG stem with distal gap (middle) and distal + lateral proximal gap (right) compared with a perfect fit model (left). Top pictures are results without interference fit, bottom pictures are results with an interference fit of 0.1mm.279

Figure 6.110: Micromotion results using Duda's stair-climbing forces (top set) and Fisher's gait cycle forces (bottom set) for the AML stem with gaps in the proximal $\frac{1}{3}$ (middle) and gaps in the proximal $\frac{1}{2}$ (right), compared to a perfect fit model (left).281

Figure 6.111: Surface area (grey colour) unfeasible for bone ingrowth for the AML modelled with $\frac{1}{3}$ proximal gap (top set) and $\frac{1}{2}$ proximal gap (bottom set). Results using Fisher's walking forces (middle) and Duda's stair-climbing forces (right).282

Figure 6.112: AP radiographs showing varus malalignment of the Alloclassic hip stem (left – picture taken from Khalily & Whiteside 1998) and the Roy-Camille hip stem (right – picture taken from Chen et al. 1998).287

Figure 6.113: Pictures showing the correct size implants and their undersized + malaligned counterparts (AML on left; Alloclassic on right).290

Figure 6.114: Micromotion results for the Alloclassic size 5 (left), 4 (centre) and 3 (right) using Duda's stair-climbing loads.292

<i>Figure 6.115: Micromotion results for the Alloclassic size 5 (left), 4(centre) and 3 (right) using Fisher’s gait cycle loads.</i>	<i>292</i>
<i>Figure 6.116: Micromotion results for the AML stem size 135 (left), size 120 and with a different scale, size 105 (right) in stair-climbing.</i>	<i>293</i>
<i>Figure 6.117: Micromotion results for the AML stem size 135 (left) and size 120 (right) in Fisher’s gait cycle. Result for the AML size 105 was not included as the analysis failed before maximum load was achieved.</i>	<i>293</i>
<i>Figure 6.118: Micromotion results for the Alloclassic size 3 in proper alignment and in varus malalignment. First set on the left using Duda’s stair-climbing, and the second set on the right using Fisher’s gait cycle.</i>	<i>294</i>
<i>Figure 6.119: Micromotion results for the AML stem size 105 in proper alignment and in varus malalignment using Duda’s stair-climbing loads (first two pictures). The last picture on the right showed micromotion results using Fisher’s gait cycle for malaligned AML size 105. Analysis for properly aligned AML size 105 failed before maximum load was achieved.</i>	<i>294</i>
<i>Figure 6.120: The femur model created separately from two CT datasets and the combined model.</i>	<i>300</i>
<i>Figure 6.121: The Young’s modulus of bones from the normal VHP dataset (left), from a patient suffering from osteoporosis (middle) and osteoarthritis (right) (Pictures were scaled to fit).</i>	<i>302</i>
<i>Figure 6.122: The micromotion result from the normal VHP dataset (left), the osteoporotic bone (middle) and osteoarthritic bone (right) using Fishers’s gait (top) and Duda’s stair-climbing forces (bottom).</i>	<i>304</i>
<i>Figure 6.123: The reduction in surface area feasible for bone ingrowth.</i>	<i>306</i>
<i>Figure 6.124: Relative micromotion results for the osteoporotic model from the 1st iteration to the 4th iteration. The grey value is micromotion in excess of the threshold limit of 50µm.</i>	<i>307</i>

<i>(6,365mm²) and horizontal groove (6,283mm²) using Duda's stair-climbing loads.</i>	<i>255</i>
<i>Table 5.17: Surface area $\geq 50\mu\text{m}$ for the blank (6,172mm²), finned (6,717mm²), ridge (6,201mm²), 135^o groove (6,324mm²), 45^o groove (6,220mm²), vertical groove (6,365mm²) and horizontal groove (6,283mm²) using Fisher's walking loads.</i>	<i>256</i>
<i>Table 5.18: Surface area with more than 50μm of micromotion for the ABG, with (5,013mm²) and without (4,816mm²) the indentation features.</i>	<i>258</i>
<i>Table 6.19: Comparison between traditional and surgical robot for femoral canal preparation (Results taken from Paul et al. 1992).</i>	<i>266</i>
<i>Table 6.20: The canal flare index for the normal, osteoporotic and osteoarthritic bone models.</i>	<i>303</i>
<i>Table 6.21: The amount of surface area more than 50μm of micromotion. The total surface area for AML size 135 is 8,976mm², AML size 150 is 9,902mm² & AML size 120 is 7,858mm².</i>	<i>305</i>
<i>Table 6.22: The increase in surface area with more than 50μm of micromotion for the normal, osteoarthritic and osteoporotic models.</i>	<i>306</i>

Chapter 1 Introduction and Literature Review

The number of people undergoing hip joint replacement surgery has increased over the past decades. In the UK alone, more than 60,000 total hip arthroplasties (THA) are performed annually, 15% of which are performed in the younger age group (less than 57 years old) (Tennent & Goddard 2000). Most hip replacements are performed on patients suffering from osteoarthritis, a joint disease associated with the wearing away of the cartilage covering the bone ends. Other degenerative hip disorders that could require THA include rheumatoid arthritis and avascular necrosis. The primary aim of the replacement surgery is to relieve pain and regain mobility. Pioneered in 1962 by the renowned English surgeon, Sir John Charnley, the development of orthopaedic implants used in hip arthroplasty has improved steadily, making it one of the most successful surgical procedures. However, with the increase in the number of hip replacements performed, the scope and frequency of complications appear to be increasing.

Complications such as stress-shielding, osteolysis and aseptic loosening remain some of the major problems in hip arthroplasty (Macdonald 1998).

There are mainly two types of hip arthroplasty in use today – cemented and cementless. Hip prostheses with the use of cement are the most commonly used but the cementless techniques are gaining popularity. Fixation of these femoral components is a major concern because bone growth could only be achieved on stable implants (Pilliar 1991; Simmons, Valiquette & Pilliar 1999). Failure to achieve a strong fixation will result in the formation of fibrous tissue layer at the bone-implant interface and the eventual loosening of the implant (Pilliar, Lee & Maniopoulos 1986). PMMA is used in the cemented type prostheses to provide strong primary fixation. However, cement debris can cause complications such as inflammation and bone lysis. One of the solutions to this problem is to abolish the use of cement, thus the cementless femoral component. However, without the cement these implants could not achieve initial fixation, unless the design is modified so that proper and adequate stability could be achieved. The design of femoral prostheses, together with the surgical techniques of implantation, continues to receive much attention in the hip biomechanics community.

This study will concentrate on the cementless hip replacement because instability is a cause of concern for this type of implant, more so than the cemented. In this study, Finite Element Analyses (FEA) is used to investigate the issues of stability by calculating, through the use of a specially written computer code, the relative motion at the bone-implant interface. The quality of results for hip joint replacement depends on various factors, several of which such as the design, the surgical error and bone quality will be analysed in this study.

In this chapter, a literature review is presented starting with brief introductions to the human musculo-skeletal system, the anatomy and physiology of the hip joint and the skeletal diseases that could be treated with hip arthroplasty. A literature review on the hip replacement then follows, addressing common major issues related to THA in general and the issue of hip stems' fixation and stability in particular. The aims and objectives of the study will follow, together with a description of the organisation of the thesis.

1.1 The Human Skeletal system

The adult human skeletal system consists of about 200 bones, held together by strong fibrous bands called ligaments, to form a protective and supportive framework for the attached muscles and the soft tissues that underlie it. It plays an important role in movement by providing a series of independently movable levers, which the muscles can pull to move different parts of the body. The skeleton is not just a movable frame however; it also produces red blood cells within the bone marrow of certain bones and white cells from the marrow of other bones to destroy harmful bacteria. Bones also store minerals - calcium, for example - which can be supplied to other parts of the body.

The human skeleton is divided into two distinct parts: the axial and the appendicular skeleton. The axial skeleton consists of bones that form the axis of the body and is subdivided into three groups; the Skull, the Thorax, and the Vertebral Column. They

support and protect vital organs such as the brain, heart and lung. The appendicular skeleton is composed of bones that anchor the limbs to the axial skeleton. They are the Upper Extremities (e.g. Humerus, Ulna, Radius), the Lower Extremities (e.g. Hip, Femur, Tibia), the Hand (e.g. Carpus, Metacarpus) and the Foot (e.g. Tarsus, Metatarsus).

1.1.1 Bone Tissue

The bones which make up the skeletal system are composed of tissue that may take one of two forms, cortical (compact) bone, and cancellous (spongy) bone. Most bones contain both types. Cortical bone is dense, hard, and forms the protective exterior portion of all bones. It has a series of Haversian canals around which concentric layers of bone cells, called osteocytes, and minerals occur. The Haversian canals form a network of blood vessels and nerves that nourish and monitor the osteocytes (*Figure 1.1*). A glistening double-layered tissue called the Periosteum covers the compact bone. It serves as a place of insertion for tendons and ligaments.

Apart from the osteocytes, there are two other types of cells – osteoblasts and osteoclasts – that carry out the repair, growth and ‘remodelling’ work of bone tissues. The osteoblasts form new bone or modify existing bone to meet new conditions, whereas the osteoclasts dissolve or break down bone tissue. An equilibrium of bone resorption by osteoclasts and bone deposition by osteoblasts maintains bone tissue. Excessive osteoclasts activity could lead to an imbalance and a loss of bone density, causing osteoporosis.

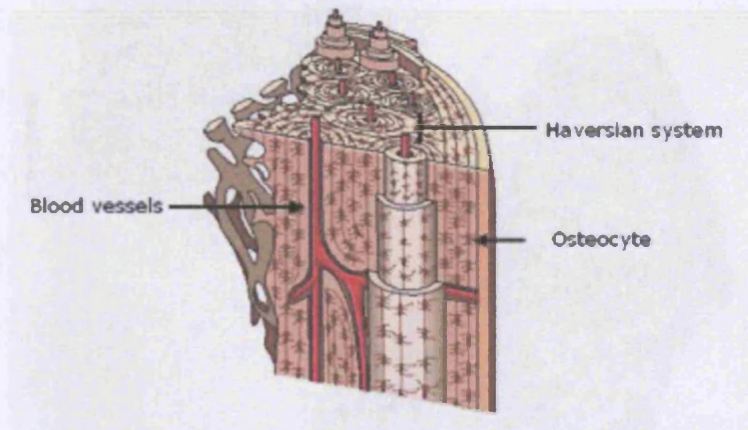


Figure 1.1: A picture of compact bone tissue (taken from www.bioedonline.org, Baylor College of Medicine).

Cancellous bone forms the inner layer of long bones and is lighter and less dense than the cortical bone. Whilst the cortical is a compact structure, cancellous bone consists of an interconnected array of plates and struts called trabeculae. It can be highly porous and irregular (*Figure 1.2*), but appears to be arranged and organised in a manner that provide maximum strength (*Figure 1.3*).

1.2.2 The Human Joints

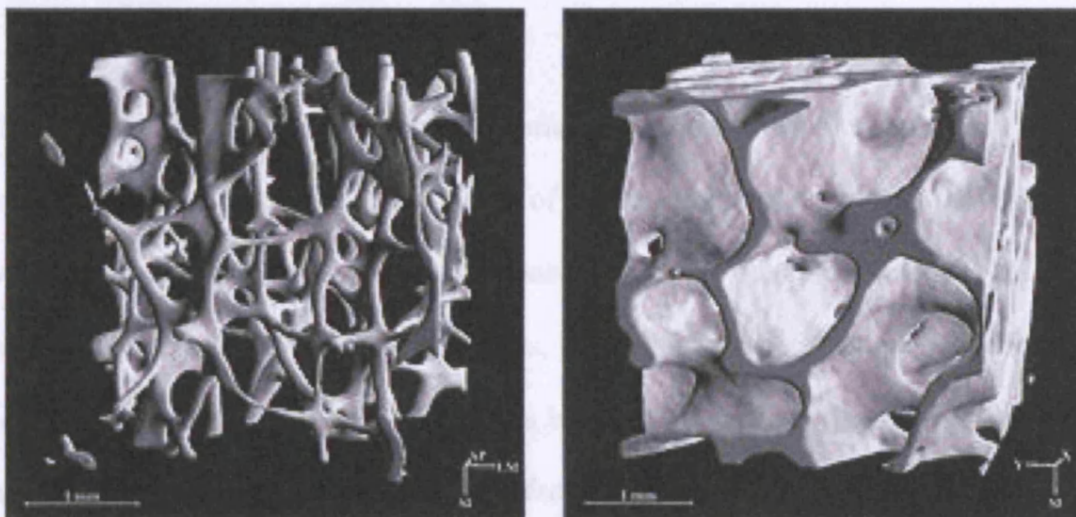


Figure 1.2: Pictures showing typical cancellous bone structures from the lumbar spine (left) and the femoral head (right) (Pictures taken from Hildebrand et al. 1999).

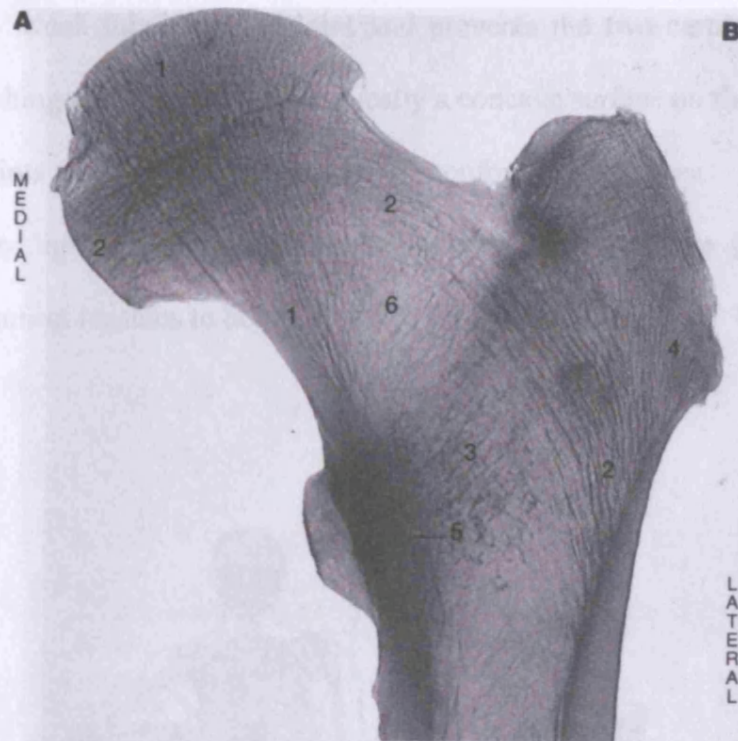


Figure 1.3: A picture of the posterior half of a proximal femur showing aligned trabeculae. The numbers represent the major groups of bone trabeculae. (Picture taken from McMinn & Hutchings 1990).

1.1.2 The Human Joints

The ability of the human body to move in many ways is attributable to complex jointing or articulation. There are three types of joints: immovable, partly movable, and synovial joints. Immovable joints, like those connecting the cranial bones, have edges that tightly interlock. Partly movable joints, such as the vertebrae, allow some degree of flexibility and usually have fibrocartilages between the bones. Synovial joints permit the greatest degree of flexibility. The surfaces are completely separated and bone ends forming the articulation are covered by a tough, smooth shiny substance called cartilage and enveloped by capsules of fibrous tissue. Friction is reduced further by a thin film of

synovial fluid, which lubricates the joint and prevents the two cartilage caps on the bones from rubbing together. There is typically a concave surface on the adjacent bone, but human joints are seldom composed of conforming surfaces. The joints are strengthened by ligaments that hold the bones in position. Some joints also have tendons that connect muscles to bones.

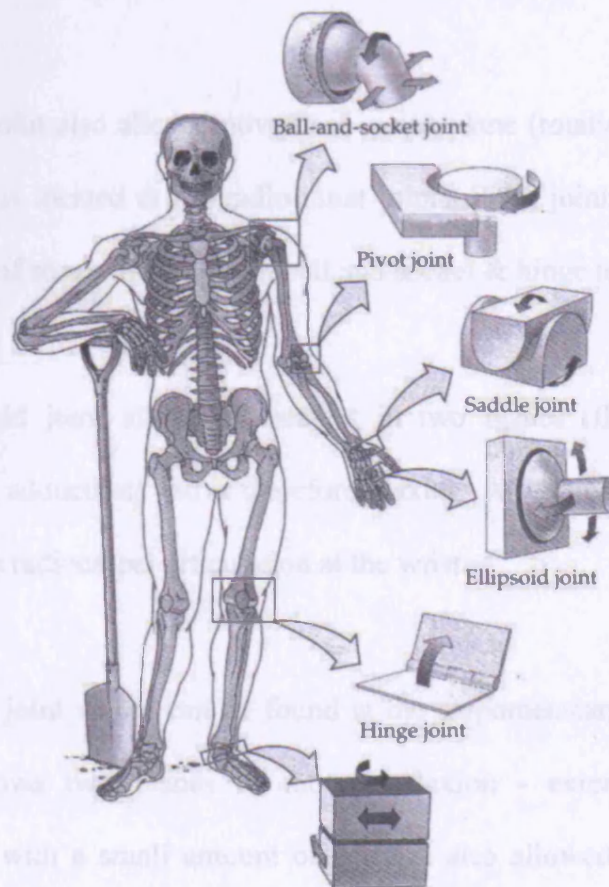


Figure 1.4: Synovial joints in the human body. Images adapted from Purves et al., "Life: The Science of Biology", 6th edition, by Sinauer Associates.

The synovial joints can be further categorised into 6 types (Figure 1.4):

The Plane Joint

Also called the gliding joint, because movement of this type of joint consists of two flat surfaces that slide over each other to allow movement. In the hand, for

example, the carpals will slide over each other as the hand is moved to positions of flexion or extension.

The Hinge Joint

The hinge joint allows movement in a single plane (flexion, extension) and is termed uniaxial. An example of the hinge joint in the body is the ulnohumeral articulation at the elbow.

The Pivot Joint

The pivot joint also allows movement in one plane (rotation). An example of a pivot joint is located at the radio-ulnar joint. Pivot joining allows freedom of movement of somewhat between ball and socket & hinge joining.

The Ellipsoid Joint

The ellipsoid joint allows movement in two planes (flexion - extension & abduction - adduction) and is therefore biaxial. An example of this joint can be found at the radiocarpal articulation at the wrist.

The Saddle Joint

The saddle joint which can be found at the carpometacarpal articulation of the thumb, allows two planes of motion (flexion - extension & abduction - adduction) with a small amount of rotation also allowed. It is similar to the ellipsoid joint in function.

The Ball-and-Socket Joint

The ball-and-socket joint allows movement in three planes (flexion – extension, abduction – adduction, rotation) and is therefore the most mobile joint. The hip and shoulder joints are examples of a ball-and-socket joint.

1.1.3 Muscle-Bone Interactions

The human body contains more than 650 individual muscles, which make up about 40% of adults body weight. They are connected to bones by tendons, have stripe-like markings, and are composed of long muscle fibres. Each of these muscle fibres is a cell which contains several nuclei. The nervous system controls the contraction of the muscle.

The muscular system consists of three different types of muscle tissues: skeletal, cardiac and smooth. Each of these different tissues has the ability to contract, which then allows body movements and functions. They are sometimes grouped into voluntary and involuntary muscles. The skeletal muscles, which we have the ability to control, are voluntary muscles, whilst the heart (or the cardiac muscle) is an example of involuntary muscle.

Bodily movement is carried out by the interaction of the muscular and skeletal systems. For this reason, they are often grouped together as the musculo-skeletal system. Muscles which cause movement of a joint are connected to two different bones and contract to pull them together. They generally work in pairs to produce a movement; when one muscle flexes (or contracts) the other relaxes, a process known as antagonism. An example would be the contraction of the biceps and a relaxation of the triceps which produces a bend at the elbow. The contraction of the triceps and relaxation of the biceps produces the effect of straightening the arm.

Skeletal muscles can be broken down into groups based upon the type of movement

they represent. The movement of the muscle is based upon the type of joint upon which the muscle works. These muscles can be broken down into groups of their own:

- Flexors – Bend at the joint, decreasing the interior angle of the joint.
- Extensors – The opposites of flexors, extensors unbend at the joint, increasing the interior angle.
- Abductors – Take away from the body, e.g. like lifting the arm to the side.
- Adductors – The opposite of abductors, move towards the body.
- Rotators – Movement in the transverse plane (rotation), either internally (towards the body) or externally (away from the body).

1.2 The anatomy and physiology of the hip joint

The hip bone is a large, irregularly shaped bone consisting of three parts, the ilium, ischium and pubis, which are fused together in adult bones. The unification of the three parts takes place in and around a large cup-shaped articular cavity, called the acetabulum, which is situated near the middle of the outer surface of the bone. The ilium is the superior broad and expanded portion which extends upward from the acetabulum. The ischium is the lowest and strongest portion of the bone, it proceeds downward from the acetabulum and expands into a large tuberosity. The pubis extends medialward and downward from the acetabulum and articulates in the middle line with the bone of the opposite side and forms the front part of the pelvis (*Figure 1.5*).

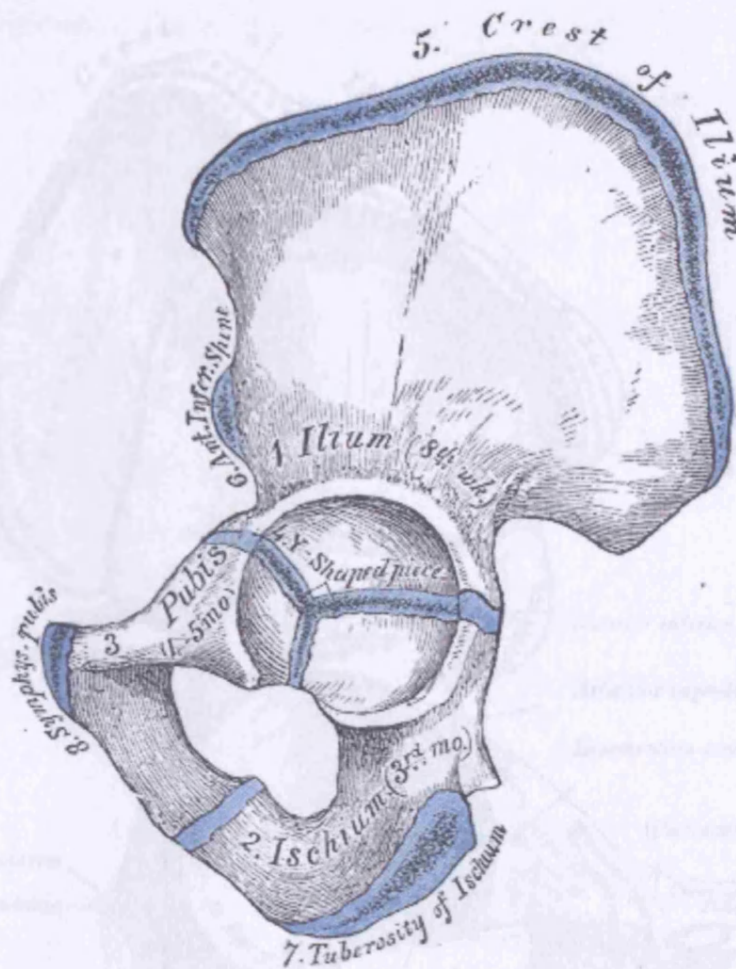


Figure 1.5: The hip bone showing three parts – the ilium, the ischium and the pubis (picture taken from the Gray's Anatomy).

The acetabulum is a deep, cup-shaped, hemispherical depression, directed downward, lateralward and forward. It is formed medially by the pubis, above by the ilium, laterally and below by the ischium. It is bounded by a prominent uneven rim, which is thick and strong above, and serves for the attachment of a ligament, which contracts its orifice and deepens the surface for articulation. The acetabulum is formed by a curved articular surface for articulation with the head of the femur (Figure 1.6).

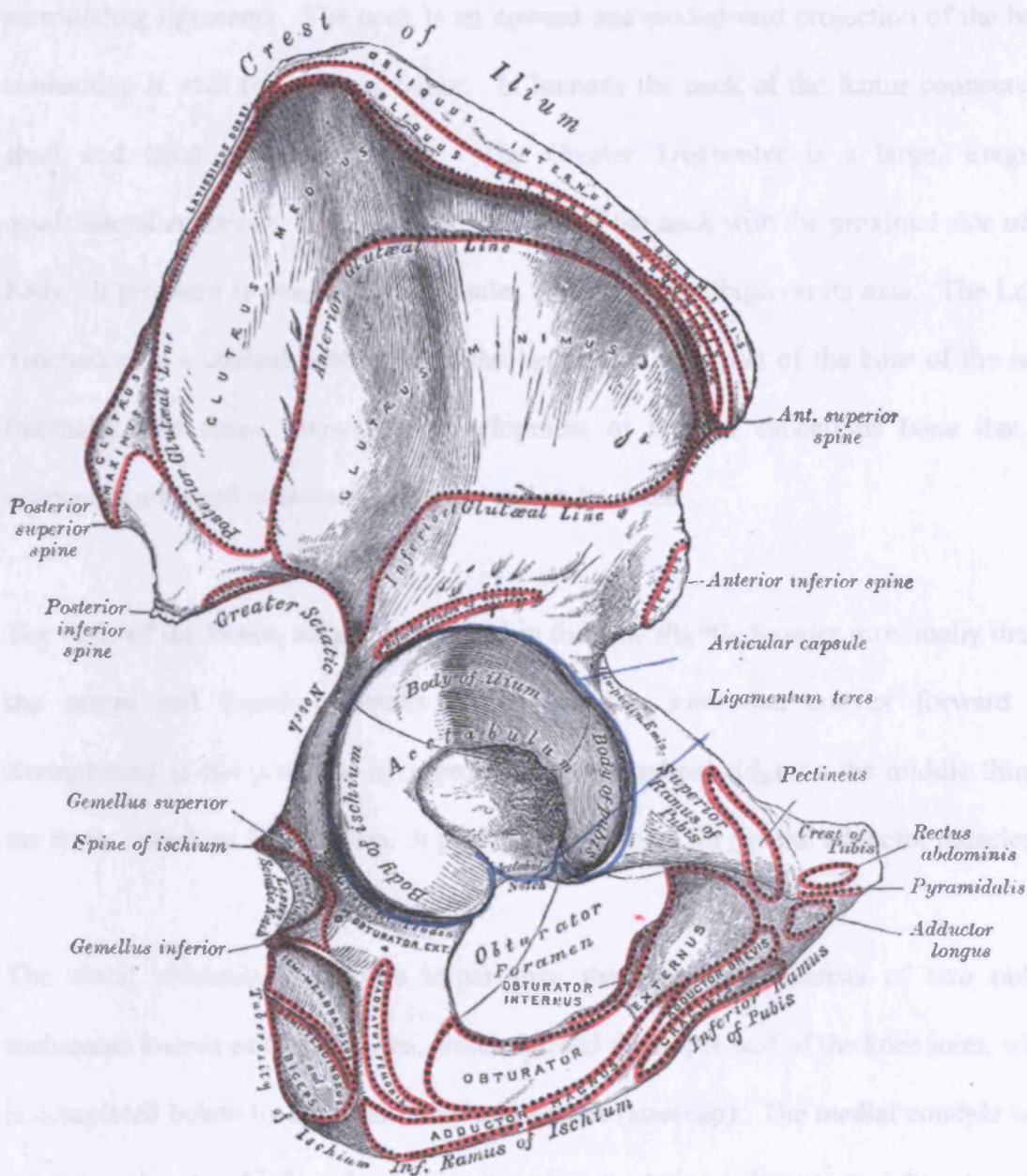


Figure 1.6: Figure showing the acetabulum (picture taken from the Gray's Anatomy).

The femur is the longest bone in the human skeletal system. It can be divided into three parts; proximal, middle and distal. The proximal part consists of a head, a neck, a greater trochanter and a lesser trochanter. The head, which is hemispherical in shape, has a smooth surface and is coated with cartilage surrounded with synovial fluids, which protect the joint whilst allowing easy motion. It forms a ball-and-socket joint with the acetabulum, being held in place by a ligament within the socket and by strong

surrounding ligaments. The neck is an upward and medialward projection of the body, connecting it with the head of femur. In humans the neck of the femur connects the shaft and head at a 125° angle. The Greater Trochanter is a large, irregular, quadrilateral eminence, situated at the junction of the neck with the proximal side of the body. It provides leverage to the muscles that rotate the thigh on its axis. The Lesser Trochanter is a conical protrusion at the lower and back part of the base of the neck. Internally, the femur shows the development of arcs of cancellous bone that are efficiently arranged to transmit pressure and resist stress.

The body of the femur, almost cylindrical in form, is slightly broader proximally than in the centre and broadest distally. The shaft is somewhat convex forward and strengthened at the posterior by a prominent longitudinal ridge on the middle third of the bone, called the *linea aspera*. It provides attachment for several adductor muscles.

The distal extremity, which is larger than the proximal, consists of two oblong eminences known as the condyles, which formed the upper half of the knee joint, which is completed below by the tibia (shin) and patella (kneecap). The medial condyle is the more prominent and is broader both in its antero-posterior and transverse diameters than the lateral condyle. They are separated from one another by the patellar surface, a smooth shallow articular depression. The lower and posterior parts of the articular surface articulate with the corresponding condyles of the tibia and menisci.

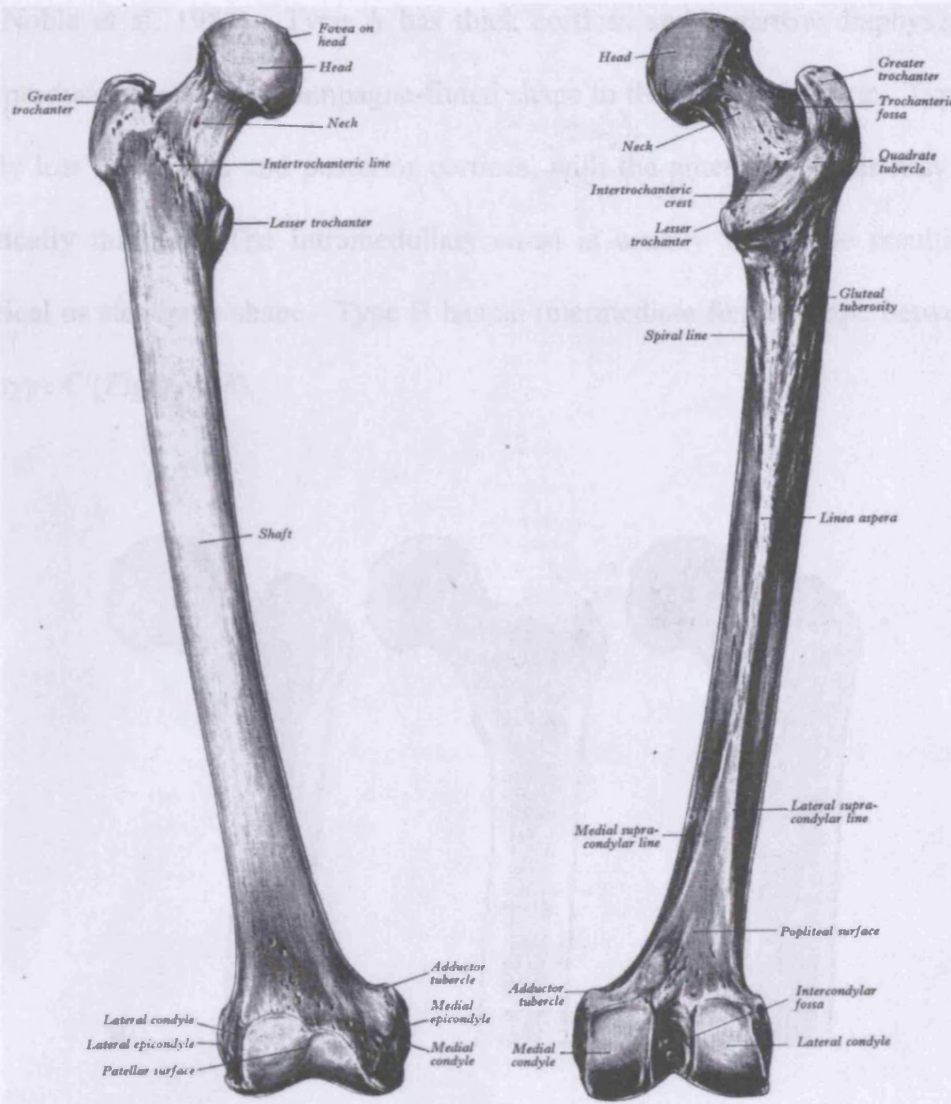


Figure 1.7: The anterior and posterior side of a right femur. (Picture taken from the Gray's Anatomy).

1.2.1 Femoral morphology classification

The proximal femur has considerable variation in morphologic features, and the density and structure changes with age. The quality and morphology of the proximal femur has been described and radiographically categorised into types A, B and C, in an attempt to guide surgical technique and implant selection during total hip arthroplasty (Dorr et al.

1993; Noble et al. 1988). Type A has thick cortices and a narrow diaphyseal canal which produce a funnel or champagne-fluted shape to the proximal femur. Type C has virtually lost the medial and posterior cortices, with the anterior cortices may also be dramatically thinned. The intramedullary canal is usually very wide resulting in a cylindrical or stovepipe shape. Type B has an intermediate funnel shape between type A and type C (Figure 1.8).

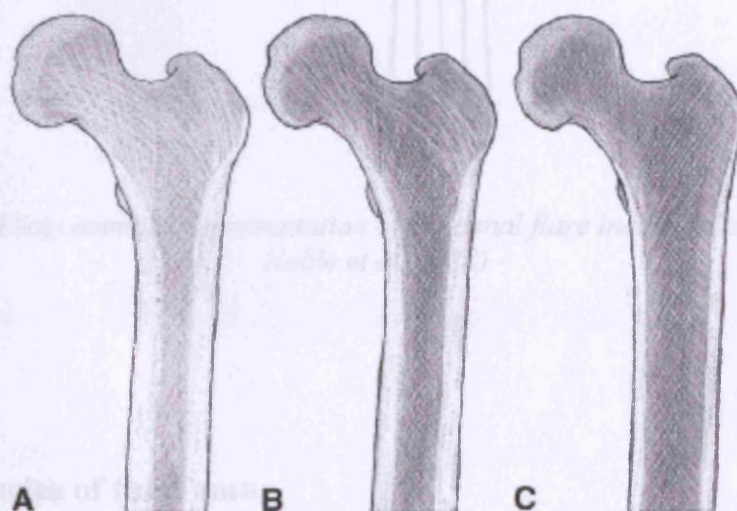


Figure 1.8: Pictures showing the morphology of internal proximal femur, from left to right, type A, B and C (picture taken from Berend et al. 2004).

The three types of femoral morphology were expressed by a single geometric parameter called the canal flare index, defined as the ratio of the intracortical width of the femur at a point 20mm proximal to the lesser trochanter and at the canal isthmus (Figure 1.9) (Noble et al. 1988). From a study of two hundred femora with age ranging from 22 to 95 years, the authors found that canal flare indices of less than 3.0 described stovepipe canals (type C), 3.0-4.7 normal canals (type B), and 4.7-6.5, canals with a champagne-fluted appearance (type A).

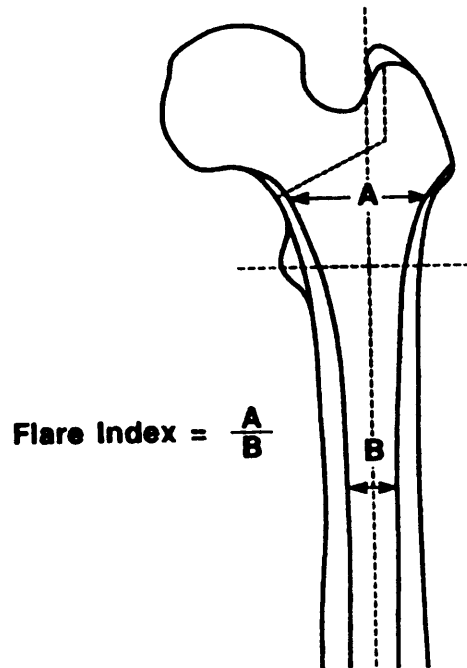


Figure 1.9: Diagrammatic representation of the canal flare index (picture taken from Noble et al. 1988).

1.2.2 Muscles of the Femur

There are many muscles that are involved in the motion of the hip and they can be categorised into several groups, depending on the type of movements available. Hip motions take place in all three planes: sagittal (flexion-extension), frontal (abduction-adduction) and transverse (internal and external rotation) (*Figure 1.10*). Different muscles are used for different kind of activities. Real movement is usually a combination of these pure movements.

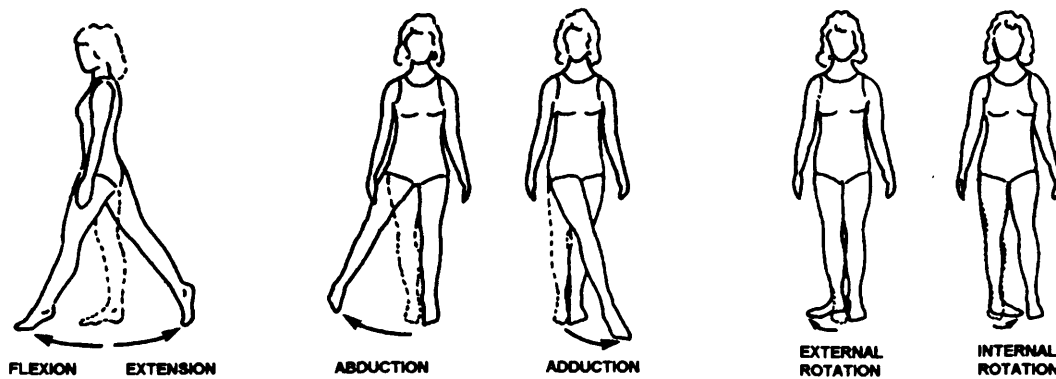


Figure 1.10: Three types of pure movement of the hip. Images adapted from (Nordin & Frankel 1980).

The following are some of the muscles which play a major role in the movement of the hip (Kapandji 1987):

The flexor muscles – the Psoas & the Iliacus, the Tensor Fasciae Latae

The Psoas and the Iliacus share a common tendon of insertion into the lesser trochanter. It is the most powerful of the flexors and has the longest range. It can also produce adduction/abduction or lateral/medial rotation as accessory movements. The tensor fascia latae, which is one of the muscles in the gluteal region, is also a fairly powerful flexor.

The extensor muscles – the Gluteus maximus

The gluteus maximus is the largest muscle of the body, and, with a force equivalent to 34 kg of weight and a contraction length of muscle equal to 15cm, it is also the most powerful and the strongest. The muscle, which is remarkably coarse in structure, lies posterior to the frontal plane that passes through the

centre of the joint. Two other glutei muscles, medius and minimus, assisted its function as extensors. The Gluteus medius is a broad, thick muscle, situated on the outer surface of the pelvis. The muscle fibres converge to a strong flattened tendon, which is inserted into the oblique ridge on the lateral surface of the greater trochanter. The Gluteus minimus, the smallest of the three Glutei, is placed immediately beneath the gluteus medius. The fibres converge to a tendon which is inserted into an impression on the anterior border of the greater trochanter. These muscles are also lateral rotators.

The abductor muscles – the Glutei muscles and the Piriformis

The main abductor muscle is the Gluteus medius, which can produce a force equivalent to 16 kg weight. The Gluteus minimus, is slightly smaller in size and produce a force one-third that of the Gluteus medius. The Gluteus maximus, on the other hand, produces abduction only with its highest and superficial fibres. The Piriformis is a flat muscle, pyramidal in shape, lying almost parallel with the posterior margin of the Gluteus medius. It is situated partly within the pelvis against its posterior wall, and partly at the back of the hip-joint. The tensor fascia latae is also a powerful abductor muscle.

The adductor muscles – the Adductor magnus and the Gluteus maximus

The Adductor magnus is the most powerful of the adductors. It is a large triangular muscle situated on the medial side of the thigh. It arises from the pubis, the ischium, and the tuberosity of the ischium and is inserted into the

linea aspera. The anterior - superior portion is often described as a separate muscle, the Adductor minimus. The large bulk of the gluteus maximus muscle is also adductors.

The rotator muscles – the Piriformis, the Glutei and the Tensor Fascia Latae

There are numerous lateral rotator muscles in the hip, some of which are the piriformis and the gluteus maximus. The medial rotators are less numerous than the lateral rotators. They are mainly three muscles, the tensor fascia latae, the gluteus minimus and the gluteus medius.

1.3 Hip Joint Diseases and Skeletal Disorders

Degenerative hip disorders are the major reason for hip joint arthroplasty. The disease can become so severe that replacement surgery is the only way to remove pain and regain mobility. In this section several major hip disorders are discussed, as well as a brief introduction to a common skeletal disorder of osteoporosis.

As mentioned previously, osteoarthritis is a degenerative condition associated with the wearing away of the cartilage covering the bone-ends. Cartilage is used to absorb the stresses put on a joint, and protects the bones from damage. Osteoarthritis occurs when the cartilage deteriorates, either due to age or injury. With age, human joints slowly

lose the ability to regenerate and repair the cartilage. Bone growths develop as the cartilage degenerates, and the bones that make up the joint rub together, causing pain and restriction of movement. It is a progressive disease that can affect any or all of the joints in the human body, with the weight-bearing joints such as the hips and the knees being more susceptible than the others. Currently, no cure exists for osteoarthritis. Treatment options centre on prevention, if possible, and control of the disease. At its worst, the disease can cause constant pain and severely reduced mobility.

Rheumatoid arthritis is another form of arthritis that is chronic and affects many different joints. It begins with an inflammation and thickening of the synovial membrane, which causes pain and swelling, followed by bone and cartilage degeneration and disfigurement. The disease is considered to be an autoimmune condition that is acquired, and in which genetic factors appear to play a role. It appears more frequently in older people, with more women being affected than men.

Avascular Necrosis (AVN) is a skeletal disease that occurs when bone tissues die off, resulting in the collapse of the bone. It is caused by the loss of blood to the bone. Hips are one of the areas most commonly affected by the disease. Common names for this disease include osteonecrosis, aseptic necrosis and ischemic bone necrosis. The disease can be caused by excessive use of drugs and alcohol or by injury. A joint that has been injured through fracture or dislocation has an increase risk of AVN because blood vessels may be damaged, and blood circulation to the bone is disrupted resulting in trauma-related AVN. Arthritis and AVN affect both men and women at higher rates as they age. The majority of cases involve people between the ages of 30 and 50 years. However, it can affect people of all ages.

Osteoporosis is a major skeletal disorder in which nutrition plays a role and can be prevented and treated. It is characterised by a significant loss of cancellous bone stock and structural deterioration of bone tissue, causing it to become fragile and more likely to fracture. If left untreated, the disease can progress without symptoms until the bones became so weak that a sudden strain, bump, or fall causes a fracture. Fractures occur typically in the hip, spine and wrist. Women are more likely to suffer from osteoporosis than men. Osteoporosis is not a cause for joint replacement, but if a replacement is required due to fracture for example, then it affects the decision made by the surgeon because of the structural deterioration of the bone.

1.4 Hip arthroplasty

People suffering from severe hip joint diseases, may choose to have their joint replaced. Total hip arthroplasty is made up of two major parts, the acetabular component and the femoral component. The acetabular component (socket portion) is a hemispherical cup that replaces the acetabulum. It comprises ~~of~~ a shell with an inner socket liner that acts like a bearing. The femoral component (stem portion) replaces the femoral head (*Figure 1.11*).

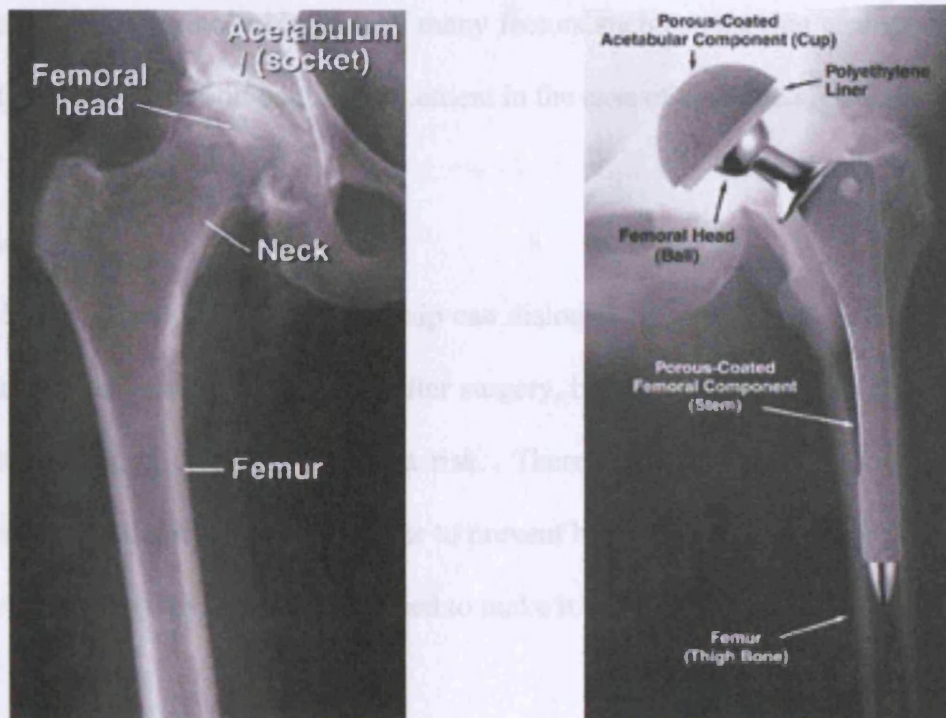


Figure 1.11: Major components of a hip joint (left) and major components of a THA (right). (Picture taken from www.aori.org).

Whilst the use of hip implants has helped patients suffering from skeletal diseases or injuries to relieve pain and gain mobility, its use in human body is not without its own shortcomings. As with all major surgical procedures, complications can occur. Failures of these implants have been reported and many studies have been conducted to identify the reasons behind the failures. Some of the most common complications following hip replacement are as follows (Macdonald 1998):

1. Infection.

Infection can be a very serious complication following an artificial joint surgery. Some infections may show up very early – even before the patient leaves the hospital. Others may not become apparent for months, or even years, after the operation. Infection can spread into the artificial joint from other infected areas. Prevention of

infection involves a combination of many factors such as ensuring clean air theatres, and the use of antibiotic-containing cement in the case of cemented hip arthroplasty.

2. Dislocation.

Just like a natural hip, an artificial hip can dislocate, where the ball comes out of the socket. There is a greater risk just after surgery, before the tissues have healed around the new joint, but there is always a risk. There are certain activities and positions which the patient must avoid in order to prevent hip dislocation. A hip that dislocates more than once may have to be revised to make it more stable.

3. Stress-shielding.

Proximal bone loss due to stress-shielding is also a cause of concern because it could lead to loosening. It is an adverse bone-remodelling phenomenon where bone is resorbed in areas where it is not loaded to physiological levels. This unwanted bone remodelling could cause failure of arthroplasty due to the weakening and deterioration of the proximal bone mass.

4. Aseptic Loosening.

The major reason that artificial joints eventually fail continues to be through a process of loosening where the implant or cement meets the bone. A loose hip is a problem because it causes pain. Once the pain becomes unbearable, another operation will probably be required to revise the hip. There are many factors that cause the loosening of hip prostheses. One of the common causes of aseptic loosening is an inflammatory reaction to particles or wear debris (Bauer & Schills 1999). Wear of polyethylene, metal and bone cement produces debris particles that induce bone

resorption (osteolysis) and implant loosening. These causes further increase in wear debris and a vicious cycle of failure begins. This cycle of wear subsequently causes implant migration, periprosthetic fractures, dislocation and pain (Macdonald 1998).

Another common mechanism of loosening is micromotion of implants that did not achieve adequate initial fixation. Without good fixation, bone cannot grow into the implant in the desired way and so cannot attach onto the surface of the implant. This is especially important for implants with relatively smooth surfaces, where fibrous tissue formation would take precedence over bone formation.

1.4.1 Types of hip implant

There are two major types of artificial hip replacements: cemented and uncemented. Both are widely used. The superiority of one compared to the other remains a topic of debate. The choice made by orthopaedic surgeons is usually based on the patient's age, type of disease, anatomy, lifestyle, and the surgeon's experience. The surgeon's criteria of a suitable hip implant include:

- Shape and design for optimum fit within the patient's anatomy.
- Shape and design which allow for optimum surgical technique.
- The implant's clinical history of stability – called fixation.
- The exterior coating of the stem, which contributes to optimum fixation.
- The type of surgery – primary, revision or fracture.

Cemented prostheses are the oldest form of hip arthroplasty. They are held in place by a type of epoxy cement that attaches the stem to the bone. Good clinical results at 10 years are achievable through this method (Emery et al. 1997). There are, however, complications arising from this conventional method of fixing artificial joints, mainly from the use of the cement itself. PMMA degrades over time and the built-up of cement debris causes inflammation of the surrounding bone and loosening at the interface (El-Warrak et al. 2001). Revision surgery, if required, will also be a problem due to the significant removal of bulk cancellous bone during the first surgery. Despite these complications cemented techniques are still widely used depending on the condition of the patients. It has been suggested for use in the older patients above 65 years (Dorr, Wan & Gruen 1997), or on patients with osteoporotic bone condition or poor bone stock to ensure strong primary fixation (Haber & Goodman 1998). However, Harris (1997) strongly believed that cemented techniques not only worked well with the elderly, but also for younger patients.

Early total hip arthroplasty using the cementing technique in the late 1960s and early 1970s showed an incidence of femoral component loosening of 30%-40% at 10 years (Stauffer 1982; Sutherland et al. 1982). These disappointing results led to revised cementing techniques (Rasquinha et al. 2003), and the use of bioactive cement to encourage rapid bone ingrowth (Oonishi 1991). Some authors also suggested limiting the cement to the proximal area only (sometimes called the hybrid option) (Monti, Cristofolini & Viceconti 2001).

The cementless alternative is used to eliminate the problems associated with the use of cement. The diameter of the stem is generally larger than its cemented counterpart in order to fill the canal, and the surface is usually roughened with particles through grit-blasting or plasma-spraying. Roughened surfaces are not recommended in cemented stems; they are usually polished in order to reduce cement wear debris (Duffy et al. 2001). Some cementless designs also have macro-features at the proximal part such as a porous coating or fibre meshing. These features are beneficial in cementless implants because they provide a medium for biological attachment that secures the implant onto its place. The roughened surface encourages bone attachment and the macro-features allow new bone to attach and grow into, creating a strong bond between the patient's own natural tissue and the implant (Whiteside et al. 1993).

The earlier generation of cementless stems performed less favourably than the cemented designs at that time (Kim, Oh & Kim 2003). However, most cementless hip stems currently in use have survival rate similar to their cemented counterpart (Bourne & Rorabeck 1998). One study reported that clinical results for cementless designs were comparable to cemented stems in terms of disease specific, patient specific, global health, or functional capacity (Mulliken et al. 1996). Another study showed that statistically, there were no significant differences in clinical and functional outcome between cementless and cemented femoral components in the first 12 months post surgery (Zimmerman et al. 2002).

Besides the promising results of cementless stems, old complications associated with the cemented technique are still not entirely eliminated. Stress-shielding, for example, still occurs in hip replaced with cementless stems (Nourbash & Paprosky 1998).

Osteolysis also occurs in cementless arthroplasty due to wear debris. It was previously thought that migration of cement debris along the bone-cement interface was the cause of osteolysis, due to the detection of particles of PMMA of various sizes found in failed interface membranes. However, a study by Boss et al. (1990) showed that the release and deposition of wear products, of whatever nature, were apparently responsible for osteolysis.

One of the major problems associated with cementless stems is thigh pain. This has been attributed to the lack of fixation, i.e. the occurrence of interface motion between the stem and the femoral shaft (Engh, Bobyn & Glassman 1987). This was confirmed by Cruz-Pardos & Garcia-Cimbrelo (2001) who found a high correlation of thigh pain with unstable fixation. Whiteside (1989) reported a similar observation; that a tight distal fit correlated with a lower incidence of thigh pain. Pain was significantly more likely to occur in those patients with a loose distal fit (20 out of 38, i.e. 53%) than in those with a tight distal fit (2 out of 67, i.e. 3%).

Debate also exists on the suitability of cementless stems in bone with stovepipe characteristic (type C bone). Some authors have recommended the use of cementless femoral fixation for patients with type A and type B only (Barrack 1998; Bourne & Rorabeck 1998; Dorr et al. 1993). Healy (2002) however, reported that cementless stems were not just reliable with younger patients who have good bone stock, but were also reliable for elderly patients (above 75 years of age) with type C bone. Reitman et al. (2003) also reported that cementless stems could be used in bones with a stovepipe characteristic.

Aseptic loosening is a major concern in cementless hip stems, and it is a failure associated with the lack of stability. It can be divided into 2 categories (Horikoshi et al. 1994). The 1st category is a late failure due to osteolysis which can be explained by excessive wear particles that migrate along the implant-bone interface and result in formation of the activated interfacial membranes. Early failure, on the other hand, can be explained by the lack of initial implant stability or catastrophic failure of metal or polyethylene materials. Aseptic loosening is still a major problem in cementless design. This could be seen in a recent follow-up report of a carbon fibre-reinforced composite stems, where 92% of the stems were revised due to aseptic loosening at 6 years (Adam et al. 2002). The authors blamed the high rate of loosening on deficient primary stability due to the bad design.

1.5 Achieving primary stability in cementless stems

Achieving good primary fixation is of crucial importance in cementless hip arthroplasty to ensure good short and long term results. One of the major direct consequences of a lack of stability is the eventual loosening of the prosthesis. This stability, or the lack of it, is commonly measured as the amount of relative motion at the interface between the bone and the stem under load. Large interfacial relative movements reduce the chance that bone will osseointegrate with the implant, and may cause the formation of a fibrous tissue layer around the prosthesis. The shear strength at the interface will reduce significantly as well as the ability to transfer load to the surrounding bone. This will

further encourage the formation and thickening of the fibrous tissue, which eventually leads to loosening and failure of the arthroplasty.

Achieving good initial stability is also important because if this is attained at surgery, immediate post-operative full weight bearing is acceptable – i.e. protected weight bearing is unnecessary (Chan et al. 2003). Another similar study also showed that when solid initial fixation was obtained intraoperatively and radiographically, bone ingrowth reliably occurred whether or not a partial or full weight-bearing postoperative protocol was followed (Woolson & Adler 2002).

Implant fixation by bone ingrowth is one of the aims of hip arthroplasty. The term bone ingrowth or osseointegration refers mainly to bone formation within a porous surface structure of an implant, but it can also refer in general to any bone formation into the irregular depths of non-smooth surfaces or an intimate implant surface-to-bone contact. Clinical success of fixation by bone ingrowth depends on a stable implant-bone interface. This primary stability can vary depending on implant design variables (geometry, means of additional fixation, stiffness mismatch), implantation technology variables (accuracy of tools for rasping, broaching, reaming, drilling, sawing), surgical technique variables (accuracy of use of the implantation technology), and patient variables (bone quality, bone defects) (Kienapfel et al. 1999).

Cementless hip stems, though eliminate^{ing} the problems associated with the use of cements, lack the very thing that the cement provides – strong initial fixation. Several in-vitro experimental studies found larger micro-movement for the cementless stems compared to the cemented stems. Burke et al. (1991) found that the micromotion was

always roughly about twice that of the cementless design at low loads and up to 3.5 times at higher loads. In a comparative study between a cemented stem and four cementless stems, Schneider et al. (1989b) found that all cementless stems tested in vitro produced more micromotion than the cemented. Another comparative study also showed similar results (Schneider et al. 1989a).

Clinically, aseptic loosening is one of the major concerns in cementless hip arthroplasty. In a two-year follow-up report of the Bichat III cementless stem (Duparc & Massin 1992), 16% from a total of 203 hips were revised due to persistent thigh pain. All the revised stems were found to be loose. From the unrevised stems 60% of them also complained of pain, and their symptoms were attributed to micromotion of the implant relative to the endosteal bone. Dickob & Martini (1996) reported that the cementless PM smooth prosthesis had 15% of its femoral components revised for loosening at 6 years. From the unrevised hip replacements, 73% were not completely free from pain. Menon & McCreath (1999) reported that the cementless Freeman stems were unsatisfactory at mid-term results. 30% were revised, 16% of which were due to aseptic loosening at an average follow-up period of 4-5 years. There was a high incidence of thigh pain (40%) and an average femoral subsidence was 5.4mm. A study on the smooth surface Moore stem showed that thigh pain on weight bearing was the main problem and was due to loosening of the stem (Phillips & Messieh 1988). The follow-up of cementless APR-I stems at 6.7 years showed that 70% of the stems had progressive loss of fixation (Dorr et al. 1997).

Radiographic signs that were correlated with instability have been reported. Kobayashi et al. (1997) concluded in his paper that predictors of aseptic loosening was either

migration of $\geq 2\text{mm}$ at two years or the presence of radiolucent lines of 2mm occupying $\frac{1}{3}$ of any zone. Vresilovic et al. (1994) reported that radiolucent lines covering greater than 50% of the bone-prosthesis interface was one of the radiographic signs correlated with instability. Khalily & Whiteside (1998) also reported the use of radiolucent lines as a predictor of future need for revision. However, there were cases where the implant migrated significantly in the first year and then stabilised – usually termed late stabilisation (Kitamura et al. 1999). No complications were found later on for these late-stabilised implants. Lautiainen et al. (1994) argued that subsidence was not a definitive hallmark of loosening between 2 to 5 years follow-up. In a 4 to 8 years follow-up study of Harris-Galante cementless femoral stem (Petersilge et al. 1997), 22% of the stems were found to have migrated more than 2mm but later stabilised.

In order to improve its stability, cementless stems are usually designed with rough surfaces or surfaces with microgeometry. Mont and Hungerford (1997) reported that proximal microfeature of any kind improved the success of cementless stems. These include the interconnected multilayered microporous beads and mesh coatings, to other various microporous coated components in use today such as plasma sprayed surfaces and variegated textured surfaces. Chen et al. (1998) reported a 5-year follow-up study of porous-coated cementless stems where 92% of the stems showed evidence of bone ingrowth into the porous coating. A strong fixation can also be achieved with multi-layered honeycomb mesh structure etched onto the stem's surface where this structure provides the anchoring effect through mechanical interlocking (Kusakabe et al. 2004). Circumferential coating in cementless stems also has the added advantage of sealing the diaphysis from wear debris, thus preventing osteolysis in the distal region (von Knoch et al. 2000). A comparative study between hip stems with and without circumferential

coating showed that the survival rate of hip stems with the circumferential coating was significantly better (Dorr et al. 1997; Dorr & Wan 1996; Jacobsen et al. 2003).

It has also been reported that these microtextures are able to influence bone-cell behaviour (Yoshinari et al. 2003). Apart from encouraging the formation of osteoblast-like cells (Matsuzaka et al. 2004), microtextured and microgrooves also helped in anchoring the bone because it has been proven that these features can determine the alignment of cells and cellular extensions (Matsuzaka et al. 2003; Yoshinari et al. 2003).

Biological fixation is achievable by the use of bioactive materials such as hydroxyapatite (Chang et al. 2001; Eckardt et al. 2003; Mouzin, Soballe & Bechtold 2001; Ricci et al. 1991), other calcium-phosphate based materials (Niki et al. 1991; Uchida et al. 1984; Yamamuro & Takagi 1991), calcium ion (Ca^{2+}) (Jinno et al. 2004) or glass and glass-ceramics (Gong, Abdelouas & Lutze 2001). The effect can also be further enhanced by covering the surface of these materials with synthetic stimulants (Kato et al. 2001a; Kato et al. 2001b). All these bioactive materials have been shown to improve the amount of bone apposition to the implant's surface. The attachment of bone does not just show intimate contact, but also exhibits a chemical bond to the surface. Resorption or dissolution will take place, over time, where new bone will replace the resorbed materials (Capello et al. 1998; Rokkum & Reigstad 1999). The rate of resorption is therefore crucial to the success of these biomaterials. Rapid resorption could lead to disintegration of the coating with loss of bonding strength and mechanical fixation.

There are, however, published reports that showed the uncertain short-term effect of bioactive coatings. Ciccotti et al. (1994) found that there were no differences between implants coated with and without HA coatings at 6 and 12 weeks in terms of plain radiographic evaluations. No instability was detected and bone ingrowth was similar in the two groups. Rothman et al. (1996) also reported that there were no significant clinical or radiographic advantages between HA-coated and non HA-coated implants two years after surgery. The same conclusion was also arrived at by Johnston et al. (2001) when comparing standard AML stem with the one coated with tricalcium phosphate (TCP). The two groups of 46 subjects showed no significant differences in terms of bone ingrowth, the degree of hypertrophy / calcar atrophy at 6, 12 and 24 months. Jinno et al. (2004) reported greater bone apposition in calcium ion coated prostheses as compared to the non-coated, but this was only significantly different at 1 month. They concluded that calcium ion was beneficial only for early fixation unless if the dissolution rate could be controlled.

Longer follow-up study also showed that there were no significant advantageous of using HA coating. A study of IPS cementless stems with and without HA coating showed that clinical and radiographic results were similar at a mean duration of 6.6 years (Kim et al. 2003). No aseptic loosening was found in both groups and the bone remodelling patterns, including calcar atrophy, were similar. In a study comparing between HA and non-HA porous coated Mallory-Head stems, no significant differences were found in terms of Harris hip scores and femoral stem survivorship at a minimum of 3 years (Yee et al. 1999). Kang et al. (2000) reported that there were no statistical clinical or radiographical differences between the HA-coated APR-II stems and the non-coated at 4 years. But there were significant differences between proximally porous

coated APR-II and the non-porous coated, with the latter having 14% rate of osteolysis and 0% for the former.

In a study comparing between implants with or without HA coating on grooved specimens, Hayashi et al. (1999) reported that geometry played a more important role than HA coating alone. Specimens with 1mm grooves HA-coated showed higher percentage of bone ingrowth in 4 weeks, but showed minimal improvements in the following 8 and 12 weeks. By 8 weeks, the uncoated control specimens showed similar percentage of bone ingrowth. However, specimens with 2mm grooves HA coated showed similar ratio of bone ingrowth to the uncoated 1mm grooves. Furthermore, specimens with porous-coated beads showed lower attachment strength at 4 weeks compared to HA coated grooves, but significantly stronger attachment strength at 12 weeks. It was concluded that the percentage of bone ingrowth increased rapidly with HA coating at a specific type of geometry, with certain types of geometry, such as the beads, proving to be better than HA coating alone.

The threshold value of relative micromotion, above which fibrous tissue layer forms, has been studied in both animals and human. In a review of dental implants in animals, the threshold micromotion value was found between 50 and 150 μ m (Szmukler-Moncler et al. 1998). The tolerated micromotion threshold varies according to surface state and/or implant's design. Femoral implants in animal, on the other hand, gave a slightly lower threshold value of 30 μ m. A similar range of threshold values were also reported for orthopaedic implants in human. A micromotion study on eleven cemented femoral specimens retrieved at autopsy found a maximum axial micromotion of 40 μ m (Maloney et al. 1989). Histologic investigation showed intimate osseointegration at the interface

with only rare intervening fibrous tissue. The same magnitude of micromotion was found in cementless femoral components with bone ingrowth at the porous coating and a higher micromotion of 150 μm was found on areas of failed bone ingrowth (Engh et al. 1992). Another micromotion study comparing the AML and the Mallory Head prosthesis with surface bone ingrowth showed a micromotion of 80 μm or less (Whiteside et al. 1993). It can be concluded from these experiments that the threshold value of micromotion for osseointegration is between 30 and 150 μm .

Computer models simulating the effect of fibrous tissue layer have also been reported in the literature. In a study comparing the effect of various fibrous tissue layer thicknesses on micromotion with a threshold value for bone-ingrowth of 200 μm , a thickness of 58 μm was found to be sufficient to increase the micromotion beyond the targeted threshold value (Bernakiewicz, Viceconti & Toni 2001). It was also reported from a similar study (Viceconti et al. 2001), that the viable region for bone-ingrowth was completely eliminated throughout the stem surface for a fibrous tissue layer of thickness 300 μm . Others have used a mathematical model which incorporates the effect of interface debonding and relative motions on bone resorption (Weinans, Huiskes & Grootenboer 1993). Three simplified models of orthopaedic implants were analysed, and the results showed reasonable qualitative agreement with resorption patterns found in clinical studies.

1.5.1 The use of Finite Element Analysis in Orthopaedic

Biomechanics

Finite element models of joint anatomy can help surgeons understand trauma from repetitive stress, degenerative diseases such as osteoarthritis, and acute injuries. FE models of prosthetic joint implants can provide surgeons and biomechanical engineers with the analytical tools to improve the life-span of implants and improve the clinical outcomes of total hip replacement surgeries (O'Toole et al. 1995). These models are created from many small "elements" of triangular or rectangular shapes. When these finite element (FE) models are loaded with proper boundary conditions, their responses are obtained by solving a set of simultaneous equations that represent the behaviour of the model under load.

FE analyses have been widely used in the study of hip joint arthroplasty and in particular the study of hip stem stability. FEA is used to complement the experimental work on micromotion and could even become a useful tool to assess the suitability of implants before surgery (Huiskes et al. 1998; McNamara et al. 1997). One advantage of using FE methods in analysing the stability of hip stems is that it is a non-destructive assessment that can measure the distribution of micromotion along the entire surface of the stem. In-vitro experiments, on the other hand, could only measure micromotion at certain points, and the drilling of holes during specimen preparation could damage and weaken the surrounding bone, thus overestimating the relative motion. FE analysis gives a clearer picture of the stem being analysed and could pointed out ways of improving the stability further. Finite elements have been shown to predict

experimental findings and long-term failure mechanisms in orthopaedic surgery with excellent accuracy (Stolk et al. 2003; Tanner et al. 1995).

With faster computers and more reliable software, computer simulation is becoming an important tool in orthopaedic research. Future research programmes will use computer simulation to reduce the reliance on animal experimentation, and to complement clinical trials (Prendergast 1997).

1.6 Aims and Objectives

Cementless hip stems are widely used and gaining popularity over its cemented counterpart, but the major concern is their stability. Analysing factors that could compromise the stability is crucial to its success, and the valuable information obtained from these analyses could be used to improve the stability and therefore improve the confidence of patients and surgeons alike. This study will concentrate on various issues surrounding the stability of cementless hip stems using finite element analyses. A variety of design features will be analysed, looking at the designs' strengths and weaknesses, and suggest ways of improving the stability. The effect of surgical errors, such as the creation of interfacial gaps during canal preparation, and implant undersizing and malalignment will also be analysed. Bone quality could also affect the stability of cementless hip stems and a study will be conducted to analyse this. It is hoped that this study will provide quantitative and qualitative data to help both surgeons

and engineers on issues related to the stability of cementless hip stems, in order to improve its short-term and long-term successes.

1.7 Structure of the Thesis

The thesis is organised into 7 chapters. Following this introductory chapter is Chapter 2, which deals with finite element model construction. Detailed descriptions on the construction of the models are presented, together with explanations of the boundary conditions used in the analysis. The micromotion algorithm for quantitatively predicting the stability is described and verified using a published data from the literature. Two convergence studies are also performed to ensure the numerical accuracy of the models.

In Chapter 3, a simple in-vitro micromotion experiment is carried out to validate the finite element predictions. Four human cadaveric femurs are each implanted with a cementless stem and loaded axially on a testing machine. One of the femurs is CT scanned and an FE model of the very same specimen is created. A parallel virtual experiment simulating the physical experiment is carried out and the results are compared with those of the experiment.

Chapter 4 looks at the effects of various parameters affecting FE micromotion predictions. It starts with the FE input parameters for which the accuracy of the values is uncertain. These are the coefficient of friction and the effect of interference fit on micromotion. Loading cycles in FE will also be looked at to see if cyclic loadings

affect micromotion results. The chapter then continues with the effects of muscle forces on FE micromotion predictions. The final section of the chapter examines the effect of bone material properties, where the stability of the implant is analysed by gradually reducing the bone's stiffness values.

The next chapter (Chapter 5) looks at the effect of hip stem designs on micromotion. An investigation is undertaken to gather as much information as possible on cementless hip stem designs. These stems were then categorised into one of three basic types. Each of these types are then analysed in terms of stability under physiological loadings. This chapter also looks at the effects of implant stiffness, and the length of the stem, on stability. A comparative study will also be conducted between a distal and a proximal fixation design. The study continues with stems incorporating proximal macrofeatures, which is increasingly popular in cementless stems, to quantitatively analyse its capabilities in terms of improving stability. Several of these macrofeatures are analysed and their distribution of micromotions compared.

Having addressed the issue of the design of the implant itself, the following chapter (Chapter 6) will raise the issue of surgical and pathological parameters on the stability of femoral stems. During bone preparation, broaching and reaming creates gaps at the interface. FEA was conducted to see if these gaps affect the stability of cementless stems. Actual CT dataset, as well as discussions with a senior orthopaedic surgeon, is used to identify the location of the gaps. The effects of hip stem malalignment and undersizing on stability are also examined. For the effects of pathological conditions on stability, two femoral models are reconstructed from CT dataset of patients suffering from osteoarthritis and osteoporosis respectively. The two models are analysed in FE

under physiological loading conditions and compared with the results from a normal healthy bone.

Chapter 7 summarises and concludes the thesis, offering suggestions of potential future work in this area that can be based on this research.

Chapter 2 Finite Element Model Construction

Good computer model construction is essential to the success and reliability of finite element analyses. In the field of biomechanics of the hip, both two-dimensional (2D) and three-dimensional (3D) models have been reported in the literature. Whilst analyses using 2D models are simple to perform, they lack important 3-dimensional information. Many implants have complex geometries and these can only be assessed properly in 3D; 2D models cannot be used to analyse asymmetrical stems for example. Though 3D models have become the standard in biomechanical analyses, they are very costly – they are more time consuming both in terms of labour and computing resources than 2D analyses.

This chapter explains the 3D reconstruction of the human bone and the implant. It also explains how implant stability can be analysed using finite elements, and the use of computer software to construct the models and carry out the analyses. The process is started with the reconstruction of the hip from CT images, and then the hip stem from CAD geometrical data. The reconstruction of hip stems uses the CAD file received from the manufacturer, where a slightly different approach was used in order to achieve good meshes. The implant was then aligned into the bone based on the surgical approach recommended by the manufacturer. Once aligned, the contact was then modelled using a 'cut-out' procedure assuming that there were no gaps at the bone-implant interface. The material properties of the bone were assigned using an in-house algorithm written by a previous PhD student (Hopkins 2004). The boundary conditions were then applied in a particular coordinate system of reference.

The chapter will also describe the 'micromotion code', an algorithm written in Visual Fortran to calculate and display interface micromotion. This code was checked for accuracy using Rohlmann's simplified cylindrical bone-implant model (Rohlmann et al. 1988). Rohlmann's model is also used to compare the differences between micromotion measured at the interface and the one measured relative to the outer surface of the cortex. As with all FE analyses converged solutions are required, that is the solution must be independent of numerical variables such as mesh densities and load increment size. These convergence studies will also be looked at in this chapter.

The chapter continues with a description of how the results will be presented for the rest of the study. There are two sets of results; one of which is the comparative micromotion results. This is a contour plot of relative micromotion at the bone-implant

interface, as has been used previously (Keaveny & Bartel 1993; Viceconti et al. 2001). Further to these micromotion studies, a novel technique of predicting the stability of hip stems is proposed. This is a technique where bone loss is simulated at the interface where micromotion is predicted to exceed the threshold limit for bone ingrowth. Iterations can be continued until either a stable state is achieved or the implant fixation fails.

The procedures described here for preparation of FE analyses will be used throughout the whole study unless stated otherwise. The protocols that have been developed or incorporated into this study will now be further explored.

2.1 Pre-processing

2.1.1 Creating a 3D model of the femur

The construction of 3D models of the hip was done using the software AMIRA (TGS software) which allows semi-automated segmentation of medical images. All images used in this study were obtained from 2-dimensional CT datasets. These images were stacked in order, with a certain thickness value between them that corresponded to the distances between the CT slices. Segmentation was then carried out manually on each slice by marking the required part on the image (*Figure 2.12*). The segmented images were then compiled automatically using the software's marching cubes algorithm, generating a 3-dimensional triangular surface mesh. The resulting mesh was very refined, and a triangular reduction and a smoothing procedure were performed on the

Give Ref.

newly created model to turn it into a more manageable mesh density with undistorted triangular shapes (Figure 2.13). The femoral neck was left uncut for the time being as the anteversion angle is required for orientation of the stem. For most of the project, CT images from the Visible Human Project (VHP) dataset were used as the standard, unless stated otherwise.

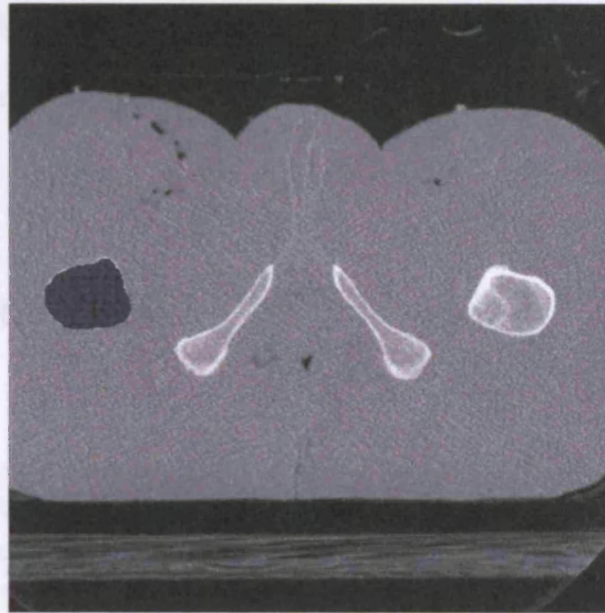


Figure 2.12: 2D slice from a VHP dataset, showing segmentation of the right femur.

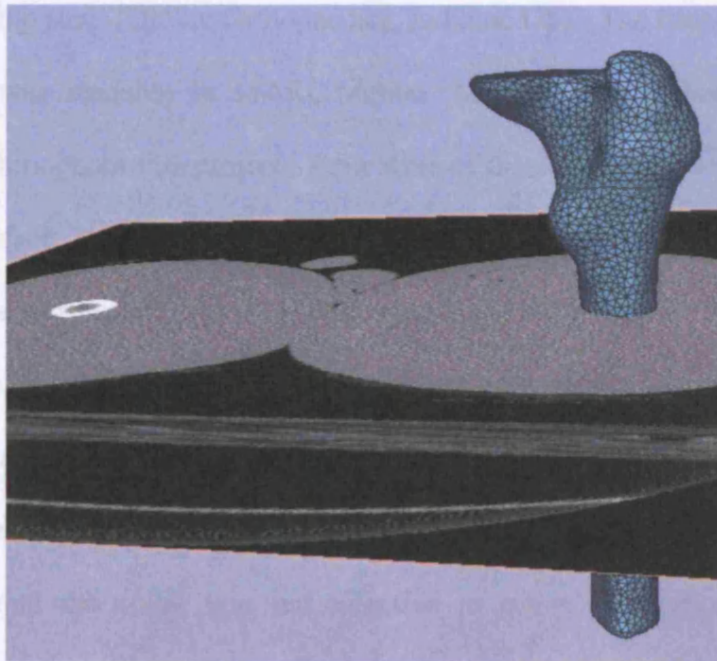


Figure 2.13: 3D model construction with triangular surface mesh of the right femur from Computed Tomography (CT) images using Amira software.

The above procedure described the construction of the femur model using 2D image-based data in Amira. Theoretically, one can also create an implant model from say a CT scan of an implanted femur using the above procedure. However, artefacts from the metal of the implant make it impractical to create the implant model using the above method. This problem will be discussed further in chapter 6 when analysing the effect of interfacial gaps on micromotion.

2.1.2 3D models of hip stems

3D CAD models of the implants were obtained from their respective manufacturers in various file formats. Creating a mesh from these models depended very much on the format of the file and the available software to do the meshing. Most of the studies here used the AML hip stem (DePuy Orthopaedics, Indiana, US). The files obtained were in a format that was readable in MARC.Mentat (MSC software), the Finite Element software used throughout this project. Four sizes of the AML stem were all received in rectangular surface mesh format (*Figure 2.14*). The mesh was then refined by subdividing the elements and then converted into a triangular surface mesh by subdividing the rectangular elements using the two corners of each rectangle. Several adjustments were made to the original AML model such as the removal of the collar and tapering the stem tip. The collar was removed because a study by Keaveny & Bartel (1993) found that the collar was not effective in terms of achieving stability and reducing micromotion. The cut bone surface usually resorbs away from contact with the collar. Further discussion on the effects of a collar on micromotion will be made in

64
Ref

chapter 5 when discussing various design aspects of cementless hip stems. The tip was tapered because the actual design has a tapered tip and, more importantly, to eliminate unnecessary stress concentration in this area. The triangular mesh was then automatically turned into solid tetrahedrals using the tetrahedral mesh generator in AMIRA.

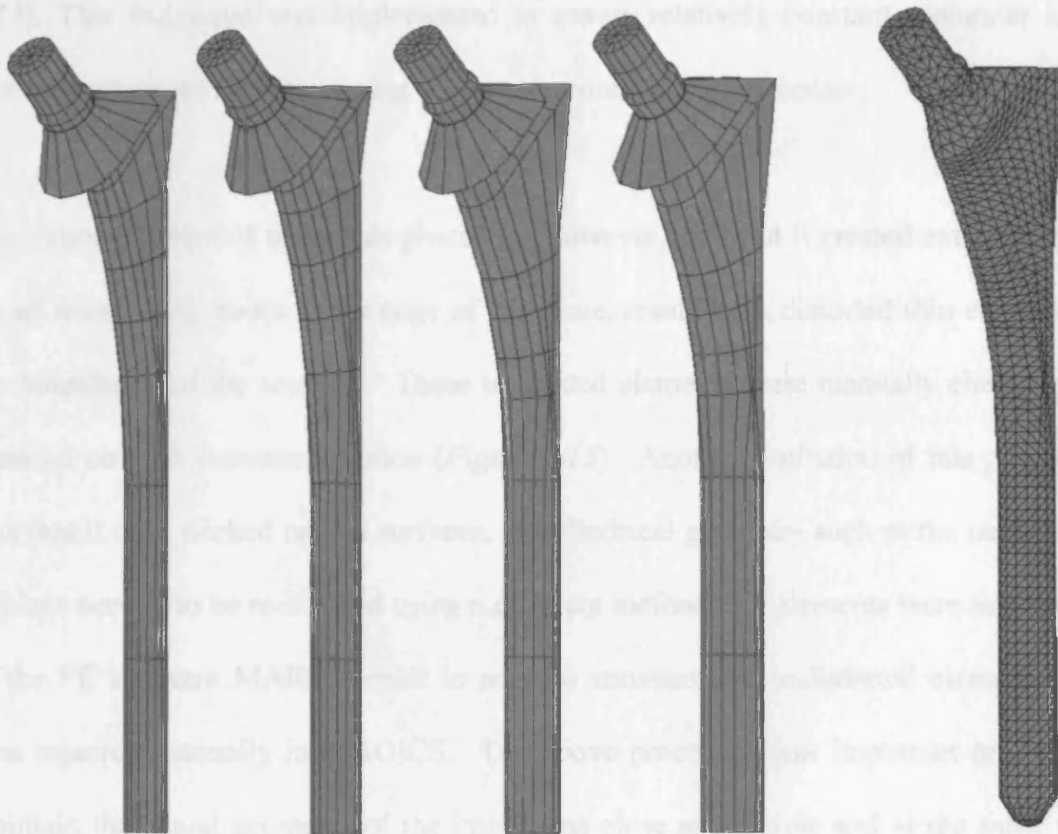


Figure 2.14: CAD models of the AML stems at different sizes (first 4 stems) received from the manufacturer, and the solid tetrahedral mesh created (right).

The method described above for the AML hip stem was rather straightforward. This is because the models supplied by DePuy were already properly meshed. However, for other 3D models of hip stems used in a later study (Chapter 5 and 6), they were not in the same format as the AML models. *Figure 2.16* below shows the original 3D CAD model of the Alloclassic hip stem (Sulzer Orthopaedics, Switzerland) received in a

stereolithographic (.stl) format, a format that is generally used as a pre-processing format for rapid-prototyping technologies (Sanghera et al. 2001). The surfaces were re-meshed because the elements were not of equal size and were highly distorted. Another computer software called MAGICS (Materialise Software) was used to re-mesh the surface, and the process was carried out manually “section-by-section”, i.e. removing a plane section and re-meshing it with a constant triangular grid of a certain size (*Figure 2.15*). This technique was implemented to ensure relatively constant triangular mesh size throughout while maintaining the actual geometry of the implant.

The major problem of using this procedure, however, was that it created extra elements on all intersecting nodes at the edge of the plane, resulting in distorted thin elements at the boundaries of the sections. These unwanted elements were manually checked and repaired on each converted section (*Figure 2.15*). Another limitation of this procedure was that it only worked on flat surfaces, so cylindrical geometry such as the neck of the implant needed to be re-meshed using a different method; the elements were subdivided in the FE software MARC.Mentat to achieve constant and undistorted elements, and then repaired manually in MAGICS. The above procedure was important in order to maintain the actual geometry of the implant as close as possible and at the same time minimising local stress concentration during FE analysis. The resulting mesh is shown in *Figure 2.16*.

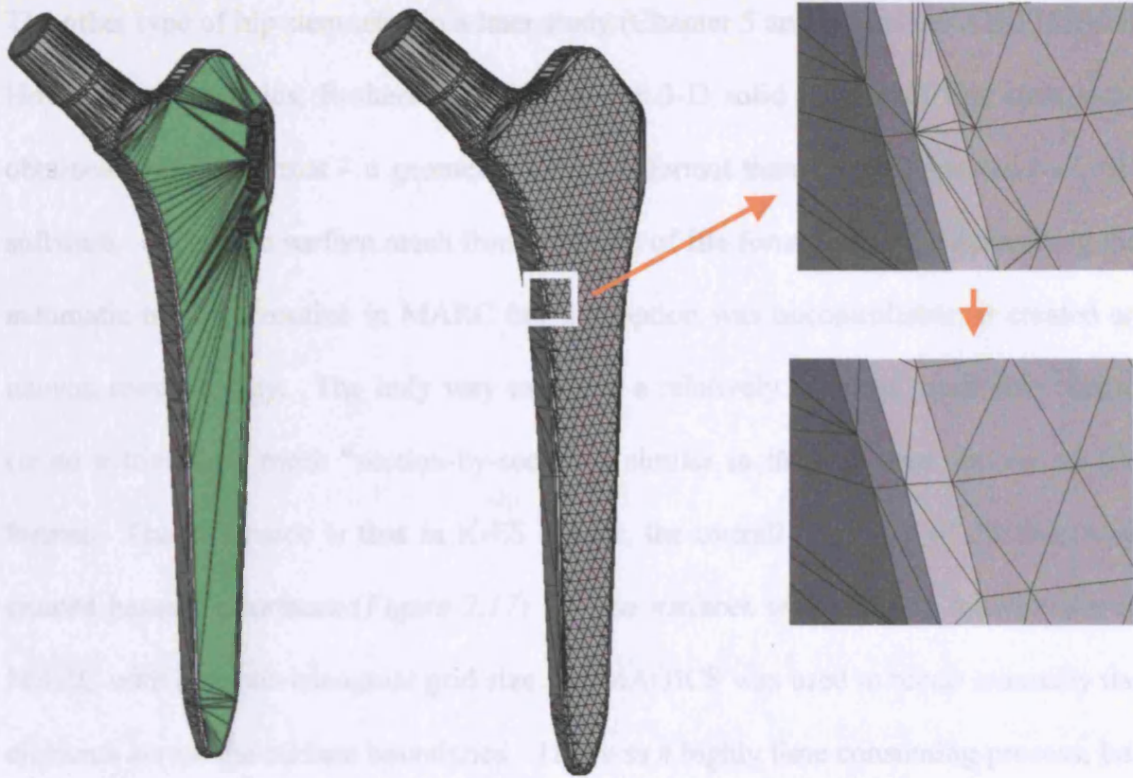


Figure 2.15: The original CAD drawing with highlighted section for remeshing (left), and after remeshing (centre). The inset pictures show the extra elements created (top) and after manual repair (bottom).

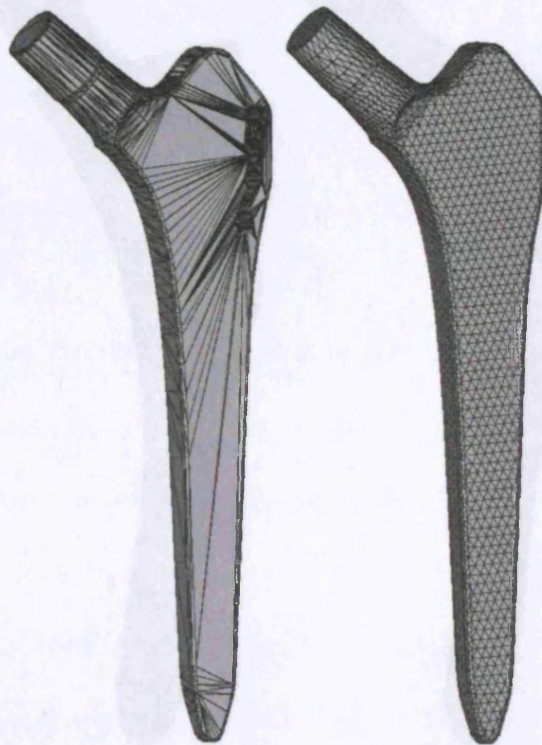


Figure 2.16: The original CAD drawing of an Alloclassic Hip Stem (left) received from the manufacturer and the completed triangular surface mesh.

The other type of hip stem used in a later study (Chapter 5 and 6) was the ABG (Stryker Howmedica Osteonics, Rutherford, NJ), and the 3-D solid models of this stem were obtained in IGES format – a geometric data file format that can be imported by CAD software. Creating a surface mesh from this type of file format could be done using the automatic meshing routine in MARC but this option was uncontrollable; it created an uneven mesh density. The only way to create a relatively constant mesh size was to create a triangular mesh “section-by-section”, similar to the one used for the stl file format. The difference is that in IGES format, the overall geometry of the stem was created based on surfaces (*Figure 2.17*). These surfaces were meshed individually in MARC with a certain triangular grid size and MAGICS was used to repair manually the elements across the surface boundaries. This was a highly time consuming process, but produced a properly-spaced and equally-sized surface mesh.



Figure 2.17: The ABG hip stem in the original IGES format surface meshed in MARC (left) and the completed model after repairing the surface boundaries in Magics (right).

All triangular surface meshes of the implants were then turned into solid tetrahedrals automatically in AMIRA software. The procedure described above was not the only method for creating 3D FE models and was very time-consuming, but based on the available software at hand, the method described above was the only way to create good FE solid meshes.

2.1.3 Aligning the stems in 3D

Once the construction of the 3D models of the femur and the implants was completed, the next step was to position the implant inside the bone to simulate hip replacement. The surface mesh, not the solid mesh, of both the implant and the bone were used for creating bone-implant contact. The simulation of stem insertion into the femoral canal was performed according to the recommended surgical procedures of the particular implant. There are similarities in the principles of positioning these hip stems. The distal half of the stem and the canal axis must be aligned, and the neck of the prosthesis must be aligned to the anteversion angle of the neck of the femur.

For the AML prosthesis, the stem and the canal axis were aligned, with the stem axis being defined as the centre line of the cross section in the distal portion of the stem, and the canal axis was defined as the centre line of the isthmus region. The isthmus region was assumed to be almost cylindrical in shape, and the maximum inscribed circle on the endosteal geometry was used as a reference for a suitable size of the stem. This is done because the AML is designed for canal filling, where canal fill is defined in cross sectional slices as a proportion between the stem area and the endosteal area of the isthmus. The stem was then rotated so that the neck of the stem was aligned to the

anteversion angle of the femoral neck. The osteotomy level was then set at 10mm above the upper end of the lesser trochanter and coinciding with the osteotomy line of the stem – for the AML it had to be in line with the placement of the collar on the medial calcar.

For the Alloclassic hip stem, similar procedures were used to align the stem and the neck. However, the Alloclassic is rectangularly tapered and was not designed to fill the canal in the medio-lateral (ML) direction. A suitable size was chosen based on the size that appropriately filled the canal in the ML direction with the lateral flare of the stem used as a reference to ensure proximal fill. Contact to the endosteal cortex in the distal half was also used to determine suitable size. As the stem was tapered, maximum cortical support like the one obtained for the AML was not possible.

Similar procedures were used for the ABG hip stem for alignment with the canal and the femoral neck. The ABG is an anatomical stem with distal endosteal bone over-reaming as a standard surgical protocol. The suitable size was therefore decided based on a proximal fill of the stem in the greater trochanter area.

Another type of cementless stem used in this study was the CLS hip stem. It is rectangularly tapered in all planes with a significant reduction in diameter in the distal half. Apart from using similar procedures to align the stem and the neck, the lateral part of the stem must also touch the endosteal lateral cortex. The CLS is also a proximal fixation design, and as such a suitable size was decided based on the stem that appropriately filled the proximal part of the femur.

The aligned and appropriately sized stems were presented to and judged by an experienced orthopaedic surgeon to confirm that the reconstruction followed the design concept and implantation of the individual hip stem. Pictures of the aligned and appropriately sized cementless hip stems used in this study are shown in *Figure 2.18* below.

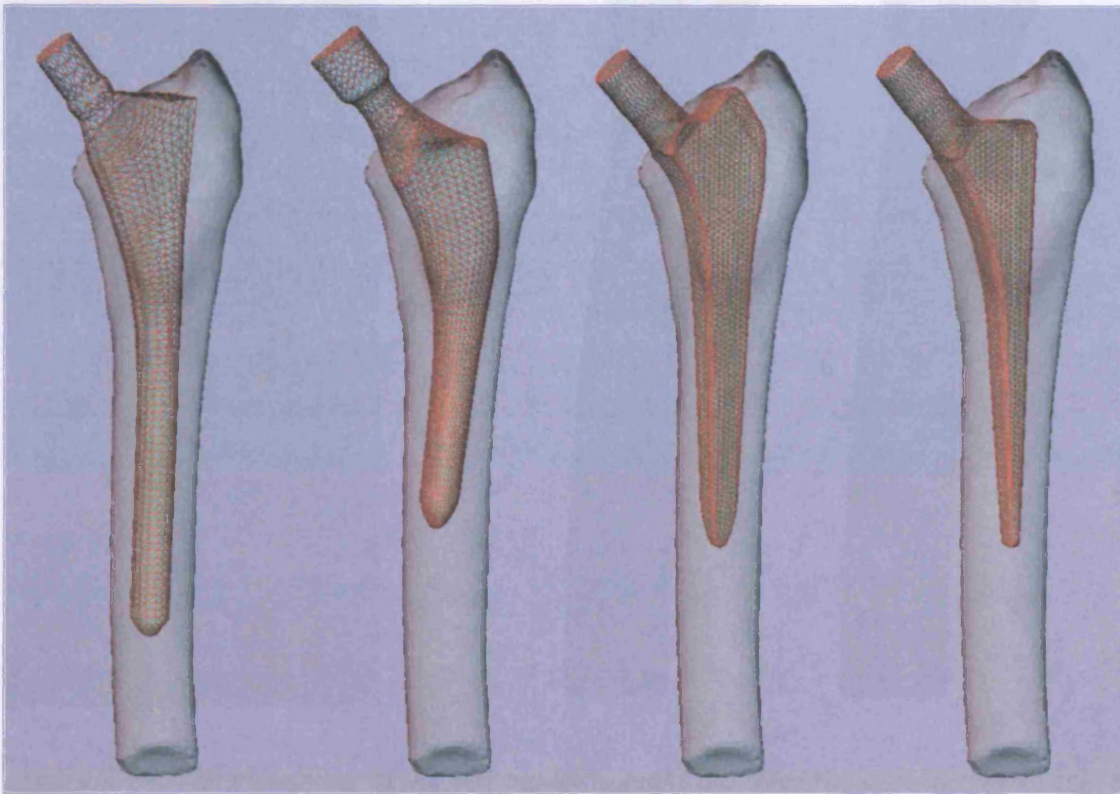


Figure 2.18: Hip stems used in the study – the AML, the ABG, the Alloclassic and the CLS – aligned inside the VHP femur model.

2.1.4 Creating bone-implant contact

Once the stem was appropriately in place, the osteotomy level was set to about 10mm above the upper end of the lesser trochanter. The cut was done using a 3D cube model

oriented to the same anteversion angle of the femur using MAGICS (Figure 2.19). The boolean operation, however, created extra unwanted elements at the boundaries between the bone and the cube model. These bad elements were repaired manually as described before.

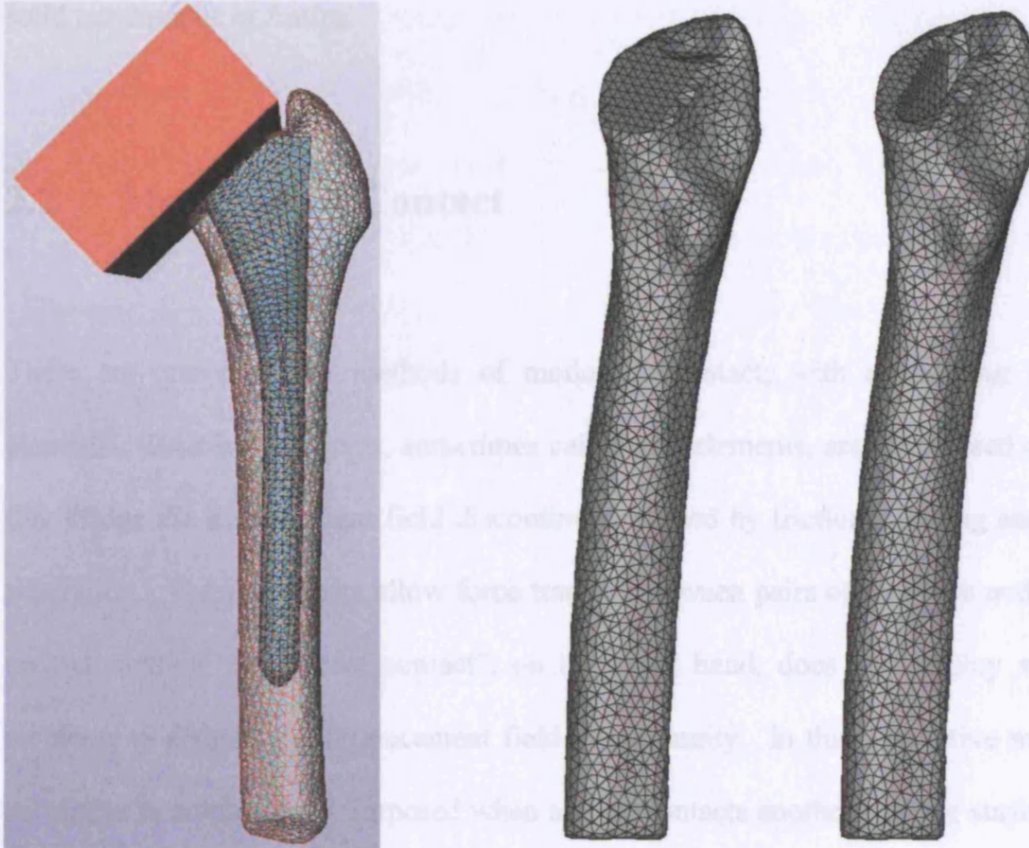


Figure 2.19: The placement of the box model to make a cut for the ante-version angle at the neck (left), the femur model with ante-version cut (middle) and the “after-reamed” femur model (right).

To create contact between the bone and the implant, an assumption was made that there would be a perfect fit between the outer surface of the implant and the inner bone. Creating a perfect match at the interface was done by using the surface mesh of the aligned stem as a “cut-out” for the resected hip model using the same boolean operation in MAGICS. The result of this operation was a resected hip model with a hole that had the exact shape of the outer surface of the implant (Figure 2.19). As with the cut of the

neck, there were bad elements created at the boundaries between the implant and the bone, and these elements were repaired manually. The bone surface mesh proximal to the lateral shoulder of the stem was also removed to simulate the actual results of reaming by the surgeon. The “operated” hip model was then automatically turned into solid tetrahedrals in Amira.

2.2 Modelling of Contact

There are currently two methods of modelling contact; with or without interface elements. Interface elements, sometimes called gap elements, are specialised elements that bridge the displacement field discontinuity caused by frictional sliding and tensile separation. These elements allow force transfer between pairs of interface nodes. The second method, the “direct contact”, on the other hand, does not employ structural elements to address the displacement field discontinuity. In this alternative method, a constraint is automatically imposed when a node contacts another node or surface. The constraint equation is such that the contacting node is forced to be on the contacted surface and allowed to slide, subject to the current friction conditions and the calculated tolerance zone. If a node slides from one segment to another during the iteration procedure, the retained nodes associated with the constraint are changed and a recalculation is automatically made. For tensile separation, a default value of 10% of the maximum reaction force is usually used as the threshold limit.

Both techniques of modelling contact have been used in FE micromotion studies with results comparable to their experiment equivalent. However, there have been reports of

potential limitation of using the interface elements. Zachariah and Sanders (2000) reported that in contact analyses between soft tissues and stiff surfaces, the direct contact method was sensitive to the coefficient of friction and better reflected the effects of local shape differences. In another study comparing gap elements and zero interface thickness elements, it was found that micromotion patterns obtained using both techniques were similar, but with higher magnitudes in the case of gap elements (Hefzy and Singh 1997). In a study comparing the use of gap elements and the direct contact procedure, Viceconti et al. (2000) showed that gap elements produced more errors than the alternative method. Furthermore, it has been reported (Tissakht et al. 1995) that when friction was simulated in a contact analysis, the predicted relative displacements were dependent on the value of the assigned axial stiffness of the gap.

Due to some potential limitations of gap elements described above, a direct frictional contact method will be used in this study to analyse micromotion. The procedure described previously for reconstruction of 3D models created a perfect fit between the stem and the bone, i.e. the interface nodes of the stem and their corresponding nodes at the bone shared the same co-ordinates. This is appropriate for the direct-contact method, and the FE software used in this study, MARC, claimed that the direct contact procedure can be very accurate if perfect contact is already known. A description of frictional contact and the study of the effects of friction coefficient on micromotion will be analysed in chapter 4.

2.3 Defining material properties

Once the solid tetrahedral mesh of the operated femur is completed, material properties will have to be assigned for the implant and the bone. This is rather straightforward for the implant as it is a homogeneous material. Bone, however, is not homogeneous. The mechanical properties of bones vary depending on location within the bone, age, level of activity and pathological conditions. Early FE models defined the properties by separating the stiff cortex from the cancellous structure and assigned a homogeneous property to each of them (Ando et al. 1999; Biegler et al. 1995; Kuiper & Huisker 1996; Viceconti et al. 2000; Viceconti et al. 2001). Cancellous stiffness values used ranged from 0.07 to 0.75GPa, whilst cortical stiffness was from 14 to 17GPa. Others used a more sophisticated approach by assigning material properties on an element-by-element basis (Keaveny & Bartel 1993). The properties were estimated from photographs or radiographs by estimating grey level values.

In this project, the second method of assigning material properties was chosen. An in-house algorithm written by a previous PhD student (Hopkins 2004) was used to assign material properties based on medical imaging data. In this algorithm, the grey-level of the CT images was related to the apparent density using a linear correlation (Cann & Genant 1980; McBroom et al. 1985). This allowed for the transformation of the spatial radiological description into the description of bone density. The modulus of elasticity of individual elements was then calculated from the assigned apparent densities using the cubic relationship proposed by Carter and Hayes (1977):

$$E = c \rho^3$$

where $c=3790 \text{ MPag}^{-3}\text{cm}^9$. This relationship was based on the assumption that cancellous and cortical bones are simply at different ends of a continuous spectrum. The material properties were assumed to be linear elastic and isotropic with Poisson's ratio set to 0.35.

2.4 Boundary conditions of the model

Once the model has been completed, loads simulating physiological activities need to be assigned before analyses could be performed. Loading configurations were different from author to author depending on several factors such as the activities analysed, the pathological condition of the patient and the weight of the patient. This study will use two loading configurations, Fisher's gait cycle and Duda's stair-climbing. A detailed description of the two physiological activities and their effect on micromotion will be discussed in chapter 4, together with a study on the effects of muscle forces.

Before these loads could be assigned, a coordinate system needs to be defined. It is important to use the same sign convention as the coordinate system used in other studies. Both Fisher and Duda used the coordinate system shown in *Figure 2.20*. The FE model of an implanted femur was then aligned to the coordinate system before loading vectors of the joint contact force and muscle forces were placed through point loads. In all cases, the model was constrained at the distal part of the bone in all directions to prevent rigid body motion.

Several parameters needed to be set such as the coefficient of friction and the interference fit. A value of 0.4 for the friction coefficient and a radial interference fit of 0.1mm was usually used in most of the analyses. The reasoning for these choices and the effects of these parameters on interface micromotion will be looked at in detail in chapter 4. Numerical parameters such as the incremental load step will be discussed later on in this chapter. An FE software program called MARC.Mentat (MSC Corporation, USA) was used for all micromotion analyses in this study.

Coordinate System at Left Femur

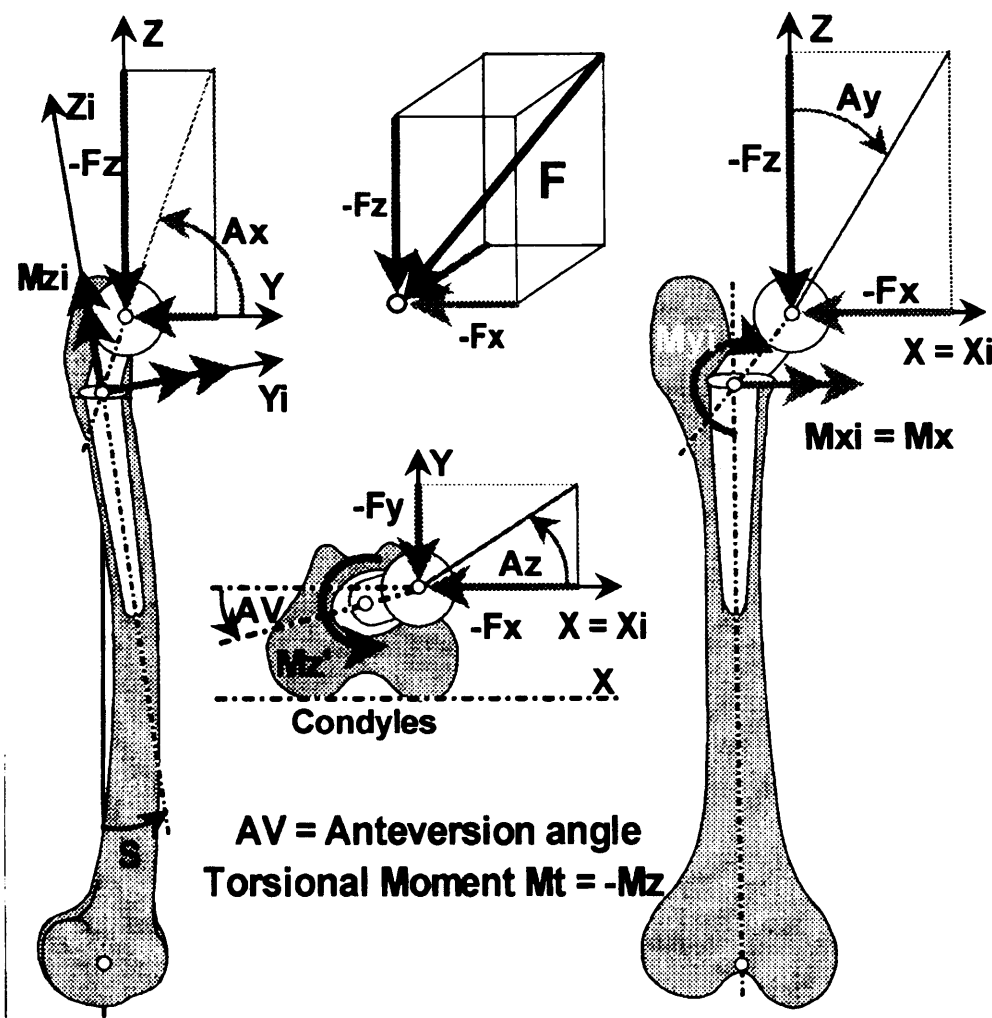


Figure 2.20: Coordinate system used in all analyses (taken from "Hip 98" CD).

2.5 Micromotion Subroutine

This section describes how micromotion and the stability of the implant were calculated and displayed. One major difference to note between FE predictions and experimental study on relative micromotion is exactly where the measurement of relative motion is made. Experimental micromotion usually involves displacement transducers mounted on the outer cortex of the bone, i.e. they are separated from the implant by the thickness of the bone. The deflection between the implant and the bone during loading must involve movement at the interface and could also involve deformation of the bone between the surface of the implant and the outer surface of the bone where the transducer is mounted (Whiteside et al. 1993). An FE micromotion study, on the other hand, calculates how much sliding occurs at the interface by subtracting the nodal displacements at the outer surface of the stem from the nodal displacements of the bone surface in contact with the stem. The difference in terms of micromotion results between the experimental and FE methods is analysed later in the chapter (see section 2.7).

A computer code (see Appendix) was written in Compaq Visual Fortran (Compaq Computer Corporation) to calculate and display micromotion from MARC.Mentat's post-processing file. Another subroutine was written to automatically store the interfacial nodes – the nodes on the implant surface and their corresponding nodes on the bone – which were involved in the micromotion calculations. These “common” nodes shared the same co-ordinates and were used in the main subroutine by subtracting the nodal displacement of the stem from the corresponding nodal displacement of the

bone. The results obtained from the calculation were then displayed as contour plots on the outer surface of the prosthesis.

As mentioned at the start of the chapter, two sets of results are presented in this study. The first one is simply the contour plots of micromotion obtained from the computer code. The results are usually compared with each other, and those with lesser micromotion are assumed to be better than those with larger micromotion. This technique has been used previously (Keaveny & Bartel 1993; Viceconti et al. 2001), although most published FE work on micromotion has simply presented average values of micromotion in various sections of the stem (e.g. proximal, middle and distal) (Ando et al. 1999; Biegler et al. 1995; Kuiper & Huiskes 1996; Rubin et al. 1993).

The above micromotion results are suitable for the comparison of micromotion between implants. However, conclusive evidence could not be made from these results about the stability of different hip stems. An orthopaedic surgeon, for example, would like to know if stability is compromised for a particular hip stem design subjected to a particular physiological loading. This question could not be answered simply by presenting the comparative micromotion results. A novel technique is therefore proposed to predict hip stem instability, where bone loss is simulated at the interface where micromotion exceeds the threshold limit for bone ingrowth.

As mentioned in the previous chapter, the threshold value of relative micromotion, above which fibrous tissue layer forms, varies between 30-150 μm . In this study a threshold value of 50 μm was chosen. The result from the first implant loading iteration was modified by creating a gap at the interface where micromotion was found to be

more than $50\mu\text{m}$ (Figure 2.21). The $500\mu\text{m}$ thickness gap was created by translating the nodes on the bone side of the interface perpendicularly outwards from the stem's surface. A second iteration was then performed with the newly-created interfacial gaps. From the new set of results, the model was modified again to include new gaps at the interface where micromotion exceeded the threshold limit. Third iterations were performed and the procedure was repeated until either a stable-state interface micromotion was achieved or the implant failed. Implant failure occurred if interfacial shear strength was exceeded or the surface of the implant was encapsulated with the threshold micromotion limit representing fibrous tissue. Interfacial shear strength varied from 6-55MPa based on implant push-out tests (Dhert & Jansen 2000). This variation depended on many factors such as implant material, surface texture, bone type and follow-up period. In this study a value of 15MPa was assumed as the interfacial shear strength based on the published data for a titanium alloy implant with cortical bone type.

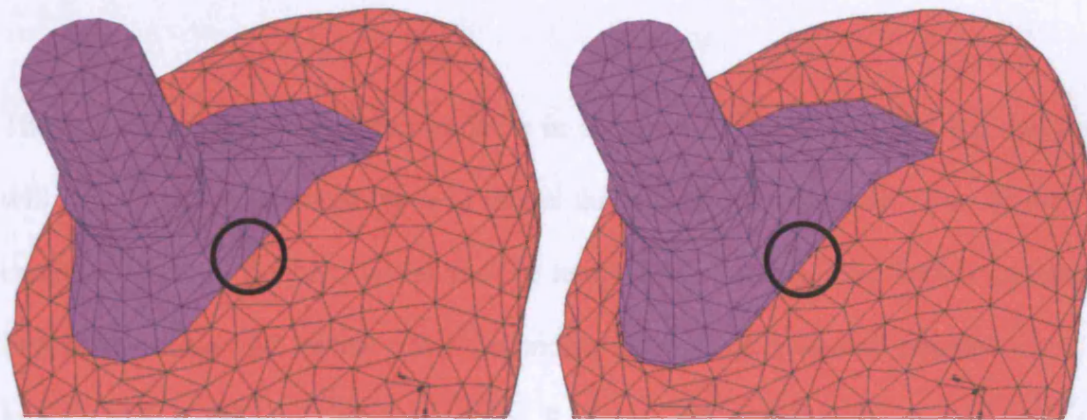


Figure 2.21: Pictures showing no interface gaps (left) and with interfacial gaps with thickness of $500\mu\text{m}$ (right).

In this study either the 'as implanted' or both 'as implanted' and 'post interface remodelling' results will be presented depending on the situation. When looking at the

effects of parameters such as the effect of muscle forces on micromotion (such as the one in Chapter 4), then only comparative micromotion results are presented. In chapter 5, however, when looking at the effect of hip stem designs on micromotion, both sets of results will be presented.

2.6 Convergence study

The results of any FE analyses must be independent of all purely numerical parameters. It is therefore crucial to perform convergence studies to ensure that the results obtained are not dependent on those parameters. In this section, two parameters will be checked for convergence; the mesh and the load increment.

2.6.1 Mesh convergence

There are many element types available in finite element analysis, but the discussion will concentrate on element types to model three-dimensional solids. Two of the most common ones are the hexahedral and the tetrahedral, which can be further categorised into lower order and higher order depending on the interpolation function used. A lower order hexahedral is made up of 8 nodes and 8 integration points whilst its tetrahedral companion has 4 nodes and 1 integration point. Both elements have three global displacement degrees of freedom and use linear interpolation functions, where the strains are constant throughout the element. A higher order hexahedral has 20 nodes, 27 integration points and a higher order tetrahedral has 10 nodes and 4

integration points. Both of them can use a quadratic interpolation function which allows the strains to vary within the element.

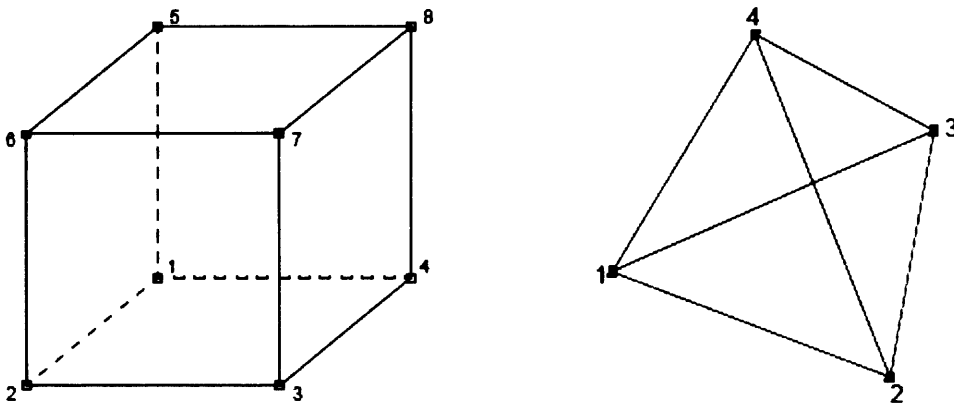


Figure 2.22: The eight-noded hexahedral (left) and the four-noded tetrahedral (right). Higher order hexahedrals and tetrahedrals have an extra node (midside node) on each edge.

Higher order elements are usually not recommended in contact analyses because the shape functions have interpolation functions which lead to the equivalent nodal forces oscillating between the corner and midside nodes. As this has a detrimental effect on both contact detection and determining contact separation, lower order elements are usually recommended in contact analyses. The choice of the type of element (hexahedral or tetrahedral) should not, in principle, change the results because both of them have to be in models with converged solutions. However, the total number of elements (or mesh density) of the model may be different between the two different element types. As the tetrahedrals have fewer nodes and therefore fewer degrees of freedom, and because of the difference in shape functions, more of this type of element is needed than the hexahedrals to produce similar converged results.

In this study, tetrahedrals are used mainly due to the availability of computer software, AMIRA and MAGICS, which can only work with triangular surfaces. Therefore a convergence study of this type of element will be carried out. To perform the convergence analyses, an AML hip stem model obtained from the manufacturer with a rectangular surface mesh was refined by subdividing the rectangles. The newly subdivided surface mesh was further subdivided until five models with increasing mesh surface density were obtained. These five models of rectangular surface mesh were then converted into triangular surface meshes before converting them into solid tetrahedrals using the automatic solid meshing function in MARC.Mentat. The results are shown in *Figure 2.23*. The bone models also followed the same procedure for refinement. *Table 2.1* shows the total number of elements and nodes for all five models. Micromotion analyses were performed on all of the models with all other parameters being the same.

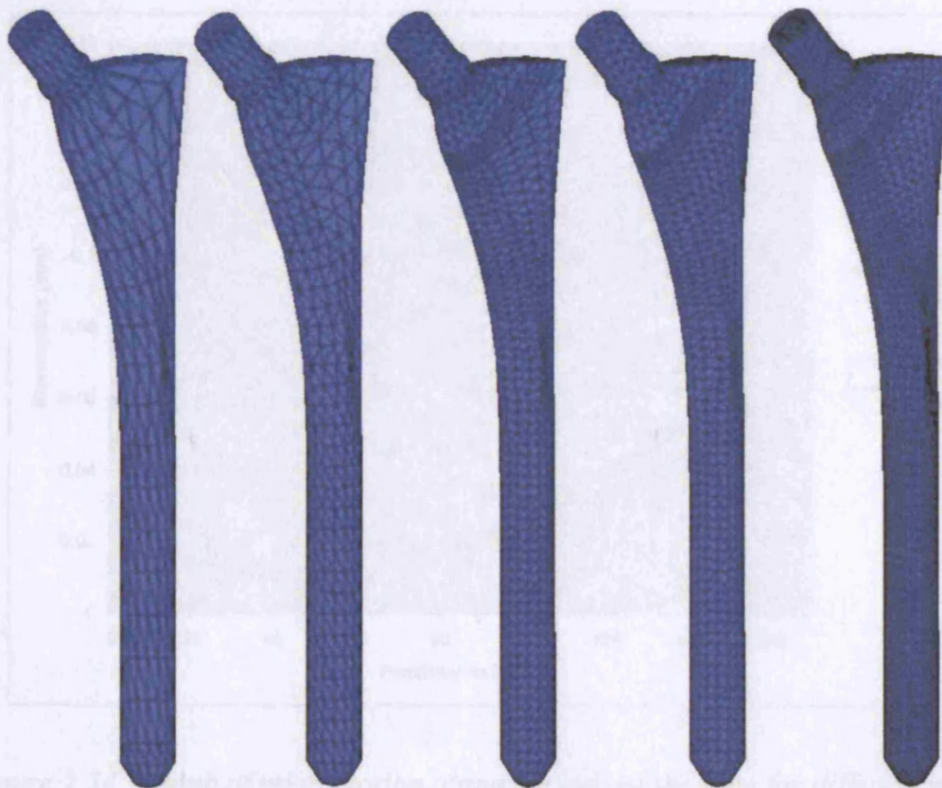


Figure 2.23: The tetrahedral elements of the implant with increasing mesh densities.

	Nodes	Elements
Tet -A	4,049	14,688
Tet -B	6,663	28,732
Tet -C	9,225	40,408
Tet-D	12,078	56,526
Tet-E	16,866	77,738

Table 2.1: Total number of nodes and elements of tetrahedral mesh with increasing density.

From the contour plot of micromotion shown in *Figure 2.25*, sixteen nodes along the length of the stem from the coarsest mesh (Tet-A) were chosen for comparison between all five models. These nodes are available in all models at exactly the same location, thus allowing proper and exact comparison. The graph of micromotion of these sixteen nodes is shown in *Figure 2.24*.

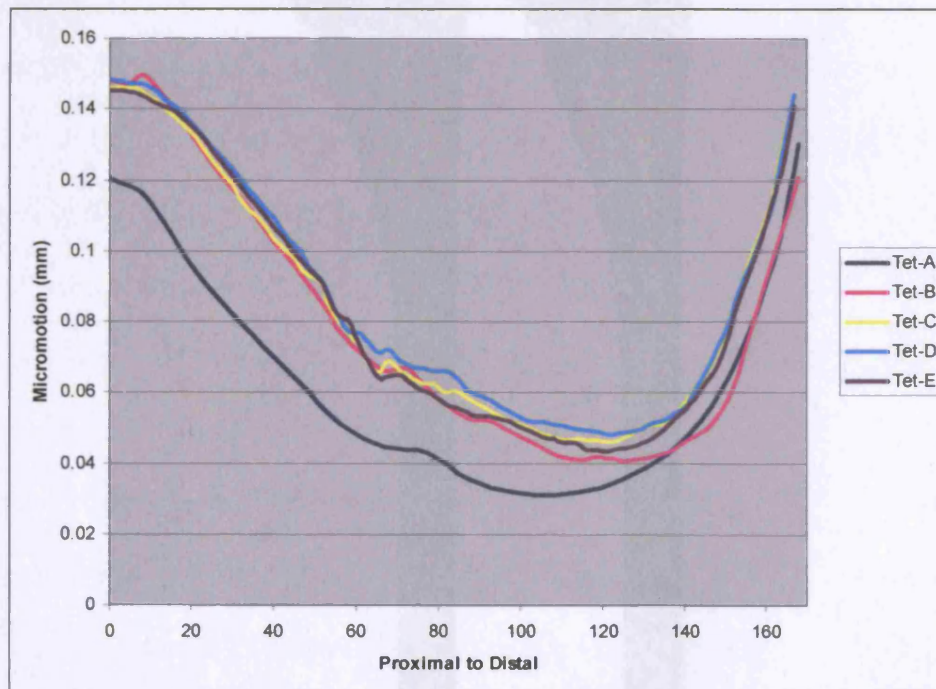


Figure 2.24: Graph of micromotion along the axis of the stem for different mesh densities.

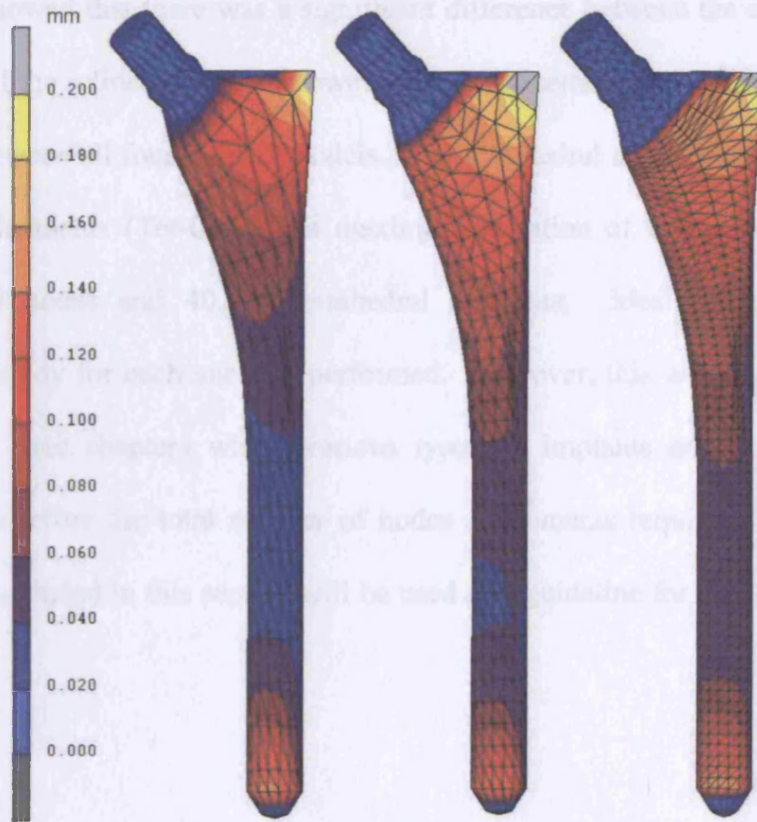


Figure 2.25: Micromotion results at increasing tetrahedral mesh densities (left to right).

The results showed that there was a significant difference between the coarsest (Tet-A) and the rest of the refined models. However, once refinement was made there was little difference between all four refined models. The tetrahedral model seemed to converge after two refinements (Tet-C) with a maximum variation of 8%. This was roughly about 10,000 nodes and 40,500 tetrahedral elements. Ideally, one would do a convergence study for each analysis performed. However, this would not be practical especially in later chapters where various types of implants and bone types were analysed. Therefore the total number of nodes & elements required for convergence which was concluded in this section will be used as a guideline for convergence in later studies.

2.6.2 Load Increment

The second FE parameter that could affect the result is the load increment size. The default setting for load increment in MARC.Mentat is 10, which means that the model is loaded with an increment of 200N on each load step if the total load is 2kN. Three models were prepared from the previous mesh convergence study with different load increment sizes of 1, 5 and 10. Micromotion analyses were then performed with all models having the same loading conditions as well as material properties and friction coefficient. The result in *Figure 2.27* below showed that similar distribution was found when 5 or 10 increments were used. The difference between these two increments was 2% and therefore 5 load increments are used throughout the study.

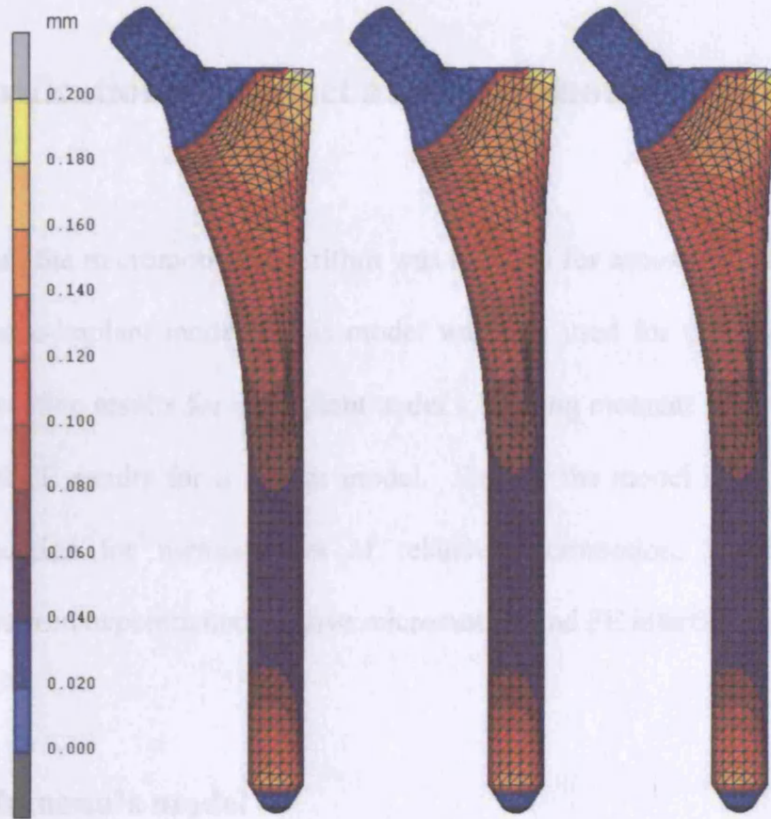


Figure 2.26: Contour plot of micromotion for load step of 1, 5 and 10 increments.

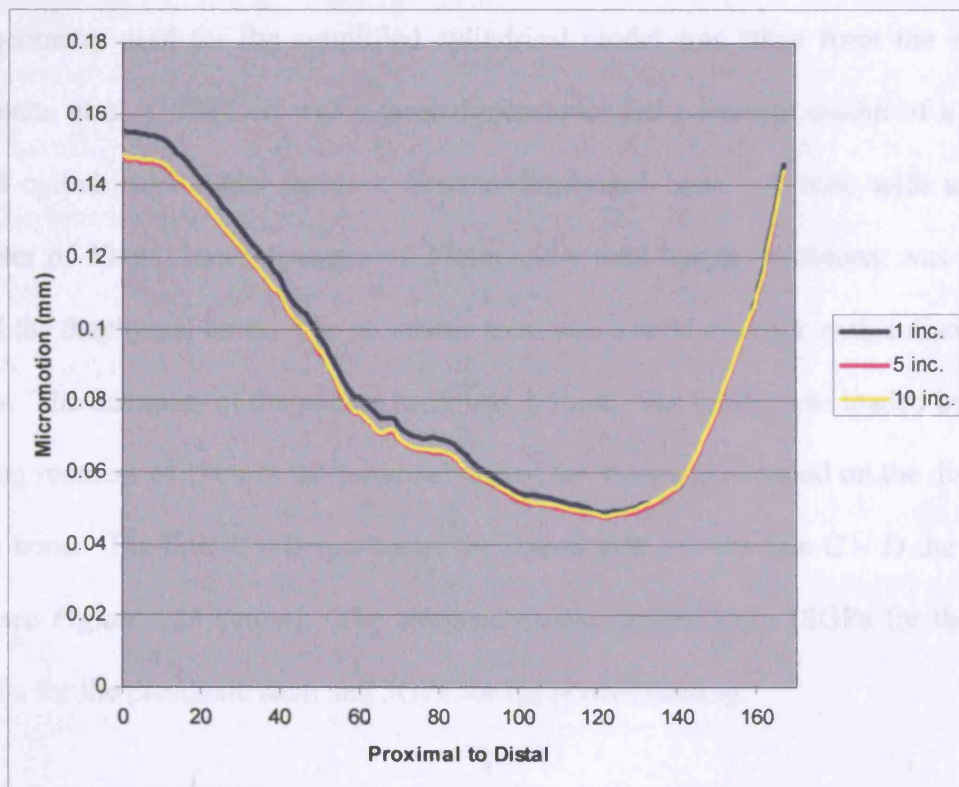


Figure 2.27: The micromotion distribution with 1 increment, 5 and 10 increments.

2.7 Verification of contact and micromotion algorithm

In this section, the micromotion algorithm was checked for accuracy using a simplified cylindrical bone-implant model. This model was also used for verification purposes, where micromotion results for an implant under a bending moment were compared with the published FE results for a similar model. Finally, the model is used to study the effect of location for measurement of relative micromotion, i.e. comparing the difference between experimental relative micromotion and FE interface micromotion.

2.7.1 Rohlmann's model

The geometry used for the simplified cylindrical model was taken from the work of Rohlmann et al. (1988). It was a three-dimensional finite element model of a porous coated cylindrical implant inside a femoral diaphyseal bone. A tube with an outer diameter of 30mm, inner diameter of 20mm and a total length of 184mm was used to model the diaphyseal bone. The prosthetic stem was a solid cylinder with a diameter of 17mm. The thickness of the porous layer was 1.5mm. The model was loaded by a pure bending moment of 1Nm at the proximal end of the stem and clamped on the distal end of the bone. The line A – B represents the lateral side and the line C – D the medial side (see *Figure 2.28* below). The assigned elastic moduli were 18GPa for the bone, 200GPa for the prosthetic stem and 5GPa for the porous coating.

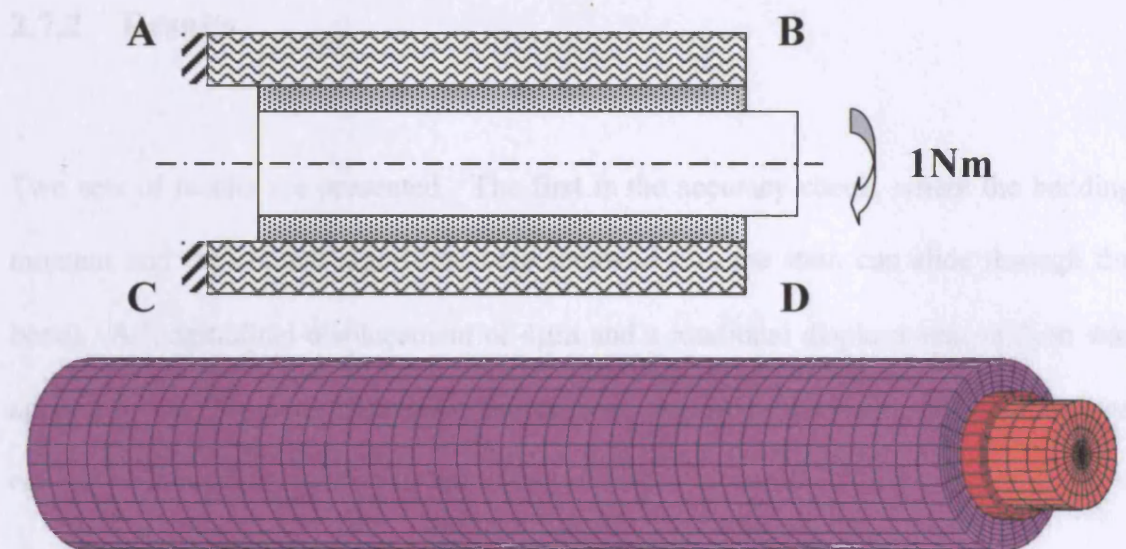


Figure 2.28: A diagrammatic sketch of a longitudinal section of Rohlmann's model and the finite element model.

Rohlmann's FE model consisted of 1,110 eight-noded hexahedral elements and 1,582 nodes. The FE calculations were performed using an FE program called ADINA and a specially developed code to represent the situation directly after implantation, when no tensile stress can be transferred across the bone-implant interface. The code had a non-linear interface condition where the connection between the elements in the interface was eliminated when tensile stress perpendicular to the interface occurred. A new FE calculation was then performed, thus allowing changes in the stress distributions. This process was repeated several times until only small changes in the stresses were found.

Ref

The FE model used in this comparative study consisted of 14,940 eight-noded hexahedral elements and 16,638 nodes. All other parameters (geometry, material properties, boundary conditions) were the same as Rohlmann's. The FE software used was MARC.Mentat, with its default contact algorithm as described in section 2.2, and a friction coefficient of 0.4.

2.7.2 Results

Two sets of results are presented. The first is the accuracy check, where the bending moment and the contact algorithm were removed (i.e. the stem can slide through the bone). A longitudinal displacement of $4\mu\text{m}$ and a rotational displacement of $3\mu\text{m}$ was applied to the prosthetic cylinder. The analysis was performed with the micromotion code and the result is shown in *Figure 2.29* below.



Figure 2.29: Contour plot showing relative micromotion of $5\mu\text{m}$ when the prosthetic stem (with the coating) was displaced longitudinally by $4\mu\text{m}$ and rotationally by $3\mu\text{m}$.

The result above shows that the micromotion code accurately calculated and displayed the interface relative micromotion of $5\mu\text{m}$.

Figure 2.30 below shows contour plots of micromotion, using the micromotion code, when the model was loaded with a pure bending moment of 1Nm . Rohlmann's published result is displayed on the right. *Figure 2.31* shows the graph of relative motion along the cylindrical stem, where the distribution of micromotion along the stem was similar to Rohlmann's. Peaks were found at both ends at the lateral and medial side, with maximum micromotion at the distal-medial point C. The rest of the surface had relatively small micromotion. The maximum micromotion obtained from the FE model was $0.517\mu\text{m}$ compared to the analysis by Rohlmann which was $0.389\mu\text{m}$.

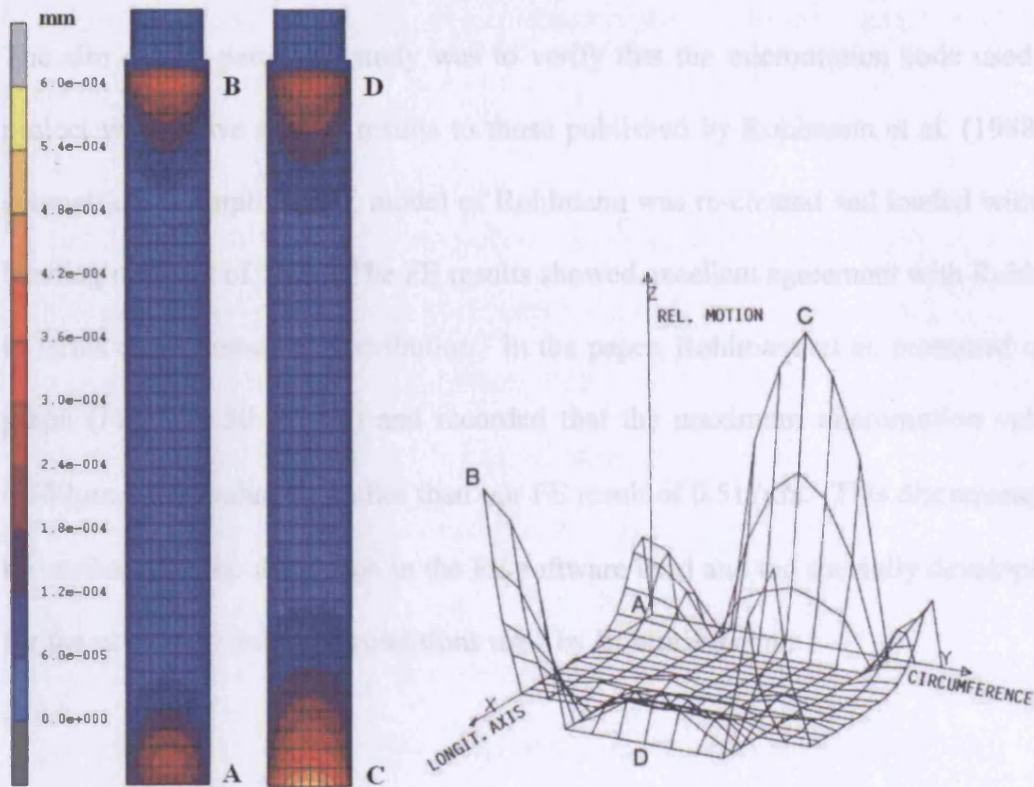


Figure 2.30: Results of the Rohlmann's model using the micromotion algorithm (left) and the published result by Rohlmann et. al. (right).

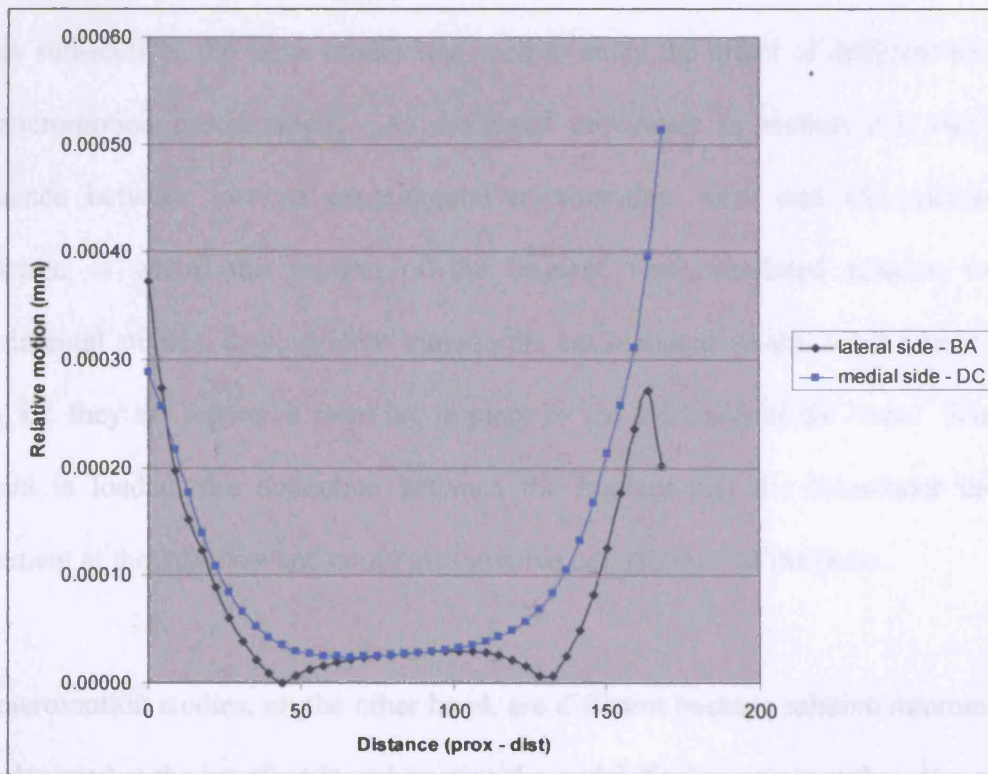


Figure 2.31: Graph of relative motion along the lateral and medial side of the cylindrical prosthesis.

The aim of this particular study was to verify that the micromotion code used in this project would give similar results to those published by Rohlmann et al. (1988). The geometrically simplified FE model of Rohlmann was re-created and loaded with a pure bending moment of 1Nm. The FE results showed excellent agreement with Rohlmann's in terms of micromotion distribution. In the paper, Rohlmann et al. presented only the graph (*Figure 2.30 - right*) and recorded that the maximum micromotion value was 0.389 μ m. This value is smaller than our FE result of 0.517 μ m. This discrepancy could be attributed to the difference in the FE software used and the specially developed code for the non-linear interface conditions used by Rohlmann et al.

2.7.3 The effect of location for micromotion measurement

In this sub-section, the same model was used to study the effect of different locations for micromotion measurement. As discussed previously in section 2.5, one major difference between in-vitro experimental micromotion work and FE micromotion prediction is where the motion of the implant was calculated relative to. In experimental studies, displacement transducers are mounted on the outer cortex of the bone, i.e. they are separated from the implant by the thickness of the bone. When the implant is loaded, the deflection between the implant and the transducer involves movement at the interface and could also involve deformation of the bone.

FE micromotion studies, on the other hand, are different because relative micromotions are calculated at the interface by subtracting the nodal displacements at the outer surface of the stem from the nodal displacements of the bone surface in contact with the stem.

The results could be different from experimental studies if the deformation of the bone is not taken into account.

To the author's knowledge there are no reports of how micromotion of the implant relative to the bone would seem to change if the measurement was made relative to the periosteal surface instead of the interface. The aim of this study is therefore to compare, using a simplified cylindrical FE model, micromotion results at the interface with micromotion of the implant calculated relative to the periosteal surface.

As explained in section 2.5, a short computer code was written to store interfacial nodes – the nodes on the implant surface and their corresponding nodes on the bone – which share the same co-ordinates. This computer code was adjusted (see Appendix) so that the nodes on the implant's surface were now paired with the nodes on the outer cortex of the bone directly normal to them. The micromotion code would therefore calculate the difference in the nodal displacements of the implant's surface relative to the outer surface of the cortex.

The bending moment of 1Nm used previously was increased to 20Nm to roughly simulate the actual bending moment during physiological loading, with the distal part of the stem fixed in all directions to prevent rigid body motion. The results are shown in *Figure 2.32* and *Figure 2.33*.

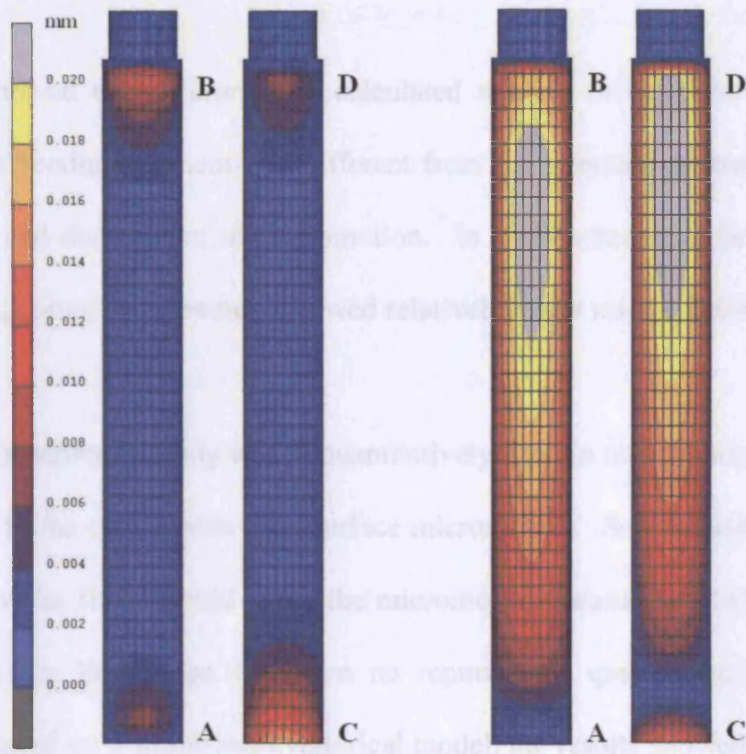


Figure 2.32: Contour plot of micromotion for the bending moment load of 20Nm. (Left – interface micromotion, right – micromotion relative to the periosteal surface).

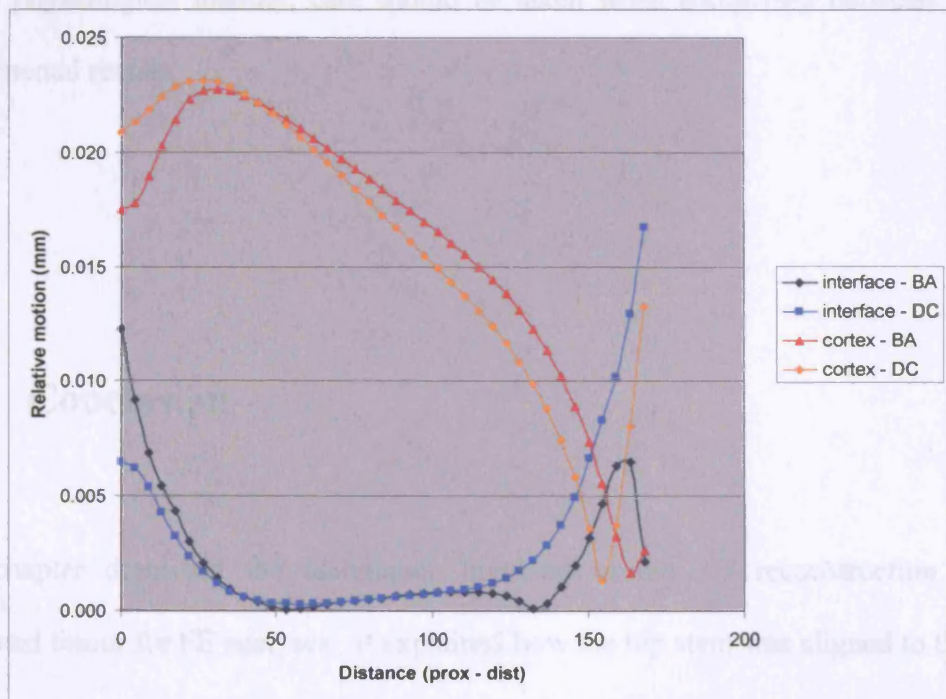


Figure 2.33: Graph of micromotion along the stem on the lateral and medial side under bending moment for the interface micromotion and micromotion relative to the periosteal surface.

The results showed that micromotion calculated relative to the outer surface of the cortex under a bending moment was different from the interface micromotion in terms of magnitude and distribution of micromotion. In areas where interface micromotion was minimum, cortex measurement showed relatively larger micromotion.

The aim of this particular study was to quantitatively analyse micromotion measurement made relative to the cortex with the interface micromotion. Several authors mentioned that bending of the femur could affect the micromotion measurement (Whiteside et al. 1993), but to our knowledge there are no reports that quantitatively analysed the hypothesis. Based on a simplified cylindrical model, the results showed that there were large differences between the interface and cortex measurement when bending deformation of the bone occurred. Since the femur is primarily loaded in bending during physiological loading, care should be taken when comparing between FE and experimental results.

2.8 Conclusion

This chapter described the techniques involved in the 3D reconstruction of the implanted femur for FE analyses. It explained how the hip stem was aligned to the bone and how contact was modelled. It also described how the material properties and loading configurations were assigned. The chapter then continued with a description of

the micromotion code and a description of how the results will be presented for the rest of the study. A novel technique of predicting hip stem instability was also proposed, where bone loss is simulated at the interface where micromotion exceeds the threshold limit for bone growth. FE mesh convergence and load increment size analyses were also presented. The micromotion code was checked for accuracy and verified using Rohlmann's simplified cylindrical model. The model was also used to compare the differences between micromotion measured at the interface and the one measured relative to the outer surface of the cortex. The results showed that there were large differences between the interface and cortex measurement when bending deformation of the bone occurred.

Chapter 3 Experimental validation

This chapter describes an experiment which was carried out in order to validate the computer predictions. Four cadaveric femora were used in the experiment and a computer model created from one of the bones was used for verification of interface micromotion. The chapter starts with a literature review of experimental work and FE analyses on micromotion, looking at various types of micromotion that can be measured in an experimental setup and the differences and similarities between experiment and computer predictions. The materials and methods used will be described for both the experiment and the FEA before comparing and discussing the results obtained from both studies.

3.1 Experimental work on micromotion

The measurement of implant stability through in vitro experiment has been done by numerous investigators (see *Table 3.2*, *Table 3.3*, *Table 3.4*). These laboratory studies can be categorised into two; the ones that were experimenting with the initial postoperative stability and the ones examining long-term assessment. For the former, the experiment was done, in general, by inserting an implant into a cadaveric human femur (Schneider et al. 1989a; Schneider et al. 1989b), or a composite femur (Otani et al. 1993) using a press-fit technique. For the latter, fresh frozen femora containing an implant, retrieved at autopsy from patients, are used (Engh et al. 1992; Whiteside et al. 1993). The femur is then potted at the distal end using cement and fixed rigidly to the load frame of a universal testing machine. In some studies, muscle groups are simulated by means of woven nylon strips. These strips are attached at the appropriate location on the outer cortex at one end and to the testing machine at the other end. The magnitudes of these muscle forces are varied by tightening or loosening the strips. The muscle group that is usually included is the abductors, but some also included the extensors (Engh et al. 1992) and the adductors (Doehring, Rubash & Dore 1999). Joint load is then applied to the head of the implant, either as axial compression (Whiteside & Easley 1989), or with the help of a custom designed mechanism, to apply a pure torque (Otani et al. 1993; Schneider et al. 1989a; Schneider et al. 1989b; Sugiyama et al. 1994; Whiteside et al. 1993). The magnitude of applied loads were usually taken to simulate the physiological loading of level walking, stair-climbing, single-leg stance and rising from a chair. Depending on the type of physiological loading, the long axis of the femur is rotated at certain angle to the vertical. For single leg stance, the femur is

positioned at about 21° to the vertical while in stair-climbing, the femur is placed at a flexion angle of 30°.

The relative motion of the implant is measured by mounting dial gauges (Whiteside and Easley 1989) or other displacement transducers such as linear variable differential transducers (LVDT) (Doehring et al. 1999; Whiteside et al. 1993) or differential variable reluctance transducers (DVRT) (Bachus, Bloebaum & Jones 1999) on the outer cortex of the bone. Holes between 3.5-5mm are drilled through the cortical bone at the required areas for measurement, where the plunger of the measuring equipments is passed through and attached to the stem of the implant. The type of motion that is measured in this case is the toggle motion in the anterior-posterior or medial-lateral direction. Other types of motion could be measured depending on the arrangement of the transducers. Measurement of axial motion is possible by inserting a metal pin into the hole and attaching the plunger of the transducer to the other end of the metal pin, with the transducer itself aligned along the axis of the femur. Rotational micromotion could also be measured in this way by positioning the displacement transducer perpendicular and tangential to the axis of the stem.

All the above techniques measured relative motion between the stem and the outer cortex of the bone. This is a reasonable estimate of micromotion at the interface assuming that the deflection in the thickness of the bone is negligible. It may not necessarily be the case, and if deflection did take place in the bone during loading, the actual interface micromotion would be different. The interface is also destroyed right at the point of measurement during instrumentation and damages the bone surrounding the area which in turn may affect the realism of measurement. Another limitation of

measuring micromotion in experimental laboratories is that the measured micromotion is restricted to certain areas, usually the proximal, middle and distal part of the stem. Though this could be enough to get a general view of how stable the implant is, it lacks information on the distribution of relative motion about an implant's entire interface which could be useful, for example, when looking at the effectiveness of various implant features.

The published experimental results are shown in the tables below. They are categorised into the types of micromotion measured. *Table 3.2* shows the results of the axial micromotion, *Table 3.3* the rotational micromotion and *Table 3.4* the transverse micromotion.

Author	Femoral	Boundary condition	Implant type	Load simulation	Measured location	Micromotion (μm)
Bachus et al. (1999)	Cadaver	Joint load	"Bridge Hip" (Prox. Cemented)	Single-leg	Ave. of 5 points	42 \pm 6
				Stair-climb		42 \pm 9
			"Nexus II" (Full cement)	Single-leg		41 \pm 5
				Stair-climb		45 \pm 8
Baleani et al. (2000)	Composite	Torsion	"Ancafit" Cementless	Torsional load	Greater troch.	9.7 \pm 8.9
			"CLU Hybrid" Lateral cemented			1.3 \pm 0.4
			"Ancafit" cemented			1.0 \pm 0.3
Berzins et al. (1993)	Cadaver	Joint load	"HG Multilock" (straight stem, cementless, proximal coat)	Walking	Proximal	3.2 \pm 2.3
					Distal	23 \pm 7
				Stair-climb	Proximal	8.7 \pm 2.3
					Distal	38 \pm 15
				Rise from chair	Proximal	18 \pm 7
					Distal	63 \pm 9
			"Anatomic" (curved stem, cementless, proximal coat)	Walking	Proximal	2 \pm 0.5
					Distal	23 \pm 7
				Stair-climb	Proximal	4.2 \pm 1.3
					Distal	38 \pm 15
				Rise from chair	Proximal	8.5 \pm 2.3
					Distal	63 \pm 9
Burke et al. (1991)	Cadaver	Joint load & Abd.	"HGP" Cementless	1-leg stance	Proximal	10.4 \pm 9.5
		Joint load & Ext.		Stair climb		10.1 \pm 6.2
		Joint load & Abd.	"THR pre-coat" Cemented	1-leg stance		11.2 \pm 14.8
		Joint load & Ext.		Stair climb		5.7 \pm 6.0
Doehring et al. (1999)	Cadaver	Joint load, Abductor, Adductor, Extensor.	"HG Multilock" (straight stem, cementless, proximal coat).	Stair climb	Medial	26 \pm 5
					Lateral	2 \pm 1
					Anterior	10 \pm 2
					Posterior	20 \pm 2
Engh et al. (1992)	Femora with implant	Joint load, Abductor	"AML" cementless 1/3 proximal coated	1-leg stance	Prox - Ant	1-4
					Prox - Pos	1-6
					Mid - Ant	1-5
					Mid - Pos	3-20
					Tip - Ant	10-94
					Tip - Pos	10-55
			"AML" cementless 4/5 proximal coated	Stair climb	Prox - Ant	1-12
					Mid - Ant	1-3
					Tip - Ant	5-74
				1-leg stance	Prox - Ant	10-21
					Prox - Pos	1-18
					Mid - Ant	2-20
Mid - Pos	1-7					
Tip - Ant	2-25					
Tip - Pos	12-50					

				Stair climb	Prox - Ant	13-30
					Mid - Ant	5-13
					Tip - Ant	53-80
			"AML" cementless fully coated	1-leg stance	Prox - Ant	2
					Prox - Pos	5
					Mid - Ant	10
					Mid - Pos	4
					Tip - Ant	4
					Tip - Pos	2
				Stair climb	Prox - Ant	2
					Mid - Ant	12
					Tip - Ant	8
Otani et al. (1993)	Composite	Joint load	Carbon composite	Axial load 2500N	Stem tip	45 ± 15
			Titanium alloy			40 ± 5
			Stainless steel			25 ± 6
Schneider et al. (1989)	Cadaver	Joint load	"CLS" cementless	Axial load & Torsional load	Prox - Med	145 ± 50
					Prox - Ventral	152 ± 35
					Dist - Lat	80 ± 22
			"Muller 85" cementless		Dist - Ventral	82 ± 10
					Prox - Med	50 ± 30
					Prox - Ventral	25 ± 5
			"Zweymuller" cementless		Dist - Lat	15 ± 5
					Dist - Ventral	45 ± 30
					Prox - Med	25 ± 5
			"PCA" cementless prox. coated		Prox - Ventral	55 ± 25
					Dist - Lat	10 ± 1
					Dist - Ventral	10 ± 1
					Prox - Med	12 ± 1
					Prox - Ventral	13 ± 2
					Dist - Lat	13 ± 1
					Dist - Ventral	15 ± 4

Table 3.2: Axial micromotion from published in-vitro experiments.

Author	Femoral	Boundary condition	Implant type	Load simulation	Measured location	Micromotion (μm)	
Bachus et al. (1999)	Cadaver	Joint load	"Bridge Hip" (Prox. Cemented)	Single-leg	Ave. of 5 points	31 \pm 15	
				Stair-climb		87 \pm 53	
			"Nexus II" (Full cement)	Single-leg		59 \pm 22	
				Stair-climb		92 \pm 32	
Baleani et al. (2000)	Composite	Torsion	"Ancafit" Cementless	Torsional load	Medial – Prox	56.2 \pm 26.1	
					Medial – Mid	49.5 \pm 25.6	
					Medial – Tip	39.5 \pm 27.7	
					Ant – Prox	10.3 \pm 9.6	
			"CLU Hybrid" Lateral cemented		Medial – Prox	11.7 \pm 7.9	
					Medial – Mid	6.7 \pm 4.0	
					Medial – Tip	0.8 \pm 0.1	
					Ant – Prox	0.7 \pm 0.1	
			"Ancafit" cemented		Medial – Prox	0.9 \pm 0.2	
					Medial – Mid	0.6 \pm 0.1	
					Medial – Tip	0.6 \pm 0.1	
					Ant – Prox	0.7 \pm 0.1	
Burke et al. (1991)	Cadaver	Joint load & Abd.	"HGP" Cementless	1-leg stance	Proximal	7.0 \pm 9.3	
				Stair climb		103.1 \pm 103.7	
		Joint load & Ext.		"THR pre-coat" Cemented		1-leg stance	4.9 \pm 5.3
						Stair climb	26.2 \pm 28.2
Doehring et al. (1999)	Cadaver	Joint load, Abductor, Adductor, Extensor.	"HG Multilock" straight stem cementless proximal coat		Stair climb	Medial	78 \pm 5
						Lateral	46 \pm 5
				Anterior		60 \pm 5	
				Posterior		46 \pm 3	
Gortz et al. (2002)	Composite	Joint load	"ABG"	Torsion	Proximal	8.76 \pm 0.66	
					Distal	10.98 \pm 0.60	
			"CLS"		Proximal	12.60 \pm 0.78	
					Distal	7.08 \pm 0.36	
			"S-ROM"		Proximal	8.40 \pm 0.66	
					Distal	4.44 \pm 0.48	
			"Alloclassic"		Proximal	25.14 \pm 0.84	
					Distal	2.22 \pm 0.30	
Otani et al. (1993)	Composite	Joint load	Carbon composite	Torsional load 30Nm	Proximal	190 \pm 80	
			Titanium alloy		Distal	5 \pm 5	
					Proximal	50 \pm 15	
			Stainless steel		Distal	28 \pm 7	
					Proximal	35 \pm 15	
			Distal		20 \pm 10		
Whiteside et al. (1993)	Femora with implant	Joint load	"AML" 1/3 prox. coat	Torsional load	Medial-Prox	4 (@ 22Nm)	
			"Mallory-Head" 1/3 prox. coat			87 (@ 10Nm)	

Table 3.3: Rotational micromotion from published in-vitro experiments.

Author	Femoral	Boundary condition	Implant type	Load simulation	Measured location	Micromotion (μm)
Bachus et al. (1999)	Cadaver	Joint load	"Bridge Hip" (Prox. Cemented)	Single-leg	Ave. of 5 points	20 \pm 6
				Stair-climb		19 \pm 10
			"Nexus II" (Full cement)	Single-leg		18 \pm 8
				Stair-climb		24 \pm 10
Gotze et al. (2002)	Cadaver	Joint load	"Alloclassic" on-the-shelf	Single-leg	Proximal	24-34
					Distal	5-8
			"Adaptiva" custom-made		Proximal	9-10
					Distal	3-24
Otani et al. (1993)	Composite	Joint load	Carbon composite	Axial load 2500N	Prox – mediolat.	82 \pm 30
					Distal- mediolat.	5 \pm 2
					Prox – anteropos.	25 \pm 20
					Distal – anteropos.	6 \pm 4
			Titanium alloy		Prox – mediolat.	18 \pm 5
					Distal- mediolat.	7 \pm 4
					Prox – anteropos.	21 \pm 5
					Distal – anteropos.	4 \pm 4
			Stainless steel		Prox – mediolat.	5 \pm 1
					Distal- mediolat.	11 \pm 4
					Prox – anteropos.	21 \pm 6
					Distal – anteropos.	3 \pm 2
Schneider et al. (1989)	Cadaver	Joint load	"Muller M84" cementless	Axial load & Torsional load	Prox – mediolat.	75 \pm 45
					Prox – anteropos	90 \pm 25
					Distal – mediolat.	75 \pm 80
					Distal - anteropos	100 \pm 40
			"Spotorno CLS" cementless		Prox – mediolat.	140 \pm 110
					Prox – anteropos	150 \pm 90
					Distal – mediolat.	80 \pm 45
					Distal - anteropos	80 \pm 30
Whiteside et al. (1993)	Femora with implant	Joint load	"AML" 1/3 prox. coat	Axial load	Prox – mediolat.	4
					Prox – anteropos	2
					Distal – mediolat	44
					Distal - anteropos	0
			"Mallory-Head" 1/3 prox. coat		Prox – mediolat.	12
					Prox – anteropos	80
Whiteside & Easley (1988)	Cadaver	Joint load	Collared cementless	Single-leg	Prox – anteropos	20 \pm 10
					Prox - mediolat	10 \pm 5
					Distal - anteropos	5 \pm 10
			Collar-less cementless		Prox – anteropos	20 \pm 20
					Prox - mediolat	15 \pm 15
					Distal - anteropos	5 \pm 5

Table 3.4: Transverse micromotion from published in-vitro experiments.

The above tables showed that various magnitudes of micromotion have been reported ranging from 0.5 μm to 250 μm . A comparison between a fully cemented stem and a proximally cemented stem showed that the magnitude of micromotion was similar (Bachus, Bloebaum & Jones 1999). Axial micromotion caused by loads simulating single leg stance and stair climbing also did not differ much. However, rotational micromotion was larger in stair climbing for both fully cemented and proximally cemented stems. Baleani et al. (2000) also found that the proximally cemented implants had similar micromotion to the fully cemented ones. Compared with the fully cementless option, the latter produced micromotion about 4-5 times more, with micromotion largest at the proximal area and gradually decreasing towards the tip. Another study (Burke et al. 1991) comparing between cementless and cemented implants showed that axial micromotion was similar in single leg stance, but halved for the cemented stem during stair climbing. Rotational micromotion was also similar for both stem types in single leg stance, but was about 4 times larger in stair climbing for cementless compared to fully cemented stems.

The effect of the implant's stiffness on micromotion has been studied by Otani et al. (1993). Two testing protocols, the axial load test and the torsional load test, were performed on three implants made of different materials. In the axial load test, axial micromotion was found to be largest for the carbon composite implant, which was the most flexible of the three, and smallest for the stainless steel implant, which was the stiffest of the three. Transverse micromotion distally was found to be similar between all three implants, but proximally the carbon-composite implant showed larger transverse micromotion than the other two. Under torsional load, the carbon composite

implant produced significantly larger rotational micromotion proximally but about 4 times smaller rotational micromotion distally than the titanium alloy or stainless steel implants. Whiteside & Easley (1989) compared transverse micromotion between collared and collarless cementless stems and found that a collar did not have a detectable effect on medio-lateral and antero-posterior proximal micromotion. The authors argued that micromotion in the proximal area was primarily controlled by the distally fixed stems and that the collar was only useful in preventing distal migration and failure of fixation.

Berzins et al. (1993) compared the micromotion of a straight stem and an anatomic stem. They found no significant difference for axial micromotion in the distal area for both types of stem in all three physiological activities analysed – walking, stair climbing and rising from a chair – with stair climbing producing almost 2 times more motion than in walking, and rising from a chair almost 3 times. The straight stem produced 2 times larger axial micromotion in the proximal area during stair climbing and rising from a chair compared to the anatomic stem. A proximal fixation coating significantly reduced micromotion in this area, by up to 10 times more than with similar coating in the distal region for both straight and anatomic stems.

Another similar comparative study looked at four different cementless stems – three of which had grit-blasted surfaces with different side grooves (the CLS, the Muller 85 & the Zweymuller), and the fourth was an anatomic stem with proximal porous coating (the PCA) (Schneider et al. 1989a). The authors found that the PCA was the most stable among the four stems, with the CLS the most unstable (up to 11 times more axial micromotion than the PCA).

The magnitude of micromotion also seemed to depend on the extent of coating. In a retrieval micromotion study of AML stems (Engh et al. 1992), the authors showed that fully porous coated implants produced less micromotion in all three measured locations – proximal, middle and tip – with magnitude less than 12µm for loads simulating both the single leg stance and stair climbing. For the partially coated implants ($\frac{4}{5}$ coated and $\frac{1}{3}$ coated) the magnitudes of micromotion were comparable between the two, with micromotion greater over the uncoated areas, and largest distally for the $\frac{1}{3}$ coated AML. Their results also showed that there was no significant difference in axial micromotion between single leg stance and stair climbing.

A retrieval micromotion study by Whiteside et al. (1993) compared AML and Mallory-Head specimens. Both stems had porous coating in the proximal $\frac{1}{3}$. The antero-posterior micromotion in the proximal area of the AML was 2.5% of that with the Mallory-Head. The Mallory-Head also produced significantly larger rotational micromotion during a torsional load test. The authors reported that the AML had a superior stability due to dense cortical-cancellous bone ingrowth. The Mallory-Head specimen, on the other hand, was a severely worn titanium implant and the joint was full of particulate metal debris, so the bone ingrowth may have been reduced.

An in-vitro experimental test that simulated physiological stair climbing activity with 4 muscle groups and a joint load showed that rotational micromotion was higher than axial micromotion in all four measured sites; medial, lateral, anterior and posterior (Doehring et al. 1999). The largest difference was found at the lateral side where rotational micromotion was found to be up to 23 times larger than axial micromotion.

3.2 Finite Element work on micromotion

There are numerous published papers predicting micromotion using FE analyses (*Table 3.5*). The FE models used varied from a simplified cylindrical model (Hefzy & Singh 1997; Keaveny & Bartel 1993; Rohlmann et al. 1988) to a more realistic three-dimensional (3-D) shape. 3-D models of hip arthroplasty are usually reconstructed from CT slices or other image-based data. The models are then analysed as a contact between two objects, the implant and the bone. Two of the methods commonly used to analyse contact are either through direct-contact or the use of interface elements, sometimes called gap-elements. The direct-contact method, as the name suggests, means that there are no elements in between the 1st body and the contacted 2nd body. Contact occurs if a node from one body touches another node or a surface of another body. For the second type of contact, a thin layer of elements is used in between the two contacting bodies with specific properties, such as a very low stiffness, assigned to these interface elements. Frictional contact is then applied either using non-linear friction (Dammak, Shiraziadl & Zukor 1997) or more commonly using the Coulomb's law of friction (Mann et al. 1995). This law states that a body in contact will move relative to the second body if the force applied to it is bigger than a product of the normal force exerted on the body and a parameter, μ , known as the coefficient of friction. This parameter is a measure of how difficult it is to move a body relative to the other.

Author	Implant Model	Material Prop. of Bone	Loading conditions	Loading simulations	Type of Contact	Friction	Measured location	Micromotion (μm)	
Ando et.al. (1999)	IDS	Cortical= 17GPa Canc.= 300MPa Poisson= 0.3	Joint load Abductor	Stair climbing, Single-leg stance	Direct contact	Coated, $\mu = 0.61$ Smooth, $\mu = 0.42$	Proximal (P)	10 (P), 18 (D)	
	FMS anatomic						Distal (D)	16 (P), 13 (D)	
								14 (P), 29 (D)	
								26 (P), 65 (D)	
								15 (P), 33 (D)	
FMS	47 (P), 80 (D)								
Omnifit	47 (P), 30 (D)								
Omniflex	109 (P), 73 (D)								
							57 (P), 28 (D)		
							144 (P), 115 (D)		
Biegler et al. (1995)	3D Mallory Head	Cort. = 14Gpa Canc. = 500MPa Poisson= 0.3	Joint load Abductor	1-leg stance	Interface elements	Smooth, $\mu = 0.42$ Coated, $\mu = 0.61$	Distal	24	
							Proximal	33	
							Coated, $\mu = 0.61$	Distal	23
				Proximal			14		
				Stair climb			Smooth, $\mu = 0.42$	Distal	14
				Proximal			58		
	Coated, $\mu = 0.61$			Distal		20			
	Proximal			56					
	3D Harris Galante			1-leg stance		Smooth, $\mu = 0.42$	Distal	33	
						Proximal	17		
						Coated, $\mu = 0.61$	Distal	32	
	Proximal			14					
Stair climb	Smooth, $\mu = 0.42$	Distal	43						
		Proximal	42						
		Coated, $\mu = 0.61$	Distal	42					
Proximal	41								
Keaveny & Bartel (1993)	3D AML full coat	QCT derived	Joint load Abductor	1-leg stance	Interface elements	Smooth, $\mu = 0$ Coated, $\mu = 1.73$	Proximal	50 – 125	
							Distal	200 - 250	
	AML part coat						Max	340	
	AML uncoated						Max	420	

Kuiper & Huiskes (1996)	2D Titanium	Cort = 17GPa Canc = 600MPa	Joint load	1-leg stance	Not mentioned	Smooth, $\mu = 0$	Proximal	480 – 520
							Distal	450 - 550
						Lubricated, $\mu = 0.15$	Proximal	20 - 60
							Distal	70 – 90
						Coated, $\mu = 0.4$	Proximal	0 – 40
							Distal	50 – 60
	2D Isoelastic	Smooth, $\mu = 0$	Proximal	570 – 630				
			Distal	520 – 610				
		Lubricated, $\mu = 0.15$	Proximal	130 – 200				
			Distal	50 – 100				
		Coated, $\mu = 0.4$	Proximal	80 – 110				
			Distal	30 – 50				
Rubin et al. (1993)	3D Spotorno CLS	QCT derived for cancellous	Joint load	1-leg stance	Contact elements	Coated, $\mu = 0.6$	Proximal	371 max
							Middle	292 max
							Distal	35 max
				Stair climb			Proximal	603 max
							Middle	298 max
							Distal	150 max
Viceconti et al. (2001)	3D Ancafit	Cortical (composite) = 14.2Gpa Cancellous (composite) = 69MPa	Torsion load	Stair climb	Contact elements (node-to-face)	Coated, $\mu = 0.2$	Thick=0	75 max
							Thick=33	125 max
							Thick=138	275 max
							Thick=244	390 max
							Thick=562	1000 max
							Thick=723	1300 max

Table 3.5: FE micromotion results from literature.

Values of friction coefficient have been measured experimentally by Rancourt et al. (1990), between tibial cancellous bone and two types of porous structure, beads and fibre mesh. With applied normal pressures between 0.1 and 0.4MPa, values of coefficient of friction between 0.44 and 0.63 were found. Most authors of FE work used values within this range for coated surfaces. However, there are also authors who used a value as low as 0.2 (Viceconti et al. 2001) and as high as 1.73 (Keaveny & Bartel 1993). For contact between bone and smooth surfaces, most authors used coefficient of friction $\mu=0$. However, there are also authors who used a value as high as 0.42 for smooth surfaced implants (Ando et al. 1999; Biegler et al. 1995). Our own study on the effect of friction coefficient on micromotion is discussed in the next chapter.

The loading conditions used in FE micromotion studies were usually taken to simulate two types of physiological loading, single-leg stance and stair-climbing. Most of the analyses used joint contact force only while others also included forces to simulate the effect of the abductor muscles. The load vectors used in these studies were also different from each other. The load vector for single leg stance, for example, varied from (-418, 0, 1402 N) (Biegler et al. 1995) to as high as (-1492, 915, 2925 N) (Keaveny & Bartel 1993). The effect of muscle forces on micromotion is further analysed in chapter 4.

The material properties used in micromotion finite element studies also vary. Assigning material properties based on the greyscale value of CT images seems to be the standard, but others have also used homogeneous material properties for the cortical and the cancellous bone. The values usually used if homogeneous properties were chosen were between 14-17GPa for cortical bone and 300-750MPa for cancellous bone. Some

authors used an even lower value – 69MPa – for cancellous bone (Viceconti et al. 2000; Viceconti et al. 2001). However, this value was chosen to represent the material properties of polyurethane foam which was used as cancellous bone substitute in their synthetic femur model. Further analyses on the effect of bone's material properties on micromotion are carried out in the next chapter.

Micromotion predictions from FE models (*Table 3.5*) vary from 5-603 μ m in models where friction is included, and 420-630 μ m in frictionless scenarios. Biegler et al. (1995) compared two types of cementless implants, the straight cylindrical Harris-Galante and the tapered Mallory-Head prostheses, with loads simulating single leg stance and stair climbing. Two kinds of surface finish were also simulated in this study: a smooth-surfaced implant and a porous coated implant for each hip stem model with both physiological loadings. There was little difference of magnitude of micromotion between smooth and porous coated implants. This may be due to the fact that the authors chose similar values of friction coefficient for the two surfaces – 0.42 for smooth and 0.61 for porous coated. Keaveny and Bartel (1993) assigned a coefficient of friction of 0 and 1.73 for both smooth and coated implants to analyse the effect of the extent of porous coating on relative micromotion. The maximum magnitude of micromotion was found to increase as the amount of coating was reduced from full coat (250 μ m) to zero coat (420 μ m). Contour plots of micromotion showed that the magnitude of relative motion increased steadily from proximal to distal. A smaller magnitude was found proximally than distally due to the effect of the collar support modelled in the analyses.

Viceconti et al. (2001) analysed the effect of interface fibrous tissue thickness on micromotion. The authors found that the stability of the implant was extremely sensitive to the presence of soft tissue. Using a threshold limit for bone ingrowth of 200 μ m micromotion, the authors found that soft tissue layers of 300 μ m thick were sufficient to compromise osseointegration on more than 90% of the stem surface.

A 2D analysis of micromotion using homogeneous properties for both cancellous and cortical bone was constructed by Kuiper and Huiskes (1996) to study the effects of implant stiffness and coefficient of friction on micromotion. A flexible stem generated motions about three to four times larger proximally than a stiff stem, which generated larger motions distally. The presence of friction reduced motions by about 85% compared with frictionless interface. However, increasing the coefficient of friction further had little effect on micromotion.

Micromotion results of various designs of hip stems have been reported by Ando et al. (1999). In their FE analyses, five 3D models of cementless stems – the IDS, the FMS-Anatomic, the FMS, the Omniflex and the Omnifit – were loaded in physiological loading simulating single leg stance and stair climbing. Two of the stems were anatomical (the IDS and the FMS-Anatomic), one was tapered (the FMS), and the other two were straight (the Omniflex and the Omnifit). Average micromotion in the proximal and distal areas was calculated and the results showed that relative micromotion was larger for all models during walking than in stair climbing. The authors did not discuss why micromotion results were larger in single leg stance than in stair-climbing. Looking at the load vector used in the analyses, the joint contact force in single leg stance had a larger magnitude (-1385, 849, 2714 N) than in the stair climbing

(-709, 601, 1553 N). This could explain the prediction of higher micromotion in single leg stance than in stair climbing.

The results obtained by Ando et al. in the previous paragraph were different from those obtained by Biegler et al. (1995) who compared the Mallory-Head and Harris-Galante prostheses. Biegler et al. showed that relative motion in the proximal area was about 2-4 times more in stair climbing than in single leg stance, though the difference was less pronounced in the distal area. This could be explained by the load vector used by the authors. They used a lower value for the single leg stance (-418, 0, 1402 N) compared to stair climbing (-709, 601, 1553 N). Note that the load vector used by Ando et al. for single leg stance was significantly larger.

Rubin et al. (1993) in their micromotion predictions for a cementless stem found that stair climbing produced maximum micromotion in the proximal area of up to 600 μ m, which was about twice as high as in the single-leg stance. However, similar to the micromotion results reported by Biegler et al., micromotion in the middle and distal areas was similar for the two physiological loadings. The load vector used in their analyses was (-600, 400, 1000 N) for single leg stance and (-550, 470, 1220 N) for stair climbing. Even though the trend of micromotion distribution was similar to Biegler et al., the magnitude of micromotion along the stem was an order of magnitude larger than Biegler et al. or Ando et al. Certainly the load vector could not explain the significantly larger micromotion observed in their analyses. However, the stem was modelled without distal canal filling which could explain the larger micromotion results.

3.3 Micromotion Experiment: Materials and Methods

This section describes how the experiment was conducted. It contains a description of the bone and implant preparation, and instrumentation for measuring micromotion. The first task was to decide what type of micromotion should be measured and compared with FE. As described in the literature above, there are various types of micromotion that can be measured experimentally. For the sake of simplicity, it was decided to use axial micromotion to validate the computer predictions. Axial load aligned to the axis of the implant and loaded at the shoulder of the prosthesis will be used for this purpose.

The next stage is to decide where the measurements are to be made. Two points have been decided – one in the proximal area and another one in the distal area. The exact location of the holes depended on the arrangement of the instrument used for measurement. A linear variable differential transducer (LVDT Model DFG5, DC Miniature series, Solartron Metrology, West Sussex, UK), which is a type of linear displacement transducer, was chosen to measure the axial component of displacement of the implant relative to the bone.

An LVDT consists of a cylindrical housing and a separate movable core (*Figure 3.34*). It is an electromechanical device that converts the displacement of the core into an electrical signal. The cylindrical housing consists of a primary coil and two identical secondary coils symmetrically spaced on either side of it.

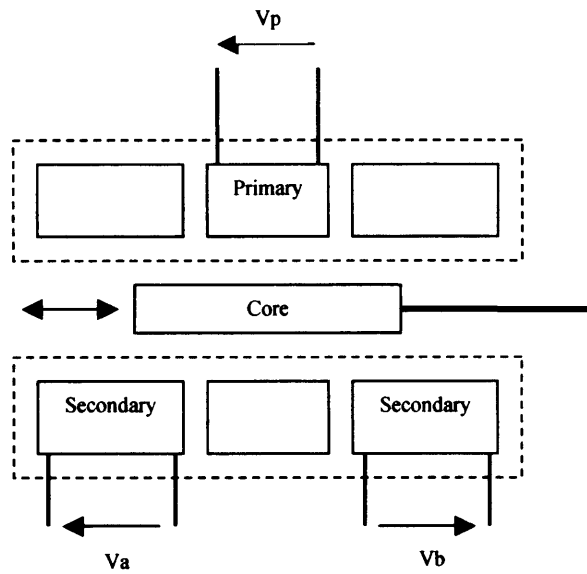


Figure 3.34: Diagram showing the main components of an LVDT.

When the primary coil is energised by an external power source, voltages are induced in the two secondary coils. With the core in a central position, the induced voltage from the primary to each secondary coil is equal and the net output of the transducer is zero. When the core is moved from the central position in either direction, the induced voltage in the coil towards which the core is moved increases, while the induced voltage in the opposite coil decreases. This action produces a differential voltage output that varies linearly with changes in core position. The difference is that when the core moves in one direction, the output voltage is in phase with the voltage on the primary, but when the core moves in the other direction, the voltage is out of phase. The LVDT used has an infinite resolution which means that it can respond to even the most minute movement of the core and produce an output. The readability of the external electronics, e.g. a digital voltmeter, represents the only limitation on the resolution.

The LVDT must first be calibrated before use. *Figure 3.35* below shows the arrangement for calibration. A 9V d.c. power supply was used, with a digital voltmeter to display the LVDT output. The LVDT was aligned in a vertical direction with a screw thread micrometer that had a graduation of $10\mu\text{m}$, using two clamps and a retort stand. The core end of the LVDT was placed on top of the spindle rod of the micrometer where readings were taken from the digital voltmeter as the spindle was displaced from 0 to $500\mu\text{m}$ at $10\mu\text{m}$ intervals. The graph of the voltmeter reading vs the displacement of the core is shown in *Figure 3.36*.

From the graph (*Figure 3.36*), a linear equation relating the voltage to the displacement was obtained,

$$\delta D \approx 1.587 \delta V$$

where D is the displacement and V is the voltage.

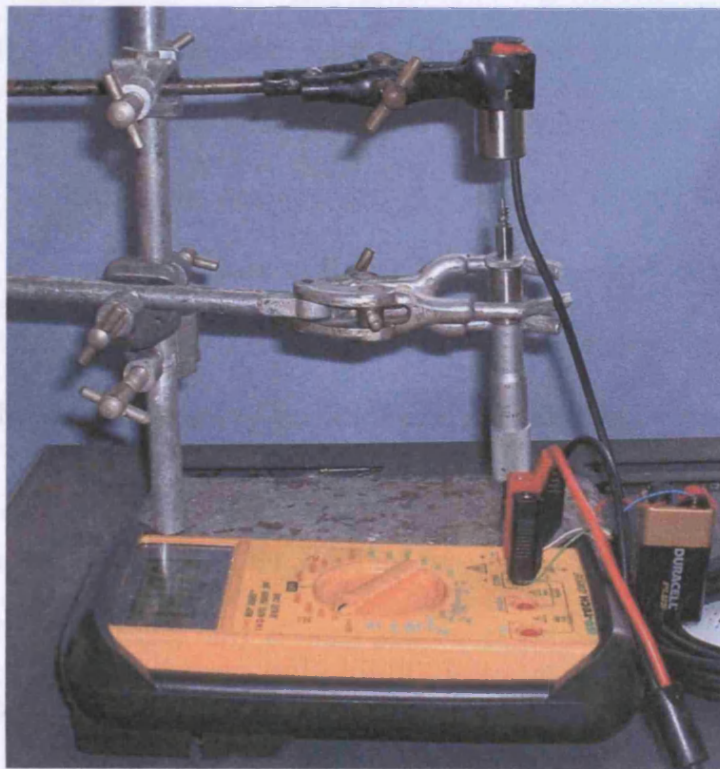


Figure 3.35: Calibration of the LVDT used in the experiment to measure relative motion.

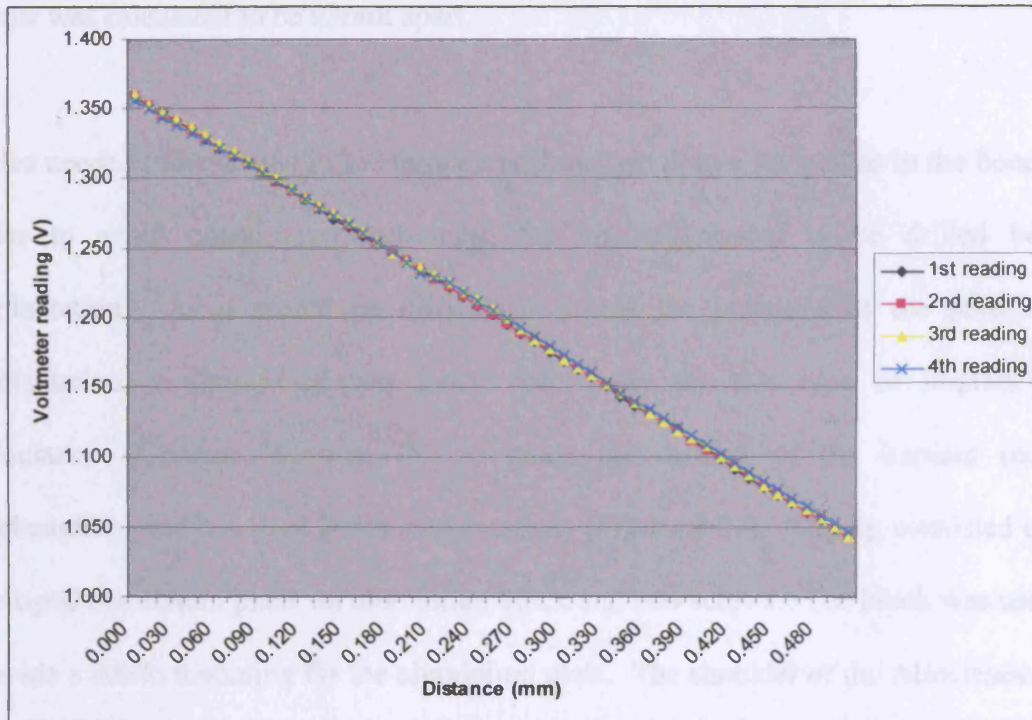


Figure 3.36: Graph of volt vs displacement for calibration of the LVDT.

Once the LVDT was calibrated, the exact location of the measuring points could be planned. Axial motions were to be measured, so the LVDT needed to be placed parallel to the axis of the stem. The anterior side of the femur slightly below the greater trochanter area was a suitable place to fix the LVDT because of its relatively straight surface. Since the core of the LVDT could work in both directions, only one LVDT was needed. The exact locations of the holes were decided based on the working range of the LVDT. The working range of the core was 10mm from one end to the other (± 5 mm from the central position), but since the relative motion of the implant would be in the range of micrometers, only a small section in the middle of either phase was needed. The length of the rod connected to the core was 27mm and the coil housing was 43mm in length. Using 25mm of the length of the connecting rod from each end,

together with the length of the coil housing, the distance between the measurement points was calculated to be 93mm apart.

Holes needed to be drilled in the implant at these two points, as well as in the bone. In order to avoid unnecessary loosening, the implant needed to be drilled before implantation. As it would be difficult to locate the positions of the holes after implantation, a simple jig was made specifically for this type of implant (the Alloclassic, Zimmer, Warsaw, IN) to guide the drilling of the implant (before implantation) and the bone (after implantation) (*Figure 3.37*). The jig consisted of an L-shaped aluminium plate, an aluminium block and two screws. The block was used to provide a stable mounting for the aluminium plate. The shoulder of the Alloclassic was machined to a depth of 2mm using a milling machine to provide a flat surface for the block. Two screws were used to fix the plate to the block; these passed into the superior part of the shoulder of the stem. The guide holes in the plate were then drilled, using a drill size slightly larger than the hole in the stem. These holes were 93mm apart, with the proximal hole 40mm from the corner of the plate.

Once the holes had been drilled into the implant, implantation was carried out by an orthopaedic surgeon. Four cadaveric femurs (3 left, 1 right) were used in this experiment. The neck of the femur was first resected, and the femur was then reamed with firm impaction using the smallest size reamer to open the canal. The process was continued with the next size increment of the reamer until no further movement of the reamer with impaction could be made and there was a change in pitch during impaction. This was the endpoint of impaction, which was based on visual and auditory clues. A

femoral stem measuring the same size as the last reamer used was then implanted in the femur. Two femurs had Alloclassic size 4 and another two had size 3.

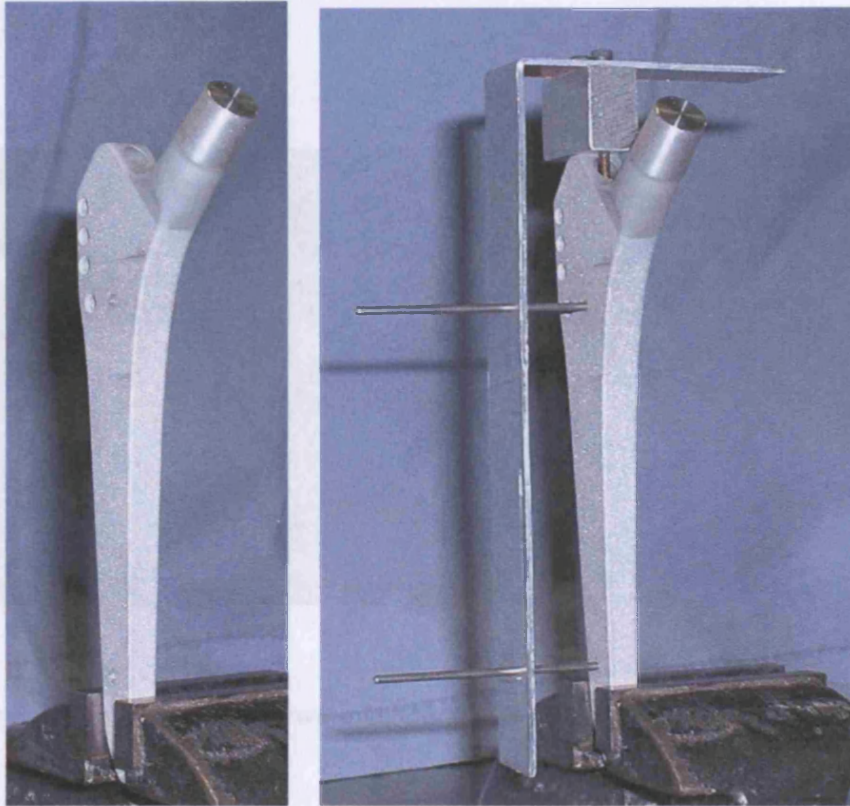


Figure 3.37: The jig used to drill holes on the implant and bone.

For comparison with FE predictions, one of the four femurs was CT scanned twice – one whilst intact and another one after implantation. Two CT scans were needed – the first one for use in FE modelling and the second one for implant alignment. This will be described later in the chapter (section 3.4) when describing the construction of the FE model.

After the implantation was completed on all four femurs, the jig was used once again to locate the holes in the implant. A $\phi 5\text{mm}$ drill was used on the bone, which was larger than the $\phi 2\text{mm}$ of the implant holes. A $\phi 2\text{mm}$ steel rod 40mm long was inserted into

each hole. The movement of this rod, which represented the movement of the implant, relative to the bone was measured by the LVDT via the connecting rod of the LVDT core. The steel rods were glued into the implant holes to avoid them from moving or becoming loose (*Figure 3.38*).



Figure 3.38: Location of the two $\phi 2\text{mm}$ steel pins for micromotion measurement.

The femur was then sectioned 250mm distal to the lesser trochanter and placed inside a grease-lubricated cylindrical metal container. These were then placed onto the table bed of a universal materials testing machine (Instron Corp., Canton, MA.) for alignment. The specimen was adjusted by means of eight screws through the sides of the metal container until the long axis of the stem was parallel to the direction of loading. Polymethylmethacrylate (PMMA) was then used to ensure that the specimen was fixed securely inside the metal container. The potted femur was then fixed onto the bed of the Instron machine via screws. The LVDT was placed at the midpoint between the two steel rods (*Figure 3.39*). The connecting rod of the LVDT core was then fixed to the free-end of the steel rod which had been roughened with glass paper using a very thin layer of bluetack and superglue. The specimen was left for two hours before the

experiment started to ensure all glue had set. After two hours, the reading on the voltmeter was checked to ensure that no movements were recorded between the steel rod and the LVDT core.

The testing machine was then set-up for a cyclical axial compression load of 0 to 2kN for 50 cycles at a rate of 1kN/min using a 5kN load cell. All implanted femurs were subjected to cyclic pre-load with the same magnitude and rate until there was no major fluctuation in the readings of the voltmeter. This protocol ensured that no significant axial subsidence was recorded during the experiment by achieving maximum press-fit and ensured repeatability of results. Once the voltmeter readings had stabilised, the experiment started. Readings from the digital voltmeter were taken manually at maximum load of 2kN and when fully unloaded at each cycle. Measurements for the distal part were performed first and after the 50 cycles had completed, the magnetic core of the LVDT was removed and placed on the other end of the coil for measurement of the proximal side. The connecting rod of the core was glued to the roughened free-end of the steel rod, and left for two hours before the experiment was started again. The process then continued as described above.



Figure 3.39: The implant loaded in compression using the Instron machine.

3.3.1 Experimental Results

Once the experiments were completed for all four specimens, raw data were collected for analyses. *Figure 3.40* below shows a typical load-crosshead displacement curve for the experiment. Each experiment started with the measurement of micromotion on the distal part of the stem before continuing to the proximal side. As can be seen from the graph below, the experiment for the distal part started with a big jump in the displacement before stabilising. Once stabilised, the load-displacement curve was similar between proximal and distal, with the proximal side having a slightly steeper curve than the distal.

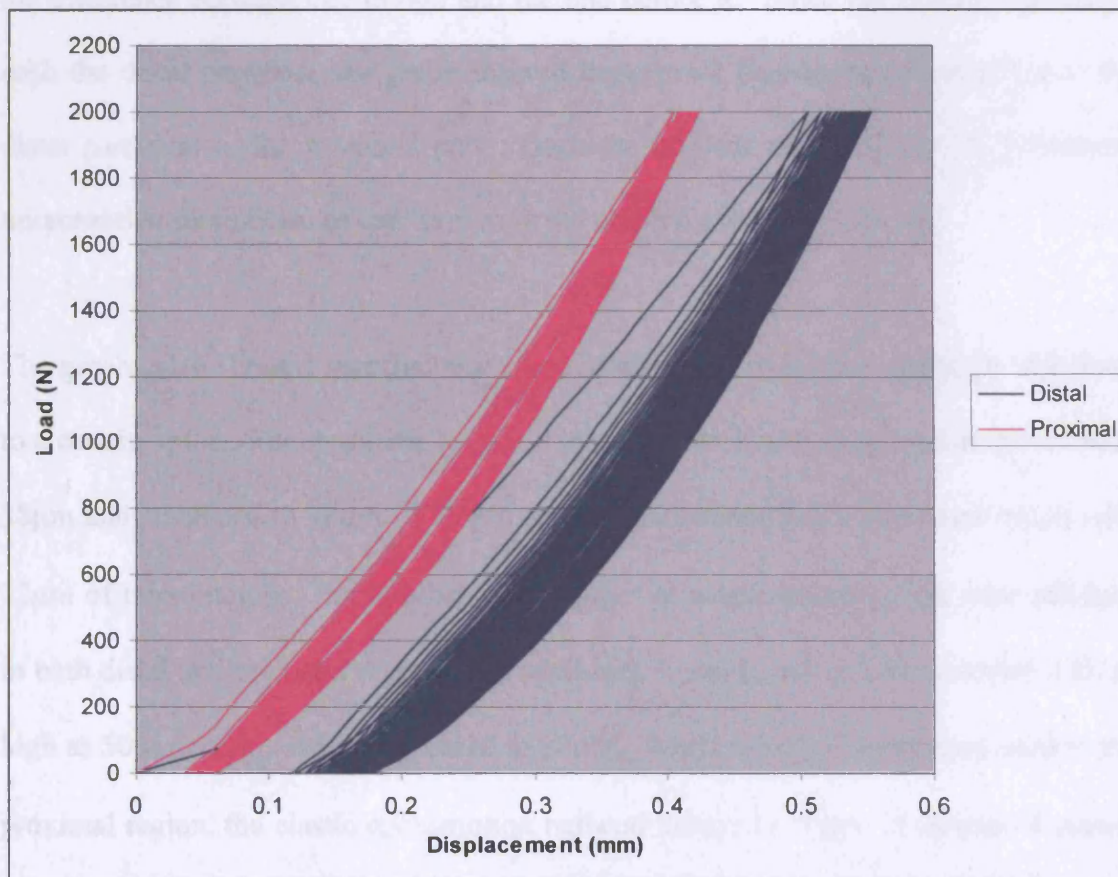


Figure 3.40: Example of Load-crosshead displacement curve from the experiment, specimen 2.

For micromotion results, the recorded voltage readings from the voltmeter were converted into displacements using the linear relationship previously mentioned. Micromotion results for each specimen were then plotted against load cycles for the distal part and the proximal part (*Figure 3.41*). Specimen 1 and 2 are Alloclassic size 4, and specimen 3 and 4 are size 3.

As can be seen from the two graphs, micromotion at each loading cycle can be categorised into two types, reversible and permanent. Reversible micromotion is a recoverable motion which can be calculated from the difference between the peak and the trough of each loading cycle. Permanent micromotion is non-recoverable and it is the difference between one trough and the one before it. Since the experiment started with the distal part first, the graph showed larger total permanent micromotion in the distal part than in the proximal part. Once the implant was fully seated, permanent micromotion diminished as can be seen in the graph for the proximal part.

The graphs also showed that the magnitude of elastic micromotion gradually stabilised to a certain value. For specimen 1, elastic micromotion in the distal region started with 38 μm and stabilised to 18 μm . The proximal region started with 20 μm and ended with 12 μm of micromotion. For specimen 2, changes in elastic micromotion were minimal in both distal and proximal region. For specimen 3, elastic micromotion started with as high as 50 μm and gradually decreased to 20 μm . When the experiment continued to the proximal region, the elastic micromotion reduced further to 14 μm . Specimen 4 started with 34 μm before reducing to 16 μm . However, in the proximal part, elastic micromotion started with 40 μm and then stabilised to 22 μm .

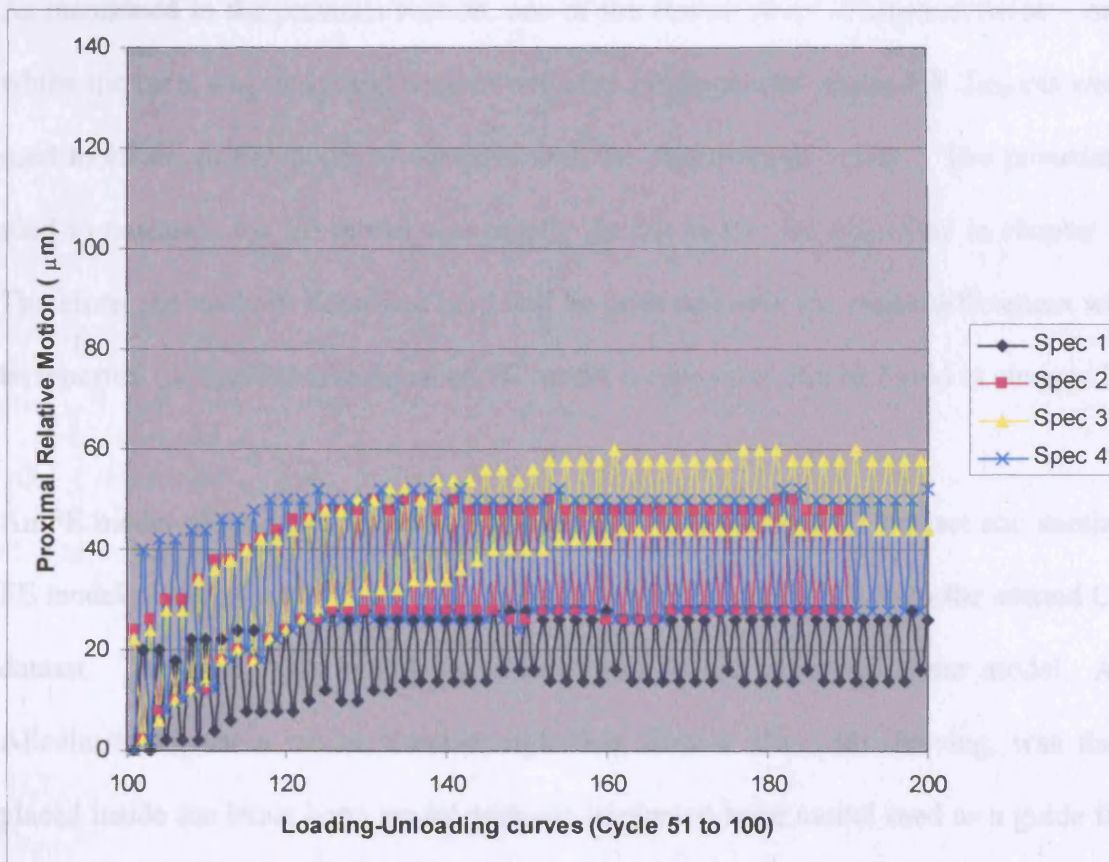
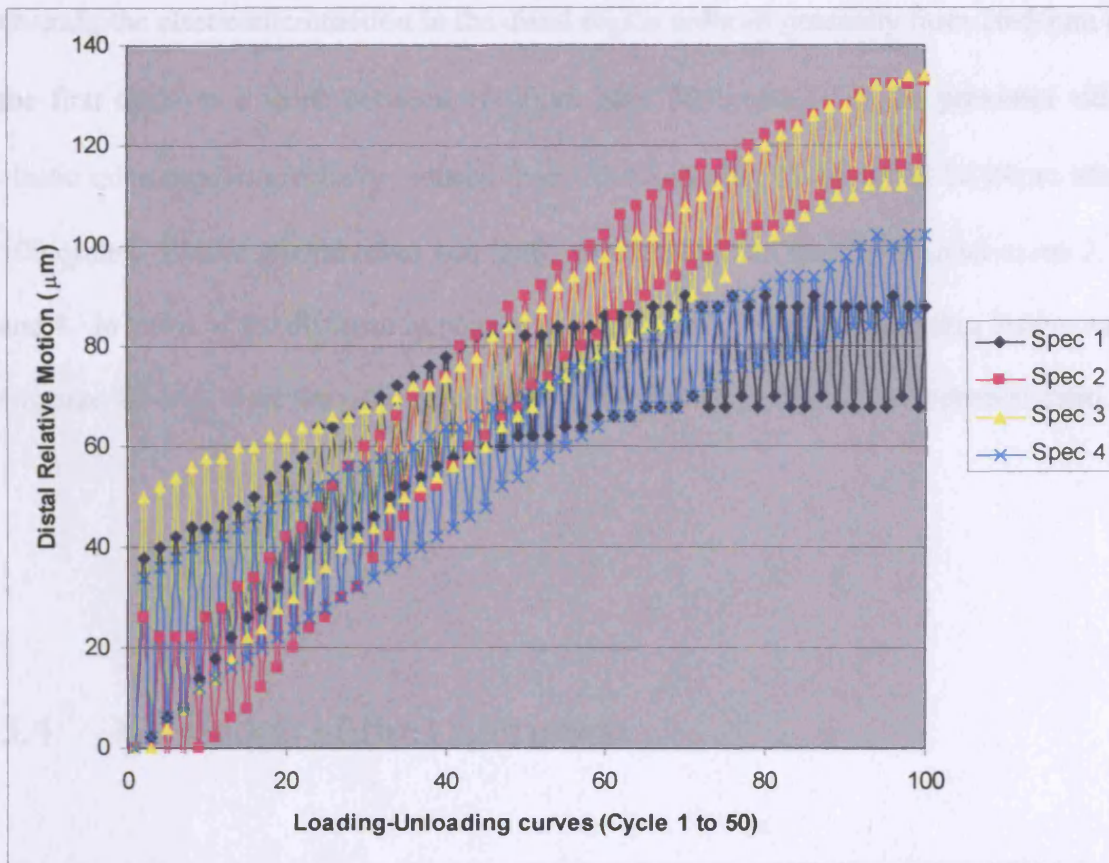


Figure 3.41: Relative motion results from the experiment.

Overall, the elastic micromotion in the distal region reduced gradually from 26-50 μm at the first cycle to a value between 16-20 μm after 50 cycles. For the proximal side, elastic micromotion gradually reduced from 20-40 μm after 50 cycles to 12-24 μm after 100 cycles. Elastic micromotion was larger proximally than distally for specimens 2, 3 and 4. In terms of the different implant size used in the experiment (two size 3 stem and two size 4 stem), there were no major differences in micromotion found between them.

3.4 FE models of the experiment

As mentioned in the previous section, one of the femurs was CT scanned twice – one whilst the bone was intact and another one after implantation. These CT datasets were used to create an FE model to compare with the experimental results. The procedure used to construct the FE model was mostly similar to the one described in chapter 2. Therefore, the methods described here will be brief and only the major differences will be reported. A detailed discussion on FE model construction can be found in chapter 2.

An FE model of an intact femur was constructed from the first CT dataset and another FE model of the resected femur with implant was also constructed from the second CT dataset. The intact bone model was then aligned to the implanted femur model. An Alloclassic hip stem model, created separately from a 3D CAD drawing, was then placed inside the intact bone model with the implanted bone model used as a guide for alignment (*Figure 3.42*). This alignment is important so that the hip stem model, which

was created separately, was in the exact location of the one found in the experiment. The implanted model created from the second CT dataset could not be used in FE analysis mainly due to the artefacts from the metal stem. So, the Alloclassic hip stem had to be created separately and then used with the intact bone model for FE analysis.

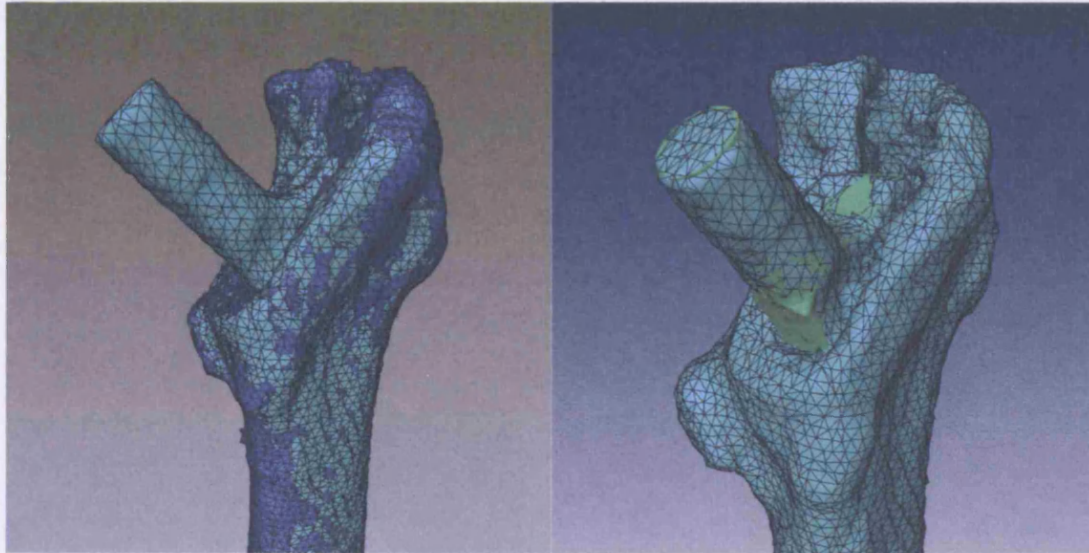


Figure 3.42: Alignment of the intact bone to the implanted bone (left) and alignment of the Alloclassic hip stem to the implanted bone (right).

From this point onwards, the construction of the FE model followed the procedure as described in Chapter 2. A coefficient of friction of 0.4 was assigned to the stem-bone interface and an interference fit of 0.05mm was assumed. The FE model was then axially loaded at the centre of the shoulder of the stem with 2kN of load to simulate the loading configuration in the experiment.

3.4.1 Results

The result of the FE analysis is shown in *Figure 3.43* below. It shows that the distribution of micromotion was similar between the anterior and posterior side, and the proximal half had relatively larger magnitude of micromotion than the distal half. The proximal half of the stem had a range of micromotion between 24 to 29 μm whilst in the distal half micromotion reduced gradually from 28 μm to 14 μm . For micromotion result at the exact location with the experiment, the value of micromotion at the proximal part was found to be between 26-28 μm and the distal part was 21 μm .

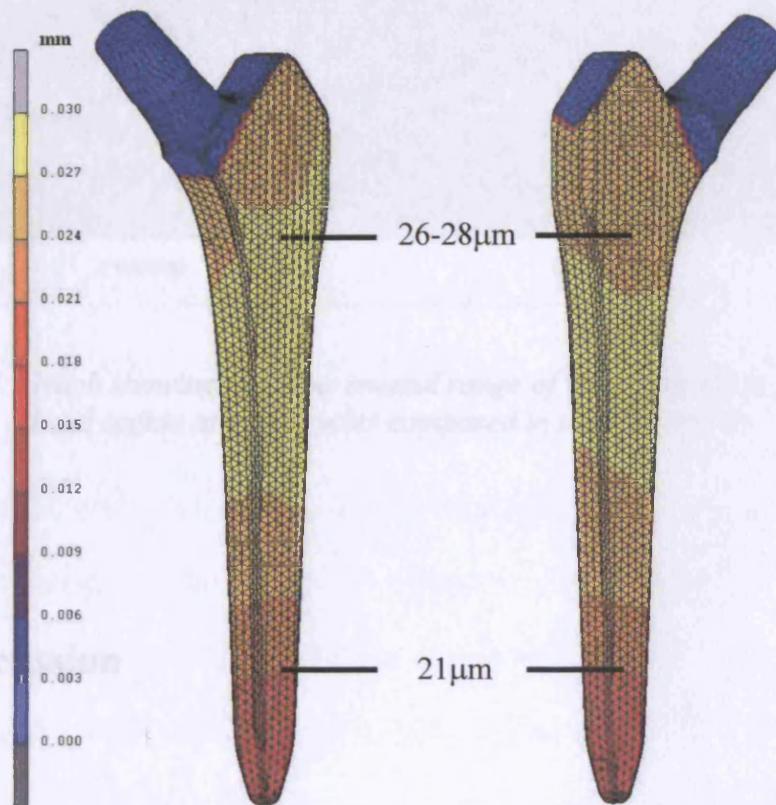


Figure 3.43: Contour plots of micromotion for the Alloclassic hip stem under axial load of 2kN.

Figure 3.44 on the next page shows a graph comparing the FE results at a specific point in the proximal and distal part and the range of elastic micromotion values obtained

from the experiment after 50 cycles. The graph shows that the FE results correlate well with the experimental findings, with larger micromotion proximally than distally.

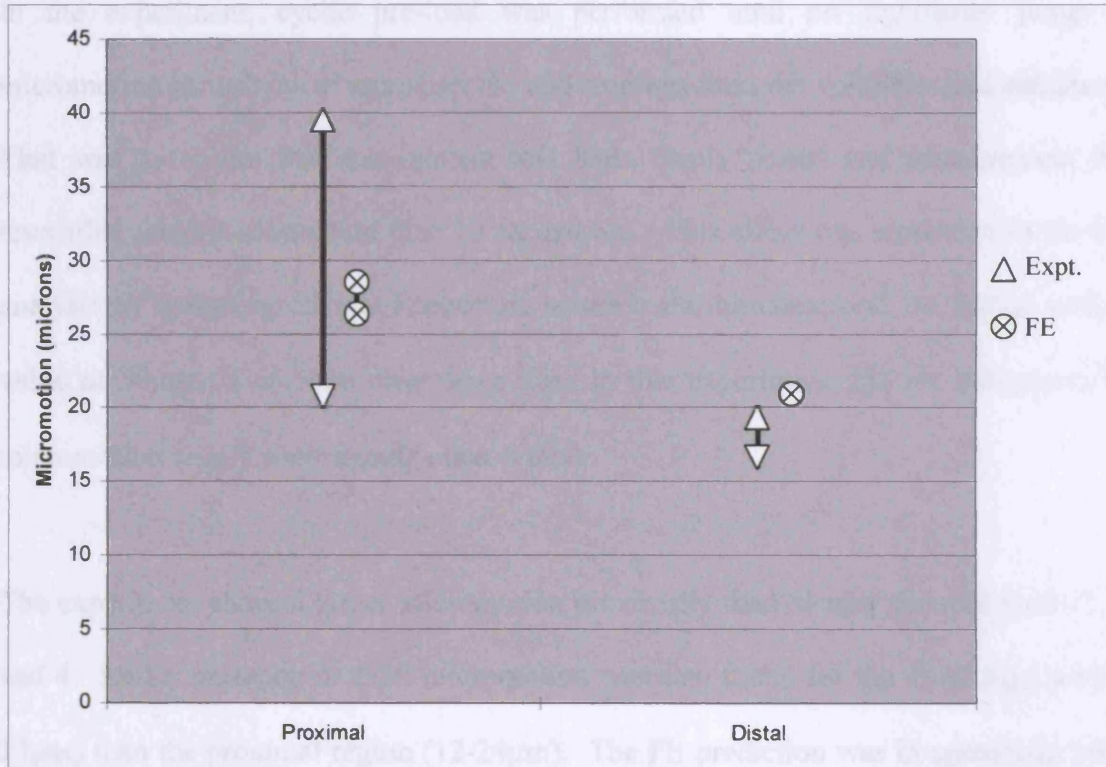


Figure 3.44: Graph showing the experimental range of values for the proximal and distal region after 50 cycles compared to the FE results.

3.5 Discussion

In this chapter, an in-vitro experiment was carried out to validate the FE predictions. Four cadaveric femurs were implanted with Alloclassic hip stems by an orthopaedic surgeon. All specimens were then loaded in cyclic axial load of 2kN using an Instron machine, where axial micromotions were recorded in the proximal and distal region via

an LVDT. One of the specimens was CT scanned twice to construct an FE model for comparison with the experimental findings.

In the experiment, cyclic pre-load was performed until no significant jump in micromotion in each cycle was observed and readings from the voltmeter had stabilised. That was to ensure that the implant had been firmly seated and measurement for reversible micromotion could then be carried out. This effect was simulated in the FE analysis by assigning an interference fit between the hip stem and the femur with a value of 50 μm . Two stem sizes were used in this experiment, but no differences in micromotion results were found between them.

The experiment showed larger micromotion proximally than distally for specimens 2, 3 and 4. Lesser variation in axial micromotion was also found for the distal region (16-20 μm) than the proximal region (12-24 μm). The FE prediction was in agreement with the experimental results where similar magnitudes were observed and proximal micromotion was found to be relatively larger than distal micromotion. This is as expected because the Alloclassic is a distally-fixed hip stem. It was press-fitted into the canal with its distal part anchored onto the endosteal cortices. These results were also similar to the experimental findings of Gotze et al. (2002) who compared micromotion between a custom-made stem and an Alloclassic hip stem. Though the loading configuration simulated in their experiment was for single leg stance, which was different from the one used in this experiment, the authors did report larger micromotion proximally (24-34 μm) than distally (5-8 μm) for the Alloclassic hip stem. Another in-vitro experimental study comparing between several designs of cementless hip stems (Gortz et al. 2002) which included the Alloclassic also showed that the

Alloclassic produced relatively small rotational micromotion distally under torsional load.

A direct comparison of the FEA results with other published FE results that used a similar hip stem design is not available. Comparison is made even more difficult due to the variety of loading configurations and magnitudes, material properties, coefficient of friction and the interference fit. Nevertheless, the magnitudes of the micromotion results were in the same range and similar order of magnitude as reported by Ando et al. (1999) and Biegler et al. (1995).

A couple of specific assumptions were used in the FE models. These were parameters that have to be assigned a certain value which was unknown from the experiment. The coefficient of friction is a parameter that determines how difficult it is for two contacting bodies to slide against each other. The values used in other published FE works ranged from 0 to 1.73 (see next chapter), and 0.4 was used in this study. The second assumption was the level of interference fit. It would be difficult if not impossible to measure the amount of press-fit achieved after implantation, and therefore a value of 50 μ m was assumed. Varying these two parameters could change the result of the micromotion predictions. The effects of friction coefficient and interference fit as well as other parameters that could affect micromotion prediction will be looked at in the next chapter.

3.6 Conclusion

This chapter validated the computer predictions of micromotion via a simple experiment. Four cadaveric femurs were implanted with the Alloclassic hip stem and cyclically loaded axially to 2kN using an Instron testing machine. An FE model was created from one of the specimens and loaded axially with the same magnitude to simulate the experimental loading. Values of reversible micromotion from the experiment varied between 12-24 μ m proximally and 16-20 μ m distally. The FE results correlate well with the experimental findings, with values between 26-28 μ m proximally and 21 μ m distally.

Chapter 4 Parameters affecting Finite Element predictions.

There are various parameters that need to be considered when analysing the stability of hip stems using FEA as these parameters could affect the predicted micromotion results. In this chapter, five major parameters are examined – the friction coefficient, the interference fit, cyclic loading, the material properties of the bone and the muscle loads.

The coefficient of friction is a parameter that corresponds to the degree of resistance to motion between two contacting bodies. This needs to be assigned a certain value, with higher values mean higher resistance to motion. The second parameter that must be consider is the amount of interference fit between the bone and the implant, because fixation of cementless stems is achieved through press-fit. The effect of press-fit on

micromotion is analysed by varying the value of the interference fit. The third parameter is the load cycle. To the author's knowledge, all FE studies on the stability of cementless hip prosthesis did not include cyclic loading. It is therefore unclear which type of micromotion these FE results represented – the permanent or the reversible micromotion. The material properties of the bone could also affect the micromotion results. A healthy normal bone has different values of apparent density than weaker bones such as the one suffering from osteoporosis. The effects of bone quality on micromotion are analysed by varying the coefficient value in the modulus-density cubic relationship proposed by Carter and Hayes (1977). The final section of this chapter looks at the effect of muscle forces on micromotion. There are many muscles acting on the femur, and the magnitudes and directions of these muscle forces vary depending on the type of activities. These values have been calculated by two researchers; Duda (1998) for physiological walking and stair-climbing, and Fisher (1999) for the three phases of a gait cycle. The values published by the two researchers will be used in this chapter to analyse the effects of muscle forces on micromotion.

One of the limitations in analysing these parameters is that the results of changing one parameter at a time could be different to the results when a combination of two or more parameters is involved. However, the results obtained from changing a parameter can provide us with a rough idea of how the results would change if other parameters are also included. In this chapter each parameter will be analysed individually by keeping the rest of other parameters constant. As the effects of these parameters on predicted micromotion could also be affected by the overall geometry of the stem, one particular hip stem, the AML, will be used throughout this chapter to ensure consistency of results.

4.1 The effect of coefficient of friction

One important feature of cementless hip stems is the texture or roughness of the surface of the stem. Without this feature, the stem lacks strong initial stability for proper bone ingrowth, resulting in aseptic loosening (Duparc & Massin 1992). This is different from their cemented counterpart where stems with polished surfaces such as the Stanmore (Biomet), the C-Stem (DePuy) and the Exeter (Stryker) performed extremely well with high rate of long-term success (Ek & Choong 2005; Emery et al. 1997; Gerritsma-Bleeker et al. 2000). Furthermore, it has been found that surface texture favours the formation of new bone (Ricci et al. 1991; Suzuki, Aoki & Ohya 1997). The strength of attachment can be further enhanced by the use of bioactive materials, such as calcium phosphate, coated on the textured surface (Niki et al. 1991).

The observation that surface topography can affect bone mineralisation has been reported in the literature. One paper (Ricci et al. 1991) investigated tissue response between implants with smooth and roughened surfaces using implantable chambers. The authors found that the implant with smooth surfaces strongly favoured the formation of fibrous tissue. The implant with roughened surfaces, on the other hand, did not favour fibrous tissue formation and direct bone apposition happened after several weeks. In another similar study (Suzuki, Aoki & Ohya 1997), smooth-surfaced titanium implants were compared with rough-surfaced titanium implants inserted in rabbits' femur. The authors found that direct bone-implant contact and bone volume around the implant were greater in the rough-surfaced titanium compared to the smooth-surfaced titanium.

Surface roughness is achievable through various methods. Probably the most common method is grit-blasting or plasma-spraying the surface with particles. This technique produces a surface texture that is irregular and is characterised by the surface roughness parameters. The most widely used parameter is the R_a , the arithmetic mean of the departure of the profile from the mean profile. Grit-blasted and plasma-sprayed surfaces usually have R_a values up to $20\mu\text{m}$. Experimental studies showed that surface roughness improved bone attachment and reduced the thickness of fibrous tissue layer (Ricci et al. 1991).

Textured surfaces with more regular geometry and relatively larger in dimension than the grit-blasted or plasma-sprayed surfaces have also been exploited. The most widely used are beads of several hundred microns in diameter bonded to the implant surface. This technique produces a more regularly spaced porous structure. Wire-meshing also gives similar type of structure (Yamamuro & Takagi 1991). There are other structures which are more cancellous-like but their uses are currently limited as bone substitutes (Hacking et al. 2000). The introduction of pores or gaps in these structures will not just introduce friction, but also allows bone to grow into the pores, thus providing an interlocking mechanism. The porous structures are filled with blood immediately after surgery, and after several weeks, new bone tissues enter and fill the spaces of the porous structure. In a retrieval study of the Mallory-Head and the AML cementless implants (Whiteside et al. 1993), the authors found extensive bone ingrown into the porous coating of both stems.

Hip prostheses with porous coated surfaces have also been reported to give higher resistance to micromotion than the use of smooth-surfaced bioactive materials alone

(Oonishi 1991). The magnitudes of micromotion also vary between different types of surface geometry. In an in-vitro experimental study looking at the stability of cementless hip prostheses (Schneider et al. 1989b), the authors found that proximally coated implant with beads produced less micromotion than those with grit-blasted surfaces. In a study looking at bone ingrowth and strength of attachment of porous tantalum (Hacking et al. 2000), the high volumetric porosity and highly interconnected network of consistent shaped pores of porous tantalum has been found to give higher strength of attachment by three to six times than porous beads.

The direct immediate consequence of implant having textured or rough surfaces is the introduction of friction at the bone-implant interface. However, these textured surfaces are impossible to model physically in global scale FE. Only the effect of these surfaces can be incorporated in finite element analyses by modelling the two bodies as a frictional contact with an assigned value of friction coefficient – the larger the assigned value, the more difficult it is for the contacting bodies to slide against each other.

The values of the coefficient of friction between tibial cancellous bone cubes and porous-surfaced metal plates have been measured experimentally by Rancourt et al. (1990). Two types of porous structure, beads and fibre mesh, were used in the experiment and compared with smooth stainless steel plates. With applied normal pressures between 0.1 and 0.4MPa, average values of the coefficient of friction of 0.28 (SD 0.03) was found for the smooth plates. For the fibre mesh and beads, the average values of friction coefficient were between 0.44 (SD 0.07) and 0.63 (SD 0.15).

In published finite element work on micromotion, the friction coefficient used varied from 0 - 0.42 for smooth surfaces, to 0.2 - 1.73 for rough surfaces. A 2-dimensional FE micromotion study by Kuiper and Huiskes (1996) used $\mu=0$ for smooth surfaces, $\mu=0.15$ for lubricated surfaces and $\mu=0.4$ for coated surfaces. Two other published papers (Ando et al. 1999; Biegler et al. 1995), however, did not use $\mu=0$ for smooth surfaces. Instead, they used $\mu=0.42$ for smooth and $\mu=0.61$ for coated surfaces. Another paper used $\mu=0$ for smooth and $\mu=1.73$ for coated surfaces in their 3D AML models (Keaveny & Bartel 1993). Viceconti et al. (2001), however, used a much lower friction coefficient ($\mu=0.2$) for their coated 3D Ancafit hip stem models.

A value of coefficient of friction needs to be assigned for all FE analyses in this study. Since the values used in FE micromotion study varied from 0 to 1.73, it is important to see how micromotion predictions are affected by the friction coefficient, and to choose a suitable coefficient for this study.

4.1.1 Methods and Results

To study the effects of friction coefficient on micromotion, 6 models of the AML stem were prepared as described in Chapter 2. Each model was analysed separately by assigning different coefficient of friction starting with 0.01, and then between 0.2 and 1.0 at 0.2 increments. All other parameters were kept the same. The models were then loaded in physiological walking with all relevant muscle forces suggested by Fisher (1999) (see section 4.4). The three figures below (*Figure 4.45*, *Figure 4.46* and *Figure 4.47*) show micromotion results from the analyses.

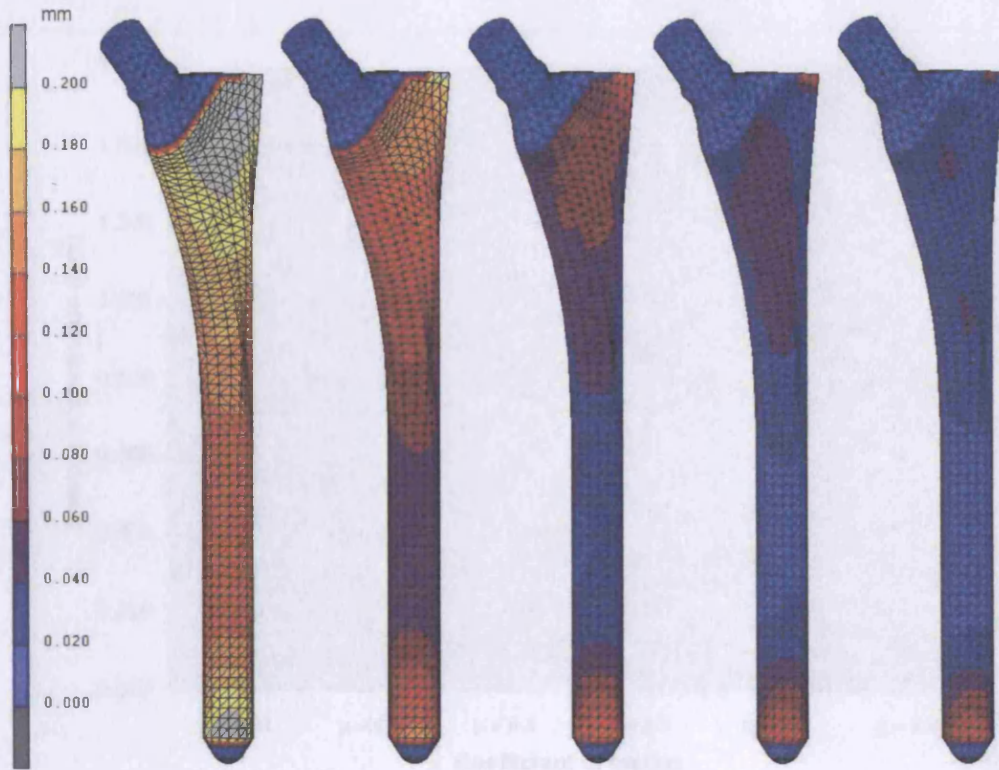


Figure 4.45: Contour plots of micromotion with friction coefficient of 0.2, 0.4, 0.6, 0.8 and 1.0 (left to right). The model with friction coefficient of 0.01 is not included as the micromotion went beyond the range of the scale.

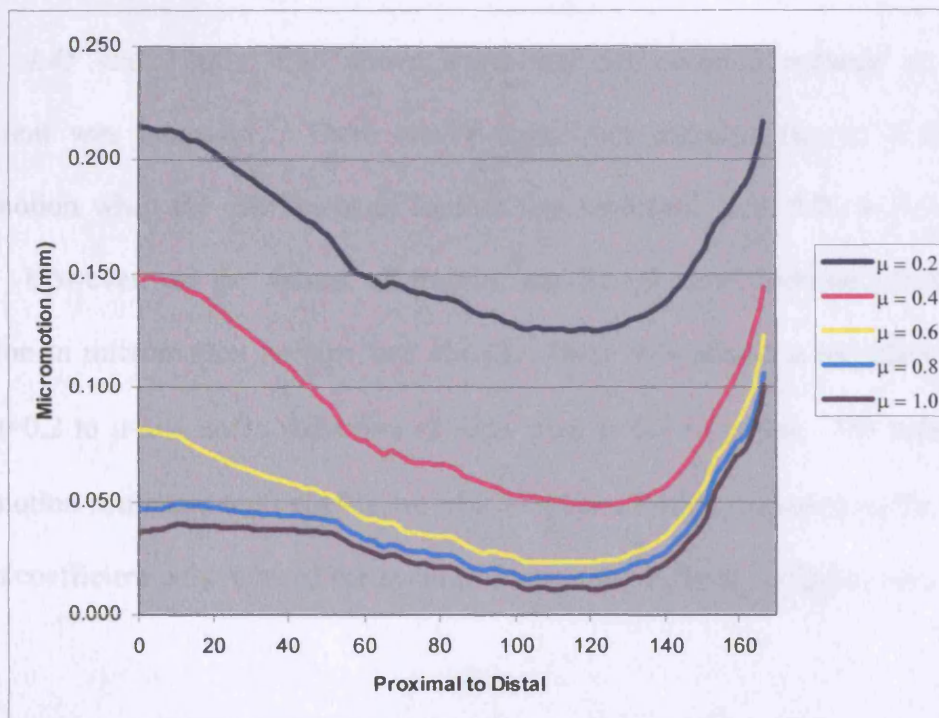


Figure 4.46: The effects of the coefficient of friction on micromotion along the anterior surface of the AML stem (proximal to distal).

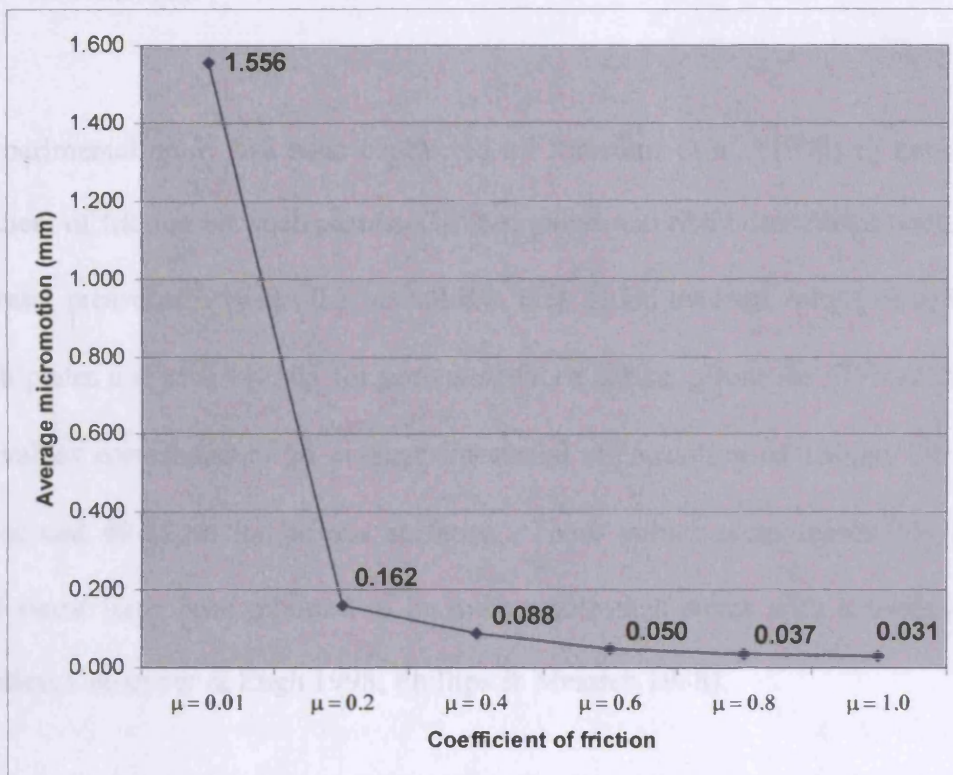


Figure 4.47: Average micromotion along the anterior surface of the AML stem as a function of coefficient of friction.

Figure 4.45 and Figure 4.46 above show that micromotion reduced as friction coefficient was increased. There was a significant decrease (up to 8 times) in micromotion when the coefficient of friction was increased from 0.01 to 0.2 (Figure 4.47). However, as the values of friction coefficient were increased further, the reduction in micromotion became less abrupt. There was almost a reduction of 50% from $\mu=0.2$ to $\mu=0.4$ and a reduction of 43% from $\mu=0.4$ to $\mu=0.6$. The reduction in micromotion continued until coefficient of 0.8 where a further increase in the value of friction coefficient only reduced the average micromotion slightly (Figure 4.47).

4.1.2 Discussion

An experimental study has been conducted by Rancourt et al. (1990) to measure the coefficient of friction between porous-surfaced plates and tibial cancellous bone. Based on normal pressures between 0.1 to 0.4MPa, they found average values of $\mu=0.28$ for smooth plates and $\mu=0.44-0.63$ for porous-surfaced plates. From the FE results above, these values correspond to an average interfacial micromotion of 130 μm for smooth surfaces and 40-88 μm for porous surfaces. These values seem reasonable because coated stems have been reported to be more stable than stems with smooth surfaces (McAuley, Culpepper & Engh 1998; Phillips & Messieh 1988).

Coefficient values of more than 0.3 can be regarded as suitable for porous-surfaced implants because the corresponding average interfacial micromotions are within the limits for osseointegration (Szmukler-Moncler et al. 1998). Coefficient values of less than 0.3 can be regarded as suitable for smooth surfaced implants because the average interfacial micromotion would be 130 μm or more – beyond the threshold limit for bone ingrowth. This is consistent with follow-up reports of stems with smooth surfaces, where they were found to be more prone to loosening and had lower survival rate than porous surfaced stems. In a follow-up study of the Moore smooth stems, Phillips & Messieh (1988) reported implant loosening as a major complication at an average of 3.4 years. Only 63% of the stems were considered to be good. Another paper (Dickob & Martini 1996) reported a follow-up study of the PM smooth prostheses and found that the survival rate with loosening as the end point was 85% at 6 years. Most of the patients were found to have thigh pain, which was attributed to micromotion and loosening of the stem.

As to which value of friction coefficient should be used, there is no straightforward answer that could pinpoint to a single universal value. Nevertheless, the FE results showed that there was a huge jump between almost frictionless surface ($\mu=0.01$) and $\mu=0.2$, and that beyond $\mu=0.8$ the choice of friction coefficient did not matter. These results are similar to the findings obtained by Kuiper and Huiskes (1996) - frictionless surface increased relative motion by up to 85% compared to the friction coefficient of 0.15, but increasing the coefficient further had little effect on relative micromotion.

Published FE studies on micromotion used various values for the coefficient of friction but still managed to predict reasonable relative micromotion. As mentioned in the introduction to this chapter, interactions between the friction coefficient and other parameters could affect the predicted interface micromotion. The results could change, for example, if different stem geometry was used, or an interference fit was introduced in the analyses. Ramamurti et al. (1997) reported that micromotion was not only affected by friction coefficient, but also by the amount of interference fit. As the amount of interference fit was increased, the effect of friction coefficient became less pronounced.

Our FE results showed that values of friction coefficient used by many authors were reasonable. As for this particular study, a value of 0.4 will be used throughout for all types of surface coating. This is based on the FE results presented in this section, and is also consistent with the experimental findings of Rancourt et al. All analyses in this project do not involve hip stems with smooth surfaces, and as such no value of friction coefficient for smooth surfaces is needed.

4.2 The effect of Interference Fit

Another important design characteristic of cementless stems is that they are pressed-fit inside the femoral canal. This characteristic can be incorporated in FEA as an interference fit of two contacting bodies – the implant and the bone. Almost all published FE analyses on micromotion ignored this essential parameter in their predictions. To the author's knowledge, only one published work included the interference fit as well as the friction coefficient (Ramamurti et al. 1997). However, the model used in their study was a simplified cylindrical model.

The degree of press fit varies depending on the design of the stem and the surgical technique involved, and the actual interference fit obtained after successful surgery is unlikely to achieve the intended press fit (Testi et al. 2004). Hip stems with distal fixation design such as the AML are more likely to have press fit distally than proximally. Proximal fixation design (such as the ABG), on the other hand, relies on press-fit in the proximal part of the stem because the endosteal cortex is over-reamed distally to avoid bone-implant contact. The surgical techniques for preparing the femoral canal could produce different amount of press-fit. The under-reaming technique, where the last reamer used in preparing the canal is slightly smaller in size than the actual implant size inserted into the canal, would theoretically produce larger interference fit than the line-to-line reaming technique (Sugiyama, Whiteside & Engh 1992). Even then, the under-reaming technique may not achieve the intended press fit

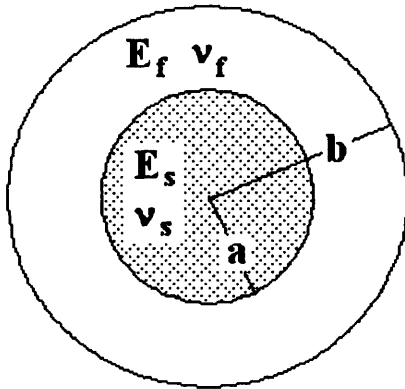
because gaps at the interface may occur due to surgical error during bone preparation (Paul et al. 1992).

The main problem of including interference fit in FE analyses is that the amount of interference fit and its distribution are unknown. It would be difficult, if not impossible, to exactly measure how much press fit has been achieved and the actual distribution of the fit post-surgery. When an orthopaedic surgeon implants a cementless hip stem, he will use visual and auditory clues until he 'feels' that the implant is 'firmly' seated. There is no way of telling how much interference fit has been achieved and its distribution – is it mainly in the distal part, the proximal part, or throughout the stem. However, to ignore the interference fit altogether in an FE study of cementless hip stems would be inappropriate as cementless stems are designed with press-fit.

In this section, the effect of interference fit on predicted micromotion will be analysed. A calculation was made using a simplified cylindrical bone-implant model to estimate the maximum amount of interference fit that could be achieved.

4.2.1 Methods and Results

As far as the author is aware, there have been no reports on the values of actual interference fit obtained post-surgery. A simple calculation was therefore made to the existing AML model to estimate the maximum amount of interference fit that could be achieved. The distal half of the stem had cylindrical shape and was used in the calculation as shown in *Figure 4.48*. Subscript 's' was used to denote the stem and subscript 'f' was used to denote the diaphyseal femur.



$$E_f = 12000 \text{ MPa} \quad \nu_f = 0.3$$

$$E_s = 200000 \text{ MPa} \quad \nu_s = 0.3$$

$$a = 13.5 \text{ mm}$$

$$K_f = \frac{b}{a}$$

$$b = 27 \text{ mm}$$

$$K_s = \frac{a}{0}$$

Figure 4.48: Diagram showing the implant (subscript *s*) and the femur (subscript *f*) for estimating the maximum interference fit.

Where E = the Young's moduli

ν = the Poisson's ratio

a = radius of the stem

b = radius of the diaphysis

The stiffness of cortical bone was obtained from the Biomedical Engineering Handbook (pg. 706, 1995), and the stiffness of the stem was taken to represent Cobalt Chromium.

The radius of the diaphysis was measured from the CT images of the VHP dataset.

The following 2 equations were used in the calculation:

$$\sigma_{\theta, \max} = \frac{P_c}{K_f^2 - 1} (1 + K_f^2) \quad \text{--- equation 1}$$

$$\frac{\delta}{c} = \frac{P_c}{E_f} \left\{ \left(\frac{K_f^2 + 1}{K_f^2 - 1} \right) + \nu_f \right\} + \frac{P_c}{E_s} \left\{ \left(\frac{K_s^2 + 1}{K_s^2 - 1} \right) - \nu_s \right\} \quad \text{--- equation 2}$$

where the maximum interference pressure (P_c) was first calculated using equation 1 by substituting values for K_f and $\sigma_{\theta,max}$. $\sigma_{\theta,max}$ is the strength of cortical bone in transverse direction and its value of 75MPa was taken from the Biomedical Engineering Handbook. The value obtained for P_c from equation 1 was then used in equation 2. Substituting values into equation 2 gives the interference fit, $\delta = 0.103\text{mm}$. This is an estimate of the maximum interference fit allowed without breaking the femur.

Two models of the AML were prepared with an interference fit of contacting bodies set to 0.050mm and 0.100mm respectively. Constant interference fit was assumed throughout the contacting bodies. Coefficient of friction was set to 0.4 and all other parameters remained the same. The results from the two models are shown below together with the result of an AML stem modelled without an interference fit obtained from the previous section (section 4.1).

Figure 4.49 and *Figure 4.50* show that interference fit affected relative micromotion significantly. The relative micromotion reduced by up to 15 times in areas of cortical contact when maximum interference fit of 0.1mm was included, and up to 3 times in the proximal area of cancellous contact. The results also showed that there was not much difference in magnitude and distribution of micromotion between interference fit of 0.050mm and 0.100mm.

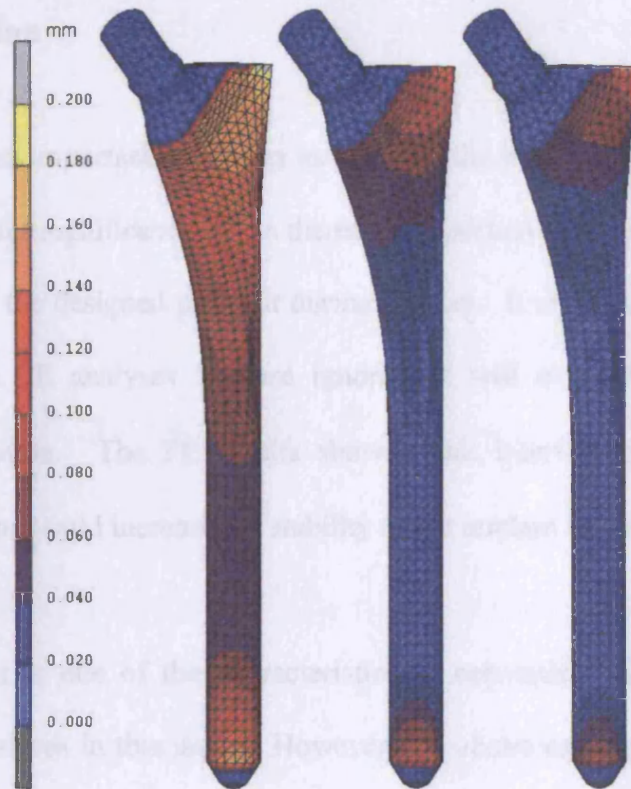


Figure 4.49: Contour plots of micromotion for the AML stem without an interference fit (left), with interference fit of 0.050mm (centre) and 0.100mm (right).

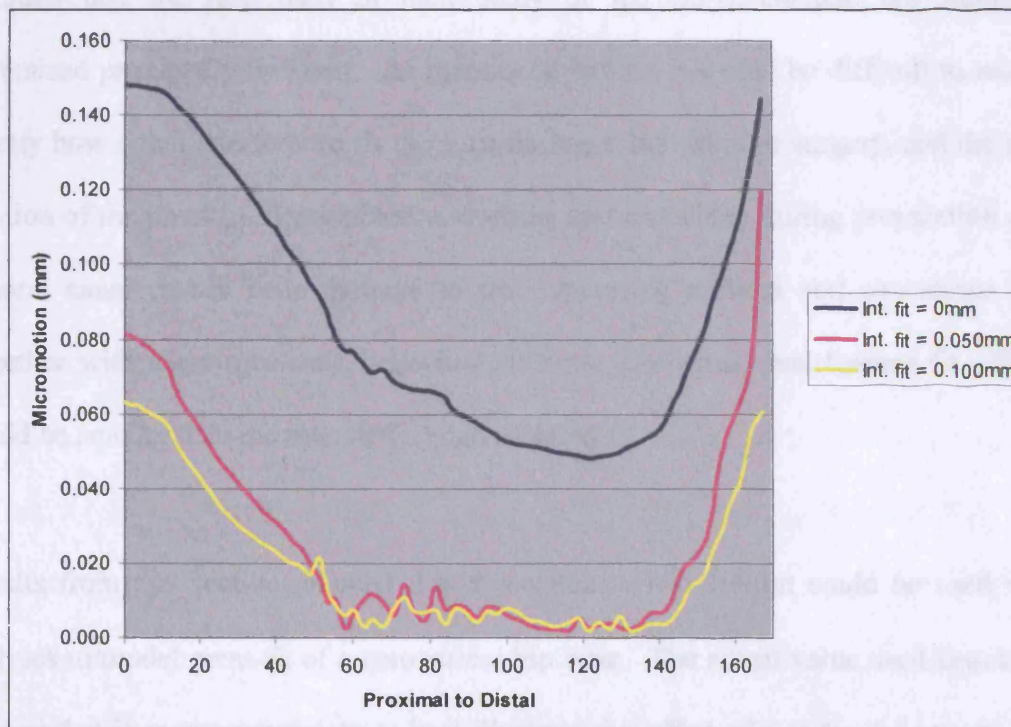


Figure 4.50: Micromotion along the posterior side of the three AML implants from proximal to distal.

4.2.2 Discussion

Interference fit is an important parameter as it affects the micromotion and therefore the stability of hip stems significantly. It is therefore important for an orthopaedic surgeon to try and achieve the designed press-fit during surgery. It is also important to include interference fit in FE analyses because ignoring it will overestimate the predicted interface micromotion. The FE results showed that interference fit of just 50 μ m throughout the stem would increase the stability of the implant by a factor of 10.

As interference fit is one of the characteristics of cementless hip stems, it will be included in all analyses in this study. However, the above estimate of interference fit was calculated based on a simplified cylindrical model of the diaphyseal femur. This estimate could well be different for other hip stem designs. Berzins et al. (1993) recorded that the rasp used in their study of the Harris-Galante hip stems was undersized proximally by 1mm. As mentioned before, it would be difficult to measure exactly how much interference fit the surgeon has achieved after surgery, and the actual location of the press fit. Undoubtedly, reaming and broaching during preparation of the femoral canal causes bone damage to the supporting cortical and cancellous bone. Together with the viscoelastic behaviour of bone, the actual interference fit obtained would be smaller than the intended design of press-fit.

Results from this section showed that any values up to 100 μ m could be used in FE analyses to model press-fit of a cementless hip stem. The actual value used depends on the one that is most appropriate or best illustrate the effect of a particular investigation

or a particular design in the analysis. Unless stated otherwise, a uniformly distributed interference fit of 100 μ m will be used for all analyses in this study.

4.3 The effect of cyclic loading on micromotion.

Micromotion can be categorised into two types – reversible and permanent (sometimes called migration or subsidence). Reversible micromotion is the difference of the measured minimum and maximum value of one loading cycle, which determines whether there will be bone apposition or loss around the stem (Pilliar, Lee & Maniopoulos 1986). Irreversible micromotion (or migration) is the total motion of the implant when it is unloaded at a particular moment in time. Migration is one of the criteria for implant revision (Kobayashi et al. 1997), although some authors reported that late stabilisation could occur on migrated implants (Chen et al. 1998; Delaunay et al. 2001).

Some in-vitro experimental studies measured only the reversible or recoverable micromotion (Burke et al. 1991; Doehring, Rubash & Dore 1999). Cyclic preload was used in these experiments to ensure that the implant has been fully seated before any measurements of micromotion were made. However, there are published results of experimental work on micromotion that measured both the total sinkage (migration) of the implant (after a few thousand load cycles), and dynamic reversible micromotion (Berzins et al. 1993; Buhler et al. 1997; Schneider et al. 1989a). These studies showed

that the first few load cycles produced relatively large motions and were mostly irreversible. These irreversible motions earlier in the load cycles can be as much as 6 times larger than motions calculated over the last few cycles. The micromotions from the last few cycles were found to be mostly recoverable and the migration was found to be negligible.

Another experimental work (Dujardin et al. 1996) measured the amount of load cycles needed to stabilise an implant before any recoverable micromotion could be measured. Three different hip stem designs were tested – on-the-shelf anatomic stem and two custom-made stems. The first custom-made stem was designed with metaphyseal filling (stem C1) and the second one with metaphyseal filling and distal stem thinning to avoid diaphyseal cortical contact (stem C2). The authors found that the anatomic stems required more load cycles to stabilise than that of the custom-made stems, and that the migration of stem C1 was greater than stem C2.

Most published FE predictions on micromotion did not differentiate between reversible and irreversible micromotions (Ando et al. 1999; Biegler et al. 1995; Keaveny & Bartel 1993). These FE studies load their models once in physiological stair-climbing or walking, and presented the relative micromotion results without discussing whether the motions were reversible or not. The major assumption used in these analyses, although not explicitly stated, was that the implant had already been firmly seated inside the femoral canal, and migration was therefore negligible and could be ignored. We believe that the main reason cyclic loading was not included in FE micromotion analyses was due to the limitation on computing resources - the amount of computing resources needed to obtain converged reversible micromotion results through cyclic loading could

be prohibitive. There is, however, one FE work on micromotion that used cyclic loading, and reported two types of micromotion – reversible and irreversible (Kuiper & Huiskes 1996). However, the model used was two-dimensional which significantly reduced the amount of computing resources.

In this study, cyclic loading is performed on a 3-dimensional AML model to analyse the reversible and permanent micromotion, and to see if reversible micromotion could be estimated from the first load cycle.

4.3.1 Methods and Results

To study the effect of cyclic loading on micromotion, the previous AML model was used with a cyclic loading input of 10 cycles. Two sets of analyses were performed; one without an interference fit, and another one with an interference fit of 100 μ m. The coefficient of friction was set to 0.4, and the models were loaded in physiological walking with all relevant muscle forces.

The next three pages (*Figure 4.51* to *Figure 4.53*) show the results of an AML modelled without an interference fit. The first set of result (*Figure 4.51*) was the total cumulative micromotion (reversible + permanent) obtained when the stem was fully loaded at each loading cycle. The contour plot of permanent micromotion (*Figure 4.52*) was obtained directly from the results when the stem was fully unloaded at each loading cycle. From these two results, the contour plots of reversible micromotion (*Figure 4.53*) were calculated by subtracting the permanent micromotion from the total cumulative micromotion. *Figure 4.54* shows a graph of an average micromotion calculated along the posterior side of the stem at each cycle.

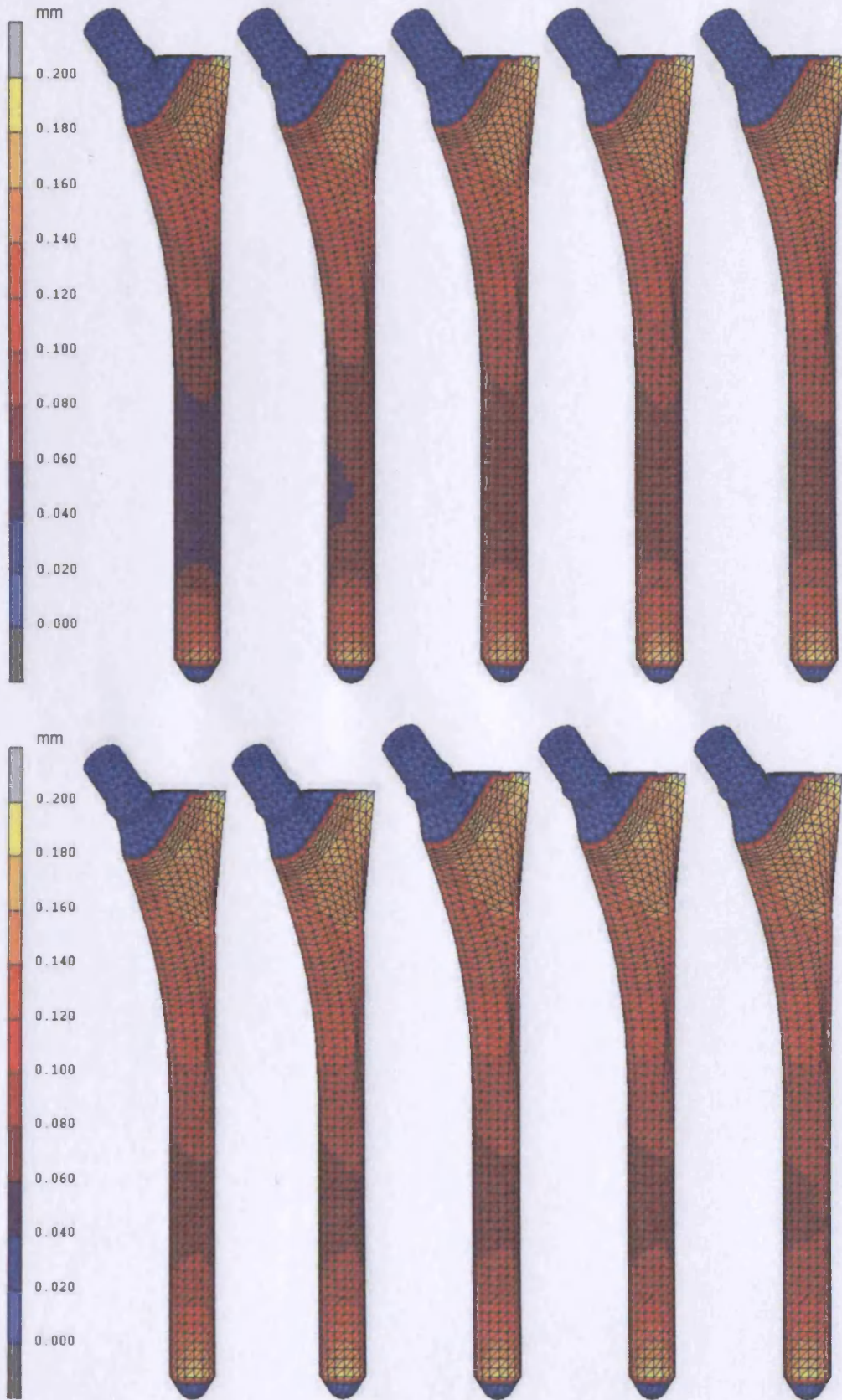


Figure 4.51: The progression of total micromotion (elastic + permanent) for up to 10 cycles.

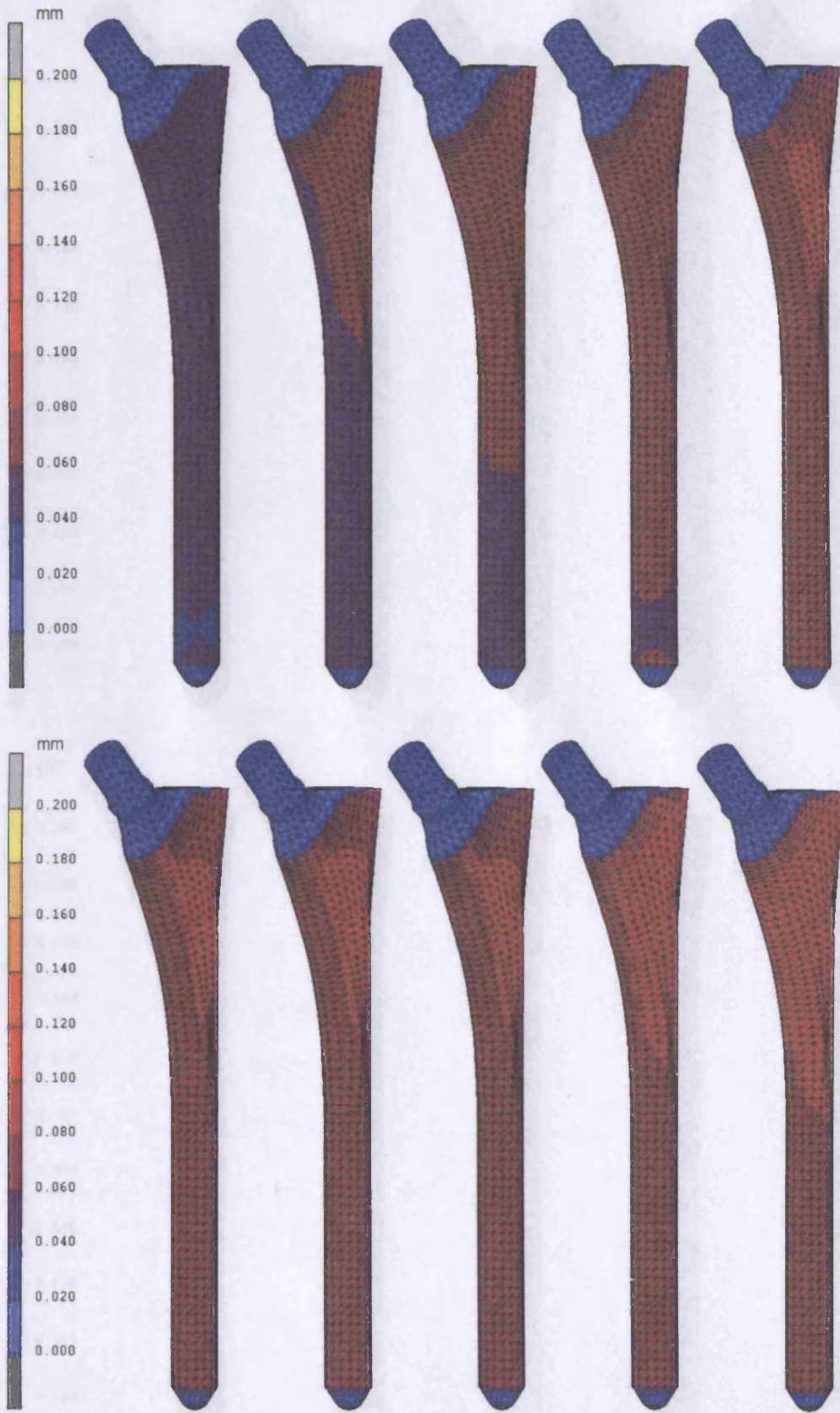


Figure 4.52: The progression of permanent micromotion for up to 10 cycles.

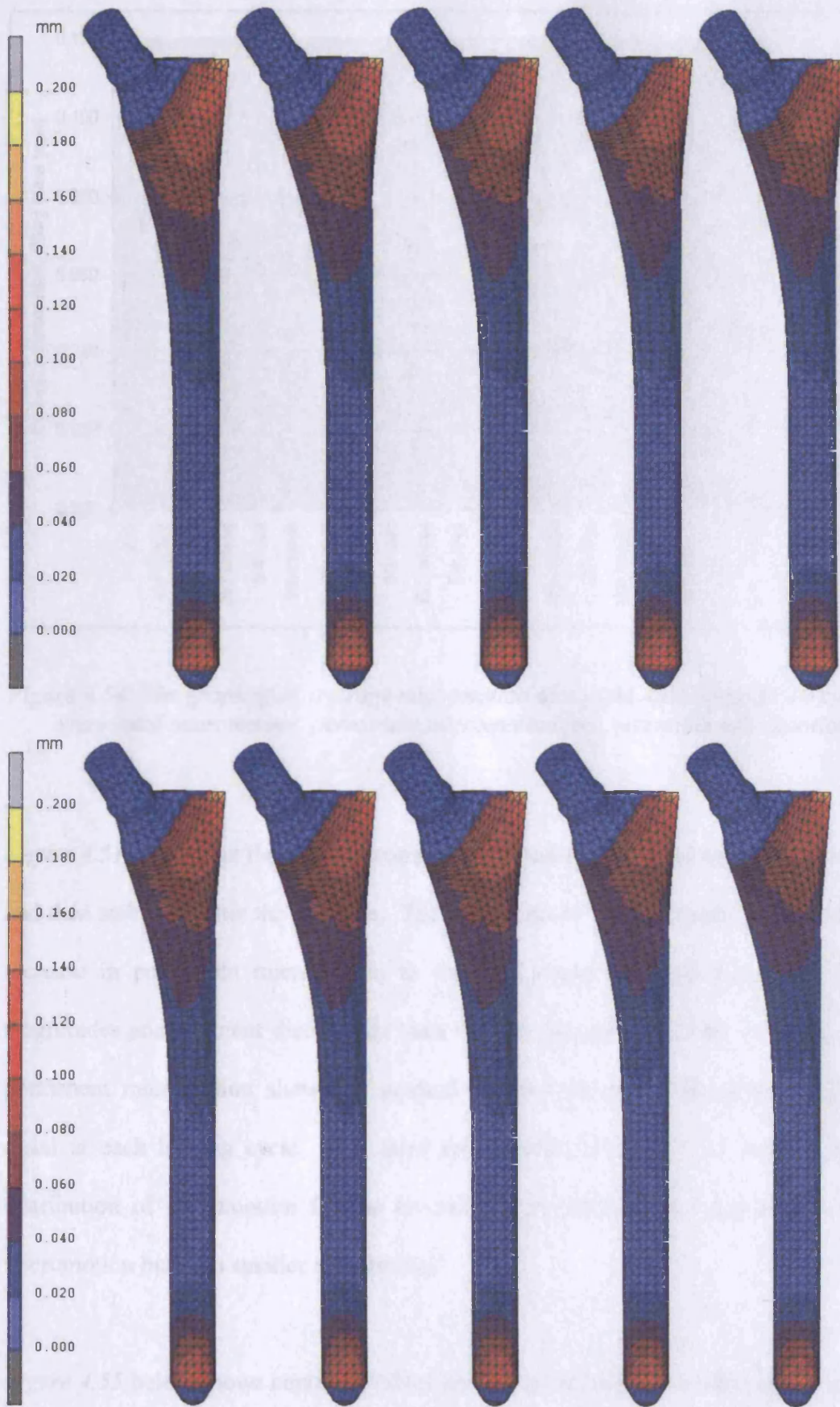


Figure 4.53: The progression of elastic micromotion for up to 10 cycles.

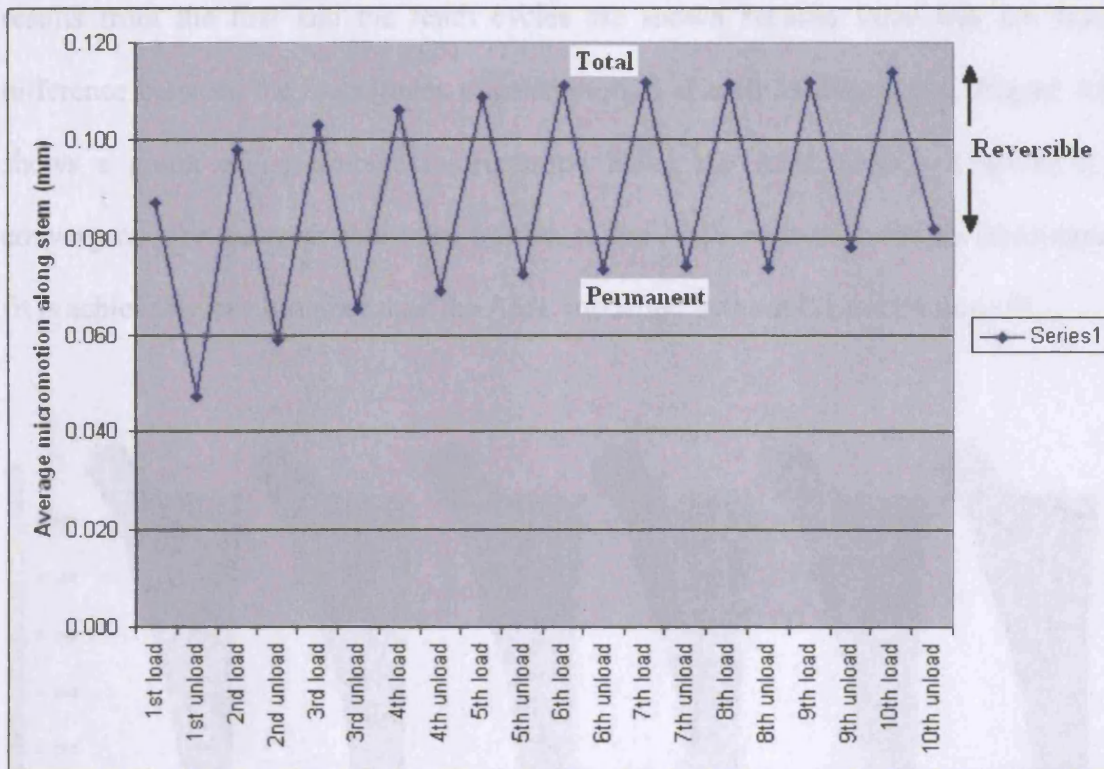


Figure 4.54: The graph of an average micromotion along the AML stem for 10 cycles to show total micromotion, permanent micromotion and reversible micromotion.

Figure 4.51 shows that the total micromotion increased as the load cycle was increased, and then stabilised after the 6th cycle. The second set of result (Figure 4.52) showed an increase in permanent micromotion as the load cycle was increased, with smaller magnitudes and different distribution than the total micromotion; the contour plots of permanent micromotion showed a gradual decrease in magnitude from proximal to distal at each loading cycle. The third set of result (Figure 4.53) showed that the distribution of micromotion for the reversible micromotion was similar to the total micromotion but with smaller magnitudes.

Figure 4.55 below shows contour plots of micromotion (total, reversible and permanent micromotions) for the AML modelled with an interference fit of 100 μ m. Only the

results from the first and the tenth cycles are shown because there was not much difference between the magnitudes of micromotion at each loading cycle. *Figure 4.56* shows a graph of an average micromotion along the AML stem - it shows that convergence for the reversible micromotion of the AML modelled with an interference fit is achievable much sooner than the AML modelled without the interference fit.

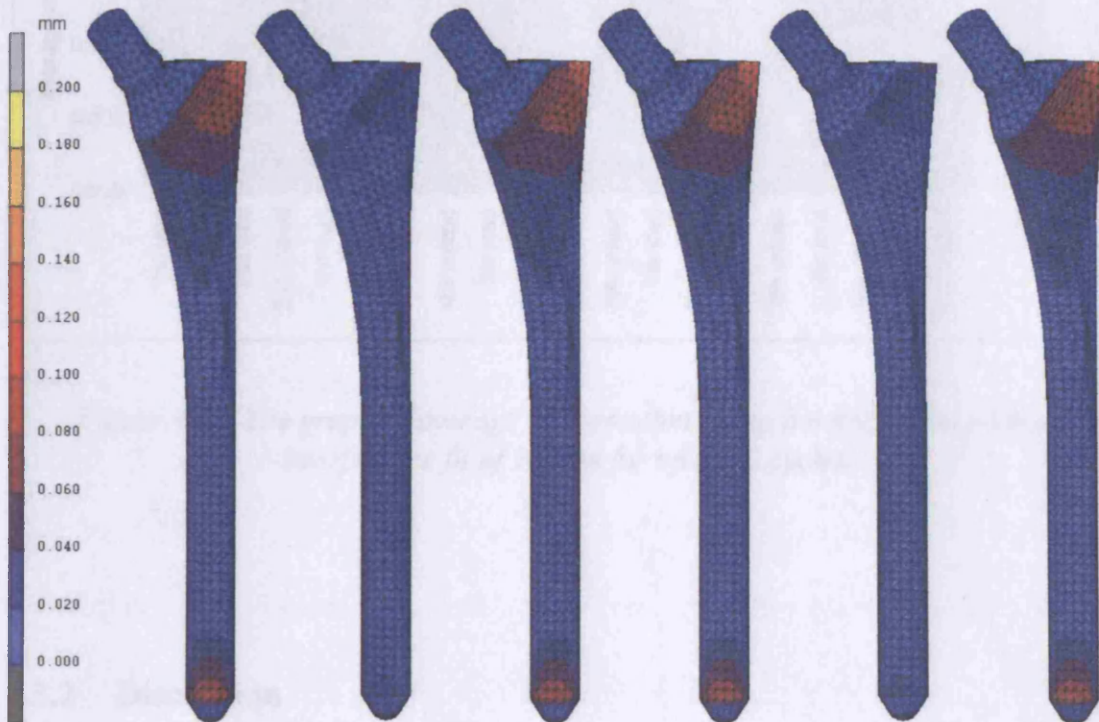


Figure 4.55: Total, Permanent and Reversible micromotion for the first cycle (first three stems) and the tenth cycle (last three stems) for the AML modelled with an interference fit of $100\mu\text{m}$.

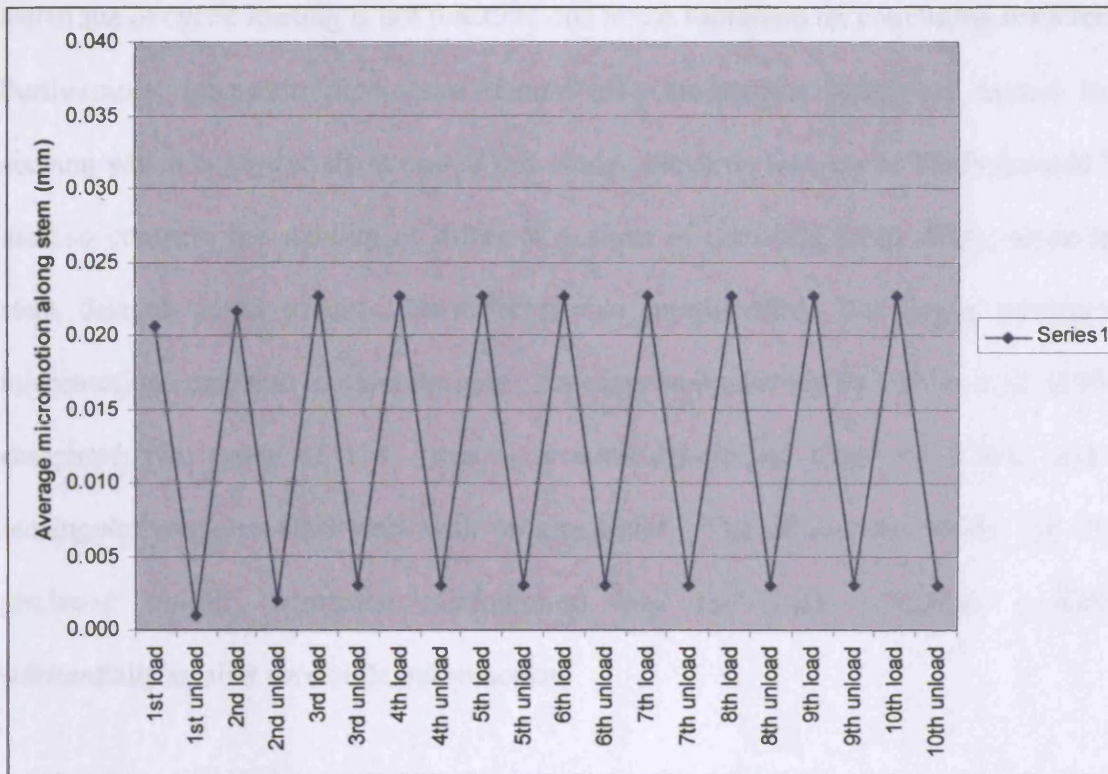


Figure 4.56: The graph of average micromotion along the AML stem with an interference fit of $100\mu\text{m}$ for up to 10 cycles.

4.3.2 Discussion

Similar to in-vitro experiments, micromotion can be categorised in FE analyses through cyclic loading. Reversible micromotion is defined as the difference of the measured minimum and maximum values for one loading cycle, and permanent micromotion is defined as the non-recoverable micromotion when the stem is unloaded at a particular time. The reversible micromotion is of particular importance because if the threshold limit is exceeded, fibrous tissue will form at the interface and fixation of the stem will be compromised. Migration, on the other hand, is one of the predictors for aseptic loosening (Kobayashi et al. 1997), but predicting long term instability using the current

technique of cyclic loading is not practical due to the limitation on computing resources. Furthermore, long-term predictions should also incorporate biological factors into account which is beyond the scope of this study. Nevertheless, cyclic loading could be used to compare the stability of different designs of cementless hip stems; some hip stem designs could produce lower reversible micromotion, but larger permanent micromotion compared to other designs. An experimental study by Buhler et al. (1997) compared two types of hip stems – a conically-shaped Cone prosthesis and a rectangularly-tapered CLS stem with proximal ribs. The authors found that the CLS produced smaller permanent micromotion, and the Cone prosthesis produced substantially smaller reversible micromotion.

Apart from the geometry of the stem, micromotion results could also be different between a cadaver micromotion study and a retrieval micromotion study. A retrieval study by Whiteside et al. (1993) of the AML and the Mallory-Head prostheses showed that recoverable micromotion was larger than permanent micromotion (average micromotion $87\mu\text{m}$ and $52\mu\text{m}$ respectively). This is different from cadaver micromotion studies where migration was found to be larger than reversible micromotion. Less migration was observed on retrieved implants because the ingrowth of bone onto the stem surface provided extra stability and prevented the stem from sinking.

Our FE results showed that reversible micromotion did not change much throughout the ten load cycles for both AML stems modelled with and without an interference fit. For the AML modelled without an interference fit, the reversible micromotion must be calculated from one complete cycle, i.e. the difference between the minimum and

maximum of one loading cycle. This is because permanent micromotion was significant when an interference fit was not included. However, when a maximum interference fit of 100 μ m was included, permanent micromotion was negligible. The micromotion result at the first maximum load is therefore a reasonable estimate of the reversible micromotion. Since all analyses in this study will include interference fit, only micromotion result from the first load is needed.

4.4 The effect of muscle loads on micromotion.

Another parameter that still remains the topic of discussion in biomechanics as a whole and in hip biomechanics in particular is the effects of muscle forces. There are many muscles acting on the hip joint as described in Chapter 1, and they are usually ignored in experimental or FE work due to their complex nature and the large variations found between patients during physiological activities.

Most in-vitro experimental work on micromotion used only the joint contact force, and ignored any muscle forces (Bachus et al. 1999; Berzins et al. 1993; Otani et al. 1993; Schneider et al. 1989; Whiteside et al. 1993; Whiteside & Easley 1988). The joint contact force is applied to the head of the implant with magnitude and direction

simulating physiological activities such as walking or stair-climbing. Several authors included the most significant muscle forces such as the abductors (Engh et al. 1992) or the extensor muscles (Burke et al. 1991) by means of woven nylon strips. These strips were attached on the outer cortex of the bone at one end and to the testing machine at the other end. The required magnitudes of these muscle forces were obtained by tightening or loosening the strips. The maximum number of muscles simulated in micromotion experimental work are three – the abductors, adductors and extensors (Doehring, Rubash & Dore 1999).

Similar observations are found in the literature for FE micromotion studies. Most of these studies used only the joint contact force (Kuiper & Huiskes 1996; Rubin et al. 1993; Viceconti et al. 2000; Viceconti et al. 2001), whilst others included the abductor muscles as well (Ando et al. 1999; Biegler et al. 1995; Keaveny & Bartel 1993). There have been no reports of FE micromotion studies that used more than one muscle forces, or to study the effects of muscle forces on micromotion and stability. There is, however, an FE study looking at the effect of muscle forces on the stress distribution in a cemented hip arthroplasty (Stolk, Verdonchot & Huiskes 2001). The authors reported that the hip-joint contact force and the abductor muscle load adequately described the stress/strain distributions in the hip during physiologic walking cycle. The other muscle loads considered in that study; the iliotibial tract, the adductors and vastii, had relatively small effects on the stress distribution. However, they did observe a slight effect of these muscles during the heel-strike phase of the gait cycle, where the magnitudes of the muscle forces were largest.

To the author's knowledge there are no FE studies looking at the effect of muscle forces on the predicted stability of hip stems. In this section, two separate datasets of muscle forces from the work of Duda (1998) and Fisher (1999) will be used to study the effects of muscle forces on the predicted stability of cementless hip prostheses.

4.4.1 Materials and Methods

Two different sets of muscle forces data were used in this section. The first one was from the work of Fisher (1999) for the three distinct phases of a gait cycle – the heel-strike, the mid-stance and the toe-off. The directions of these muscle forces were derived from the geometric data extracted from the VHP dataset, and the magnitudes of the muscle forces and the hip joint contact forces were based on predictions by Brand and co-workers (Brand et al. 1994; Brand, Pederson & Friederich 1986). The second dataset was obtained from the work of Duda (1998) where muscle forces for two physiological loadings – walking and stair climbing – have been measured.

Two different datasets were used because there are differences between the Fisher's dataset and the Duda's dataset. The first was the muscle forces measured by the researchers. Fisher calculated forces for muscles such as the Glutei muscles (Maximus, Medius and Minimus) and the Piriformis around the greater trochanter area, the Iliopsoas in the lesser trochanter area, and the Adductor muscles (Magnus and Minimus) along the linea aspera on the posterior side of the femur (*Figure 4.58*). Some of these muscles, such as the Adductor Magnus and Minimus, have several points of attachment, whilst the Gluteus Medius and Minimus were separated into components

based on multiple tendons which converged into one point of attachment. Duda, on the other hand, calculated forces for muscles such as the Abductor, Tensor Fascia Latae and the Ilio-tibial tract on the greater trochanter area, the Vastus Lateralis on the lateral femur and the Vastus Medialis on the medial femur (*Table 4.6*).

Apart from differences of the muscle forces, the loading vector of the joint contact force was also different. Fisher's joint contact force for the toe-off phase of the gait cycle was much larger than Duda's walking and stair-climbing loads. The heel-strike phase, which had the lowest magnitude compared to the mid-stance and the toe-off, was almost similar in magnitude to Duda's stair-climbing (1,966N in Fisher's compared to 2,017N in Duda's). The toe-off phase of the gait cycle had magnitude almost 1kN more than Duda's stair-climbing (2,942N in Fisher's compared to 2,017N in Duda's). The difference in the joint contact force between Duda's walking and stair-climbing was also not significant (1,910N for walking and 2,017N for stair-climbing). The torsional component of the joint contact force (the Y component), however, was almost twice in stair-climbing compared to walking (263.8N in walking compared to 486.8N in stair-climbing).

FE models of the femur and the hip implant were constructed as described in Chapter 2. The implant used was the AML hip stem and the material properties of the bone model were derived from the VHP CT dataset. The model was fully constrained at the distal end and loaded with three load cases representing the three phases of a gait cycle. Two cases were analysed for each phase - with muscle loads included (Loadcase 1) and without any muscle loads (Loadcase 2). The magnitude of the hip joint contact force, together with seven major muscle forces involved during walking are presented in *Table*

4.6, and the location of the muscle forces are presented in *Figure 4.57*. Both the magnitudes and the locations of muscles attachment to the outer cortex were taken directly from the work of Fisher (1999).

Another set of model was loaded with physiological walking and stair climbing using the muscle forces data from Duda (*Figure 4.58*). The table in *Figure 4.58*, taken directly from the HIP CD 98 (1998), was originally in percentage of body weight (%BW) and has been calculated into magnitudes based on a patient body weight of 800N. Two cases were again compared – the one with muscle forces (loadcase 1) and the one without muscle forces (loadcase 2). The global coordinate system used in these analyses has been described in Chapter 2. The models were solved using the FE package MARC-Mentat.

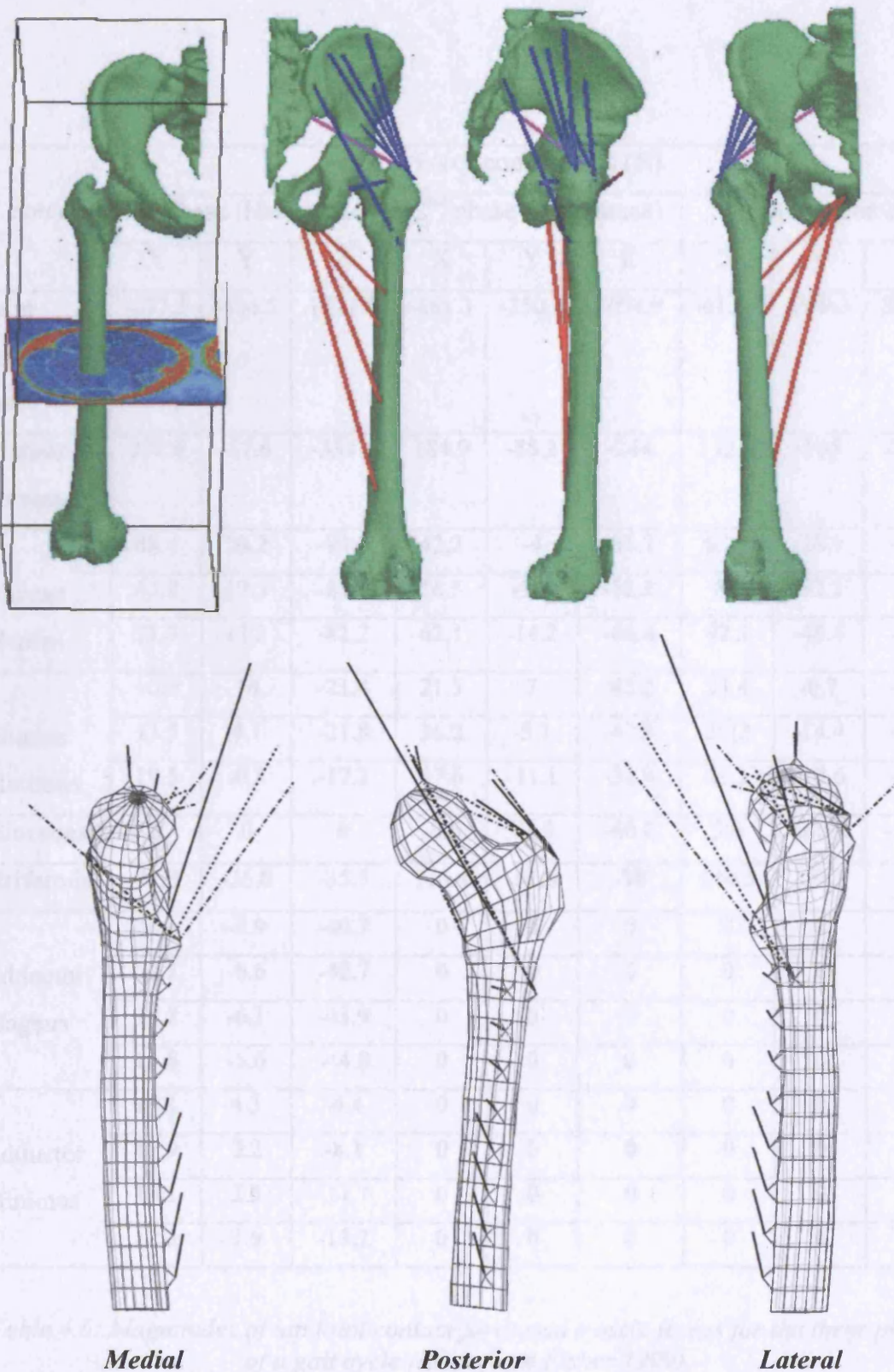
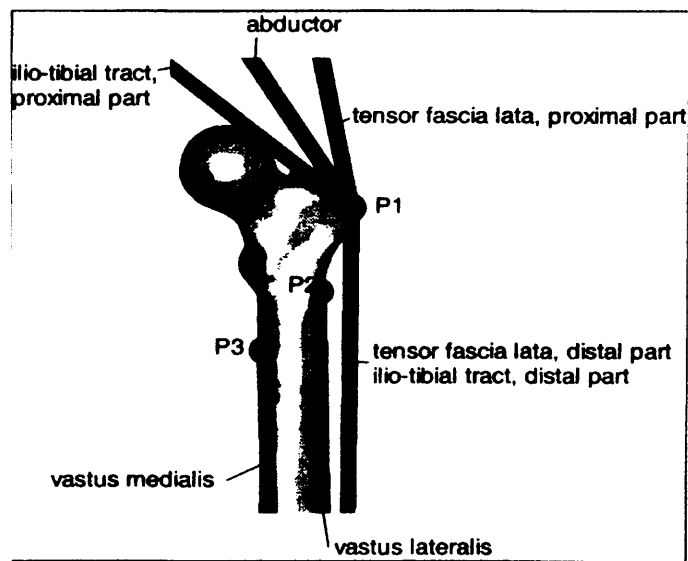


Figure 4.57: Identification of muscle paths from the VHP dataset (top). The magnitude and direction of the muscle forces and joint contact force for the three phases of the gait cycle (bottom). Solid lines are for heel strike, short-dots are for mid-stance and long-dots are for toe-off. (Picture taken from Fisher 1999)

Force	Force components (N)								
	1 st phase (Heel strike)			2 nd phase (Mid stance)			3 rd phase (Toe-off)		
	X	Y	Z	X	Y	Z	X	Y	Z
Joint contact force	-857.3	-404.5	1722.5	-861.3	-250.8	2056.9	-613.7	-219.3	2868.7
Gluteus Maximus	234.8	-37.6	-334.9	184.9	-85.2	-244	172.3	-105	-203.8
Gluteus Medius	48.4	26.2	-93.7	42.2	-4	-81.7	63.7	-28.9	-113.3
	64.8	19.5	-85.1	56.5	-7.8	-72.2	85	-32.2	-97.4
	71.3	11.3	-81.2	62.1	-14.2	-66.4	92.3	-40.4	-87.1
Gluteus Minimus	10.9	10	-21.4	21.5	7	-45.2	25.4	-0.7	-51.6
	13.5	4.1	-21.8	26.2	-5.1	-42.9	30.2	-14.4	-46.8
	19.5	-0.8	-17.2	37.6	-11.1	-31.9	43.2	-18.6	-33.2
Illiopsoas	0	0	0	-0.6	71.5	-60.8	3.6	160.6	-158.5
Piriformis	75.8	-26.0	-35.5	113.4	-61.6	-38	110.5	-70.1	-22.4
Adductor Magnus	24.1	-6.9	-40.7	0	0	0	0	0	0
	20.3	-6.6	-42.7	0	0	0	0	0	0
	17.8	-6.1	-43.9	0	0	0	0	0	0
	15.8	-5.6	-44.8	0	0	0	0	0	0
Adductor Minimus	17.1	4.3	-4.4	0	0	0	0	0	0
	15.9	3.2	-8.1	0	0	0	0	0	0
	14.1	2.5	-11.1	0	0	0	0	0	0
	12.3	1.9	-13.2	0	0	0	0	0	0

Table 4.6: Magnitudes of hip joint contact force and muscle forces for the three phases of a gait cycle (taken from Fisher 1999).



Normal walking				
Force (N)	X	Y	Z	Acts at point
Joint contact force	-433.8	-263.8	1841.3	P0
Abductor	465.9	34.5	-695.0	P1
Tensor fascia lata, proximal part	57.8	93.2	-106.0	P1
Tensor fascia lata, distal part	-4.0	-5.6	152.6	P1
Vastus Lateralis	-7.2	148.6	746.3	P2

Stair climbing				
Force (N)	X	Y	Z	Acts at point
Joint contact force	-476.4	-486.8	1898.3	P0
Abductor	563.1	231.4	-682.1	P1
Ilio-tibial tract, proximal part	84.4	-24.1	-102.8	P1
Ilio-tibial tract, distal part	-4.0	-6.4	135.0	P1
Tensor fascia lata, proximal part	24.9	39.4	-23.3	P1
Tensor fascia lata, distal part	-1.6	-2.4	52.2	P1
Vastus Lateralis	-17.7	180.0	1085.3	P2
Vastus Medialis	-70.7	318.1	2145.8	P3

Figure 4.58: Location of the muscles attachment used by Duda together with maximum loading configurations during walking and stair climbing (Taken from Hip CD 98).

4.4.2 Results

The following sets of results are contour plots of micromotion, and tables showing surface area with micromotion more than $50\mu\text{m}$. *Figure 4.59* shows that, in general, the distribution of micromotion was similar between loadcase 1 and loadcase 2, with the magnitude of micromotion in loadcase 1 (with muscles) being larger than in loadcase 2. *Table 4.7* shows that the area with more than $50\mu\text{m}$ of micromotion was greater by up to 6 times in loadcase 1 than that in loadcase 2 at all phases of the gait cycle. For loadcase 1, the results for the heel-strike and the mid-stance were more or less similar, with a small increase in micromotion for the toe-off phase of the gait cycle.

Figure 4.60 and *Table 4.8* show the results using Duda's muscle forces for loadcase 1 (with muscles) and loadcase 2 (without muscle forces). Similar to the results using Fisher's loadcases, the distribution of micromotion was similar between loadcase 1 and 2, with the magnitudes of loadcase 1 being larger than in loadcase 2. However, the difference in surface area with more than $50\mu\text{m}$ of micromotion was now even greater – up to 20 times more in loadcase 1 than in loadcase 2.

Results from Duda's loadcases with muscle forces also showed that stair-climbing activity was more critical than walking, because the surface area beyond the chosen threshold limit of $50\mu\text{m}$ was doubled in stair-climbing than in walking (*Table 4.8*). However, when the result of Duda's stair-climbing was compared to Fisher's toe-off phase of the gait cycle, the difference in the surface area was small.

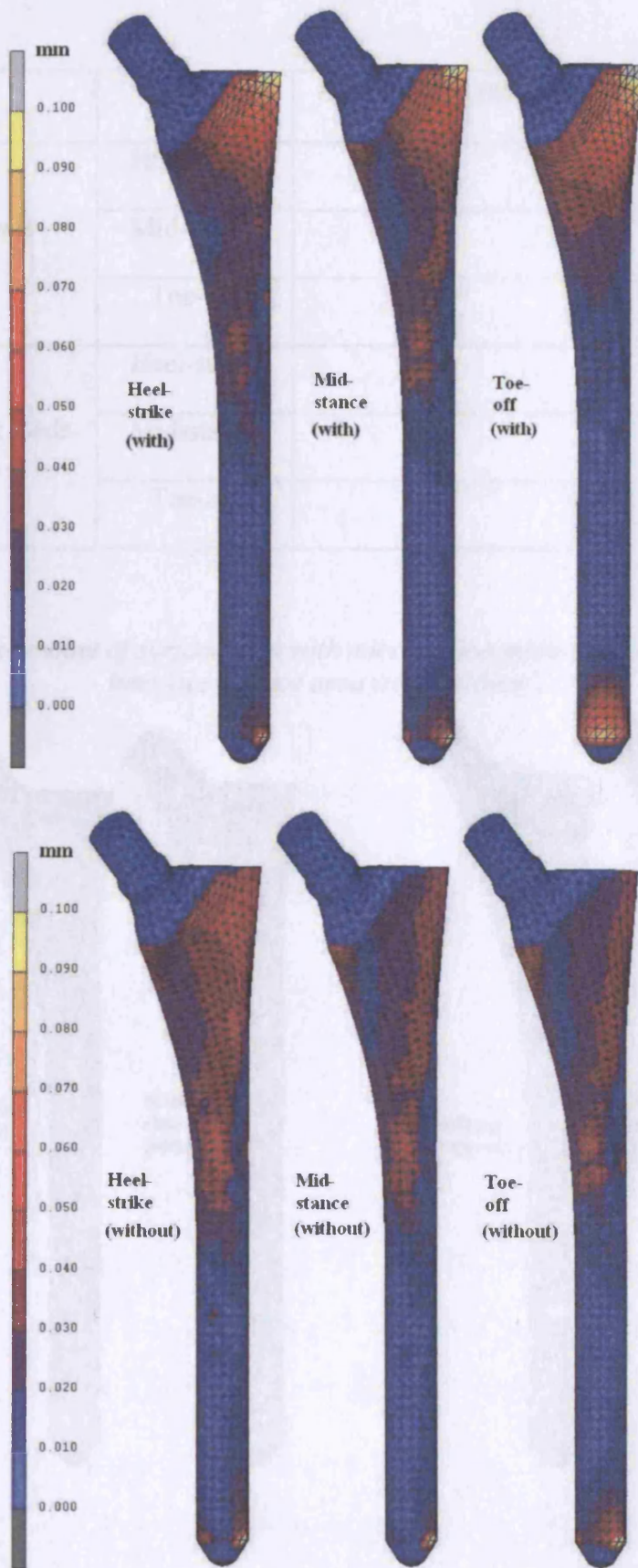


Figure 4.59: Contour plots of micromotion for the three phases of the gait cycle with (top) and without (bottom) muscle loads.

		Area > 50 μm (mm ²)	Percentage (%)
With Muscle loads	Heel-strike	529	6%
	Mid-stance	383	4%
	Toe-off	769	9%
Without Muscle loads	Heel-strike	89	1%
	Mid-stance	64	1%
	Toe-off	183	2%

Table 4.7: The amount of surface area with micromotion more than 50 μm . The total interface surface area was 8,976mm².

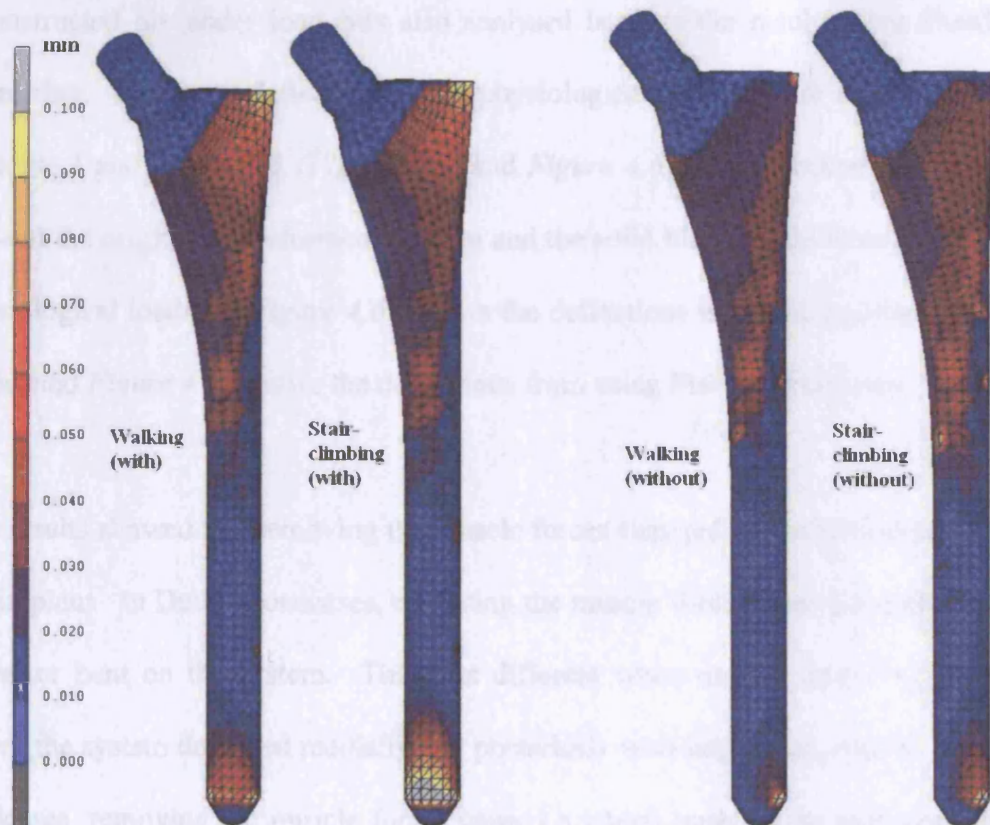


Figure 4.60: Contour plots of micromotion for walking and stair climbing with muscle loads and without muscle loads using Duda' loadcases.

		Area > 50 μ m (mm ²)	Percentage (%)
With muscle loads	Walking	540	6%
	Stair-climbing	999	11%
Without muscle loads	Walking	28	0%
	Stair-climbing	49	1%

Table 4.8: The amount of surface area more than 50 μ m of micromotion using Duda's loadcases.

Apart from analysing the contour plots of micromotion, the deflection of the reconstructed hip under load was also analysed because the results were found to be interesting. The stems deflections under physiological loading were compared between loadcase 1 and loadcase 2 (*Figure 4.61* and *Figure 4.62*). The outline of the implants showed the original un-deformed position and the solid blue models were implants after physiological loading. *Figure 4.61* shows the deflections using the muscle forces from Duda, and *Figure 4.62* shows the deflections from using Fisher's loadcases.

The results showed that removing the muscle forces changed the deflection behaviour of the implant. In Duda's loadcases, removing the muscle forces caused a relatively small posterior bent on the system. This was different when muscle forces were included where the system deflected medially and posteriorly with larger magnitudes. In Fisher's loadcases, removing the muscle forces caused a lateral push by the joint contact force on the head of the stem during heel-strike and mid-stance. The deflection was different when muscle loads were included, where the implant bent posteriorly. During the toe-off phase of the gait cycle, the implant bent further in the posterior and medial direction

when muscle forces were included. Without muscle forces, the implant would only bent very slightly in the posterior direction.

The deflection results obtained from Duda's loadcases with muscle forces were similar to the deflection during the toe-off phase of Fisher's. The magnitude of the deflection was slightly larger on Fisher's model because the joint and muscle loads were larger than Duda's. Duda's model also showed that the deflection during walking was similar to stair-climbing, with more deflection on the latter.

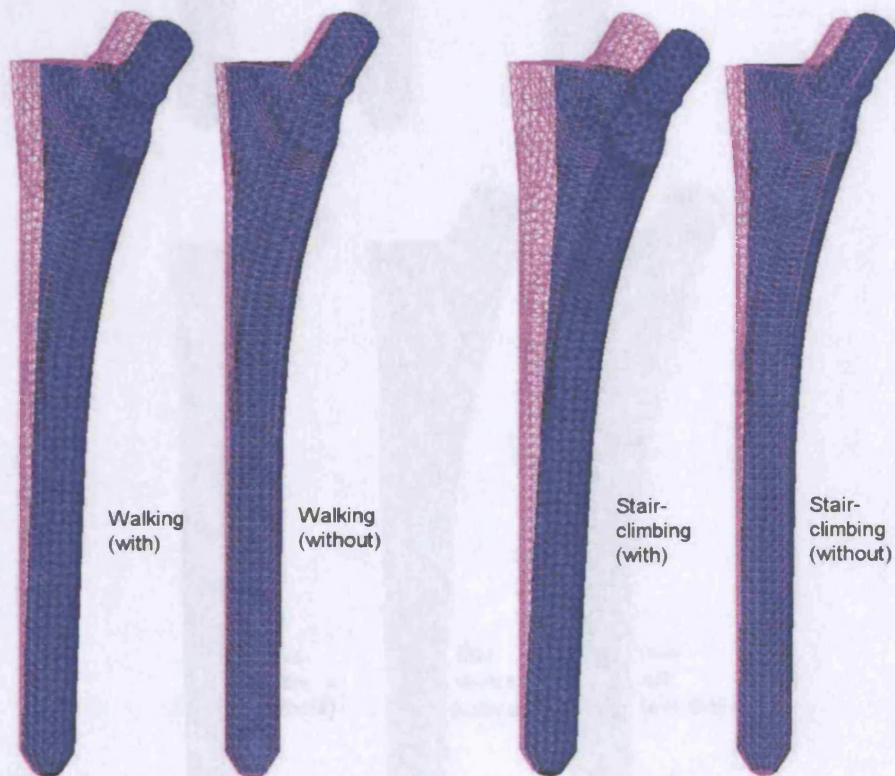


Figure 4.61: Deflection of the AML implant during walking and stair-climbing using Duda's loadcases for both with and without muscle loads.

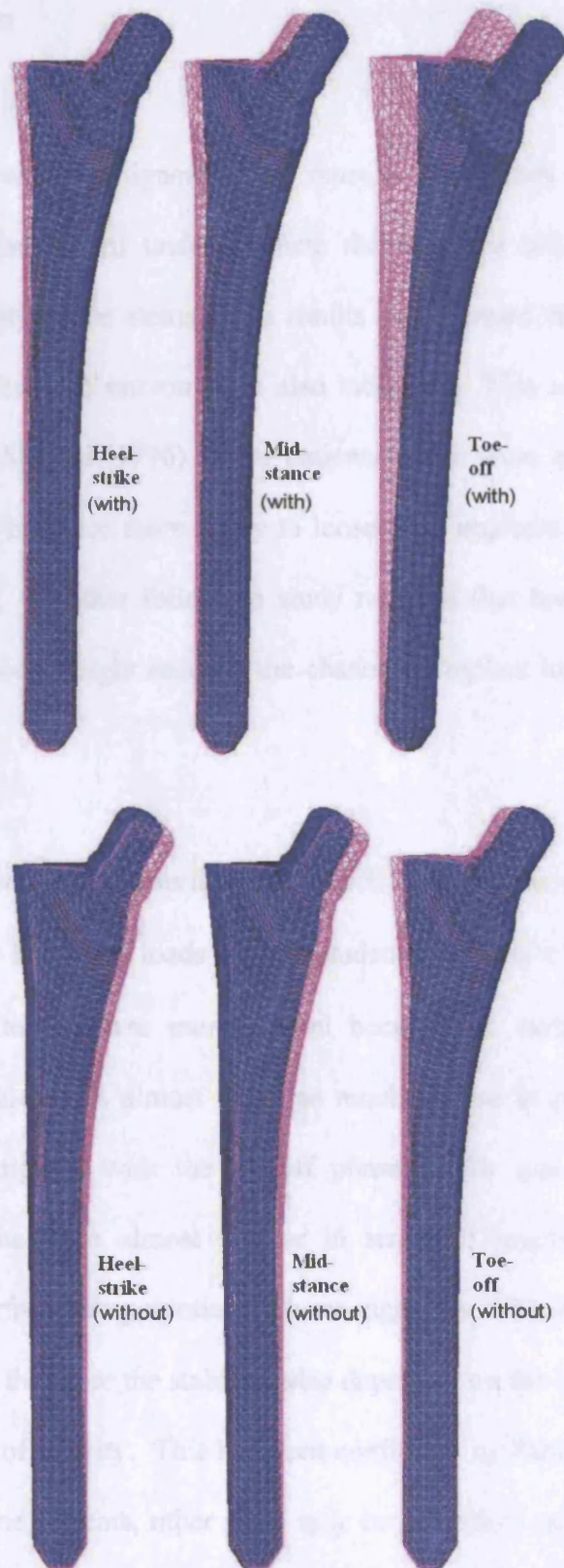


Figure 4.62: Implants deformation between with (top set) and without (bottom set) muscle forces for the three phases of the gait cycle.

4.4.3 Discussion

Our FE results showed that ignoring the muscle loads from FE analyses ^{is} ~~are~~ not recommended because it will under-estimate the interface micromotion, thus over-estimating the stability of the stems. The results also showed that as the loading was increased, the magnitude of micromotion also increased. This is in agreement with a study by Dickob & Martini (1996) where patients which were overweight by 30% or more were found to be twice more likely to loose their implants compared to patients with normal weight. Another follow-up study reported that lower hip joint force in patients with light body weight reduced the chance of implant loosening (Kim & Kim 1994).

The results also showed that the surface area which exceeded the chosen threshold limit of 50 μ m was larger if muscle loads were included. In Duda's loadcases, the results showed that stair-climbing was more critical because the surface area of potential fibrous tissue formation was almost twice as much as that in physiological walking. However, when compared with the toe-off phase of the gait cycle from Fisher's loadcases, the results were almost similar in terms of magnitude, distribution of micromotion and surface area potential for bone ingrowth. This shows that the amount of micromotion, and therefore the stability, also depended on the loading vector, and not just by specific type of activity. This has been confirmed by Pancanti et al. (2003) who reported that for some patients, other tasks may be as critical as stair climbing. Their micromotion study showed that the inter-subject variability had much more influence on the primary stability of cementless implants than the inter-task variability. Another

paper (Kotzar et al. 1995) reported that in their telemeterized study, maximum torque during walking (35Nm) was found to be larger than during stair-climbing (23Nm).

The FE results presented above showed that muscle forces must be included in FE micromotion analyses. This is in agreement with a couple of published FE work on the effect of muscle forces. As mentioned in the introduction to this section, one paper reported that abductor muscle load was required to adequately describe the stress-strain distribution in a cemented hip reconstruction (Stolk, Verdonshot & Huiskes 2001). A similar study on the effect of muscle loads on femoral strains during gait cycle showed that several muscle groups were important in order to reproduce correct physiological strain distribution. A 26% difference was found between a simplified loading configuration, and the one that included all muscle loads (Duda et al. 1998).

Our FE results that show deflections of cementless hip arthroplasty under load were also similar to other published FE work (Stolk, Verdonshot & Huiskes 2001). The authors found that the inclusion of abductor muscle force neutralised lateral bending of the reconstruction and increased medial bending. This is another reason why muscle forces should always be included in FE micromotion studies to ensure proper physiological deflection of the femur.

For the rest of the studies on hip micromotion, the loadcases simulating the toe-off phase of the gait cycle and/or the stair-climbing loadcase from Duda's will be used. The toe-off phase of the gait cycle is chosen because it has the largest magnitude of the joint contact force, whilst the stair-climbing has a larger torsional moment. This could be important when analysing hip stem designs because certain design could be better in

sustaining torsional moment (as found during stair-climbing) than others. Further analyses on the effects of hip stem geometry will be discussed on the next chapter.

4.5 The effect of bone material properties on micromotion

The final important parameter that needs to be addressed is the bone's material properties. Published FE studies on micromotion used various stiffness values for the femur. Whilst there is a couple of FE studies that used grey-scale values of CT datasets to assign bone material properties (Keaveny & Bartel 1993; Rubin et al. 1993), most of these studies used a simplified dual-properties – one stiffness value for cortical bone and another value for cancellous bone (Ando et al. 1999; Biegler et al. 1995; Kuiper & Huiskes 1996; Ramamurti et al. 1997; Viceconti et al. 2000; Viceconti et al. 2001). It is yet unknown if the difference in the bone's stiffness could affect micromotion predictions.

Even the assignment of bone properties using the grey-scale values raised some questions in terms of repeatability of results because the material properties vary depending on location within the bone, age and pathological condition. Most notably, human bones get weaker due to aging or due to skeletal diseases such as osteoporosis. In osteoporotic bone there is a significant loss of cancellous bone stock and structural deterioration of bone tissue. Although osteoporosis is not a disease leading to primary hip arthroplasty, patients which required hip replacement due to osteoarthritis or other

complications may also suffer from osteoporosis (Li and Aspden 1997). The reduced bone quality due to osteoporosis may affect the decision made by the surgeon in terms of a suitable hip stem (e.g. cemented or cementless, etc.) because osteoporosis increases the likelihood of fracture and may affect the primary stability of cementless hip prostheses.

This section will look at the interface micromotion of a cementless hip stem with regards to changes in the material properties of the bone using the density-modulus relationship proposed by Carter & Hayes (1977). Actual comparison between a normal healthy bone and bones suffering from skeletal disorders such as osteoporosis and osteoarthritis will be analysed further in chapter 6.

4.5.1 Methods and Results

As described in Chapter 2, material properties were assigned on an element-by-element basis based on medical imaging data. An in-house algorithm written by a previous PhD student (Hopkins 2004) was used, where the grey values of the CT images were related to the apparent density using a linear correlation (Cann & Genant 1980; McBroom et al. 1985). The modulus of elasticity of individual element was then calculated from the apparent densities using the cubic relationship proposed by Carter and Hayes (1977), $E=c\rho^3$, where $c=3790 \text{ MPa g}^{-3}\text{cm}^9$. This relationship is based on the assumption that cancellous and cortical bones are simply at different ends of a continuous spectrum.

To study the effect of bone quality on micromotion, the value of the constant ‘c’ was reduced, which reduced the stiffness value ‘E’ accordingly. Three values were chosen, as well as the original constant ‘c’ value of 3790, to reduce the ‘E’ value up to 35% (Table 4.9). In these analyses, the changes in stiffness value were assumed to be constant throughout the bone. Results from the analyses are shown in the following two pages.

Bone Quality	100%	75%	50%	35%
‘c’ value	3790	2843	1895	1327

Table 4.9: The percentage of bone quality together with the constant ‘c’ value used in the Carter & Hayes relationship.

Figure 4.63 shows contour plots of micromotion under simulated physiological walking and stair-climbing. The contour plots showed that as stiffness was reduced, micromotion increased accordingly in both physiological loadings. Table 4.10 and Figure 4.64 show the amount of surface area with micromotion $\geq 50\mu\text{m}$ for all four bone models. In general, the increase in surface area was similar between walking and stair-climbing, with physiological walking had more surface area unfeasible for bone ingrowth as the bone quality was reduced. When the stiffness was reduced to 35% of normal value, the surface area unfeasible for bone ingrowth increased to 50% in the case of physiological walking and 45% in the case of stair-climbing.

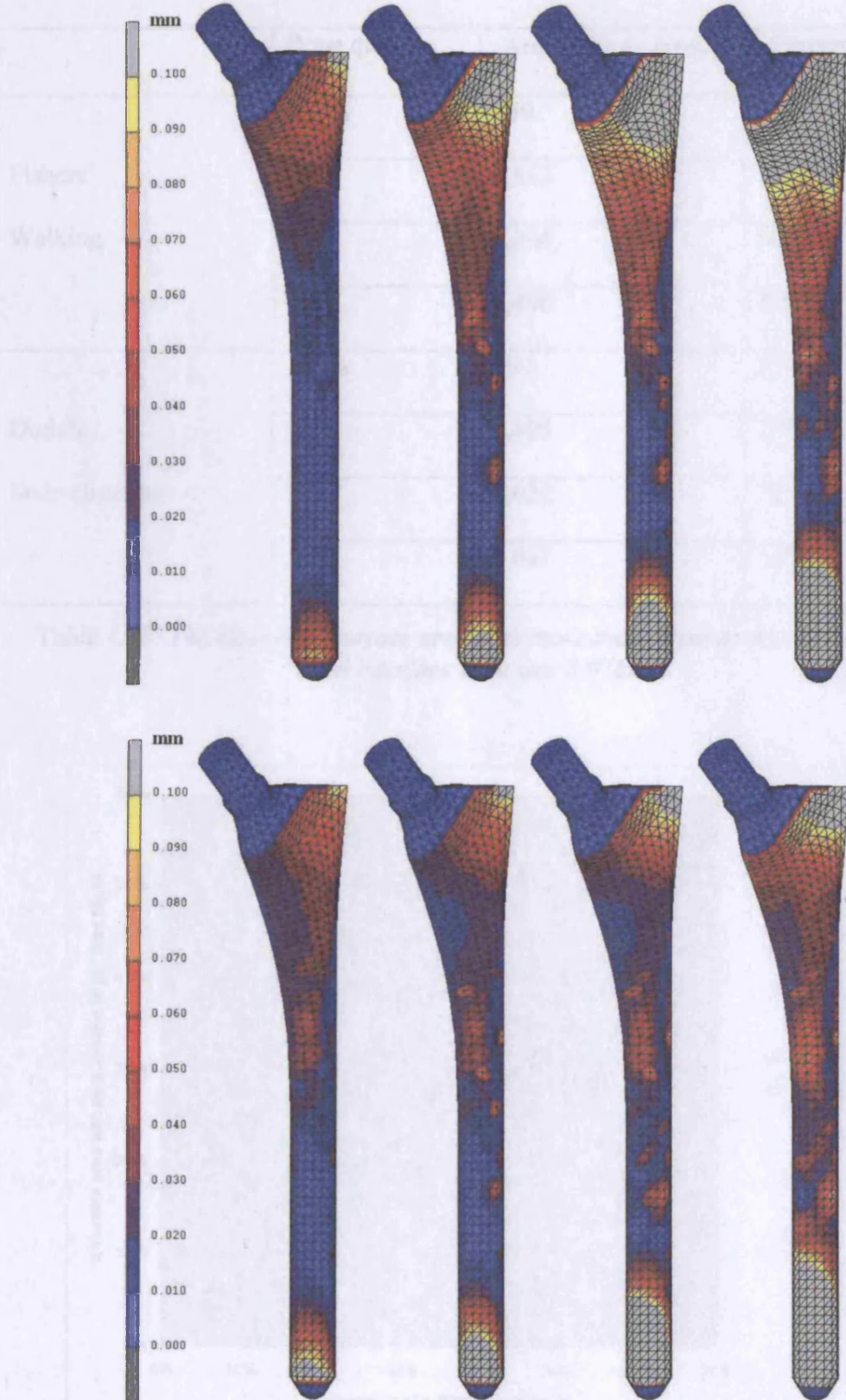


Figure 4.63: Contour plots of micromotion with decreasing stiffness values using Fishers's walking (top) and Duda's stair-climbing loads (bottom).

	Bone quality	Area > 50 μm (mm ²)	Percentage (%)
Fishers' Walking	100%	769	9%
	75%	1,813	20%
	50%	3,095	34%
	35%	4,496	50%
Duda's Stair-climbing	100%	999	11%
	75%	1,495	17%
	50%	2,622	29%
	35%	4,047	45%

Table 4.10: The amount of surface area with more than 50 μm of micromotion. The total interface area was 8,976mm².

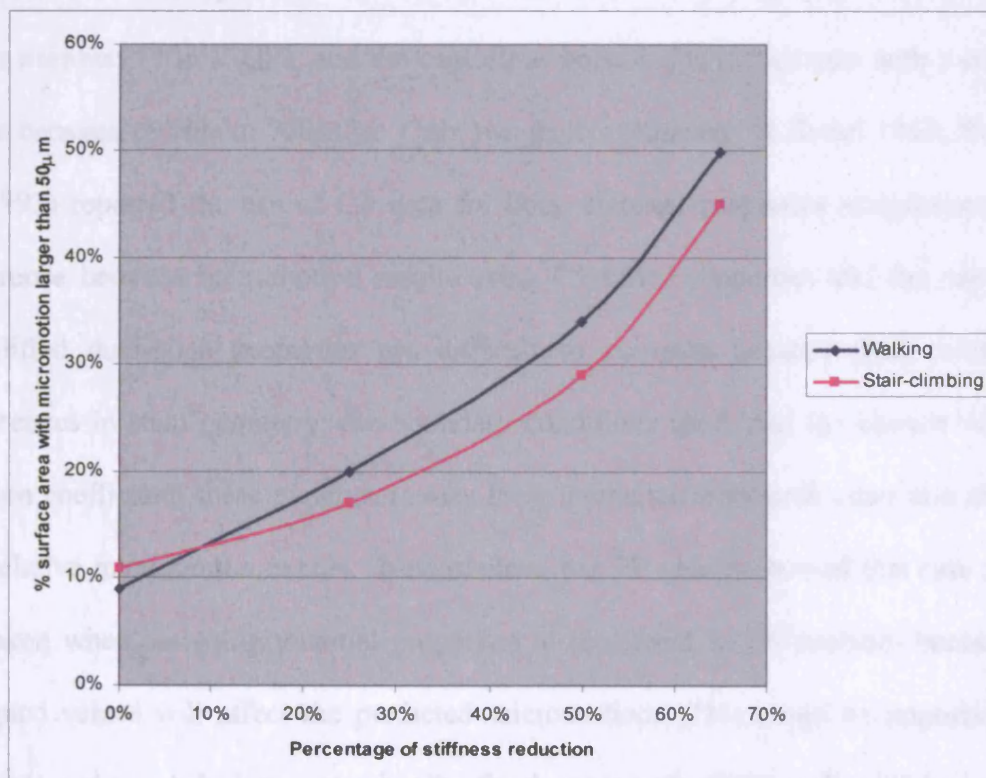


Figure 4.64: Graph showing the increase in surface area unfeasible for bone ingrowth vs the percentage of stiffness reduction.

4.5.2 Discussion

In this section we tried to answer if bone material properties affect the FE micromotion predictions by reducing the stiffness values of the bone using the modulus-density relationship. The results showed that bone stiffness affected the micromotion results of cementless hip stems; the stiffer the bone, the stable the implant. This is important to note because published FE studies on micromotion used various stiffness values for the femur. Most of these studies did not assign material properties based on medical imaging data (Ando et al. 1999; Biegler et al. 1995; Kuiper & Huiskes 1996; Ramamurti et al. 1997; Viceconti et al. 2000; Viceconti et al. 2001). The femur was separated into two types of bone – the cortical bone in the diaphysis with a constant value between 14 to 17GPa, and the cancellous bone in the metaphysis with a constant value between 69MPa to 750MPa. Only two papers (Keaveny & Bartel 1993; Rubin et al. 1993) reported the use of CT data for bone material properties assignment. The difference between micromotion results using CT-based properties and the one using simplified dual-bone properties are difficult to compare because there were also differences in stem geometry, the boundary conditions used, and the chosen value of friction coefficient; these parameters may have interacted with each other and affected the relative micromotion results. Nevertheless, our FE results showed that care should be taken when assigning material properties to the femur in FE analyses because the assigned values will affect the predicted micromotion. This could be important, for example, when analysing a proximally fixed stem with distal endosteal bone over-reaming; a constant value of 69MPa for the cancellous bone would produce larger micromotion than a value of 750MPa.

One major assumption used in this study was that the changes in bone stiffness were constant throughout the bone, and this was reflected in the results where there were minimum changes in the distribution of micromotion as the stiffnesses were reduced. This assumption may not be appropriate to bones with skeletal disorders such as osteoporosis or osteoarthritis because the changes may not be constant throughout the bone. Osteoporosis is characterised by the loss of cancellous bone stock mostly in the proximal area and the thinning of cortex in the diaphysis. The changes in stiffness may therefore be different – much lower stiffness would be found in the proximal area than in the diaphysis, and the thinning of the cortical diaphysis would mean an increase in the diameter of the stem used to ensure proper fill of the canal, thus increasing the stiffness of the stem (Li & Aspden 1997). Nevertheless, our FE results showed that bones with reduced stiffness values such as the one with osteoporosis would increase the chances of instability. The analyses from this study will be taken further in chapter 6 where actual CT datasets of osteoporotic and osteoarthritic bone will be used.

4.6 Conclusion

This chapter looked at five major parameters that could affect the prediction of interface micromotion. The chapter started with a study on friction coefficient where the results showed that there was a huge difference in micromotion between frictionless and frictional cases. Micromotion reduced as the values of friction coefficient were

increased until $\mu=0.8$, where a further increase in the coefficient did not cause significant changes to the micromotion results. A coefficient value of 0.4 was chosen for the rest of the study based on the FE results, which is also consistent with the experimental findings of Rancourt et al. The effect of interference fit on micromotion was also examined. The results showed that a press-fit of just $50\mu\text{m}$ was found to increase the stability of the stem by a factor of 10. The study continued with the analyses on cyclic loading. Two types of micromotion found in in-vitro experiments – the permanent and the reversible micromotion – could be modelled in FEA. However, when a maximum interference fit was included, permanent micromotion was negligible; this could be used to simulate the effect of a stem which has been firmly seated inside the canal. The micromotion results obtained when the implant is fully loaded could be used as a reasonable estimate to the reversible component of micromotion. The analyses were then continued with the effect of muscle forces on micromotion. The results showed that muscle forces must be included in all FE analyses in order to achieve proper deflection of the whole system, and not to over-estimate the stability of cementless hip stems. And the final section of this chapter concluded that micromotion prediction does depend on the material properties of the bone. More micromotion was found in bone modelled with lower stiffness values.

Chapter 5 The Effect of Hip Stem Designs on Interface Micromotion

The design of hip prostheses has been evolving since the inception of hip replacement three decades ago. Design changes occurred due to various radiographic and clinical problems and failures after hip arthroplasty. These problems included osteolysis due to wear particles, adverse bone remodelling due to unphysiological loading of the femur, and thigh pain and aseptic loosening due to inadequate stability.

Controversy exists with regards to the type of fixation that could achieve sufficient stability. Should it be cemented, cementless or a combination of both? The earlier generation of cementless stems showed inferior outcomes compared to the cemented designs at that time (Kim, Oh & Kim 2003). However, recent follow-up reports of both cemented and cementless designs showed that they are both successful and stable

implants. The key point is to get the right stem design for the method used. Stems which are designed for a cemented technique may not work in a cementless environment. The design may need some modification in order to achieve proper and adequate stability. For example, the stem in a cementless design needs to be made broader than its cemented counterpart so that it can appropriately fill the canal. The surface finish of cemented stems may also not be suitable in a cementless design. Cemented hip stems with proven clinical success such as the Stanmore (Biomet), C-Stem (DePuy) and Exeter (Stryker) have polished surfaces. These surfaces, however, are not suitable for cementless design because they lack friction and the surface texture that is needed for proper primary and secondary fixation. The result can be thigh pain and eventual loosening of the stem (Phillips & Messieh 1988).

The design of cementless femoral components is controversial. Debate exists regarding the most suitable type of material (e.g. CoCr or Ti alloy), surface finish or texture (e.g. grit-blasted or HA-coating or beads), extent of porous coating (e.g. partly coated or fully coated), and overall geometry (e.g. cylindrical or anatomic). Companies manufacturing cementless stems have certain objectives and differing philosophies regarding what they believe to be a successful implant design. There are two main schools of thoughts on the philosophies of cementless hip stems' fixation – Proximal fixation and Distal fixation. As the name suggests, proximal fixation relies on the proximal part of the stem to achieve stability, which in turn means relying on the cancellous bone in the greater trochanter area. Distal fixation, on the other hand, relies on the stiff cortical support distally. Apart from the proximal and distal fixation, there is also a design philosophy based on the principle of tapered fixation; a wedge-shaped femoral-component geometry with decreasing proximal-to-distal dimension. This design

philosophy proposes a gradual proximal-to-distal off-loading in an effort to mimic the normal physiological loading of the femur (Mallory et al. 2002).

Getting a hip stem designed with adequate stability is important. One of the major problems associated with unstable stems is that it causes thigh pain. In a two-year follow-up report of the Bichat III cementless stem (Duparc & Massin 1992), 16% from a total of 203 hips were revised due to persistent thigh pain. All the revised stems were found to be loose. From the unrevised stems 60% of them also complained of pain, and their symptoms have been attributed to micromotion of the implant relative to the endosteal bone. The now defunct Bichat III was anatomically shaped, fluted, made of titanium and had a smooth surface. Another follow-up study (Dickob & Martini 1996) was conducted on the PM prosthesis which had a similar rate of revision (15%) to the Bichat III. The PM stem has a tapered design with a collar, made of titanium alloy, and has a smooth surface with drop-shaped macrofeatures on its anterior and posterior surfaces. Clinical assessment from the unrevised group showed that only 27% of the patients were completely free from pain. The study, however, did not conduct any radiographic assessment, and as such it was unknown if the reported thigh pain could be associated with loosening.

A follow-up study of the Harris-Galante stem (Zimmer) showed that 28 out of 77 hips (45%) had slight, occasional, or mild pain (Clohisy & Harris 1999). Twelve of them (16%) were revised for aseptic loosening and osteolysis. From the unrevised hips, 11% of the components were found to be loose. Another stem with similar geometry to the Harris-Galante, the HGP-1, has also been reported (Cruz-Pardos & Garcia-Cimbrello 2001). A total of 93 HGP-1 were analysed and thigh pain was found in 28 hips (30%)

and loosening in 15 stems (16%). The authors found a high correlation of thigh pain with unstable fixation, subsidence and poor femoral fill.

Other cementless designs, however, have shown better results in terms of reported thigh pain. A 6 year follow-up study of the Bi-Contact stem (Aesculap) showed that none of the 153 implanted stems was revised for aseptic loosening (Badhe, Quinnell & Howard 2002). Only 6% reported having anterior thigh pain and the authors commented that this was due to unsatisfactory fixation of the proximal stem against rotational forces which caused micromotion at the bone-stem interface. A longer 9 year follow-up study of the same stem (Eingartner et al. 2000) showed that only 3 out of 214 stems were revised due to subsidence and aseptic loosening. The rest were found to be stable with no radiographic evidence of loosening (no significant radiolucent lines) and 85% reported no pain or slight pain.

Another cementless design, the Alloclassic, has also shown good results at 8 years follow-up (Delaunay, Cazeau & Kapandji 1998). The authors reported that at the end of the first year, thigh pain was recorded in 6 hips (4%) and a subsidence rate of more than 2mm in 21 hips (14%). However, at the last follow-up, only 1 hip out of 147 had slight thigh pain and no radiographic loosening was found. A longer follow-up study of the same stem (Delaunay et al. 2001) showed that thigh pain only occurred in 3 hips (2.5%) at 10 years. Again no loosening was found radiologically.

Another cementless stem with different design geometry to the Alloclassic is the AML – the latter is a straight cylindrical, slightly longer stem whereas the former is rectangularly tapered. A follow-up report (Engh, Bobyn & Glassman 1987) showed

that the fully porous-coated AML had 14% incidence of occasional thigh pain felt at the stem tip. They associated this with proximally well fixed stems but occurrence of interface motion between the tip of the relatively stiff stem and the relatively more flexible femoral shaft. They have also found that good press-fit stems showed lower incidences of thigh pain, and that the correlation was statistically significant. Another author (Whiteside 1989) also reported a similar observation, that a tight distal fit correlated with a lower incidence of thigh pain. Pain was significantly more likely to occur in those patients with a loose distal fit (20 out of 38, i.e. 53%) than in those with a tight distal fit (2 out of 67, i.e. 3%).

In an attempt to reduce or eliminate the micromotion that causes thigh pain, several authors reported design adjustment to cementless stems. One paper (Incavo et al. 2004) reported the use of distal slots, arguing that the reduced stiffness obtained from the slots could reduce the high incidence of postoperative thigh pain reported for stiffer stems. However, at follow-up between 2 to 5 years, 13% of these hips had reported thigh pain – a similar rate to the stiffer non-slotted AML stem. Other modifications include over-reaming of the femoral medullary canal, as used for the ABG cementless stem. This anatomically shaped stem has distal endosteal bone over-reaming as a standard procedure, in order to reduce the postoperative incidence of thigh pain (Giannikas et al. 2002). The authors reported that only 2 out of 61 hips (3%) complained of intermittent thigh pain at 5 years. Another follow-up report (Rogers, Kulkarni & Downes 2003) of the same hip stem showed that mild thigh pain was noted in 6% of patients at 1 year, dropping to 2% at 3 years. Late bone ongrowth which reduces instability has been associated with this clinical result.

Excessive subsidence or migration has also been accepted as one of the criteria of loosening (Jacobsson et al. 1993). One paper (Petersilge et al. 1997) reported two Harris-Galante hip stems revised for aseptic loosening. The two stems had subsidence of 7mm and 10mm respectively. Another study reported subsidence of a different design to the Harris-Galante. The Roy Camille is anatomically shaped and had 5% (4 out of 77) of femoral component loosening (Chen et al. 1998). All of the revised components had more than 5mm subsidence and had continuous radiolucency greater than 2mm in width along the stem. Less than 5mm subsidence was seen in 8 stems, which occurred up to the 2nd postoperative year and then stabilised with evidence of bone ongrowth.

Aseptic loosening is a failure associated with the lack of stability and has been found to be one of the major problems in some cementless designs. Although this characteristic of implant failure could also be secondary to osteolysis due to wear, some authors reported that in some systems where wear was minimal, aseptic loosening still occurred. A follow-up study of a prototype carbon fibre-reinforced composite stem showed a very high rate of loosening – 92% at 6 years (Adam et al. 2002). No osteolysis was found and thigh pain only occurred in 4 cases. All revised stems showed fibrous fixation without any bone ongrowth. The femoral component had an anatomical shape, with distally smooth stem and proximal roughness achieved by interlaced carbon fibres. This stem, made of carbon fibre-reinforced composite, was more flexible than usual - the stiffness was about one third of that of metal stems. The authors blamed the high rate of loosening on deficient primary stability due to the bad design. Another stem with a similar reduction in stiffness, on the other hand, has been reported with success at 2 years follow-up (Karrholm et al. 2002). The reduced stiffness Epoch (Zimmer) was

compared with stiff Anatomic (Zimmer) stems, and both stems were found to be stable with no evidence of loosening.

There are also numerous follow-up studies comparing the results of various hip stems. One of these studies was mentioned in the previous paragraph, comparing between the straight cylindrical, less stiff Epoch stem to the anatomically shaped, stiff Anatomic stem. The results of the stems at 2 years were compared radiographically and clinically. The migration of the Epoch was not found to be statistically significant than the Anatomic, but the proximal loss of bone mineral density was significantly reduced for the Epoch.

Another follow-up study compared the results of three different implant designs – the AML, the PCA and the LSF (Haddad, Cook & Brinker 1990). The AML had a straight femoral stem with a collar and was coated in the proximal $\frac{2}{3}$, the PCA had an anatomically shaped collarless femoral stem and the LSF had an anatomically shaped femoral stem with a porous coated medial collar. Both the PCA and the LSF had circumferential proximal coating. The authors reported thigh pain and ≥ 3 mm subsidence rates of 22% and 9% respectively for the AML; 20% and 15% for the PCA; and 8% and 6% for the LSF. Micromotion at the distal end of the prostheses was believed to contribute to thigh pain. The LSF had a low incidence of subsidence and thigh pain and this was correlated to the design of the LSF which had a curved femoral stem with an anatomically designed cross-section, which was better in filling the canal.

Another comparative study was made between the long, collared, titanium alloy Butel stem with the short, collarless, cobalt-chromium PCA (Jacobsson et al. 1993). The

authors reported femoral component loosening of 43% for the Butel, but only 11% for the PCA. The Butel stem showed fewer signs of stress shielding radiologically, but the Harris hip score and reported thigh pain showed significantly inferior results at 2-years and 3-years follow-up than the PCA.

There is also a report comparing three different hip stem designs in patients younger than 40 years of age (Duffy et al. 2001b). The stems used were the PCA (39 stems), the HGP-1 (24 stems) and the Osteonics (18 stems). The HGP-1 was a straight cylindrical stem with proximal porous coat and the Osteonics had a tapered design. At the follow-up between 10 to 14 years, aseptic loosening was found in 8 PCA hips (21%), 2 HGP-1 hips (8%) and none of the Osteonics had been revised due to aseptic loosening.

A comparative follow-up study was also conducted on the tapered distally-fixed Bi-Metric stem and the anatomic proximally-fixed ABG stem (Laine et al. 2000). The tapered stem was found to be more stable than the anatomic; subsidence of ≥ 2 mm was more frequent with the anatomical ABG. The Bi-Metric showed excellent stability, but the good bone ingrowth around the distal area increased stress shielding of the proximal metaphyseal femur.

Apart from the global geometries, local features have also been introduced in an attempt to improve the stability of cementless hip stems. Local features can be found in the proximal and distal parts of the prostheses. Proximal macrofeatures include fins, grooves and other patterns of indentations and projections. Distal macrofeatures include fins, slotted and fluted designs. However, these features were found to have minimal impact on reducing micromotion or improving stability (Kendrick, Noble &

Tullos 1995). Most of these features were mainly designed to reduce the overall implant stiffness, particularly in the distal region. For proximal macrofeatures, there are papers reporting on various design features that could improve the stability of the stem. The introduction of a lateral flare, a proximal lateral expansion which was designed to engage the lateral cortex of the femur, was found to improve stability (Leali et al. 2002). Average subsidence of the stem with a lateral flare was 0.32mm at 2 years. Another paper reported the effectiveness of a proximal ridge on the press-fit titanium alloy SPF prosthesis in terms of subsidence at 5 and 6 years (Donnelly et al. 1997). They found that the migration of the ridged SPF was 0.6mm/year, slightly less than the one without proximal ridge at 0.8mm/year.

The effect of design changes on the APR-II cementless stems has been reported (Dorr & Wan 1996). Three APR-II stems were compared – the original (APR-II), the one with a distal modular sleeve (APR-IIS) and the one with circumferential coating with distal stiffness relief (APR-IIT). These changes were accomplished without any alterations in the original geometry of the stem. They were anatomically shaped with a collar and the first two stems had porous coating on the proximal part but not extended onto the lateral side of the stem. The APR-IIT showed better fixation than the APR-II and the APR-IIS. This better fixation was attributed to the circumferential coating of the APR-IIT and the stiffness relief due to the hollow section of the distal stem. Patients with the APR-IIT also had less significant thigh pain.

Another cementless design was adjusted and compared in a follow-up study of up to 5 years (Knight, Atwater & Guo 1998). The PCA prosthesis was adjusted to a midstem PCA, where the collarless proximal stem geometry in the trochanteric area was made

larger in the AP direction than the original stem, designed to bring the prosthesis into greater contact with cortical bone in the metaphyseal region. Distally the stem length was extended and contained an anterior curve to match the anterior curve of the femur. These modifications were found to enhance fill proximally, reduce the tendency to produce varus alignment and improve rotational stability.

There are also numerous reports of in vitro experimental work comparing the stability of various cementless hip stem designs. One paper (Gustilo et al. 1989) reported an experiment comparing the rotational stability of a long curved stem (232mm), a short straight stem (160mm), and a short, proximally curved stem (130mm). Synthetic femurs were used in the experiment to ensure reproducible results. These stems were tested under torsion for rotational stability. The effect of the long, curved stem was evaluated further by sequentially shortening it in increments of 15mm from 232mm to 157mm. The authors found that the long, curved stem was the most stable in torsion, followed by a shorter straight stem, and a short, proximally curved stem. As the long, curved stem was incrementally shortened by 1.5-7.5cm, the initial torsional stability was reduced in proportion to the amount of shortening.

An in vitro experiment has also been carried out to compare the stability of curved stems compared to straight stems (Berzins et al. 1993). They found that curved stems were more stable than straight stems at high angles of flexion such as during stair-climbing and rising from a chair, i.e. under torsional loads.

The other global design feature that has also been studied is the use of a collar – a projection between the neck and the body of the stem that sits on the medial calcar. The

effectiveness of a collar in terms of providing stability is still a subject of controversy. It was found that the collar could increase the stability of the implant, preventing further subsidence in distally fitted or loose hip stems (Whiteside, Amador & Russell 1988; Whiteside & Easley 1989). This could be particularly useful in earlier generations of hip stems, such as the PM prostheses where early migration, or total micromotion, was the main problem (Dickob & Martini 1996). However, elastic micromotion was not affected by the presence of a collar (Whiteside & Easley 1989). Another paper reported that clinical results at 5 years revealed that the presence of a collar had no effect on the adequacy of fixation (Meding et al. 1997). A perfect collar to calcar contact is needed in order for the collar to be effective, but this is difficult to realise in practice and difficult to maintain post-operatively (Kwong 1990). A finite element study on the effect of a collar on stability (Keaveny & Bartel 1993) showed that collar support was not necessarily important because relative motion could also be effectively controlled by having surface treatments which result in a high coefficient of friction at the bone-implant interface.

A comparative experimental study was made between the rectangularly tapered, proximally-finned CLS and the conically-shaped Cone prosthesis (Buhler et al. 1997). Two types of micromotion were measured – the total motion, usually termed subsidence, and the dynamic micromotion. The CLS was found to produce larger dynamic motion, whereas the Cone prosthesis was found to produce larger total motion. Another study compared the loosening loads between the straight cylindrical AML and the anatomical PCA (Phillips, Messieh & McDonald 1990). They found that the difference in loosening loads was not statistically significant.

Another in-vitro experimental work looked at four different types of cementless stems (Schneider et al. 1989b). Three of them, the CLS, the Zweymuller and the Muller 85 had a tapered design, and the fourth was the anatomical PCA. They found that the PCA had lower mean interface micromotion than the three tapered designs, with the CLS having the largest mean interface micromotion – up to 10 times more motion than the PCA. Another study also looked at a number of cementless hip stems under torsional loads (Gortz et al. 2002). Rotational micromotion was measured on the proximally-fixed anatomical ABG, the tapered with proximal fins CLS, the tapered with lateral flare Alloclassic and the straight cylindrical S-ROM. Synthetic femurs were used in the experiment for consistency of results. The rotational micromotion for the Alloclassic was larger proximally, but for the ABG and the CLS stems larger micromotion was found distally. These stems were therefore found to be true to their design concepts; the Alloclassic was distally-fixed whereas the ABG and the CLS were proximally-fixed. The rotational micromotion of the S-ROM was found to be similar between the distal and the proximal parts, showing that it was equally fixed along the stem.

A stability study on retrieved implants has also been conducted (Whiteside et al. 1993). Two femoral specimens – 1 Mallory-Head and 1 AML – were retrieved and tested for axial and rotational stability. No permanent micromotion was found for both specimens. The tapered design of the Mallory-Head, however, was found to have more elastic deformation than the straight cylindrical AML.

Apart from in-vitro experimental work and follow-up reports, there are also finite-element studies looking at the effect of design variables on the stability of cementless hip stems. However, these FE studies are fairly limited and were not comprehensive.

The effect of implant stiffness has been studied using FE, with 2D models (Kuiper & Huiskes 1996). The effect of the extent of coating has also been studied using the AML stem and varying the coefficient of friction along the stem (Keaveny & Bartel 1993). FE studies looking at the effect of stem lengths on bone remodelling have been done using the ABG (van Rietbergen & Huiskes 2001) and the An. C.A. cementless stems (Toni et al. 1996). However, an FE study on the effect of cementless stem lengths on stability has not been reported.

To the author's knowledge, there are only two papers comparing different designs of cementless stems. One paper reported an FE study comparing the Harris-Galante and the Mallory-Head prostheses (Biegler et al. 1995). In this study, the authors reported that both designs had similar micromotion. Stability was found to be most affected by the type of loading (more micromotion during stairclimbing than walking) than the overall geometry of the stem. Another study compared five types of cementless stems, two of them anatomic and the other three were straight cylindrical designs (Ando et al. 1999). Small changes were introduced in these five stems – the first anatomic model was asymmetric with a proximal anterior flare (FMS Anatomic), the second anatomic model was curved in the A-P plane and had proximal canal filling (IDS), one of the straight cylindrical models had a lateral flare (FMS), one without (FT) and one with a distal sleeve (FX). The authors showed that the anatomic stems, which were modelled with a perfect interface fit throughout the stem, were more stable than the straight stems.

It is widely accepted that the stability of cementless stems is crucial to their success and that their design plays a role in establishing fixation. In this chapter, FE analyses will be conducted on various design parameters to study their effects on micromotion and

therefore the stability of cementless hip stems. Based on the collected information from the literature, hip stem manufacturers and orthopaedic surgeons, several major aspects of the design of cementless stems will be analysed. It starts with the global geometry of cementless hip stems and then continues with other design parameters such as the stiffness of the materials, the length of the stem, proximal vs distal fixation design, and the effects of proximal macrofeatures. It is hoped that a better understanding of various design features on stability and the interactions between them would be beneficial in the design of new femoral prostheses.

5.1 The global geometry

Cementless hip stems come in different shapes and sizes. In order to analyse practically the effect of these different geometries on primary stability, the stems were grouped into several categories based on their features. There is no consensus at the moment in terms of grouping cementless stems according to their geometry, mostly due to the large variety of cementless stems available in the market today. Healy (2002) grouped cementless femoral components into 5 basic types with examples of each – the cylindrical distal filling (the AML, the Solution), the anatomic, proximal fit and fill (the PCA, the Anatomic), combination (the S-ROM, the Bridge), dual, tapered wedge (the Omnifit, the Osteolock, the Mallory-Head, the Synergy, the Summit), and flat, tapered wedge (the Tri-Lock, the Taperloc, the Accolade). Mallory et al. (2001) grouped them into three distinct design geometries & philosophies – the extensive porous coating with distal fixation (the AML), the anatomic proximal fixation (the PCA, the Anatomic) &

gradual proximal to distal off-loading tapered geometry (the Mallory-Head). Two other papers reported similar groupings (Bourne & Rorabeck 1998; Reitman et al. 2003). They grouped the overall geometry into three main categories - cylindrical, tapered and anatomic. Another paper, although it did not categorically group the different types of cementless stems, did mention a comparison between the tapered Taperloc stem to the anatomic PCA and cylindrical stems such as the Harris-Galante, the APR-1 and the AML (Parvizi et al. 2004).

A search was conducted in the literature for all follow-up studies and in-vitro experimental work to get as much information as possible on the various designs of cementless hip stems. Apart from the literature, nine cementless primary hip stem manufacturers were also included in the search:-

1. Aesculap, Tuttlingen, Germany.
2. Biomet, Warsaw, IN.
3. Corin Medical, Gloucestershire, UK
4. DePuy, Warsaw, IN.
5. Smith & Nephew, Memphis, TN.
6. Stryker Howmedica Osteonics, Rutherford, NJ.
7. S & G Implants, Lübeck, Germany.
8. Wright Medical Technology, Arlington, TN.
9. Zimmer, Warsaw, IN.

From this search, three groups based on the overall geometry of the stem were chosen similar to the one proposed by other authors mentioned above – the tapered design, the anatomic and the straight cylindrical. Hip stems which were not tapered in any plane in

the distal half were grouped together. Because all hip stems in this group were also cylindrical, the group was termed straight cylindrical (*Figure 5.65*). The tip of the stem may or may not be tapered. Tapered stems were defined as stems that have a proximal to distal taper in either or both the sagittal or longitudinal planes (single-planar / bi-planar tapered) (*Figure 5.66*). Some tapered designs such as the Mallory-Head also have a posterior-to-anterior taper in the coronal plane (tri-planar tapered). Anatomic stems were defined as stems designed with an anterior-posterior curve that mimics the natural curve of the human femur (*Figure 5.67*). The stems must therefore come in a left and right component.

All cementless femoral stems create a press-fit mechanical interface where contact pressures between two components of dissimilar modulus, the bone and the implant, produce deformation. The bone exhibits viscoelastic behaviour, which limits the effectiveness of the press-fit by relaxing the contact pressures at the interface (Howard et al. 2004). The cylindrical distal fixation stems rely on cortical support in the distal aspect of the stem for stability, whereas tapered stems rely on proximal, cancellous bone contact and a 3-point fixation pattern. The Anatomic stems employ a curved design in both A-P and M-L planes, and have a large proximal segment to achieve a closer match to the natural endosteal cavity of the proximal part of the femur. It has been claimed that this design feature optimise resistance to axial, bending and rotational forces (Kim, Oh & Kim 2003).



Figure 5.65: Femoral components with straight cylindrical design (the pictures are not resized to scale).



Figure 5.66: Femoral components with tapered design (the pictures are not resized to scale).




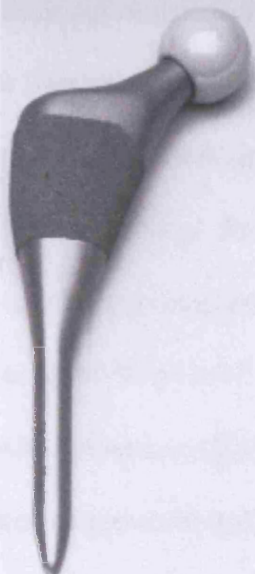



			
ABG (Stryker)	APR-II (Zimmer)	Carbon Fibre-reinforced composite (Adam et al. 2002)	IPS (DePuy)
			
Lubeck (S & G Implants)	PCA (Stryker)	Profile (DePuy)	

Figure 5.67: Femoral components with anatomic design (the pictures are not resized to scale).

The above groupings were made based on the overall geometry of the stem. The philosophies may or may not be grouped together. The straight cylindrical design, for example, may have two types of fixation – proximal and distal. The Prodigy is a distal fixation design, whereas the AML, though intended for distal fixation, can also work as proximal fixation design (Kim & Kim 1994). Similarly for the tapered group, the Alloclassic is distally fixed, whereas the CLS is also known to be a proximal fixation design. For the anatomical group, the ABG and the IPS employ a distal bone over-reaming technique for proximal fixation, but the Profile prosthesis, which uses a similar fixation concept does not use the over-reaming procedure. The issues of proximal and distal fixation concepts will be looked at in section 5.4.

In order to analyse the stability of these hip stems, a member of each group was chosen and analysed. The chosen design was only based on the availability of the 3D CAD model obtained from the respective manufacturer. They are the AML for group 1, the Alloclassic for group 2, and the ABG for group 3.

The Anatomic Medullary Locking (AML) hip stem (Depuy, Warsaw, Indiana) is a non-tapered collared design with a relatively longer stem. The shape of the stem is cylindrical to fit the medullary canal and tapered at the tip to help reduce the potential for thigh pain. Because the stem is not tapered, the implant does not wedge in place. Instead, fixation depends on a so-called ‘scratch fit’ between the rough external surface of the implant and a similarly shaped bone canal (Engh 1998). The stem is porous coated for about 80% of its length from the proximal end and is polished distally. It is made of Cobalt Chromium (CoCr) with the porous coating made of sintered CoCr beads with a mean pore size of 200 microns. The pores have been shown to provide a suitable

surface to encourage tissue ingrowth and improve the stability of hip stems (Engh et al. 1992).

The Alloclassic (Zimmer, Warsaw, IN) is a cementless, flat, tapered, collarless hip stem using distal fixation press-fit technique. The surface is fully grit-blasted (4-6 microns) with corundum particles for future bone ongrowth. A better proximal fit is achievable by having a lateral wing engaging the greater trochanter, claimed to improve axial stability. It is made of Protasul-100 titanium alloy (TiAlNb) where Niobium is used instead of the usual Vanadium used in titanium alloy. The straight taper is flat in transverse section and wedged shaped mediolaterally. It is designed to fit the femoral canal in the frontal plane but does not fill in the lateral plane. It achieves self-locking to the endosteal bone by way of 4 corners of its rectangular shape along the entire stem.

The Anatomique Benoist Giraud (ABG) hip stem (Stryker Howmedica Osteonics, Rutherford, NJ) is a cementless anatomic femoral component of roughened titanium alloy with a 50 microns coating of hydroxyapatite applied to its proximal $\frac{1}{3}$. A proximal press-fit technique is applied with distal femoral over-reaming as standard surgical procedure to avoid bone contact in this area. This design of proximal metaphyseal fixation in the ABG was an attempt to transfer stresses more proximally to maintain bone density.

5.1.1 Methods & Results

Although all three chosen implants - the AML, the Alloclassic and the ABG – have been grouped into different categories of hip stem designs, these implants had other unique characteristics or special features of their own (see *Figure 5.68* and *Table 5.13*). This made the analyses difficult as the specific features of the implants may have interacted with the global geometry and affected the overall primary stability. Therefore, these implants were adjusted, so that a proper comparison based on the groupings above could be made. For the AML, the collar was removed, the stem was shortened to the average length of the Alloclassic and the ABG, and the distinction between the porous-coated and the smooth section was ignored. The prosthesis was regarded as having a homogeneous surface structure throughout the stem. This also applied to the ABG, where the different surface finish between the proximal and distal part was ignored. The indentation features in the proximal part of the ABG were removed. The effects of this macrofeature on stability, however, will be looked at in the last section (section 5.5) of this chapter. The surgical technique of the ABG requires that the distal part is over-reamed to avoid cortical contact in this area. For the sake of analysing the different groups in this section, bone over-reaming was not modelled. It was assumed that there was perfect contact at the interface between the stems and the bone for all models. The coefficient of friction was set to 0.4 and an interference fit of 0.1mm was used throughout. The adjusted models will therefore be referred to as the ‘cylindrical’ (group1), the ‘tapered’ (group 2) and the ‘anatomical’ (group 3) designs respectively. The models were loaded in accordance with both Fisher’s gait analysis and Duda’s stair climbing loads and the results were then compared between each other.



Figure 5.68: Pictures of the AML, the Alloclassic and the ABG, taken from the manufacturer’s website.

	Fixation type	Material	Stem length	Stem shape	Symmetry	Surface finish
The AML	Distal	Co Cr	Long	Cylindrical	Yes	Porous-Coated
The Alloclassic	Distal	Ti Al Nb	Medium	Rectangular	Yes	Grit-blasted
The ABG	Proximal	Ti Al	Medium	Cylindrical	No	macrofeature

Table 5.11: The three types of hip stem designs analysed and their characteristics.

From the first set of results, bone elements with a surface area of more than 50µm of interface micromotion were adjusted so that contact between these elements and the implant was no longer available. This was done to simulate the effect of interfacial bone loss. A detailed description of the method has been explained in Chapter 2. The

models were then reloaded with physiological walking and stair-climbing loads to check for instability. The results are shown in the next few pages.

Figure 5.69 below shows that the magnitudes and distribution of micromotion were similar in all three types of implants, in both physiological walking and stair-climbing. Large micromotions were found in the proximal areas and around the distal stem tip. In terms of the amount of surface area with more than 50 μ m of interface micromotion, the range was between 8-10% for all designs (*Table 5.12*). It showed that no specific global design feature was better than the other.

After removing the bone with micromotion in excess of the chosen threshold limit to simulate interfacial bone loss, results were then compared once more (*Figure 5.70*, *Figure 5.71* and *Table 5.12*). In general, all designs were found to be stable with bone loss only increased slightly (up to 13%). The anatomical design was found to be the most stable with a very small increase in surface area above 50 μ m. The cylindrical design was the worst in stair-climbing with an increase in unfeasible surface area from 9% to 13%. The tapered design was the worst in physiological walking where there was an increase from 8% to 10%.

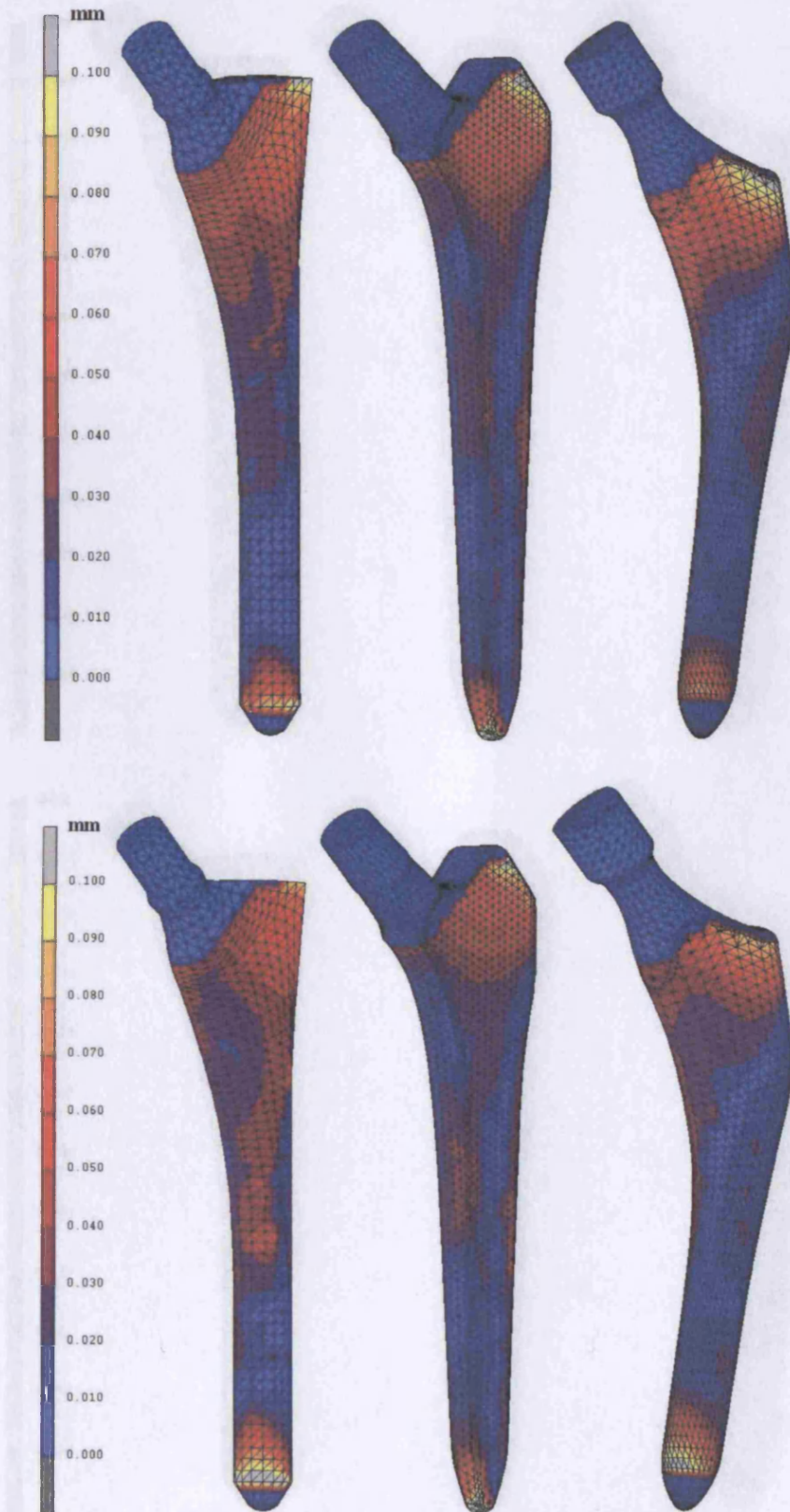


Figure 5.69: Contour plots of micromotion for the cylindrical (left), the tapered (middle) and the anatomical (right) using Fisher's gait loading (top) and Duda's stair-climbing loads (bottom) after the 1st iteration.

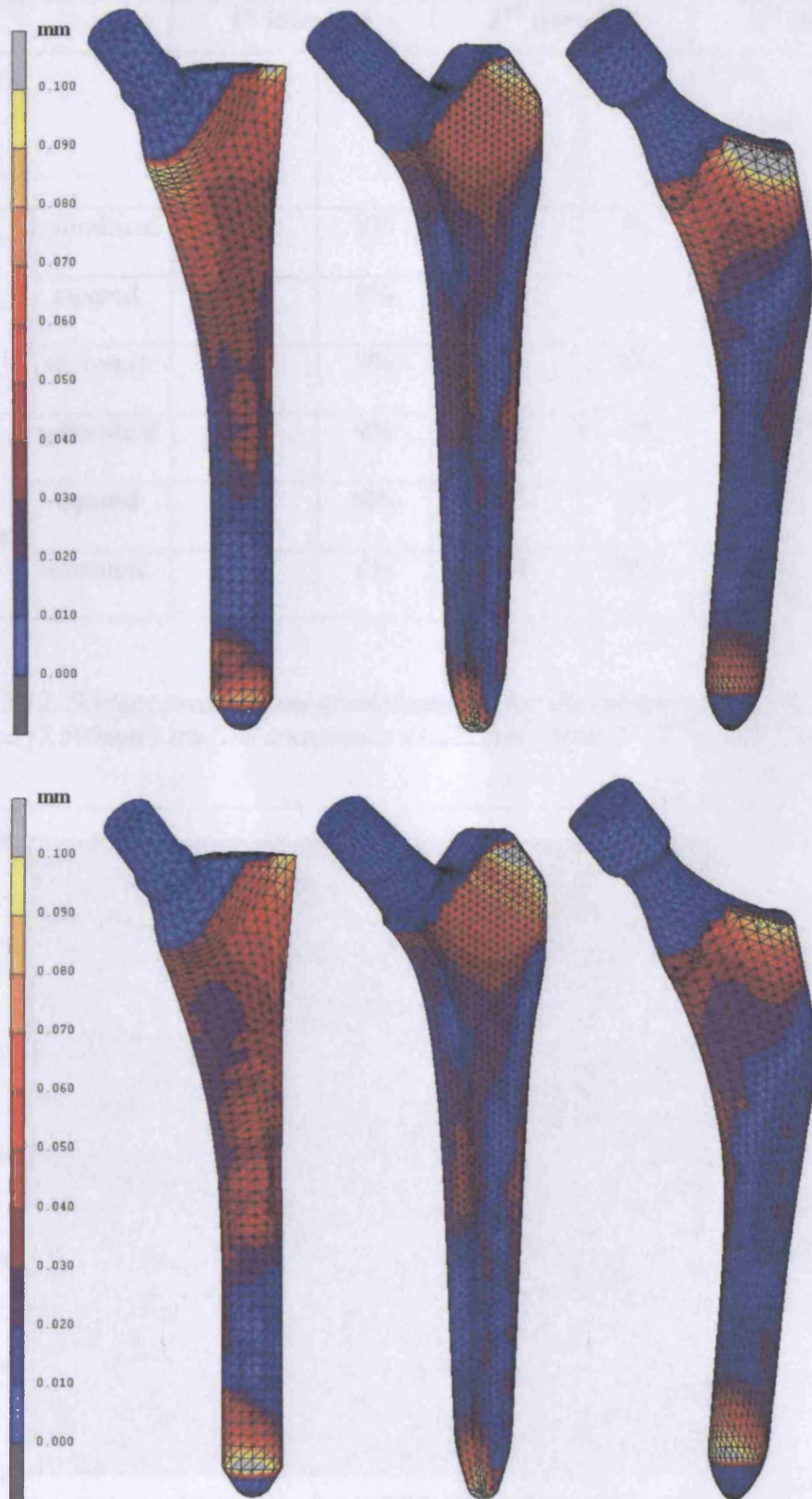


Figure 5.70: Contour plots of micromotion for the cylindrical (left), the tapered (middle) and the anatomical (right) using Fisher's gait loading (top) and Duda's stair-climbing loads (bottom) after simulated interfacial bone loss.

		1 st iteration		2 nd iteration		3 rd iteration	
		Area >50µm (mm ²)	%	Area >50µm (mm ²)	%	Area >50µm (mm ²)	%
Fisher's gait	cylindrical	604	8%	674	9%	695	9%
	tapered	642	8%	740	10%	771	10%
	anatomic	633	9%	653	9%	-	-
Duda's stair-climbing	cylindrical	647	9%	875	12%	951	13%
	tapered	757	10%	893	12%	925	12%
	anatomic	562	8%	584	8%	-	-

Table 5.12: Surface area >50µm of micromotion for the cylindrical (7,345mm²), the tapered (7,690mm²) and the anatomical (7,222mm²) after 1st, 2nd and 3rd iterations.

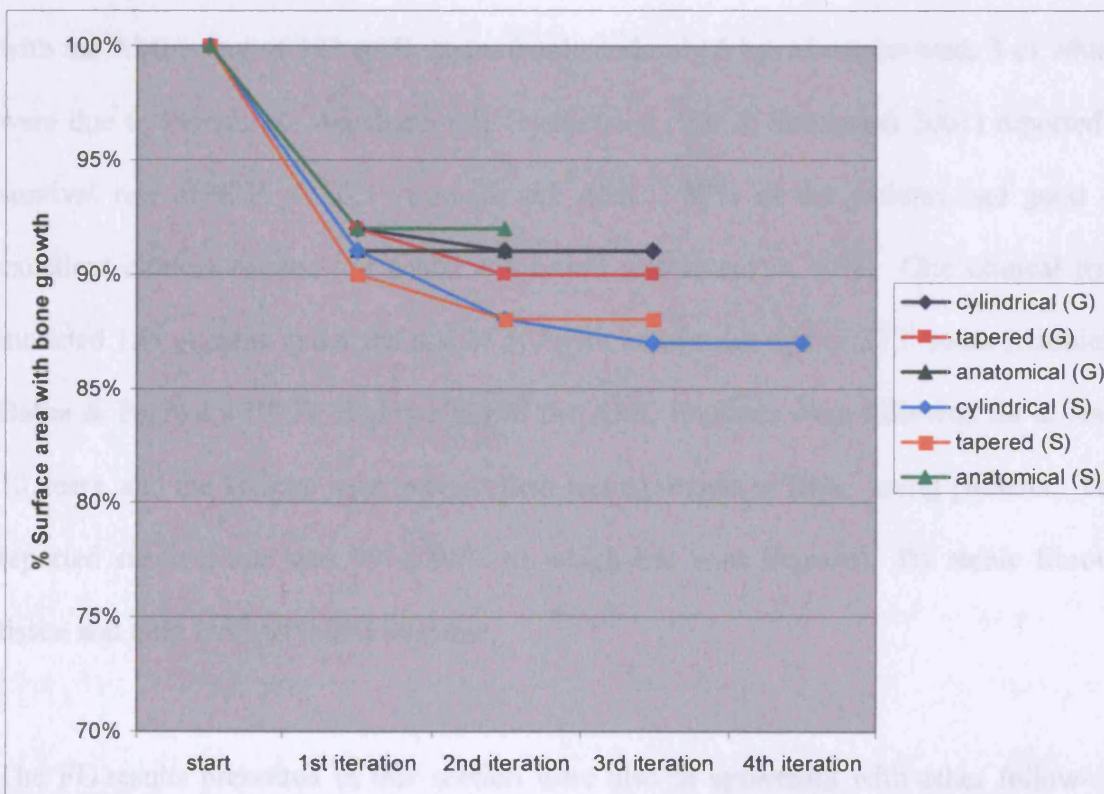


Figure 5.71: Percentage area of predicted bone ingrowth for the cylindrical, the tapered and the anatomical stem designs using Fisher's gait (G) and Duda's stair-climbing (S) loads.

5.1.2 Discussion

The above results showed that the three categories of hip stems analysed in this section, the cylindrical, the tapered and the anatomical designs had similar distribution of micromotion and were all stable when bone loss was simulated. The results are in agreement with published results of actual hip stems belonging to these groups. The AML, the Alloclassic and the ABG are all implants with excellent survival rates in short-term, medium-term and long-term.

The AML is a successful hip stem and performed well in hip arthroplasty (Chess et al. 1996). The results are well-published and the studies covered patients with a wide range of ages. One paper (Engh et al. 1994) reported 15 years of clinical experience with the AML. Out of 393 AML stems implanted only 6 have been revised, 3 of which were due to loosening. Another study (Nercessian, Wu & Sarkissian 2001) reported a survival rate of 92% at 10.5 years for the AML. 88% of the patients had good or excellent clinical results, but calcar resorption was found in 40%. One clinical trial included 154 patients under the age of 50, with an average age of 37.6 years (Kronick, Barba & Paprosky 1997). Eighty-eight of the AML implants were followed for at least 10 years, and the authors reported excellent lasting results in these young patients. The reported survival rate was 99%, 96% of which has bone ingrown, 3% stable fibrous tissue and only 1% was found unstable.

The FE results presented in this section were also in agreement with other follow-up studies in terms of predicting bone ingrowth. One study (Woolson & Adler 2002) reported that when solid initial fixation is obtained intraoperatively and radiographically

using the AML stem, bone ingrowth reliably occurs whether or not a partial or full weight-bearing postoperative protocol is followed. Another study (Engh, Bobyn & Glassman 1987) reported that bone ingrowth occurred in 93% of the cases where maximum stability was achieved. An early retrieval study of an AML stem prior to gross failure showed dense cortical and cancellous bone ingrowth (Whiteside et al. 1993). Strength of attachment of the metal implant to bone was good and no slippage was found at the interface when tested under torsional and axial load. Another study used backscattered scanning electron microscopy (SEM) to analyse bone growth of the AML stem (Engh et al. 1994). They reported that average bone ingrowth was found on 57% of the porous-surfaced area of the femoral components.

An experimental study has been conducted comparing a freshly implanted AML stem and a specimen retrieved from a deceased patient (Sugiyama et al. 1994). They found that micromotion was greater proximally for the freshly implanted stem compared to the bone-ingrown retrieved specimen. They also found that the smooth distal stem of the retrieved specimen caused larger micromotion than the freshly implanted. The authors concluded that the flexibility of the femur causes increased micromotion of the femur around the smooth distal stem despite the initially tight distal fit.

For the anatomical design, there are also follow-up reports confirming the FE predictions. The ABG hip stem has been reported to have excellent clinical and radiographic results at short-term (Rossi et al. 1995; Tonino et al. 1995) and in 5 years follow-up (Araujo, Gonzalez & Tonino 1998; Giannikas et al. 2002), though the survival rate dropped due to the wear of the polyethylene cup. Others (Herrera et al. 2004) reported a survival rate of 97% at 7-10 years, but again substantial polyethylene

wear was observed in a significant percentage of the acetabular cups. It may not be appropriate, however, to compare these FE results with the follow-up studies of the actual ABG as the over-reaming of the distal part was not modelled. Other anatomical designs, which do not use an over-reaming technique, are the Profile and the APR-II. A follow-up study of the Profile at 10 years showed excellent clinical and radiographic results, with no stems revised for aseptic loosening and thigh pain was found in only 10% of hips (Kim, Oh & Kim 2003). The APR-II stem has also been found to be very successful (Kang, Dorr & Wan 2000). Out of 99 total hip arthroplasties followed for up to 4 years, 100% had proximal bone ingrowth fixation and no patient reporting thigh pain after 3 years. Distal cortical hypertrophy associated with tip fixation occurred in 49%, whereas proximal stress shielding was present in 43% of hips.

An in-vitro experimental comparison study between a curved anatomical stem and a straight stem (Berzins et al. 1993) found that at low angles of flexion, the curved and straight stems demonstrated similar patterns of motion. However, at high torsional moments such as the one observed during stair climbing, the curved stem was found to be more stable than the straight stem. In another experiment comparing between straight and asymmetrical hip stems with 1000N of load applied to the prosthetic head, the axial micromotions were found to be small for both stems, with the symmetrical stem having the least axial micromotion – an average of $6\mu\text{m}$ – compared to the asymmetrical stem with an average of $19\mu\text{m}$ (Hua and Walker 1994). However, a torsional loading test showed that the straight stem had about ten times greater relative rotational motion than did the other two stems. Another study (Callaghan et al. 1992) showed that straight and curved stems performed similarly in terms of micromotion during single leg stance and at low loads during stair climbing. When large torsional

moments (22Nm) were applied, the straight stem produced 2-4 times more micromotion than the curved stems. All these three papers reported that straight stems produced more micromotion than curved anatomic stems during stair-climbing. The FE results, however, did not show a significant difference between the two designs at this physiological loading. The reason could be that in the FE models, a perfect fit was created with an interference of 0.1mm across the surface of the stem. The FE results showed that the straight stem had 9% surface area in excess of the threshold limit of 50µm interface micromotion compared to the anatomic with 8%. However, when the bone elements were adjusted to simulate bone loss, the area for the straight stem increased to 12%, but the anatomic design was maintained at 8%. This showed that straight stems were more susceptible to micromotion during stair-climbing when a perfect fit at the interface was not achieved.

The Alloclassic stem, which represented the tapered group, is also a successful design with a survival rate of 99.3% to 100% between 5-11 years (Delaunay, Cazeau & Kapandji 1998; Pieringer et al. 2003a; Pieringer et al. 2003b). In one of the follow-up reports of the Alloclassic (Huo et al. 1995), 98% of the hips were rated good or excellent clinically at a median of 4 years. No stem was classified as definitely loose and no hips required revision. There was also no incidence of femoral osteolysis. Another study (Delaunay et al. 2001) reported that only 3 out of 133 stems subsided 2-5mm and one subsided 5-10mm within the first year, but no progressive subsidence could be detected beyond this period. Another (Effenberger et al. 2002) reported excellent results at 8 years for the Alloclassic with 83% showing no radiolucency and 17% showing radiolucency only proximally. A retrieval study of the Alloclassic (Lester 1997) found that extensive bone-to-prosthesis apposition occurred at the interface along

the stem between 6 weeks to 60 months. The mean appositional bone index was 48%. Other tapered designs have also been shown to have excellent results at 5 years (Keisu et al. 2001) and 10 years (Eingartner et al. 2000; Park et al. 2003; Reitman et al. 2003).

The models representing the three groups have been modified as much as possible so that a proper comparison could be made between them. However, the lateral flare feature of the Alloclassic was not removed because of the difficulty in redesigning the prosthesis in three-dimensions. The lateral flare is a proximal lateral expansion, which is designed to engage the lateral cortex of the femur in the metaphysis, allowing for a much broader base of support in this area. This allows a more concentric loading in the proximal femur and relieves distal stress transfer. It has been reported that this feature provides extra initial stability in cementless hip stems (Leali et al. 2002). Another study (Effenberger et al. 2001) reported that prostheses with a lateral flare, such as the Alloclassic, have better rotational stability compared to the Schenker prosthesis, a stem without a lateral flare. The micromotion algorithm could only display resultant interface relative motion and could not separate this into axial and rotational components. As such the superior rotational micromotion of the Alloclassic could not be measured. The effect of a lateral flare feature will be analysed in section 5.4 when proximal and distal fixation designs are discussed.

Rotational stability under torsional loads has been reported by Gortz et al. (2002). Four hip stems were measured experimentally, two of which belonged to the tapered group (the Alloclassic and the CLS), one to the anatomical group (the ABG), and one belonged to the straight cylindrical group (the S-ROM). They found that the relative rotational motion for the anatomical ABG and the tapered CLS was larger distally than

proximally, whereas the Alloclassic, which is in the same group as the CLS, showed the opposite - larger proximally than distally. Though their findings could not be related to the FE results here, due to the limitation of the micromotion algorithm, it showed that the overall geometry alone could not totally account for the variable stability of cementless hip stems. Different concepts of fixation, namely proximal and distal fixation, also play a role in the stability of femoral components.

In conclusion, this section showed the results of an FE micromotion study that proved the stability of three categories of hip stems – the cylindrical, the tapered and the anatomical designs. Specific features of these implants were removed as much as possible so that a proper comparison between the three categories could be made. One of the limitations of this study was the inability to separate the resultant micromotion into axial and rotational components. It is therefore not clear, for example, which type of hip stem was better in terms of sustaining torsional loading. Despite these limitations, this study confirmed the stability of these types of hip stem designs.

5.2 Material stiffness effects.

One of the design factors that must be taken into consideration is the type of material used, where a trade off between load transfer and implant stability is the key issue (Maistrelli et al. 1991). The earlier generation of cementless stems were too stiff compared to the bone – about 10 times too stiff. A stiff material will make load transfer inefficient, and eventually cause ‘stress-shielding’ – an adverse bone remodelling

phenomenon where bone is resorbed in areas where it is not loaded to physiological levels. This stiffness mismatch between the stem and the bone causes loss of proximal cancellous bone and thickening of distal cortical bone. It was, and still is, one of the major problems in hip arthroplasties, both cemented and cementless.

The problem of load transfer from stiff implants to bone led to the development of low-stiffness stems, sometimes called 'isoelastic' stems. The aim of isoelasticity was to deform the implant and the bone as one unit, thus maintaining the bone structure better. In terms of maintaining bone stock, compliant stems have been shown to be better than stiff stems. An in-vivo study (Sumner et al. 1998) on canine models showed that reduced stem stiffness enhanced proximal load transfer, thus reducing proximal bone loss. In another study of 14 patients, where 6 patients had isoelastic implants, their overall Bone Mineral Density (BMD) - a parameter that measures bone quality - increased by a mean of 12.6%. For those with a relatively stiff titanium implant, BMD decreased by a mean of 27% after 12 months (Ang et al. 1997). An FE bone remodelling study comparing the effects of the modulus of elasticity of various stems also revealed that low stiffness material such as a CFRP composite reduced stress shielding in the proximal bone by approximately one-half in comparison to the titanium alloy (Cheal, Spector & Hayes 1992).

Though there seems to be an advantage of using isoelastic stems, several authors reported that the use of these stems caused high rate of aseptic loosening. The RM prosthesis and the Morscher prosthesis were two of the earliest isoelastic cementless stems. There was a high rate of aseptic loosening at follow-up period of nine years (Morscher & Dick 1983). A later generation of isoelastic stems such as the prototype

carbon fibre-reinforced composite also suffered a similar fate (Adam et al. 2002). The authors reported macroscopic aseptic loosening and fibrous interface fixation for 92% of carbon fibre hip prosthesis at 6 years.

As far as the author is aware, FE analyses on the effects of material stiffness on micromotion have only been done using a simplified cylindrical model (Rohlmann et al. 1988) or a simplified 2-dimensional model (Kuiper & Huiskes 1996). In this section, 3D FE analyses were conducted on three different material properties – Cobalt Chromium (CoCr), Titanium alloy (TiAl) and composite material – to compare the micromotion between them under physiological loading.

5.2.1 Methods & Results

Three AML stems prepared in Chapter 2 were analysed by assigning three different elastic moduli representing Cobalt Chromium (200GPa), Titanium alloy (110GPa) and composite material (20GPa). All stems were loaded using Fisher's walking loadcase and the results of interface micromotion were displayed. From these results, surface areas of bone with more than 50µm of micromotion were removed as described before to simulate interfacial bone loss. Further iterations were performed on each model with the same load cycle, and the new set of results were plotted and analysed as shown in the following pages.

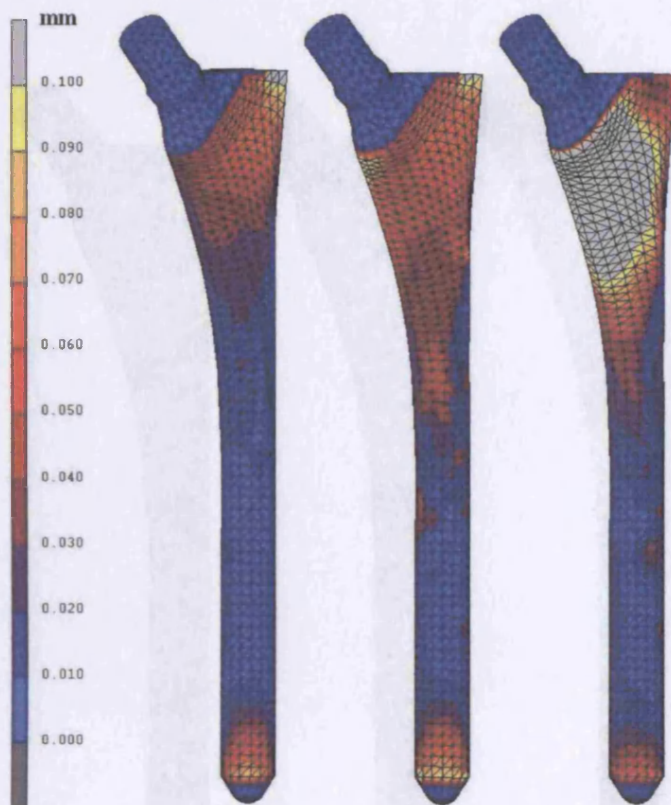


Figure 5.72: Micromotion results for the AML stem made of CoCr (left), TiAl (middle) and Composite (right) after 1st iteration.

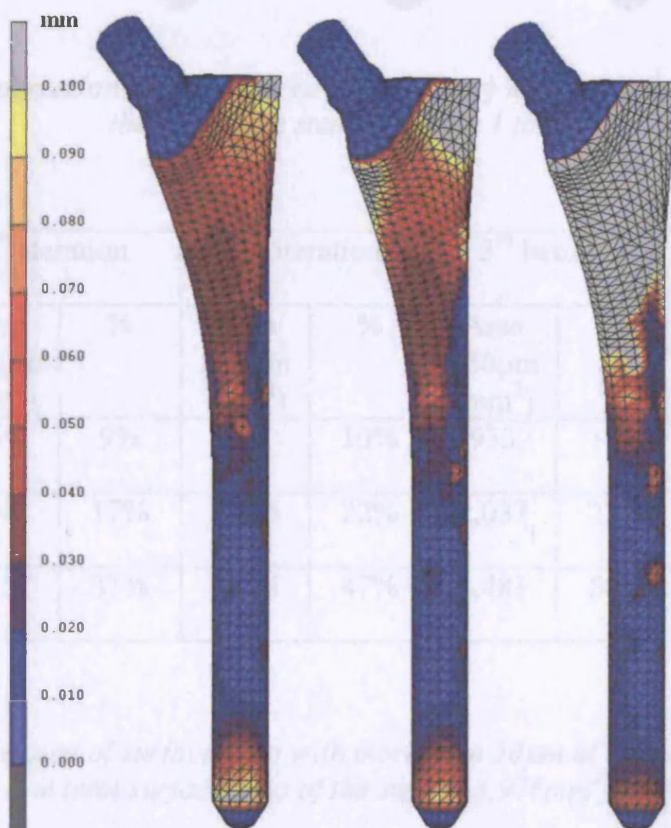


Figure 5.73: Micromotion results for the AML stem made of CoCr (left), TiAl (middle) and Composite (right) after final iteration.



Figure 5.74: Progression of surface area (grey colour) unfeasible for bone growth for the composite stem (iteration 1 to 5).

	1 st iteration		2 nd iteration		3 rd iteration		4 th iteration	
	Area >50µm (mm ²)	%	Area >50µm (mm ²)	%	Area >50µm (mm ²)	%	Area >50µm (mm ²)	%
CoCr	769	9%	890	10%	933	10%	-	-
TiAl	1,542	17%	1,955	22%	2,037	23%	2,105	23%
Composite	2,757	31%	4,204	47%	4,481	50%	4,546	51%

Table 5.13: Amount of surface area with more than 50µm of micromotion and its percentage area (the total surface area of the stem is 8,976mm²) up to the 4th iteration.

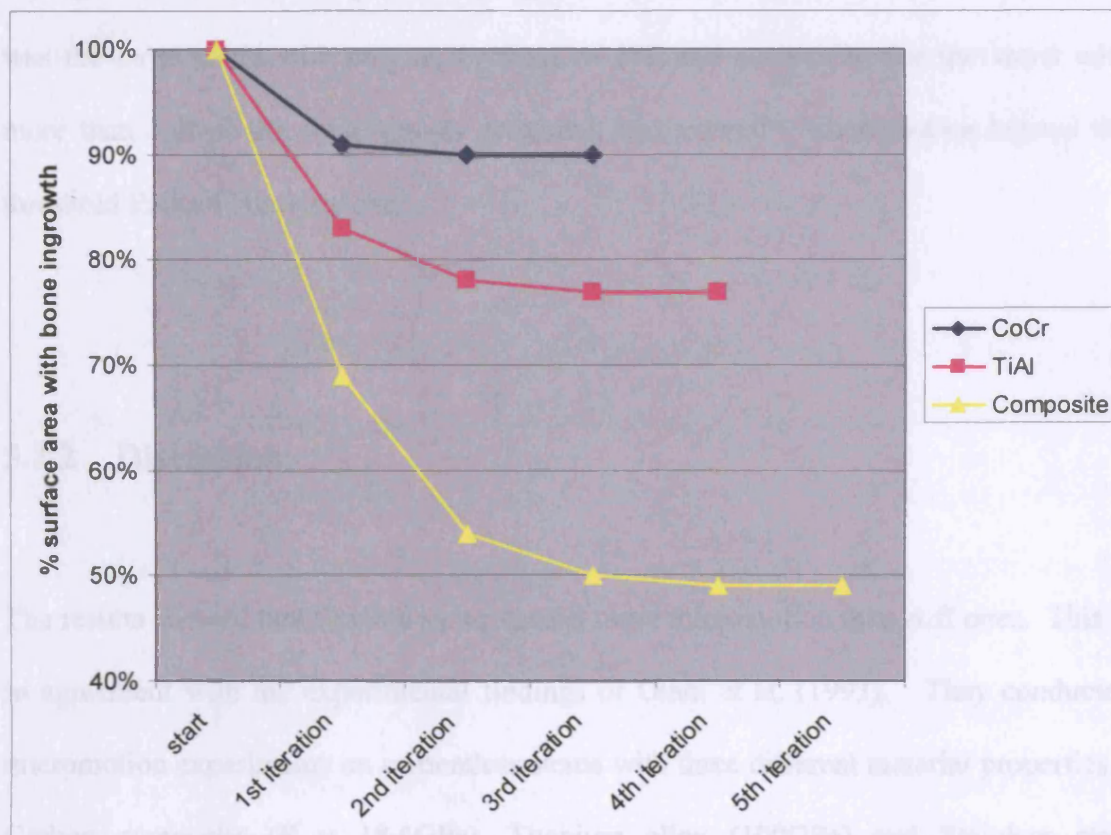


Figure 5.75: The reduction in surface area with less than $50\mu\text{m}$ for the CoCr, TiAl and Composite stems.

Figure 5.72 shows that interface micromotion increased as the stiffness was reduced, with the feasible area for bone ingrowth reduced from 91% for the Cobalt Chromium to only 69% for the composite. The area that was affected most by excessive micromotions was the proximal part, thus reducing the effectiveness of the implant in terms of maintaining stability. All load transfer then occurred in the distal part, relying on stiff cortical contact in that area.

When the unfeasible areas of bone ingrowth were removed and the analyses were repeated, the results showed that the areas with excessive micromotion increased for all implants (Figure 5.73). However, the most compliant material extended the most

among the three stems (*Figure 5.74, Figure 5.75 and Table 5.13*). Cobalt chromium was the most stable with only an increase of 1%, and composite was the worst with more than half of the stem, mostly proximal, had excessive micromotion beyond the threshold limit of bone ingrowth.

5.2.2 Discussion

The results showed that flexible stems caused more micromotion than stiff ones. This is in agreement with the experimental findings of Otani et al. (1993). They conducted micromotion experiments on cementless stems with three different material properties – Carbon composite ($E = 18.6\text{GPa}$), Titanium alloy (100GPa) and Stainless steel (200GPa). They found that the carbon composite stem produced significantly larger micromotion proximally and significantly smaller micromotion distally than in the two metals. They concluded that proximal stress transfer may be improved by a flexible stem, but they raised the possibility of increased micromotion in the proximal area. They have also suggested that improved proximal fixation may be necessary to achieve clinical success with flexible composite femoral components.

There are numerous other studies comparing implants with different stiffnesses that showed significant increase in proximal micromotion for a flexible implant compared to titanium alloy or steel implants (Sumner et al. 1991; Yildiz, Chang & Goodman 1998; Yildiz, Ha & Chang 1998). A pilot study on the goat (Buma et al. 1997), also revealed that stiff implants showed favourable initial interface micromotion for bone ingrowth.

These experimental observations were further supported by numerical analyses (Rohlmann et al. 1988). Using a simplified cylindrical model, the authors found that the interface micromotion reduced by about half for Co-Cr-Mo alloy compared to an implant with a stiffness ten times lower. Another finite element study on the effects of material stiffness used 2-dimensional model of an implanted prosthesis (Kuiper & Huiskes 1996). The authors found that a flexible stem generated motions about three to four times larger proximally than those of a stiff stem. These published results together with our findings showed that even if flexible implants could optimise load transfer, their flexibility could eliminate the environment that is needed for osseointegration.

Whilst rigid stems caused bone loss due to stiffness mis-match, compliant stems caused problems in stability because the implant is easier to displace and rotate than its stiffer counterpart (Engh, Sychterz & Engh 1999; Otani et al. 1993). As a compromise between the effect of 'stress shielding' of a stiff stem and the effect of 'excessive micromotion' of flexible stems, most hip stems nowadays are made of titanium alloy. Apart from having high structural strength and being relatively bio-inert, it has a stiffness value of around 100GPa – still larger than the stiffness of bone, but less stiff than implants made of steel or cobalt chromium.

Early examples of flexible stems were the RM prosthesis (Morscher et al. 1981; Niinimaki, Puranen & Jalovaara 1994) and the Morscher prosthesis (Morscher & Dick 1983). Both implants showed promising early results but a high rate of aseptic loosening in long-term follow-up. Femoral components were found to be extremely loose and easily removable, with a thick, shiny fibrous membrane at the interface – no evidence of any bone ingrowth whatsoever (Jakim, Barlin & Sweet 1988). Too high

flexibility in the proximal part of the prosthesis was blamed for bone resorption and implant loosening (Morscher & Dick 1983). Adam et al. (2002) reported macroscopic aseptic loosening and fibrous interface fixation for 92% of carbon fibre-reinforced composite hip prostheses at 6 years. Another study comparing between isoelastic Butel stems and stiffer PCA stems showed that isoelastic stems showed a significantly higher rate of loosening (43%) than the stiff stems at 4 years post-operatively (Jacobsson et al. 1993). The Butel stems, however, gave fewer signs of stress shielding radiologically.

Despite the above reports of hip stems loosening with the use of compliant material, a recent short-term (2 years) follow-up study (Karrholm et al. 2002) reported an encouraging result of the isoelastic Epoch stems. The migration of the Epoch was not found to be statistically significant ^{compared to} than the relatively stiffer Anatomic stems. Both stems stabilised with migration below 100 μm at 2 years with the Anatomic showing less migration than the Epoch. None of the stems were revised at the time of follow-up and the Epoch showed significantly reduced bone loss in Gruen zones 1, 2, 6 and 7 at 2 years compared to the Anatomic. The Epoch isoelastic stem seemed to show better short-term stability than the early generation of isoelastic stems such as the RM, the Morscher and the Butel. This could be attributed to other design aspects of the implant such as the overall geometry of the stem and the surface finish. The RM prosthesis, for example, was not designed to fill the canal whilst the Butel prosthesis had a smooth surface. The Epoch on the other hand is a 'fit and fill' design and has porous coating throughout the length of the stem. The FE results above also showed that even though a compliant material produced larger micromotion than stiffer implants, with a 'fit and fill' design, the distal half of the stem was as stable as its stiffer counterpart.

This section analysed the effect of material stiffness on interface micromotion. Our analyses showed that micromotion increased as the stiffness was reduced. Our results were in agreement with other published reports with regard to material stiffness, whether FE, experimental or follow-up studies. In this study, not just comparative micromotion results were presented, but stability was also predicted for the three different hip stems' elastic moduli by simulating interfacial bone loss. The results showed that even though flexible stem produced larger micromotion and significant proximal interface bone loss, it should still be stable if tight fit was achieved distally.

5.3 The effect of stem length on micromotion

The study of stem length is particularly relevant for implants that are to be used in revision surgery. Due to loss of bone stock mostly in the proximal femur after a failed primary arthroplasty, surgeons have to rely on the cortical bone distally. As such, revision hip stems are normally longer than their primary counterparts in order to achieve proper stability through distal fixation. The optimum stem length is still a topic of discussion and debate in revision surgery (Mann, Ayers & Damron 1997).

There have been few studies on the optimum length of hip stems for primary arthroplasty. These looked into the effect of stem length for a specific type of hip prosthesis where the distal part of the stem was thinner than the medullary canal. Since the distal part of the stem did not fit and fill the canal, it may be hypothesized that the

distal portion of the stem had no mechanical function, thus the study of stem length. One of these studies (Tanner et al. 1995) compared three stem lengths of the Freeman hip stem - the full length of 172mm, an intermediate length of 132mm and a short stem of 92mm. An FE model of each of them was created and analysed, and the actual prostheses with different stem lengths were tested experimentally. They found that increasing the length of the stem resulted in a sharp increase in the level of compressive stresses laterally at the tip. For the short stem, there was an increase in the proximal stresses medially while still having similar lateral stresses distally. All femora with short stem components also failed at loads between 800 and 1200N, whereas no femora with longer stems failed. They concluded that a suitable length of stem was the intermediate one. Another FE study (van Rietbergen & Huiskes 2001), on the other hand, showed that reducing stem length so as to effectively remove it did not increase failure probability, and it did not reduce stress-shielding either. They concluded that reducing the stem length to the metaphyseal area was not advantageous. These two studies, however, did not mention if stability was compromised by having a short stem.

Even though the study of stem length is mainly popular in revision surgery, it is also important for primary hip arthroplasty. If we could use as short a stem as possible initially, then should the need for revision surgery arise, the loss of bone stock would be much less than if we were to use a longer stem. As the two papers described above have already looked at the stresses at various stem lengths, the aim of this study is to investigate, using finite element analysis, the effect of stem lengths on interface micromotion.

Before starting to analyse the effects of stem length, it is important to note that this study could also be related to the study between proximal and distal fixation design, which will be discussed in the next section of this chapter. In the concept of proximal fixation, if the implant is loaded proximally, then there may be no need of a long stem. However, design characteristics of a proximally-fixed design are more than just having a short stem, and as such a separate study of proximal vs distal fixation stems is presented in a separate section.

5.3.1 Methods & Results

Four models of the AML stems were adjusted to a different length – the standard 175mm and three shorter ones - 135mm (medium length), 95mm (short length) and 74mm (very short). The length of the shortest one was determined using the CT dataset so that minimum cortical contact was obtained. All stems were loaded in Fisher's physiological walking loadcase and the micromotion results were plotted. Areas with more than 50µm of micromotion were then removed to simulate interfacial bone loss and the analyses were repeated until a stable-state was achieved or failure occurred. Results are shown in the following figures below.

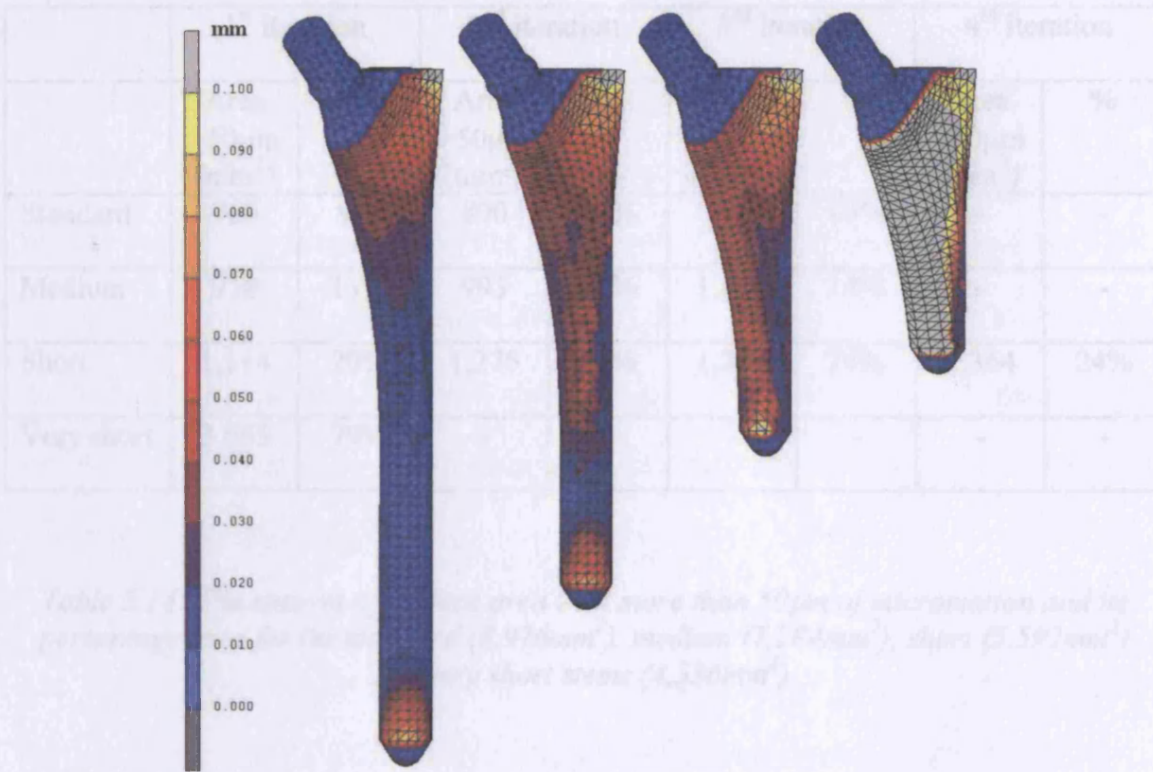


Figure 5.76: Micromotion results for the AML at various stem length for the 1st iteration.

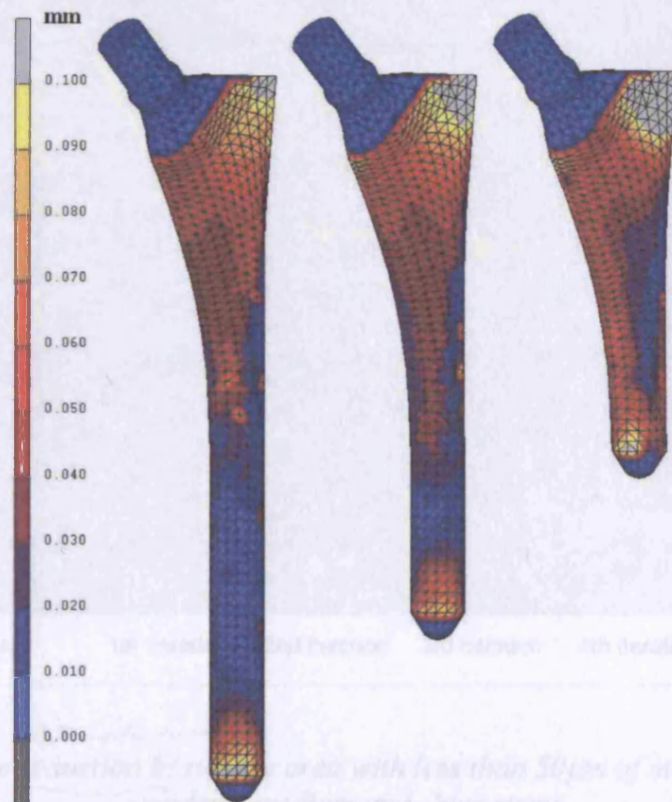


Figure 5.77: Micromotion results for the AML at various stem length for the final iteration. The fourth model was not included as the surface was surrounded with micromotion in excess of the chosen threshold limit.

	1 st iteration		2 nd iteration		3 rd iteration		4 th iteration	
	Area >50µm (mm ²)	%	Area >50µm (mm ²)	%	Area >50µm (mm ²)	%	Area >50µm (mm ²)	%
Standard	769	9%	890	10%	933	10%	-	-
Medium	938	13%	993	14%	1,040	14%	-	-
Short	1,114	20%	1,275	23%	1,342	24%	1,364	24%
Very short	3,565	79%	-	-	-	-	-	-

Table 5.14: The amount of surface area with more than 50µm of micromotion and its percentage area for the standard (8,976mm²), medium (7,284mm²), short (5,592mm²) and very short stems (4,536mm²).

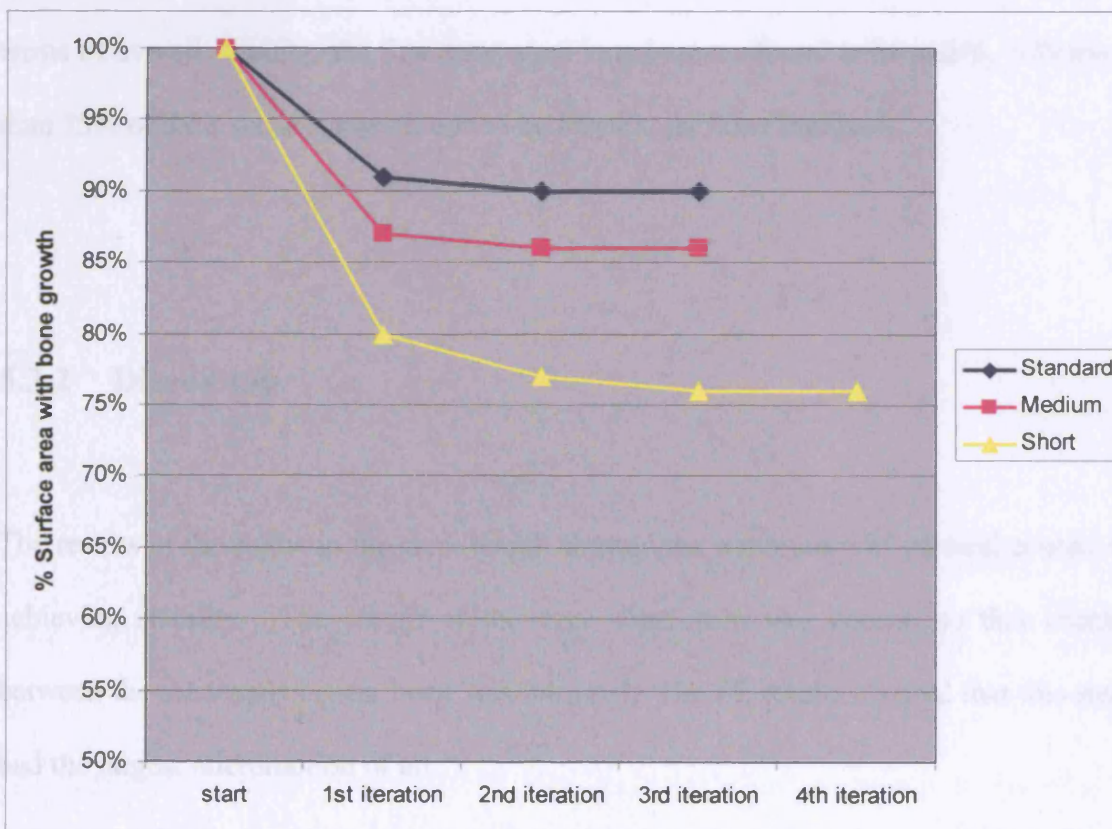


Figure 5.78: The ^{remaining} reduction in surface area with less than 50µm of micromotion for the standard, medium and short stems.

The results in *Figure 5.76* show that shortening the stem increased the interface micromotion, with a huge increase in micromotion between the third stem (short length) and the fourth stem (very short). For the shortest implant, further iterations were not conducted because 79% of the stem had micromotion in excess of 50 μ m. The results of the first three stems from the final iteration (*Figure 5.77*) showed similar results – all stems showed an increase in interface micromotion with the short stem having the largest micromotion (*Figure 5.78*).

The surface area feasible for bone ingrowth reduced as the length of the stem was reduced, both in terms of quantity and relative percentage (*Table 5.14*). However, in terms of overall stability, the first three stem lengths were found to be stable, with more than 75% of their surface areas found to be feasible for bone ingrowth.

5.3.2 Discussion

The results of the study on the stem length showed the importance of cortical contact in achieving stability. The length of the very short stem was chosen so that contact between the stem and cortical bone was minimal. The FE results showed that this stem had the largest micromotion of all.

Among the first three stem lengths, the short stem had micromotion larger and more widely spread. However, the results from the final iteration of simulated bone loss showed that this did not affect its stability. The only available paper to compare these

results with was the work of Sakai et al. (1999), where 60 patients underwent hip replacement with custom-made femoral components of two different lengths. At the period of follow-up, there were no statistical differences clinically and radiographically between the 125mm long stem and the 100mm long stem. Apart from this comparative study, there is also a follow-up study of short-stem Mayo prosthesis (Morrey 1989). The prosthesis has a double-wedged contour and fixed in place using 3-point proximal femur fixation. The follow-up period was 1 year and from out of 20 patients, 1 was revised for loosening while the rest were classified as satisfactory. It is surprising that a longer-term review has not been published, and it is certainly discouraging to see that a stem had loosened in 1 year. As there are not so many reports on short-stemmed prostheses, it is difficult to make a solid conclusion on their stability. However, the two reports above showed that as long as there was stiff cortical contact on the stem, primary stability was not compromised. This is confirmed by this FE study, that even though shorter stems have more and larger micromotion than longer stems, they should still be stable.

The main advantage of having a short-stemmed prosthesis over long-stemmed is the ease of converting to another implant should failure occur. Since less bone is removed, it provides a possibility of long-term compatibility. As far as interface micromotion is concerned, a short-stemmed prosthesis could be made more stable through other design features, such as a pronounced lateral flare that rests on the inferolateral part of the greater trochanter or by having proximal macrofeatures, all of which will be looked at in the next two sections. This study showed that shorter stems could have the potential of becoming the next generation of cementless hip stems if their stability can be improved.

5.4 Proximal vs Distal fixation designs.

As described at the start of this chapter, there are two main design philosophies of fixation of cementless hip stems; proximal fixation and distal fixation. Distal fixation is usually achieved through the press-fit technique where the distal part of the stem is fixed to the cortical diaphysis, one example of which is the AML. Proximal fixation, on the other hand, relies for its stability on the cancellous bone surrounding the proximal part, such as the ABG hip stem. Design features for both concepts of fixation can vary, such as having a straight or curved stem, rectangular or cylindrical shape, collared or non-collared, types of materials used, length of stem and types and extent of coating.

Proximal or distal fixations are both design concepts for reducing bone loss, especially in the proximal area by improving the load transfer (Longjohn & Dorr 1998). Which design concept is better remains a controversial issue. Advocates of the distal fixation concept argue that strong primary stability is crucial and it is achievable through strong and reliable cortical contact distally. Once the implant is stably fixed, bone ingrowth can then take place throughout the stem. Advocates of the proximal fixation concept argue that bone resorption in the proximal area can be reduced if the forces from the hip joint are transmitted to the most proximal part of the femur. An additional rationale for using a metaphyseal filling, proximal fixation design is to preserve the endosteum of the diaphysis for later surgery, should a revision be required in the future.

The design of the distal and proximal fixation varies. The proximal fixation design was attributed to anatomical stems such as the APR-II stem where the proximal implant geometry should fit and fill as much as possible of the proximal femur (Longjohn &

Dorr 1998). As such, the proximal part is widened in the anteroposterior and mediolateral directions to allow a greater area of bone attachment proximally. However, the surgical technique of the APR-II stems employs a tight circumferential diaphyseal fit (Dorr & Wan 1996). It is therefore uncertain if total proximal load transfer is achievable. Later generations of proximal fixation design, such as the ABG and the IPS, used distal over-reaming technique as standard surgical protocol. Theoretically this will allow more proximal loading than the diaphyseally fit technique used for the APR-II. Another advantage of distal over-reaming is that it significantly reduced thigh pain (Giannikas et al. 2002). This over-reaming technique has also been tested on the distal fixation AML stem (Kim & Kim 1994). The authors reported that fractures were more likely to occur using the under-reaming technique, and therefore switched to over-reaming the distal endosteal bone. Both techniques were found to give successful outcomes.

A tapered design can be either distally or proximally fixed because stability is achieved by wedging the implant into the femur. The Alloclassic, for example, achieves a wedge-fit in the diaphysis and therefore is categorised as a distal fixation design. The CLS, on the other hand, has a tri-tapered design with a rectangular cross-section and a narrow stem tip. A wedge-fit is achieved in the metaphyseal area and therefore it is considered to be a proximal fixation design.

In this section FE analyses will be conducted to compare interface micromotion, and therefore the stability, of two design concepts for cementless fixation - the proximal fixation design and the distal fixation design.

5.4.1 Methods & Results

In order to make a proper and general comparison between proximal and distal fixation stems, a design was chosen to represent both concepts so that the minimum changes possible can be made while maintaining the main features of the design concept. The AML was chosen as the distal fixation design. To create a proximal design from the AML, the stem was shortened by a half, and the proximal part was enlarged in the medio-lateral and antero-posterior directions in order to help it to engage the proximal cortical shell (*Figure 5.79*). The medio-lateral size was enlarged by having a lateral enlargement that filled the infero-lateral part of the greater trochanter. The distal part of the stem was shortened by 80mm, and the endosteal cavity was over-reamed by 28mm distally, making the effective length of the stem 74mm. This was done because stems intended for proximal load transfer usually have the distal cavity over-reamed; therefore the distal stem (if perfectly aligned) plays no part in load transfer. Both designs were loaded in walking and stair-climbing modes, and the results are shown on the next page.



Figure 5.79: The distal fixation design (left) and the proximal fixation design showing enlargement in medio-lateral and antero-posterior directions (right).

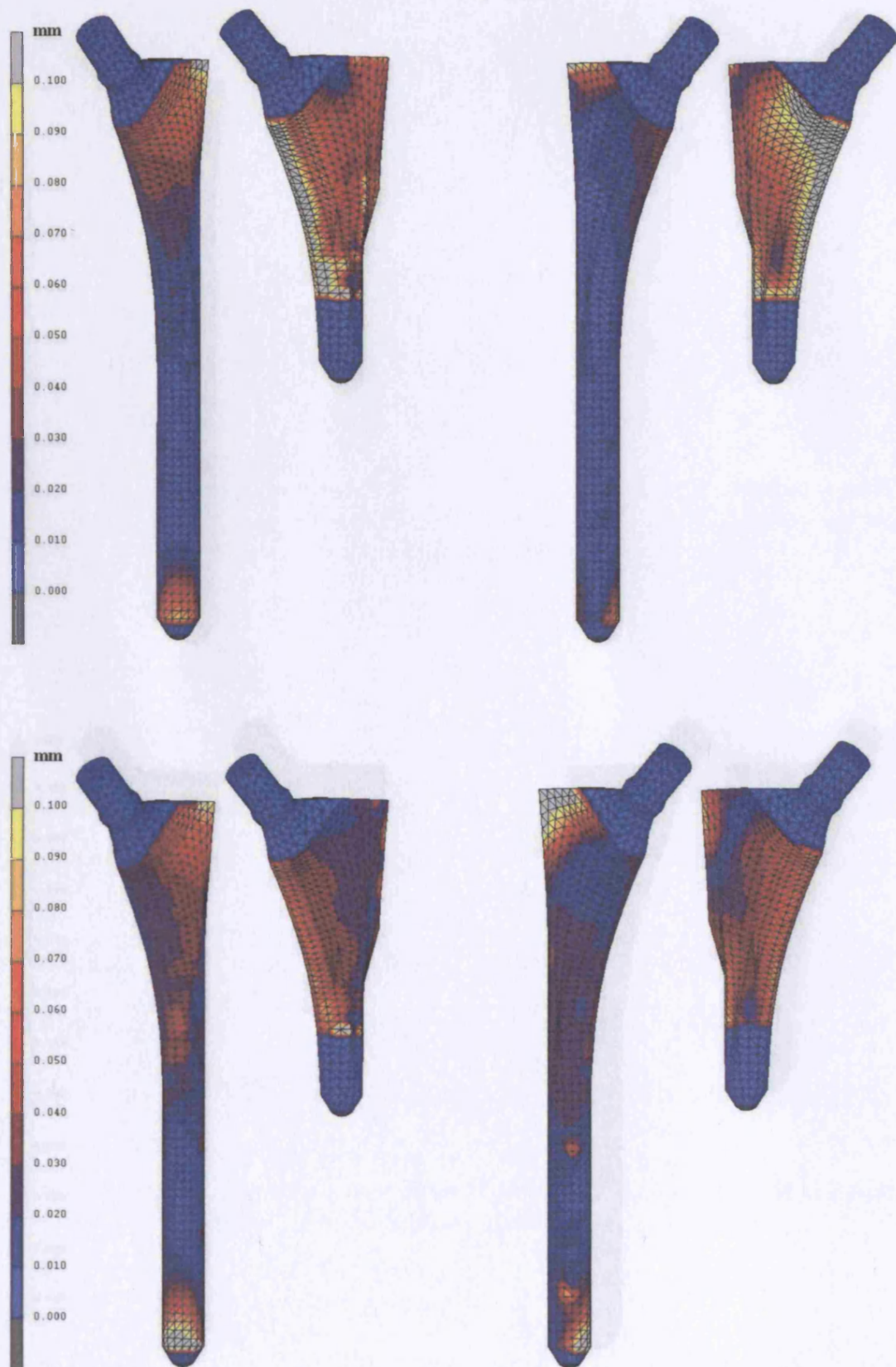


Figure 5.80: Contour plots of micromotion for a distal fixation and a proximal fixation design using Fisher's gait cycle (top) and Duda's stairclimbing (bottom) after 1st iteration. Posterior side on the left, anterior side on the right.

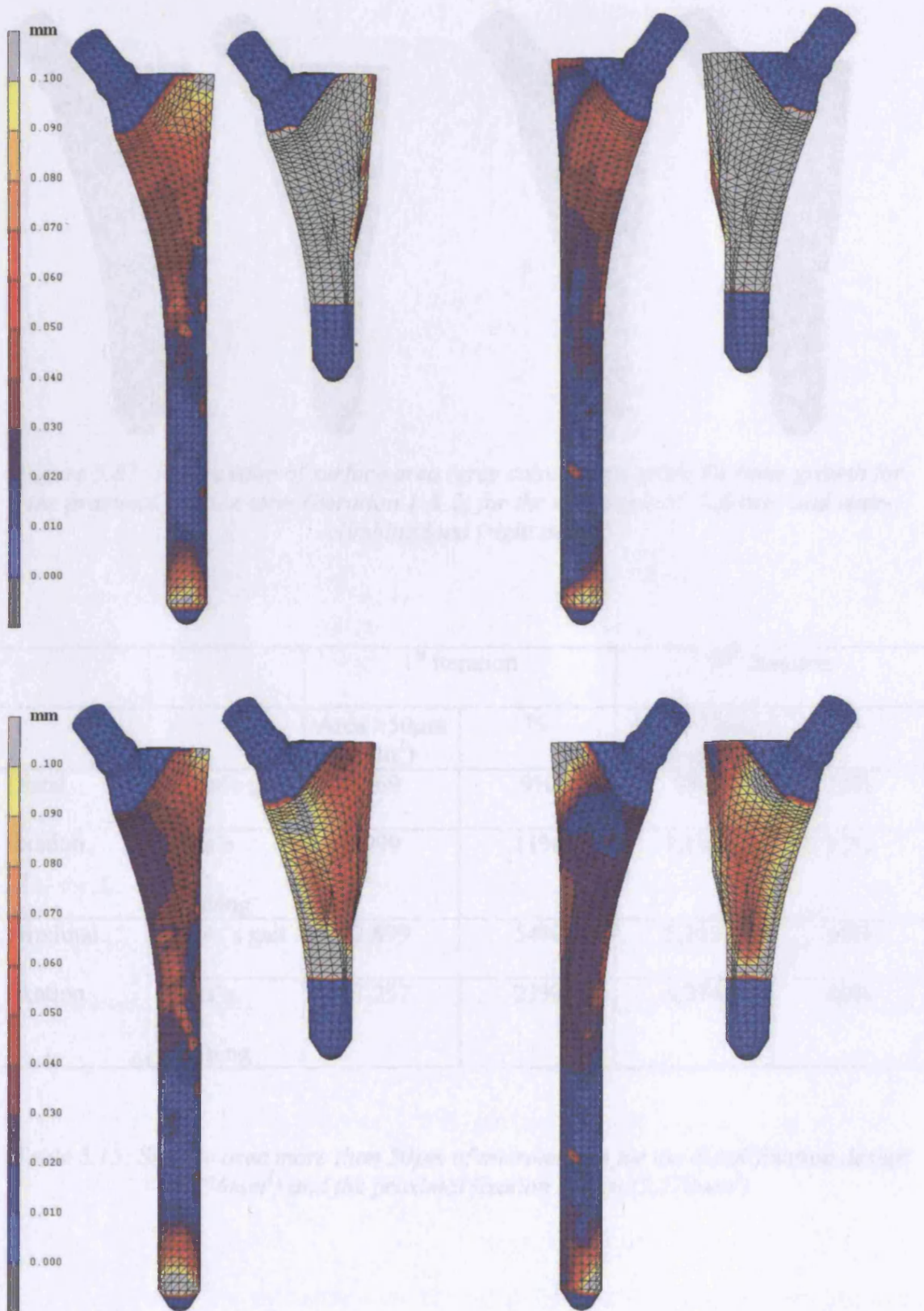


Figure 5.81: Contour plots of micromotion for a distal fixation and a proximal fixation design using Fisher's gait cycle (top) and Duda's stairclimbing (bottom) after final iteration. Posterior side on the left, anterior side on the right.

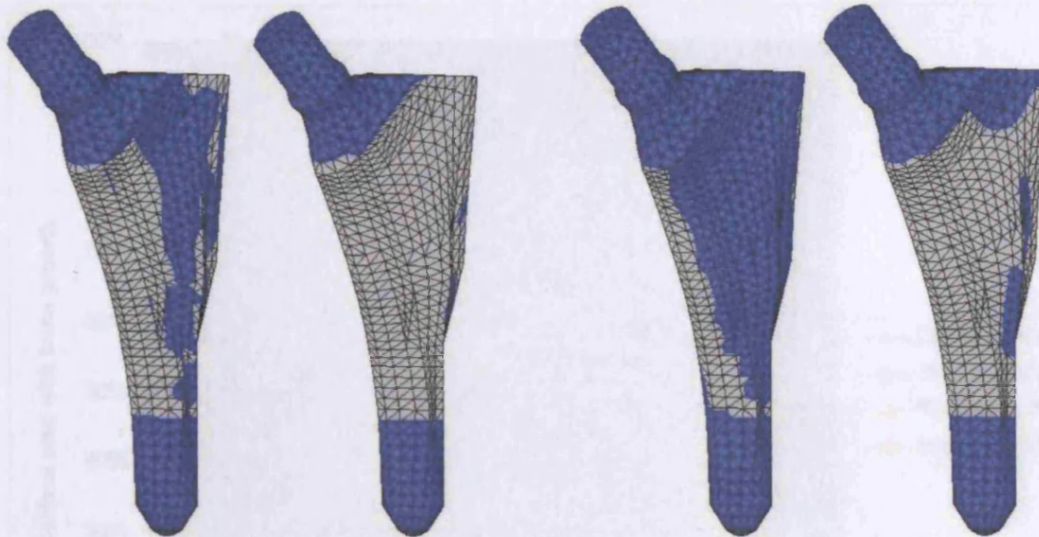


Figure 5.82: Progression of surface area (grey colour) unfeasible for bone growth for the proximal fixation stem (iteration 1 & 2) for the walking load (left two) and stair-climbing load (right two).

		1 st iteration		2 nd iteration	
		Area >50µm (mm ²)	%	Area >50µm (mm ²)	%
Distal fixation	Fisher's gait	769	9%	890	10%
	Duda's stair-climbing	999	11%	1,113	12%
Proximal fixation	Fisher's gait	2,899	54%	5,105	95%
	Duda's stair-climbing	1,257	23%	4,274	80%

Table 5.15: Surface area more than 50µm of micromotion for the distal fixation design (8,976mm²) and the proximal fixation design (5,370mm²).

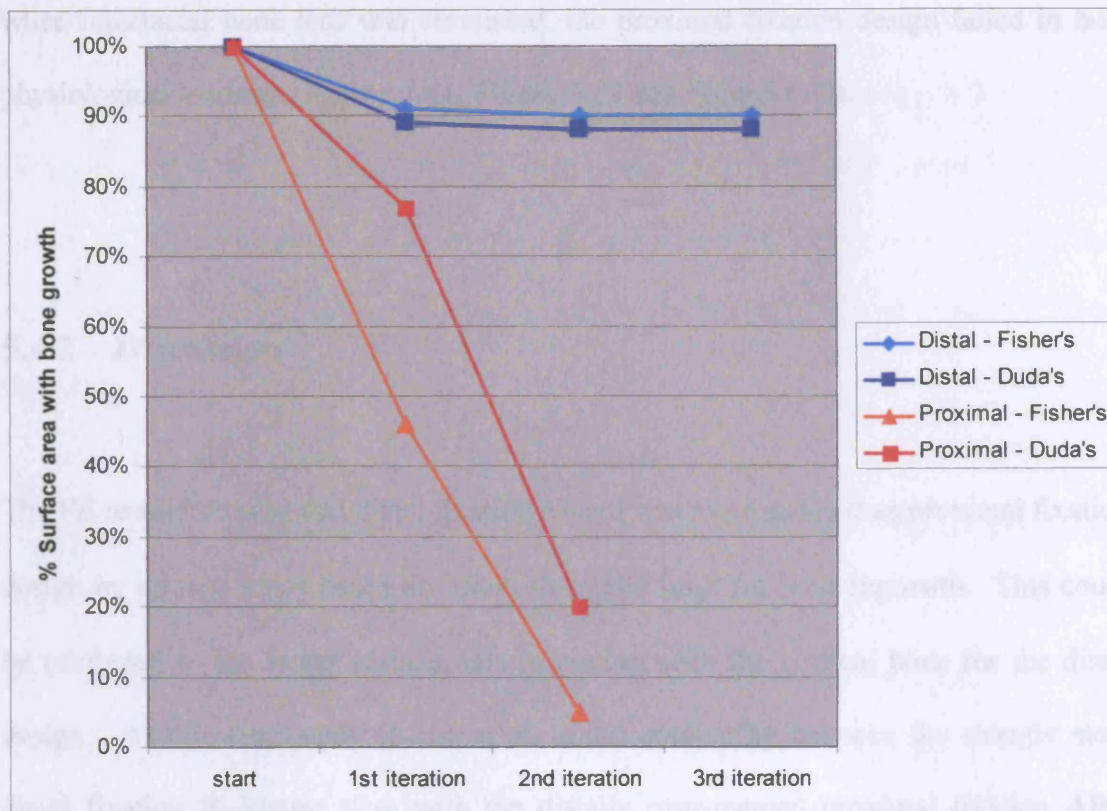


Figure 5.83: The reduction in surface area with less than $50\mu\text{m}$ of micromotion for the distal and proximal fixation designs using Fisher's gait cycle and Duda's stair-climbing loads.

The results on Figure 5.80 showed that the proximal fixation design had more micromotion than the distal fixation design in both walking and stair-climbing. The distribution of micromotion was also different between the two designs. The distal fixation model had micromotion largely in the lateral area of the proximal part and around the anterior tip of the stem. The proximal design, on the other hand, had micromotion concentrated more on the medial part of the stem.

Table 5.15 shows that unfeasible areas for bone ingrowth were larger in the proximal design by 2-6 times compared to the distal design. For the proximal fixation design, the stem seemed to be more unstable in walking, with surface areas exceeding the threshold limit more than double compared to surface areas during stair-climbing. However,

when interfacial bone loss was simulated, the proximal fixation design failed in both physiological loadings (*Figure 5.81, Figure 5.82 and Figure 5.83*).

5.4.2 Discussion

The FE results showed that distal fixation design was more stable than proximal fixation design by up to 6 times based on 50 μ m threshold limit for bone ingrowth. This could be attributed to the larger surface area in contact with the cortical bone for the distal design. A follow-up study (Laine et al. 2000) comparing between the straight stem distal fixation Bi-Metric stem with the distally over-reamed proximal fixation ABG stem, showed that there was substantially more cortical contact in the diaphyseal area for the distal fixation design as expected, and that subsidence of more than 2mm was more frequent in the proximal fixation ABG, though the stability was not compromised. Both hip stem designs, however, were found to be clinically excellent at 5 years. There was a tight diaphyseal fit that produced excellent stability for the distal fixation design, but this meant that stress was transferred in this region and as a result increased stress shielding in the proximal metaphyseal compared to the proximal fixation ABG.

For the stability of proximal design in stair-climbing, this has also been confirmed by others, as mentioned in the previous section. Hips stems with a lateral flare feature in its design, has been proven to provide extra initial stability particularly the rotational stability compared to a stem without lateral flare (Effenberger et al. 2001). Another study (Walker et al. 1999) also confirmed that a lateral flare contributed positively to a cementless stem design and that the stems could be made shorter than designs without a

lateral flare. In their FE study, migration was found to be less for the lateral flare compared to a simple straight stem model. A follow-up study of the lateral flare system by the same authors also showed that trabecular bone attached to the lateral flare coated with HA. Another paper (Leali et al. 2002) reported that cementless stems with a lateral flare provided primary stability and produced a low subsidence – an average of 0.32mm at 2 years.

An experimental study looking at the rotational stability of the two fixation designs has been reported (Gortz et al. 2002). Two proximally fixed stems, the ABG and the CLS, were found to have more rotational micromotion distally than proximally. The distal fixation Alloclassic, however, was found to produce more rotational micromotion proximally than distally. The rotational micromotion in the proximal area was larger for the Alloclassic by two times compared to the CLS and almost three times compared to the ABG. Better rotational stability for the two proximal fixation designs could be due to the proximal macrofeatures on the anterior and posterior sides of both hip stems. The CLS had tapered fins macrofeature and the ABG had semi-circular indentations macrofeature. The effect of these macrofeatures on micromotion will be looked at in the next section.

Another in-vitro experiment looked at four different cementless stems (Schneider et al. 1989b). One of the tested stems was the CLS and another one was the Zweymuller which has a tapered design similar to the distally fixed Alloclassic. The others were the Muller 85 and the anatomical PCA. They found that the CLS had the largest mean interface micromotion under load simulating single leg stance – up to 10 times more motion than the most stable stem (the anatomical PCA). Another paper reported the

migration of the proximally-fixed CLS stems (Davies et al. 1999). The mean femoral stem migration was 2mm at 2 years and 3.66mm at 7 years. Although these reports showed more migration and micromotion for a proximal fixation design, follow-up studies of the ABG and the CLS showed that these prostheses were successful (Rogers, Kulkarni & Downes 2003; Schreiner et al. 2001).

The results from this section showed that the proximal fixation design, though less stable than the distal fixation design, has some potential. As discussed in the previous section, the advantage of having a short-stemmed prosthesis is its long-term compatibility. Should the need for revision arise, less problems will be encountered as the cortical bone distally is available for fixation. However, the results from the previous section showed that full proximal load transfer by having a very short stem caused large interface micromotion and instability. In this section, the micromotion of short-stemmed prosthesis was reduced by having a proximal enlargement in the antero-posterior and medio-lateral direction. The stem failed in both physiological loadings when bone loss was simulated because most of the excessive micromotion concentrated on the medial area; stability was compromised because contact in the medial area was lost. The relative lack of stability for the proximal fixation design in this section could be improved further by having an anatomic design and introducing macrofeatures in the proximal part as will be discussed in the next section.

5.5 Proximal macrofeatures

Another important design feature of cementless stems is the introduction of proximal macrotexturing or macrofeatures. This is different from cemented stems, where the surface is normally polished – macrotexturing is bad for cemented stems because it causes abrasion at the stem-cement interface and could cause loosening (Duffy et al. 2001a).

Probably the most common macrotextures are beads and fibre-mesh. It has been shown that stems with these macrofeatures have excellent survival rates (Grant, Groggaard & Nordsletten 2004). Retrieval studies showed that bone had grown into these porous structures (Chen et al. 1998; Kusakabe et al. 2004). The challenge with analysing these macrofeatures physically in FE studies is due to their irregular arrangement and relatively small size. Usually the effects of these surface textures are incorporated simply by assigning a friction coefficient at the bone-implant interface.

Apart from beads and fibre-mesh, there are other macrofeatures which are more regular in shape. The most common type is probably grooves. These provide a space for bone to grow into and if the stem is tapered, initial stability could be achieved through bone locking the stem into place. Other types of proximal macrofeatures include tapered fins, such as the one found on the CLS hip stem, or the semi-circular indentations on the anterior and posterior sides of the proximal surface of the ABG stem.

To the author's knowledge, there are no reported studies looking at the effectiveness of proximal macrofeatures in improving the primary stability of cementless hip stems. It is

hypothesised that these macrofeatures are useful in terms of providing extra stability. In order to prove this hypothesis, several common regular macrofeatures described above will be created and then compared with a control model.

5.5.1 Methods

Two sets of models were created, one based on the CLS stem and another one based on the ABG stem. From the first group, the CLS model which has fixation fins was created. The stem had three semi-circular fins on both the anterior and posterior sides, covering almost the proximal half of the stem. The 2.5mm wide fins were tapered longitudinally with maximum thickness of 2.5mm. Six other models were also created, two of which were the blank CLS (no macrofeatures) as control and another one had ridges on the medial proximal side. The other four CLS models had grooves at different angles – vertical, horizontal, 45° to the vertical and 135° to the vertical (*Figure 5.84*). The grooves were 2.5mm wide and 1.25mm deep and the ridges 1.5mm wide and 0.75mm deep. The geometries of the grooves and medial ridges were chosen to best fit the implant. The ridges were chosen to be placed on the medial side only, as this is the only suitable place for this type of macrofeature, considering the surgical technique involved.

These models were then analysed in physiological walking and stair-climbing. Further iterations were performed after adjusting the bone elements with micromotion more than $50\mu\text{m}$ to simulate interfacial bone loss. Contour plots of micromotion and graphs of feasible surface area for bone ingrowth are then presented.

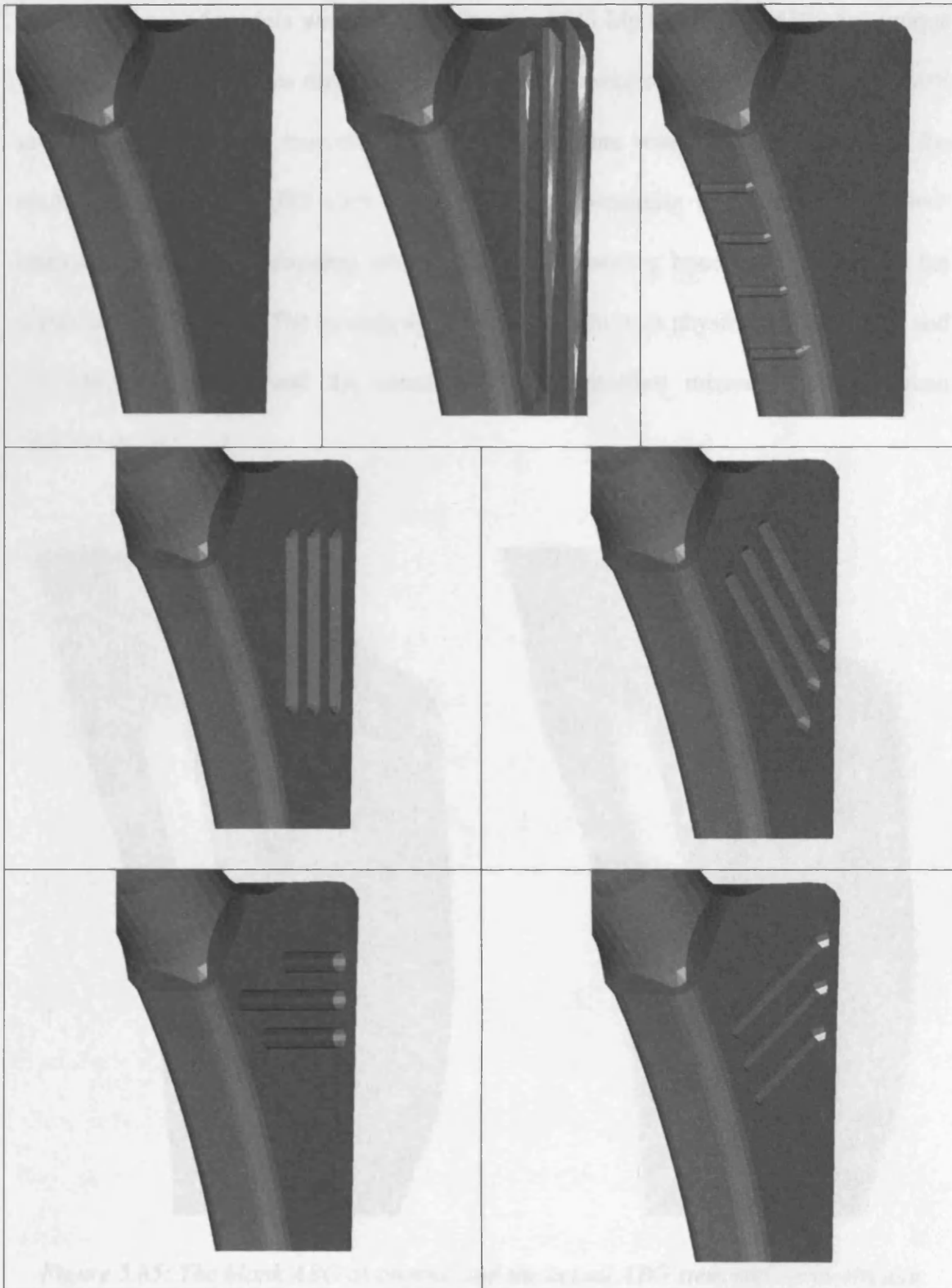


Figure 5.84: The blank, fins, medial ridges, vertical grooves, 45° grooves, horizontal grooves and 135° grooves. These resemble the most common types of macrofeatures.

Figure 5.84: Types of macrofeature studied. From left to right, top to bottom – blank, fins, medial ridges, vertical grooves, 45° grooves, horizontal grooves and 135° grooves. These resemble the most common types of macrofeatures.

The second set of models was created using the ABG hip stem. The ABG has unique indentation macrofeatures on both its anterior and posterior sides. Two models were created, one with these macrofeatures and another one without macrofeatures as the control model. The ABG uses a distal bone over-reaming technique and in these analyses the bone over-reaming was modelled by removing bone elements around the distal half of the stem. The models were then loaded in both physiological walking and stair-climbing modes, and the contour plots of interface micromotion were then calculated.

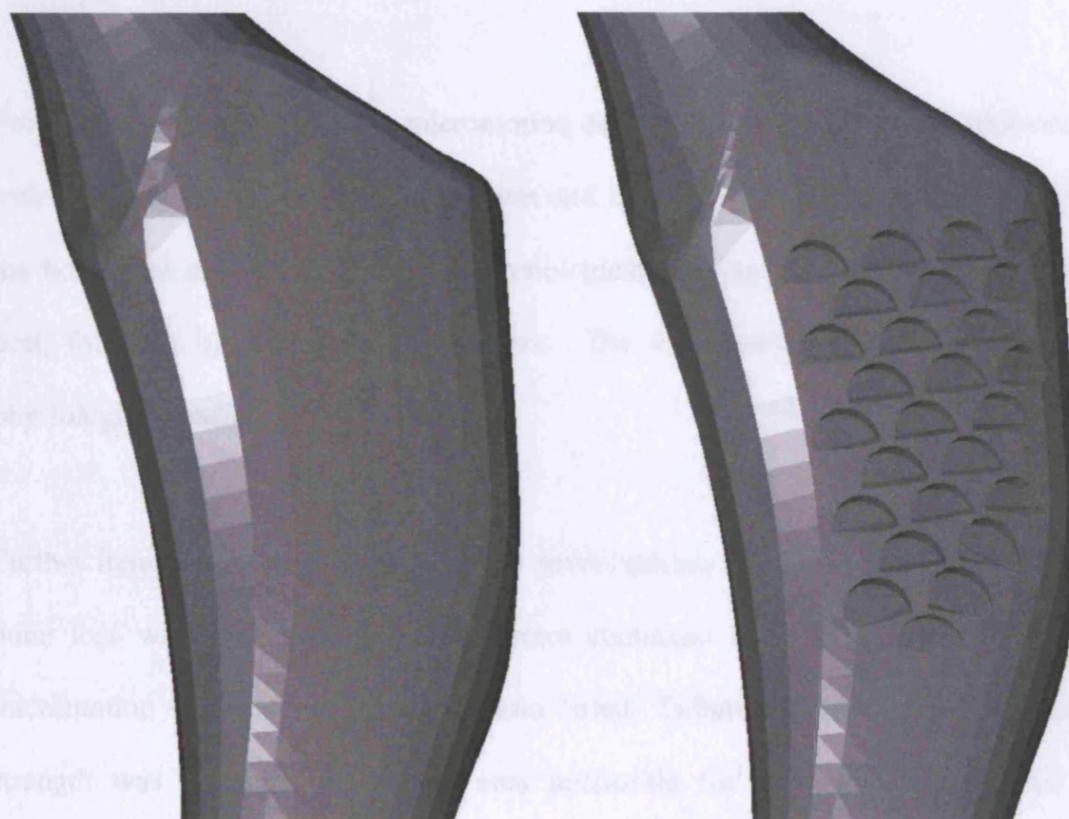


Figure 5.85: The blank ABG as control and the actual ABG stem with semi-circular indentation feature.

5.5.2 Results

Figure 5.86 and *Figure 5.87* show the contour plots of micromotion for the CLS group under loads simulating physiological stair-climbing and walking respectively. The results showed that proximal macrofeatures were effective in reducing interface micromotion, thus contributing to the initial stability of the implant. The results also showed that some types of macrofeatures were better than others. The stem with the tapered fins was the most stable with a significant reduction in micromotion in both physiological loadings, whilst the introduction of medial ridges only managed to improve stability slightly compared to the 'blank' control CLS.

For the grooved CLS, interface micromotion depended on the angle of the grooves. In stair-climbing modes, the vertical grooves and the 135^o grooves performed better than the horizontal and 45^o grooves. In physiological walking, the 135^o grooves was the best, followed by the horizontal grooves. The 45^o grooves was the worst in this physiological loading.

Further iterations were performed on all seven models to predict their stability when bone loss was simulated. Iterations were continued until either a stable state of micromotion was achieved, or the implant failed. Failure occurred if interfacial shear strength was exceeded or surface area unfeasible for bone growth exceeded the proximal half of the stem – the part where fixation is supposed to take place. The results of the iteration are shown in *Figure 5.96*, *Figure 5.97*, *Table 5.16* and *Table 5.17*.

When the analyses were repeated after simulating bone resorption, the finned CLS maintained its stability with insignificant increase in micromotion in both physiological loadings (*Table 5.16* and *Table 5.17*). The blank CLS was the worst, where further iterations showed that the surface area unfeasible for bone ingrowth kept increasing. The surface area was larger in physiological walking, where it covered almost the proximal $\frac{1}{3}$ of the stem. When second iteration was performed after simulating interfacial bone loss, the percentage of surface area with micromotion $>50\mu\text{m}$ increased to 72% (*Figure 5.89*, *Table 5.17* and *Figure 5.97*). In stair-climbing modes, the increased of unfeasible surface area was more gradual (*Figure 5.88*). However, in the 5th iteration, the stem failed with 81% of the surface area exceeded the threshold limit for bone ingrowth (*Figure 5.96*).

The medially ridged CLS had lesser micromotion compared to the blank CLS in both physiological loadings particularly in the area surrounding the ridges (*Figure 5.88* and *Figure 5.90*, *Figure 5.89* and *Figure 5.91*). When bone loss was simulated, the stem was found to be stable in stair-climbing modes. In physiological walking using Fisher's loadcase, the stem eventually failed in the 4th iteration with 67% of the surface of the stem was unfeasible for bone ingrowth. However, the increase in the surface area was less abrupt compared to the blank CLS (*Figure 5.97*). In the 2nd iteration, the surface area increased from 18% to 21%, and to 30% in the 3rd iteration. Once interfacial gaps occurred around the ridges, and the support in the medial calcar was lost, the stem behaved similar to the blank CLS with an abrupt increase in the unfeasible surface area for bone ingrowth in the 4th iteration from 30% to 67%.

There were mixed results for the stability of grooved CLS. The 135^o grooves and the horizontal grooves were stable after simulated bone loss in both physiological loadings. The vertically grooved CLS stem was stable in stair-climbing modes, but in physiological walking, the surface area unfeasible for bone ingrowth increased from 18% in the first iteration to 55% in the second iteration (*Figure 5.94* and *Figure 5.95*). The 45^o groove was also found to be stable in stair-climbing (*Figure 5.92*), but not in walking. In the first iteration, 21% of the surface area had micromotion in excess of 50 μ m (*Figure 5.93*) and in the 2nd iteration the surface area increased to 61%.

Results for the ABG system are shown in *Figure 5.98* and *Table 5.18*. No further iterations were performed as it can be clearly seen that the effect of the indentation macrofeatures was very significant. In terms of bone ingrowth, the ABG with macrofeatures had more surface area with bone ingrowth than the blank by 7-10 times. The ABG, with and without the macrofeature, also seemed to be able to sustain torsional loading better as the unfeasible areas for bone ingrowth was less in stair-climbing than in walking.

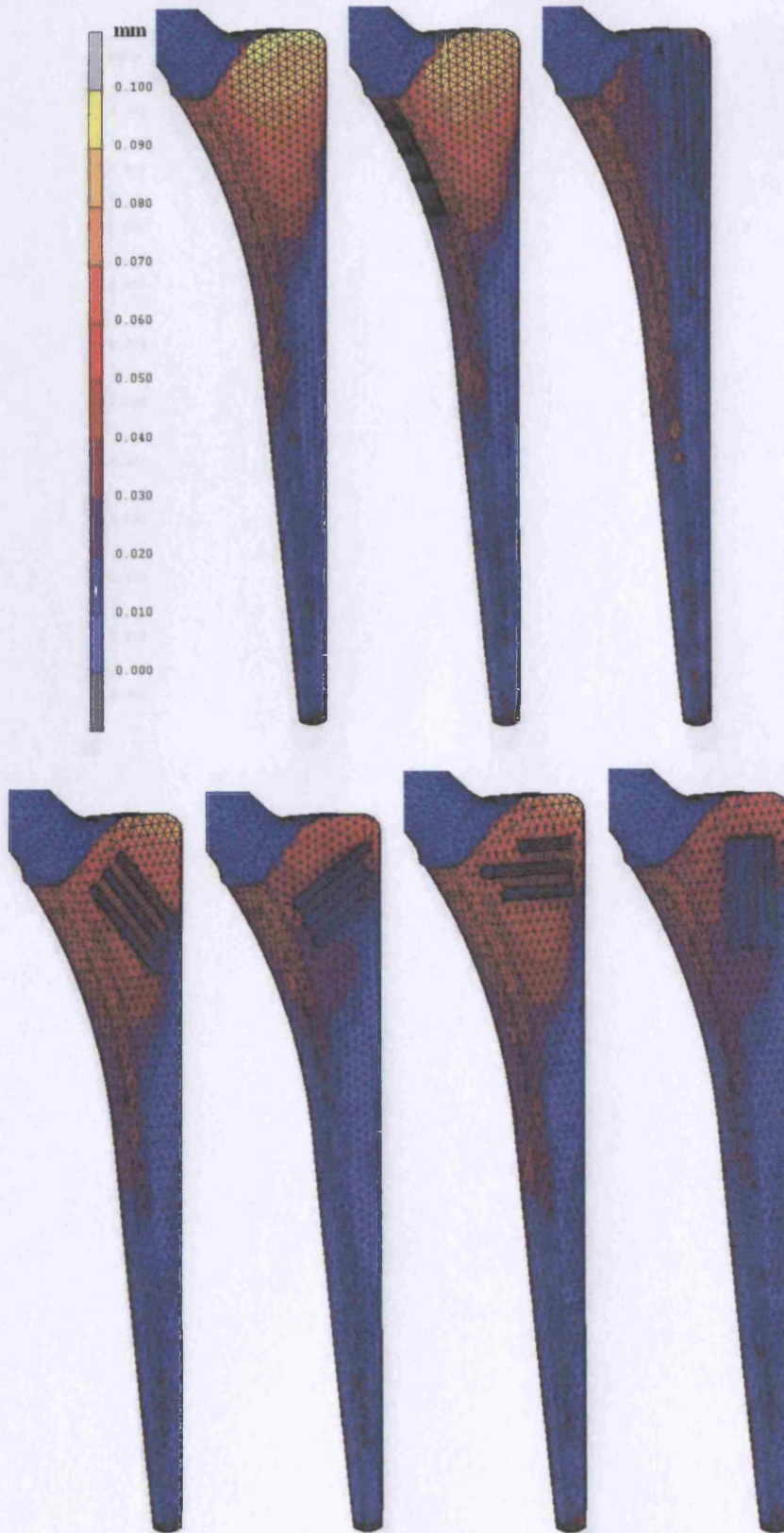


Figure 5.86: Contour plots of micromotion for the blank CLS, the ridged CLS, the finned CLS and the grooved CLS at various angles using Duda's stair-climbing loads after the 1st iteration.

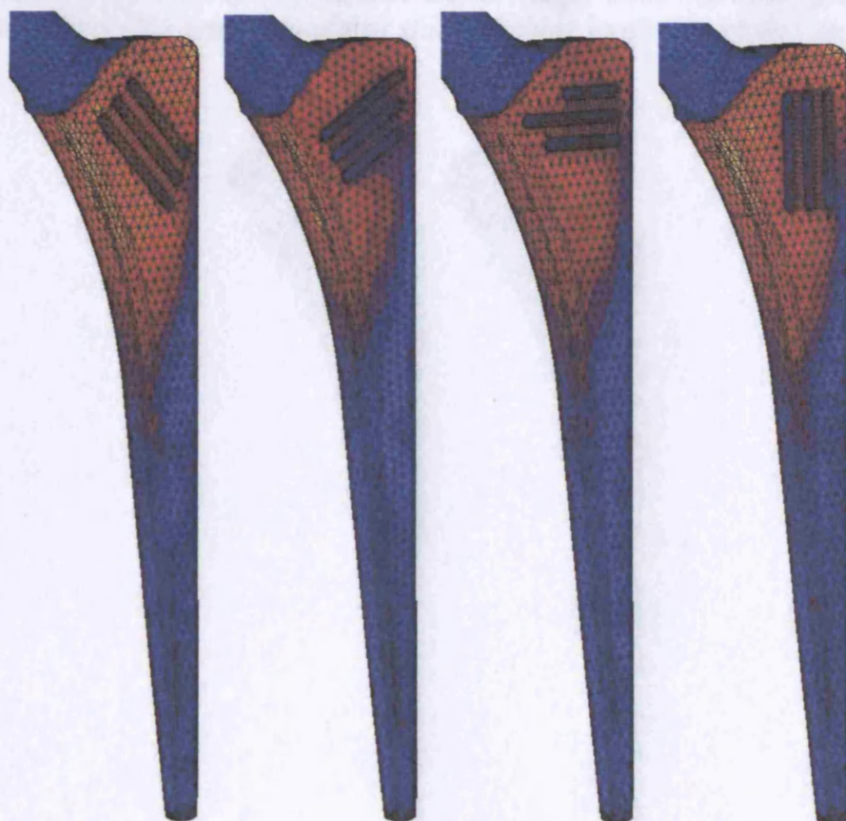
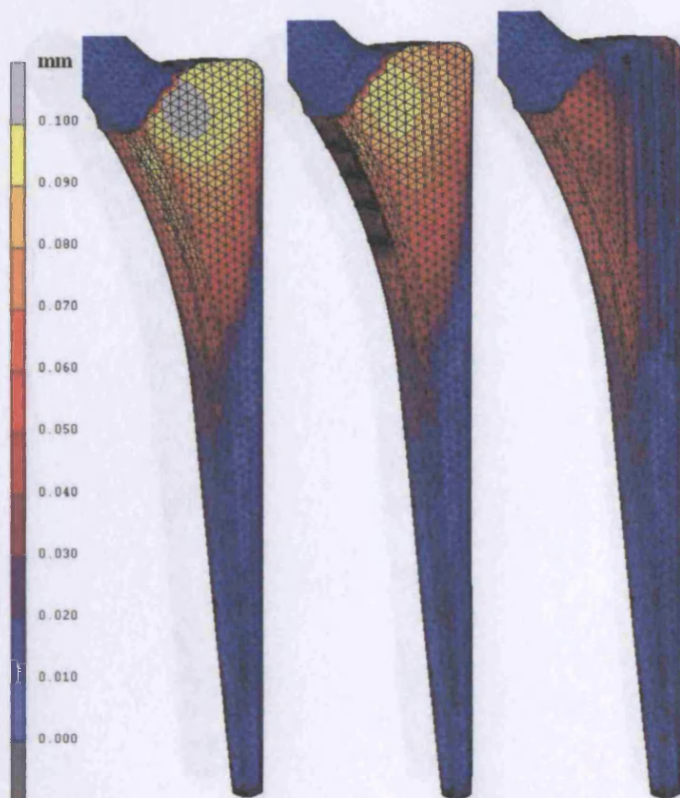


Figure 5.87: Contour plots of micromotion for the blank CLS, the ridged CLS, the finned CLS and the grooved CLS at various angles using Fisher's gait cycle loads after the 1st iteration.

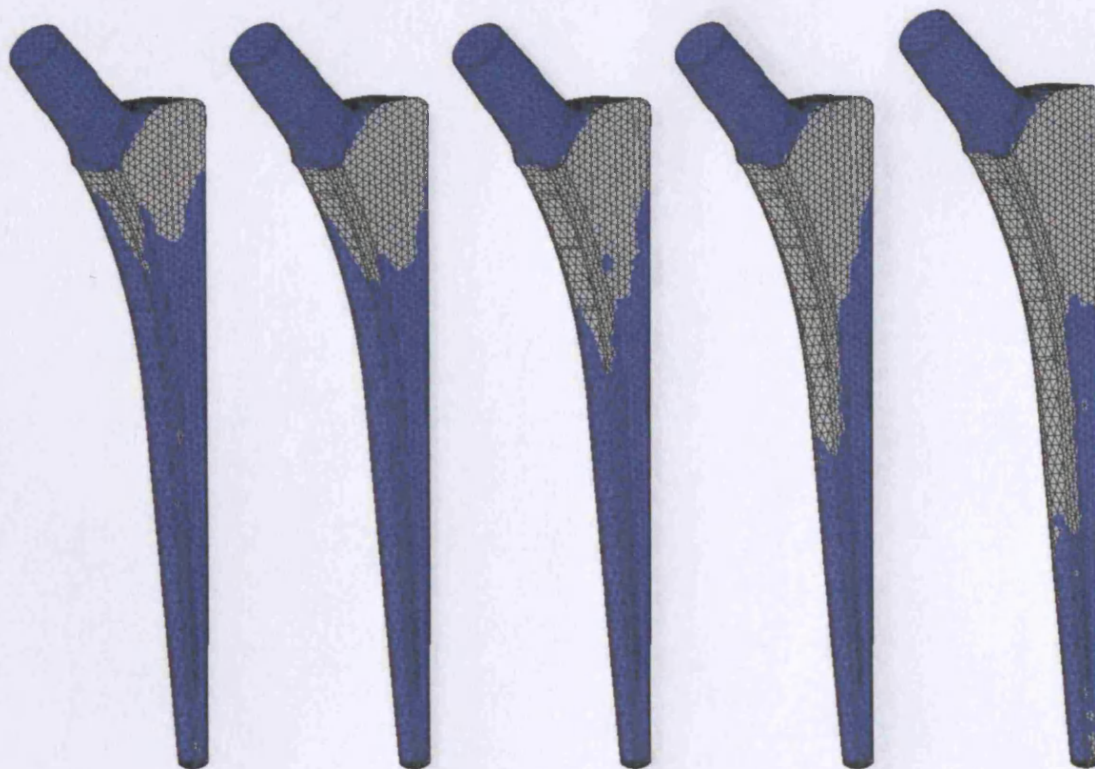


Figure 5.88: Progression of surface area unfeasible for bone ingrowth (grey area) for the blank CLS under simulated stair-climbing loads (iteration 1 to 5).

Copyright © 2010 by Taylor & Francis Group, LLC



Figure 5.89: Progression of surface area unfeasible for bone ingrowth (grey area) for the blank CLS under simulated walking loads (iteration 1 and 2).



Figure 5.90: Progression of surface area unfeasible for bone ingrowth (grey area) for the ridged CLS under simulated stair-climbing loads (iteration 1 to 3).

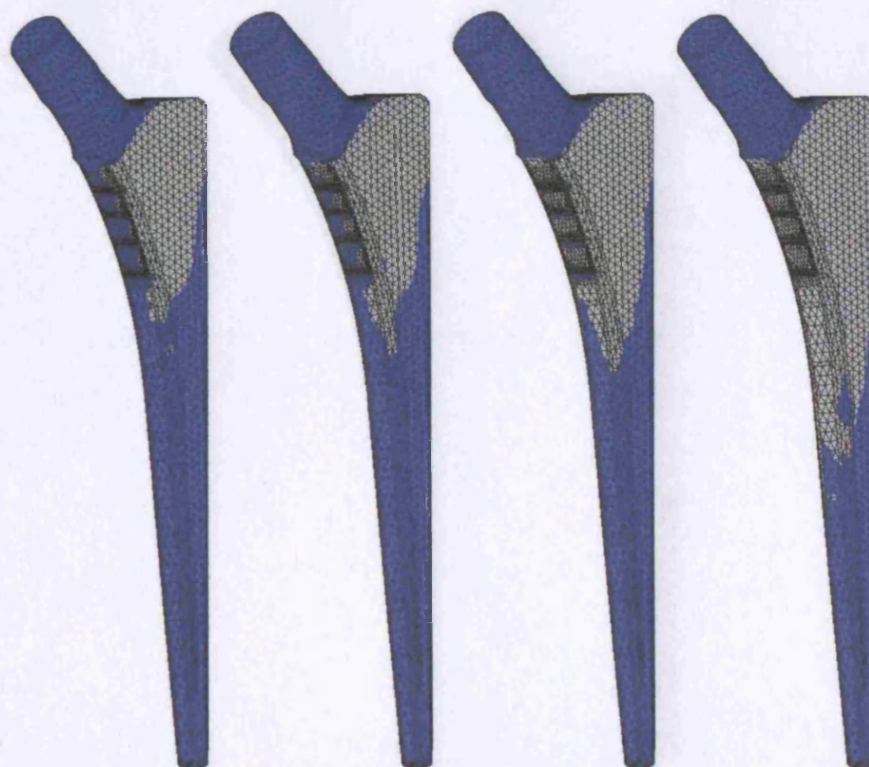


Figure 5.91: Progression of surface area unfeasible for bone ingrowth (grey area) for the ridged CLS under simulated walking loads (iteration 1 to 4).



Figure 5.92: Progression of surface area unfeasible for bone ingrowth (grey area) for the 45° grooved CLS under simulated stair-climbing loads (iteration 1 to 3).



Figure 5.93: Progression of surface area unfeasible for bone ingrowth (grey area) for the 45° grooved CLS under simulated walking loads (iteration 1 and 2).

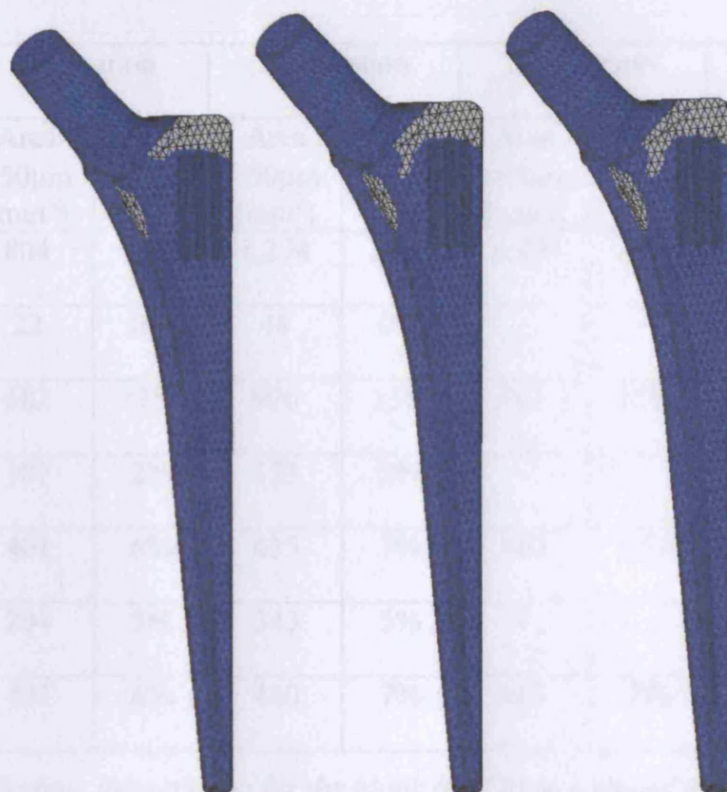


Figure 5.94: Progression of surface area unfeasible for bone ingrowth (grey area) for the vertically grooved CLS under simulated stair-climbing loads (iteration 1 to 3).



Figure 5.95: Progression of surface area unfeasible for bone ingrowth (grey area) for the vertically grooved CLS under simulated walking loads (iteration 1 and 2).

	1 st iteration		2 nd iteration		3 rd iteration		4 th iteration	
	Area >50µm (mm ²)	%	Area >50µm (mm ²)	%	Area >50µm (mm ²)	%	Area >50µm (mm ²)	%
blank	804	13%	1,294	21%	1,990	32%	2,861	46%
fins	22	0%	48	0%	-	-	-	-
ridge	682	11%	906	15%	961	15%	-	-
135 ^o	107	2%	153	2%	-	-	-	-
45 ^o	401	6%	435	7%	460	7%	-	-
Vertical	294	5%	343	5%	-	-	-	-
Horizontal	405	6%	440	7%	465	7%	-	-

Table 5.16: Surface area $\geq 50\mu\text{m}$ for the blank (6,172mm²), finned (6,717mm²), ridge (6,201mm²), 135^o groove (6,324mm²), 45^o groove (6,220mm²), vertical groove (6,365mm²) and horizontal groove (6,283mm²) using Duda's stair-climbing loads.

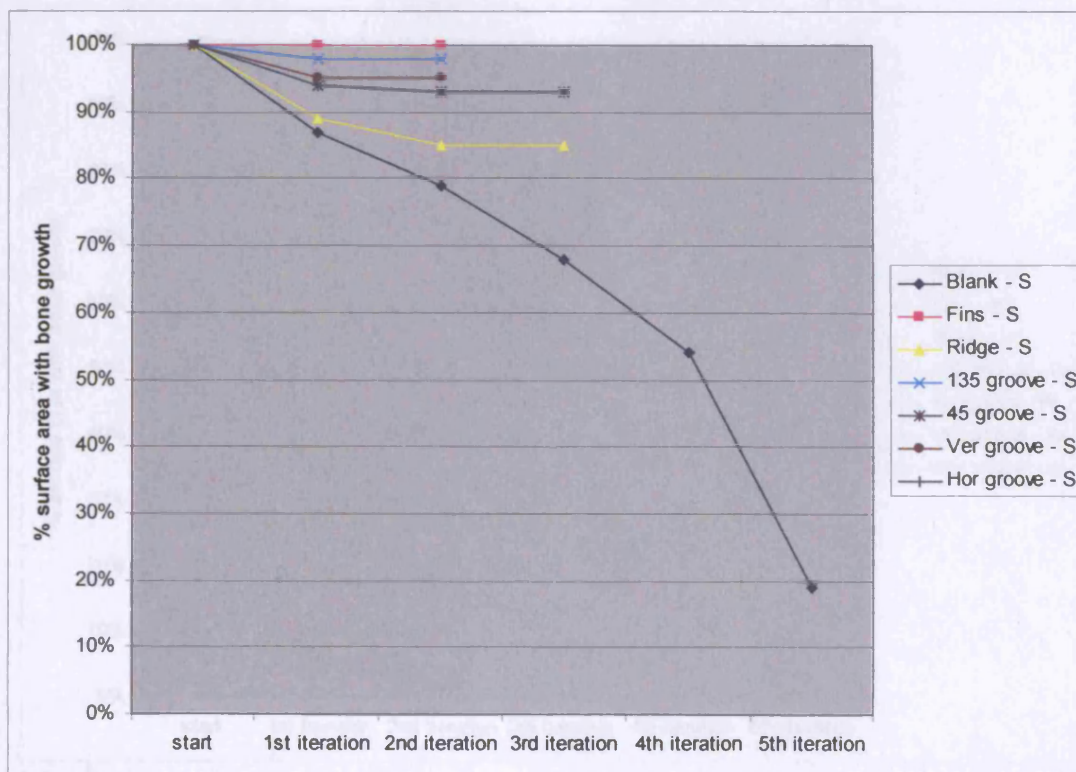


Figure 5.96 : Percentage of surface area feasible for bone ingrowth for the blank, finned, grooved and ridged CLS under simulated stair-climbing loads.

	1 st iteration		2 nd iteration		3 rd iteration		4 th iteration	
	Area >50µm (mm ²)	%	Area >50µm (mm ²)	%	Area >50µm (mm ²)	%	Area >50µm (mm ²)	%
blank	1,359	22%	4,429	72%	-	-	-	-
fins	255	4%	301	4%	-	-	-	-
ridge	1,112	18%	1,302	21%	1,878	30%	4,142	67%
135 ^o	316	5%	341	5%	-	-	-	-
45 ^o	1,331	21%	3,816	61%	-	-	-	-
Vertical	1,128	18%	3,492	55%	-	-	-	-
Horizontal	628	10%	679	11%	716	11%	-	-

Table 5.17: Surface area $\geq 50\mu\text{m}$ for the blank (6,172mm²), finned (6,717mm²), ridge (6,201mm²), 135^o groove (6,324mm²), 45^o groove (6,220mm²), vertical groove (6,365mm²) and horizontal groove (6,283mm²) using Fisher's walking loads.

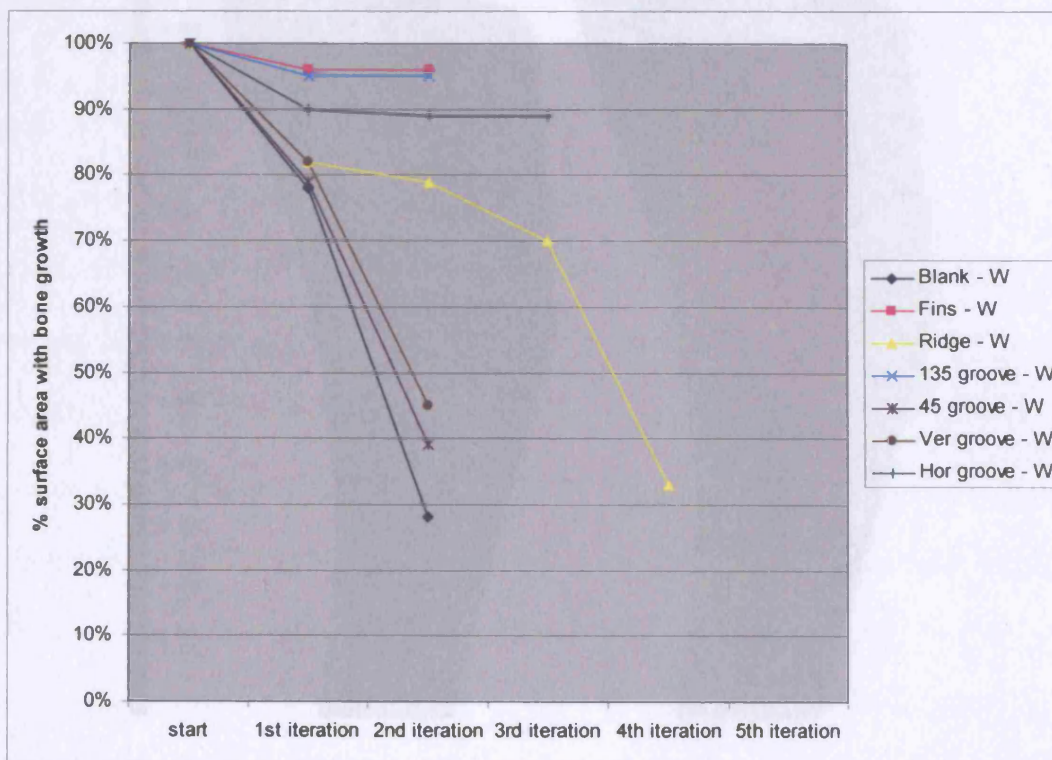


Figure 5.97: Percentage of surface area feasible for bone ingrowth for the blank, finned, grooved and ridged CLS under simulated walking loads.

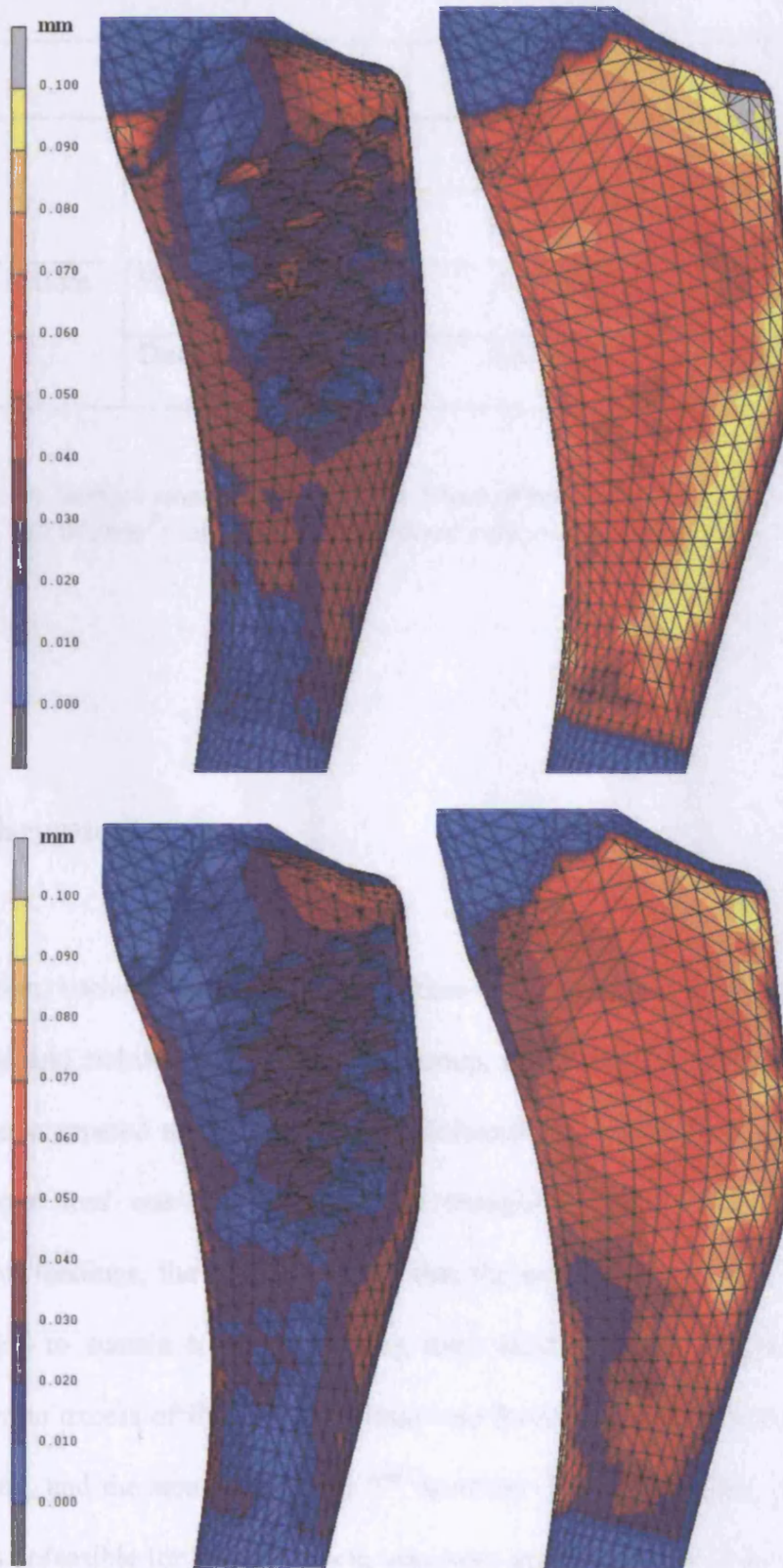


Figure 5.98: Contour plot of micromotion for the ABG with and without proximal indentation macrofeatures. Results for Fisher's gait (top) and Duda's stairclimbing (bottom).

		Area > 50 μ m	%
No feature	Fisher's gait	3,023 mm ²	63%
	Duda's stair	1,657 mm ²	34%
Indentation feature	Fisher's gait	447 mm ²	9%
	Duda's stair	163 mm ²	3%

Table 5.18: Surface area with more than 50 μ m of micromotion for the ABG, with (5,013mm²) and without (4,816mm²) the indentation features.

5.5.3 Discussion

In this section, various proximal macrofeatures were compared in terms of interface micromotion and stability. From the CLS group, the blank CLS produced the largest micromotion compared to those with macrofeatures and was the most unstable when interface bone loss was simulated. Even though the blank CLS failed in both physiological loadings, the results showed that the overall geometry of the CLS was more capable to sustain torsional loading than axial loading. In the 1st iteration, micromotion in excess of the threshold limit was found to be more in walking than in stair-climbing, and the stem failed after 2nd iteration. In stair-climbing, the increase in surface area unfeasible for bone ingrowth was more gradual and the stem failed after the 5th iteration.

The overall results showed that primary stability was improved with the introduction of proximal macrofeatures. The magnitude of improvement, however, depended on the type of macrofeatures. The CLS with its actual macrofeatures showed maximum stability because the vertical tapered fins allow bone interlocking in between them, making the stem very stable especially under torsional loading such as the one experienced during stair-climbing. The effect of a medially ridged CLS stem on micromotion, on the other hand, was found to be localised to the area surrounding the ridges. Even though micromotion was reduced compared to the blank CLS, the medial ridges were not found to be enough to maintain stability especially in physiological loading where axial motion was predominant. Once contact with the medial calcar was lost (after 3rd iteration), the stem behaved exactly like the blank CLS.

Micromotion reduction due to grooves varied according to their orientation. Grooves that aligned to the joint load had the largest micromotion and were the most unstable. These can be seen in the results for the CLS with the vertical and 45^o grooves under physiological walking loads. Grooves opposing the direction of loading had the lowest micromotion and were more stable in both physiological loadings. These can be seen in the results of the CLS with 135^o grooves in walking and stair-climbing modes, the vertically grooved CLS in stair-climbing, and the horizontally grooved CLS in walking. However, when compared with the results of the actual CLS stem with tapered fins macrofeature, the latter showed superior results in terms of interface micromotion particularly in the anterior and posterior sides and was the most stable after simulating bone loss. This could be attributed to the geometry of the tapered fins where they covered almost the proximal half of the stem. There were three fins on both sides of the stem and the thickness of the most lateral fin was larger than the other two, creating a

tri-planar tapered stem. Hip stem with a similar tri-planar tapered design has been shown to be very stable (Mallory et al. 2002).

The CLS is a type of hip stem that relies on proximal fixation. FE analyses showed that the stem was very stable with its original macrofeature of tapered fins. This is in agreement with a couple of follow-up studies on the CLS where a 100% survival rate was reported at 3 years (Robinson, Lovell & Green 1994) and 8.9 years (Schreiner et al. 2001). Out of 335 primary THA performed, only one was found to have subsided, but no stem was found to be loose clinically or radiologically. Other type of stem with similar macrofeatures, such as the vertically ridged SPF, was also found to perform better than the non-ridged SPF with migration of 0.8mm/year for the latter and 0.6mm/year for the former (Donnelly et al. 1997).

The ABG is another hip stem designed with a proximal fixation concept. It is anatomically shaped and has a narrow and tapered distal stem where this area of the femur is over-reamed to avoid stem contact and reduce distal load transfer. It is so designed in an attempt to transfer loads more proximally and maintain bone density in that area. The anatomical shape and proximal fit design provides initial stability in the metaphyseal area. This is further enhanced by the semi-circular indentation macrofeatures whose functions are theoretically converting shear forces into compression and thus prevention of early subsidence of the implant (Giannikas et al. 2002). Long-term stability is achieved through osseointegration of the implant at the metaphyseal region, which is coated with HA.

The ABG system showed excellent results with good initial stability at 2 years (Rossi et al. 1995). Another paper (Rogers, Kulkarni & Downes 2003) reported that the ABG hip stems performed well at the average 6 years follow-up, with 100% survivorship of the stem. The overall survivorship was brought down however, due to the high failure rate of the acetabular cup liner due to excessive wear. Analysis of the femoral component showed that 88% of the hips were centred, 9% were implanted in varus and the other 3% in valgus. However, no stem migration was radiographically evident.

Overall, this study confirmed the usefulness of proximal macrofeatures in improving stability of cementless stems. This is even more important in proximal fixation stems designed with distal over-reaming because strong cortical support in the metaphyseal region was relatively lacking and as such any features that can provide bone interlocking would be beneficial in terms of providing primary stability.

5.6 Conclusion

This chapter dealt with design aspects of cementless hip stems with regards to primary stability. Various design details of uncemented stems were obtained from the literature and from the manufacturers, and have been discussed; several major aspects of these designs were modelled and analysed by FEA. The study started with the overall geometry by grouping the cementless stems into three distinct categories – the straight cylindrical, the tapered and the anatomical. A representative stem from each group was

analysed in physiological walking and stair-climbing and the interface micromotion results were compared. The results showed that the three stem types had similar distribution of micromotion and were all stable prostheses. The straight cylindrical was relatively less stable than the other two types, especially when interfacial gaps were present. The study then continued with the effect of material stiffness on stability. Too flexible a material was not recommended as it increased interface micromotion; the unfeasible surface area for bone ingrowth increased up to 5 times compared to the most rigid stem. However, the FE results showed that the implant should still be stable if tight fit was achieved distally. The effect of stem length was also analysed. A longer stem was found to be more stable than shorter ones due to the larger surface area in contact with strong cortical bone in the distal area. A very short stem with minimal contact to cortical bone was found to be the most unstable. But short stems have the advantage of causing less bone damage in case revision surgery is needed. And the stability of a short stem, which could also mean a proximal fixation design, could be improved by widening its proximal part in the antero-posterior direction and having a lateral flare. Macrofeatures, of whatever type, were also found to reduce micromotion and were found to be very beneficial to stems with proximal fixation design.

Chapter 6 Surgical & pathological parameters affecting micromotion

The previous chapters have looked at various design parameters of cementless hip stems and their effects on primary stability. However, implant selection alone does not ensure successful implant fixation or successful outcome after hip replacement. The strength of primary fixation seems to depend not only on stem design, but also on other factors such as the quality of the bone and canal preparation for implantation (Amstutz 2000; Thomsen et al. 2002). Successful implant fixation in a hip replacement requires precise, accurate surgical technique (Healy 2002). An imprecise surgical procedure will cause problems in terms of achieving the maximum possible fit and could cause implant undersizing and malalignment. In cementless press-fit stems, for example, maximum fit

is difficult to achieve in the line-to-line reaming technique compared to the under-reaming technique (Sugiyama, Whiteside & Engh 1992). This is because gaps between bone and implant may occur because of inaccurate bone preparation. This chapter will not look at surgical approaches or the different available techniques for implant preparation. Rather we would like to answer the question of whether the existence of interfacial gaps, due to surgical error or otherwise, will weaken the stability of the implant. The chapter will also look at surgical errors in terms of implant sizing and alignment, using finite element analysis to see if these have any effects on primary stability. The tendency to undersize an implant normally happens when the surgeon is being too cautious and decides not to have a tight fit as this could lead to fracture of the bone or bone-splitting. It could also happen if the reamer was not properly aligned to the femoral canal during bone preparation, causing the tip of the reamer to touch the cortex sooner than it should. This causes not only implant undersizing but also implant malalignment in a valgus or much more commonly varus position.

Another factor that affects stability is the quality of the bone. Most hip replacement surgeries are performed due to joint disease such as arthritis and rheumatoid arthritis in order to remove pain and regain mobility. These skeletal diseases mostly affect the areas around the joint – the femoral head and the acetabulum. As such, the quality of the bone further away from the joint is usually affected to a lesser extent. However, there are also cases where patients are not only suffering from joint disease but also suffering from osteoporosis, a bone disease which affects mostly women and the elderly. And contrary to osteoarthritis, osteoporosis affects the overall bone quality (Li & Aspden 1997). The thinning and subsequent loss of trabecular bone in osteoporotic patients means that the apparent density of the bone stock is reduced significantly, thus

reducing the overall femoral stiffness and strength. In chapter 4, the effect of varying the stiffness of the bone on micromotion was examined by varying the constant in the density-stiffness relationship proposed by Carter & Hayes. In this chapter the effect of skeletal diseases on stability will be analysed using actual bone samples from patients suffering from osteoarthritis and osteoporosis. Comparison will then be made with a normal bone from the VHP femur dataset.

6.1 The effect of interfacial gaps on micromotion

Implantation of cementless hip stems requires specific surgical procedures based on their design. However, the principles of implantation are similar; satisfactory femoral exposure, opening the femoral canal, broaching the proximal femur (either hand-broaching or power-reaming), irrigation of the femoral canal, and implanting the femoral stem to a position which is stable to bending, tilting, rotation, subsidence and pull-out force (Healy 2002).

Gaps between implant and bone may occur especially when contemporary broaching techniques are used which are subject to surgical error. Gaps occur at various locations along the stem because the broach that prepares the bony bed passes outside the outline of the femoral component (Mont & Hungerford 1997). Noble et al. (1988) have reported the difficulties of achieving interfacial contact due to the anatomical variations of the femur. Surface-to-surface contact between implant and bone was not achieved

except at discrete areas of the interface. A study was conducted by Paul et al. (1992) to compare the accuracy of traditional broaching and reaming for femoral canal preparation versus a surgical robot for milling the cavity. In their study they measured 'cavity oversizing', 'linear gap' and 'percentage of perimeter in contact with the bone' and the results showed that robotic milling produced a superior accuracy in terms of implant fit (*Table 6.19*). The study, however, fell short of analysing the effect of the inadequacies of using traditional techniques on primary stability.

	Traditional	Surgical robot
Cavity oversizing	22-40%	0.4-0.7%
Linear gap	1.0-3.5mm	0.03-0.08mm
Perimeter in contact with bone	21%	96%

Table 6.19: Comparison between traditional and surgical robot for femoral canal preparation (Results taken from Paul et al. 1992).

The experimental findings of Paul et al. have led to the development of an algorithm that can show interfacial contact and the existence of gaps at the bone-implant interface (Testi et al. 2004). Though the paper only described the validation procedure of the algorithm, the examples presented in the paper showed that interfacial contact did not occur throughout the stem-bone interface.

Pazzaglia et al. (1998) studied the effect of interfacial gaps on rats. Two groups of roughened titanium rods were examined – one with an interference fit and the other with a 0.3mm diametrical gap at the interface. They found that there was no bone integration at the interface of the over-reamed canal, whether the surface of the rod was coated with

hydroxyapatite or not. The interface was surrounded by a thick layer of fibrous tissue, with no bony connections with the endosteal surface.

To the author's knowledge, there are no reported studies that have looked into the effects of gaps on primary stability. In order to carry out this study, a technique of identifying interfacial gaps is proposed (the 1st method), where multiple CT scans of the specimen are required. In cases where specimens are not available, discussions are conducted with experienced orthopaedic surgeons to determine the areas where interfacial gaps are most likely to occur (the 2nd method). The aim is to discover if these interfacial gaps created due to surgical error or otherwise, have any effects on the primary stability of cementless hip stems.

6.1.1 1st Method

In order to study interfacial gaps created during broaching, two sets of images from two separate cadavers implanted with the Alloclassic hip stem were scanned using normal CT and PQCT. From these two sets of images interfacial gaps were found on both (*Figure 6.99*). However, artefacts from the metallic implant made it difficult to determine the interfacial gaps accurately. In order to see more clearly the existence of gaps at the interface, a procedure is proposed as described in the following paragraphs.

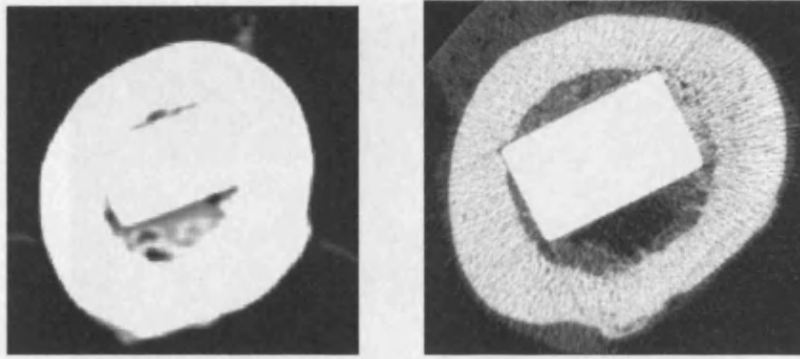


Figure 6.99: Normal CT and PQCT from two different cadavers with Alloclassic hip implant showing interfacial gaps on the posterior side.

A single dataset of implanted bone such as the one shown above is not sufficient to create an FE model to study interfacial gaps. The artefacts due to the metallic material of the implant caused several problems. Apart from the problem in analysing the gaps, the implant model created from the digitised image was also not appropriate to be used in FE analyses. Implant construction using this single dataset failed to create a perfectly shaped implant – they are coarse and slightly larger in size than the actual implant (*Figure 6.100 - right*). The model of the implant must therefore be created from the original 3D CAD model. The CT dataset of an implanted femur also cannot be used even if the implant model was constructed separately. This is because bone material properties assignment, as described in chapter 2, will show high stiffness at the interface due to an imaging artefact (*Figure 6.101*). All these problems can be overcome by using multiple CT datasets.

Three sets of CT data are needed: the intact bone, the bone after reaming and the bone after reaming (*Figure 6.102*). The 1st set (the intact bone) will be used as the overall model, which is the model without interfacial gaps. The 2nd dataset (bone after reaming) will be used to identify interfacial gaps. This is done by creating a 3D bone

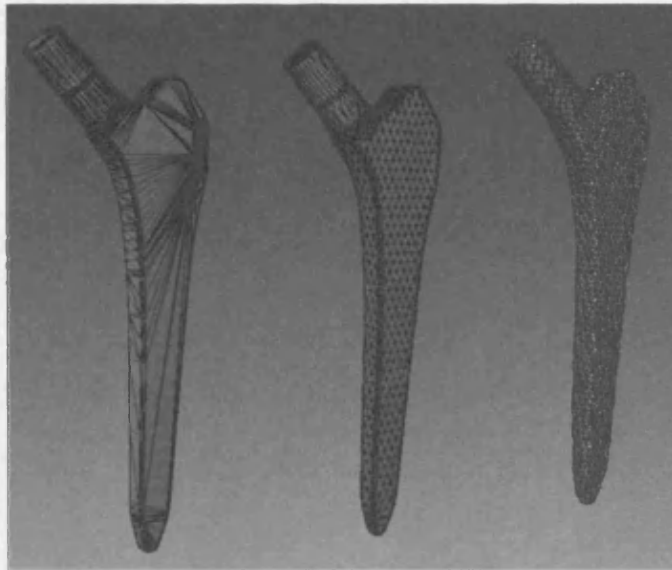


Figure 6.100: The original CAD drawing from the manufacturer (left), the created surface-meshed model (centre) and model constructed from CT images (right).

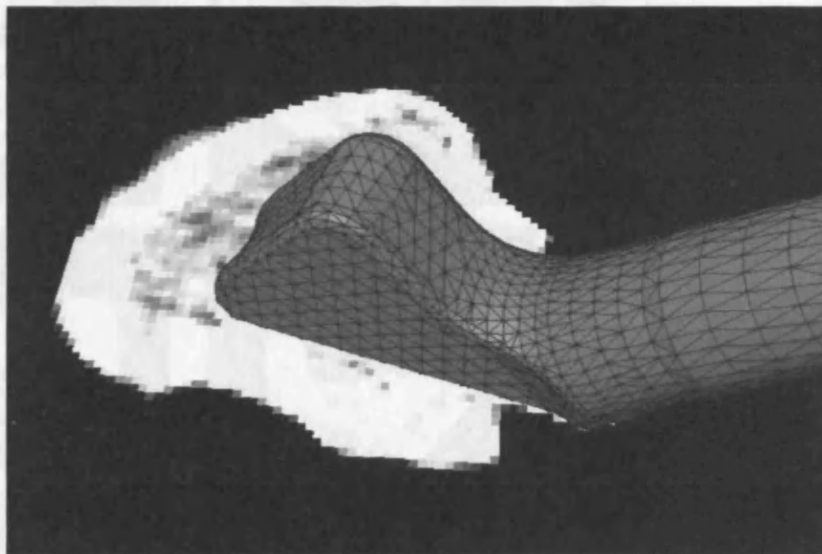


Figure 6.101: The Alloclassic hip stem on a CT slice of an implanted femur, showing the artefacts at the interface (strong white mark) that translate into high stiffness at the interface using the Carter & Hayes density-stiffness relationship.

Three sets of CT data are needed; the intact bone, the bone after reaming and the bone after implantation (Figure 6.102). The 1st set (the intact bone) will be used as the control model, which is the model without interfacial gaps. The 2nd dataset (bone after reaming) will be used to identify interfacial gaps. This is done by creating a 3D bone

model from the 2nd dataset and the implanted femur from the 3rd dataset. The two models were then aligned so that the model from the 2nd dataset coincided with the model from the 3rd dataset. The model of the implant, created separately in stereolithographic format, was then loaded into the software and aligned so that it coincided with the implant from the 3rd CT dataset. Once the implant model was properly aligned, the 3rd dataset and its model were removed leaving the implant model and the 2nd CT dataset. The interfacial gaps can now be clearly identified (*Figure 6.103*).

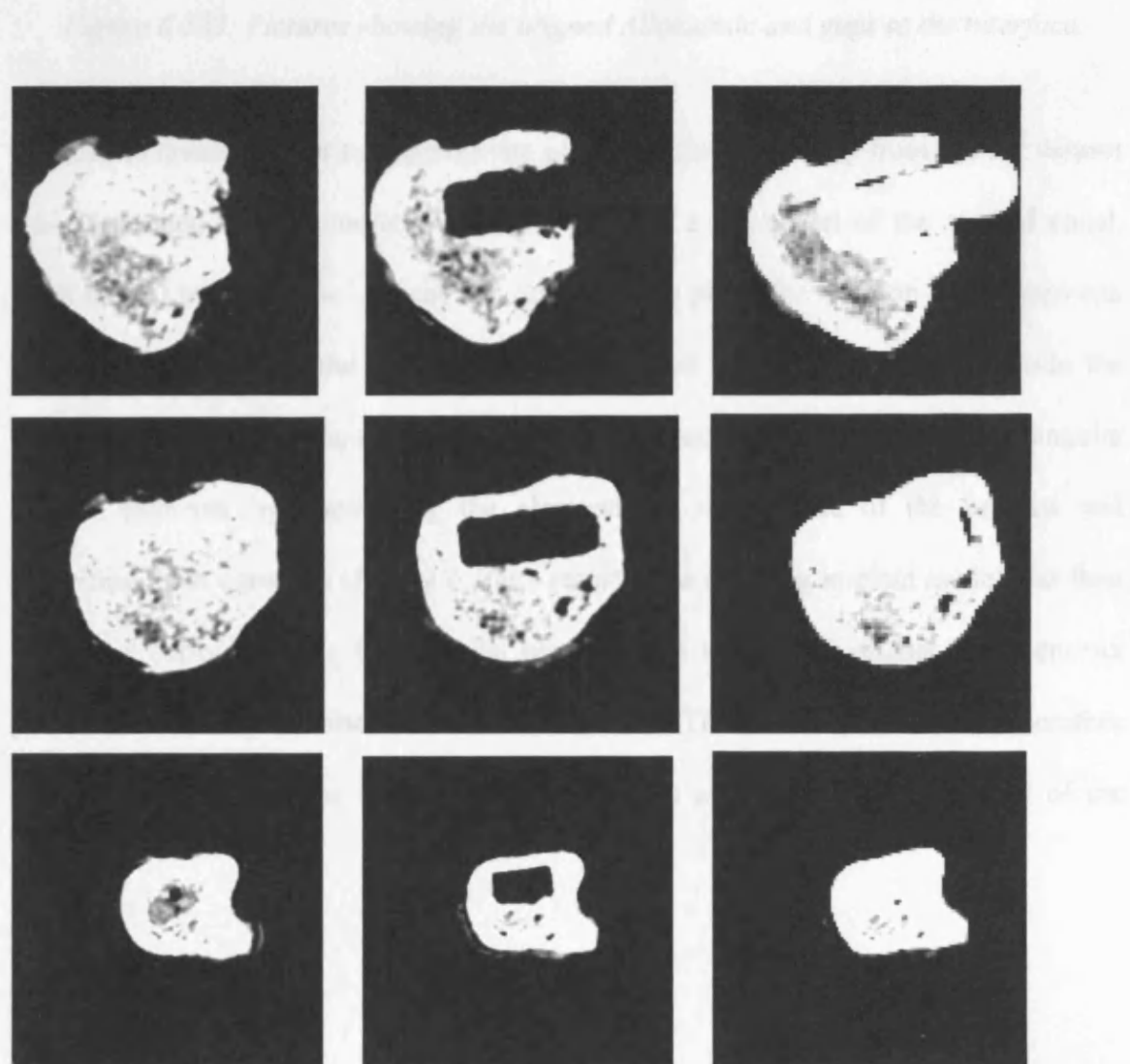


Figure 6.102: The three sets of CT data – Intact bone (left), after reaming (middle) and after implantation (right).

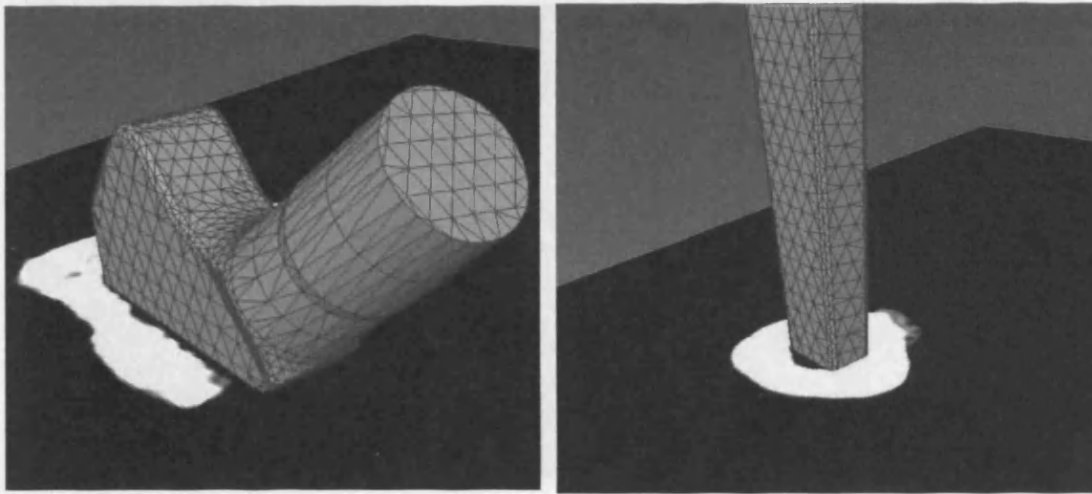


Figure 6.103: Pictures showing the aligned Alloclassic and gaps at the interface.

In order to create gaps at the appropriate place, the femoral cavity from the 2nd dataset was segmented in the computer software to create a 3D model of the reamed canal. With the 3D model of the implant still aligned in its place, the location of the gaps can be identified based on the 3D model of the reamed canal that projected outside the surface of the implant (*Figure 6.104 - left*). These gaps were then turned into triangular surface elements by duplicating the elements on the surface of the implant and projecting them outwards (*Figure 6.104 - right*). The resulting implant model was then used as a cut-out for the bone model created from the 1st CT dataset. The cut-out procedure has been described in detail in Chapter 2. The resulting bone model therefore contained interfacial gaps at the appropriate places and perfect fit on the rest of the interface.

The material properties for the bone in both models were taken from the 1st CT dataset. All other FE parameters used in the models were the same as those used in Chapters 2 and 4.

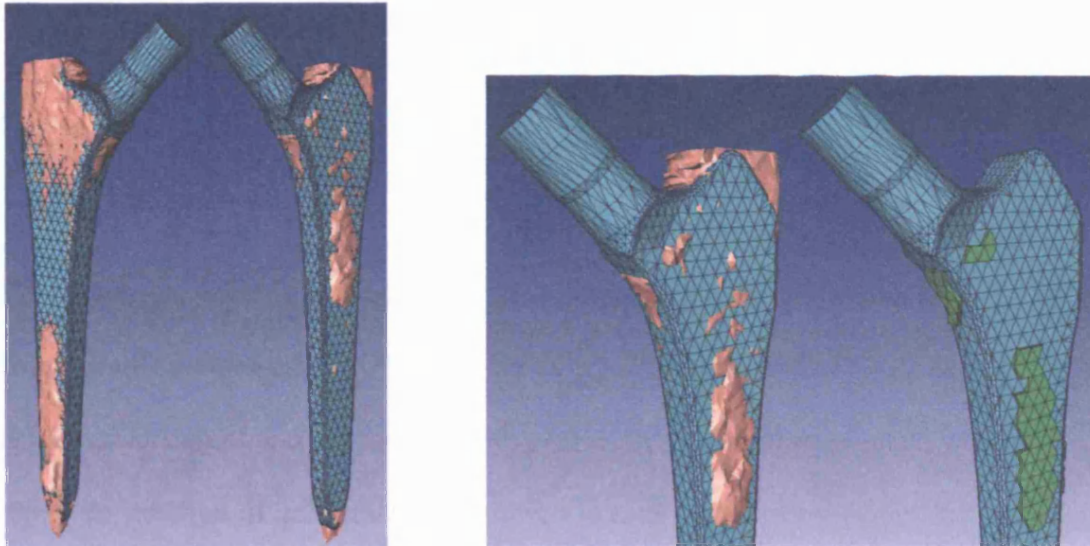


Figure 6.104: Pictures showing interfacial gaps on the anterior and posterior side of the stem (left). The interfacial gaps turned into elements (right).

Another bone model to simulate perfect fit was created from the 1st CT dataset using the aligned implant without additional elements representing gaps. This bone model, together with the bone modelled with gaps, were then turned into solid tetrahedrals. The Alloclassic hip stem model was then merged into the two bone models separately, creating two separate FE models – one with interfacial gaps and another one with perfect interface fit.

Both models were then loaded in physiologic activities representing walking (Fisher's loadcase) and stair-climbing (Duda's loadcase). The material properties for the bone in both models were taken from the 1st CT dataset. All other FE parameters used in the models were the same as those used in Chapters 2 and 4.

6.1.2 Results

The results are shown in *Figure 6.105* below for the Fisher's gait cycle (left) and Duda's stair-climbing (right). There were no significant differences between the models with interfacial gaps and the models with perfect fit in both physiological loadings. The overall distribution of micromotion is similar in each case, even though there are gaps at the interface, showing that these gaps did not endanger the stability of the prosthesis.

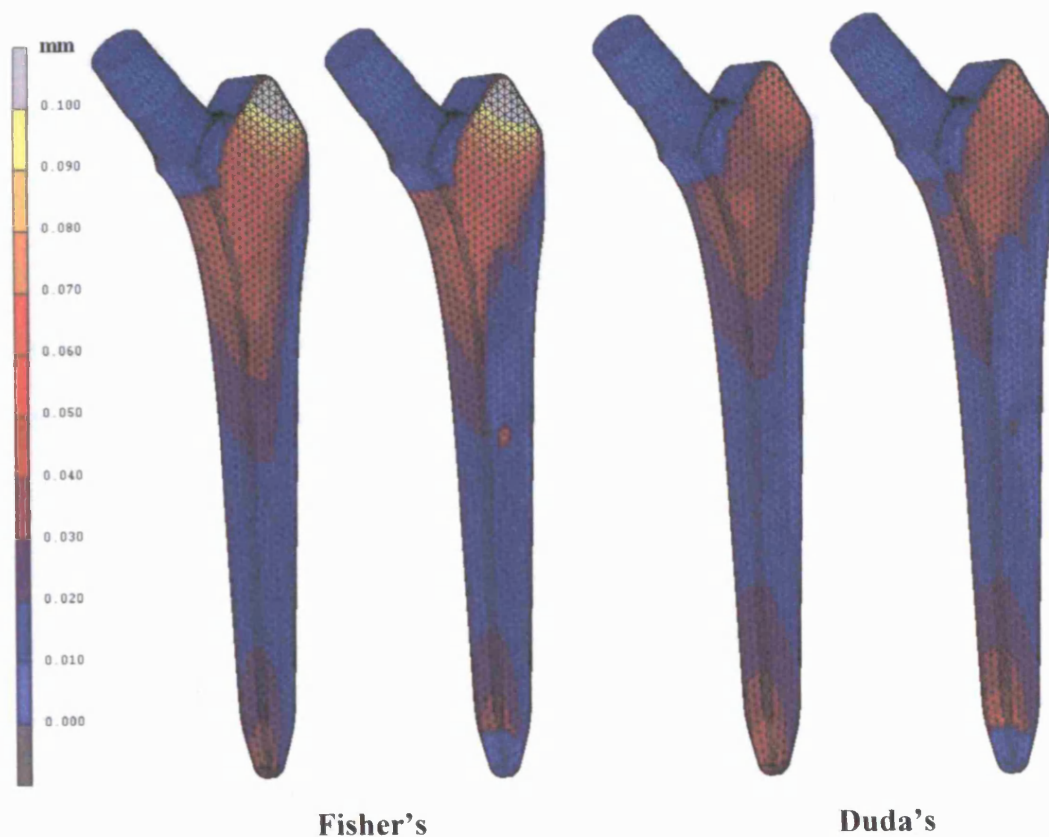


Figure 6.105: Micromotion results using Fisher's loadcase (left) and Duda's loadcase (right). Each set contains the micromotion result for without gaps (left) and with gaps (right).

6.1.3 2nd Method

Another comparison on the effect of gaps on primary stability was made using the ABG and the AML hip stems. The ABG is a proximal fixation design, where the distal endosteal part is over-reamed to avoid cortical contact, a condition which may cause thigh pain (Giannikas et al. 2002). Over-reaming the distal region also means that load will be transferred mostly through the proximal part of the implant. In this section, physical examination of interfacial gaps using CT datasets as described in the previous section could not be used due to the unavailability of specimens. Therefore, discussions with senior and experienced orthopaedic surgeons were carried out to determine the likelihood of interfacial gaps during femoral canal preparation. It was said that perfect fit in the proximal part of the ABG is crucial as this is the only area where loading is supposed to take place. However, the curved shape of the ABG meant that there are possibilities of gaps created during manual broaching in the lateral-proximal region. From these discussions, two FE models of the ABG were created, one with the lateral-proximal gap and another one with perfect proximal fit (*Figure 6.106 – middle and right*).

As mentioned above, the ABG stem is anatomically shaped with distal endosteal over-reaming as standard procedure. However, there are other anatomically-shaped hip stems that do not use the same surgical procedure as the ABG. The PCA (Howmedica), the Profile (DePuy) and the Citation (Stryker) cementless hip stems, for example, are not distally over-reamed. Compared to the ABG, the PCA is the earlier anatomic hip stem. Complications from the use of PCA stems, such as thigh pain and adverse bone remodelling (distal bone hypertrophy & proximal bone atrophy) have led to the distally

over-reamed anatomical ABG. It is unknown however if the gap in the distal region of the ABG system could compromise its primary stability. Based on this argument, another model was created with a perfect fit throughout the stem in order to compare the effect of distal over-reaming on anatomical hip stems (*Figure 6.106 - left*).

There is one published report of a computer simulation study looking at the effect of totally removing the distal half of the ABG stem, thus allowing in theory complete proximal load transfer (van Rietbergen & Huiskes 2001). The authors concluded that the predicted bone remodelling pattern did not change much between the distally-cut ABG and the normal ABG. They also mentioned that reducing the stem length to the metaphyseal region only is not advantageous from a mechanical point of view. However, they did not carry out any stability simulation analyses.



Figure 6.106: Three cases of the ABG stem analysed – without interfacial gaps (left), distal gap (centre) and distal & lateral-proximal gap (right).

The three ABG models were loaded with physiological walking and stair-climbing loads, with and without an interference fit of 100 μ m. The bone model used was created from the VHP bone dataset and all other parameters remained the same as previous studies.

The other hip stem analysed in this section is the straight cylindrical AML. Contrary to the ABG, the AML is a distally-fixed cementless stem; fixation depends on a press-fit between the rough external surface of the implant and a similarly shaped femoral canal. Under-reaming surgical procedure is used to achieve tight fit with the cortical bone distally. However, achieving strong cortical support distally means that interfacial gaps could occur in the proximal region.



Figure 6.107: Three cases of the AML stem analysed – without interfacial gaps (left), with gaps in the proximal $\frac{1}{3}$ (middle) and with gaps in the proximal $\frac{1}{2}$ (right).

Three AML models were created – a model with a perfect interface fit as control, an AML with interfacial gaps in the proximal $\frac{1}{3}$, and an AML with interfacial gaps in the proximal half (*Figure 6.107*). The three models were loaded with physiological walking and stair-climbing loads with an interference fit of $100\mu\text{m}$. The VHP femur dataset was used as the bone model, and all other parameters remained the same as previous studies.

6.1.4 Results

Figure 6.108 and *Figure 6.109* below show the contour plots of micromotion for the three ABG models using Fisher's gait cycle and Duda's stair-climbing loads. For each loadcase (Fisher's / Duda's) two sets of results are displayed, without interference fit (top pictures) and with an interference fit of $100\mu\text{m}$.

The general trend in all cases shows that micromotion increased as gaps were introduced, first on the distal region and then in the distal + lateral proximal region. There was a substantial increase in micromotion between the perfect fit model and the other two ABG modelled with gaps. However, lateral-proximal gaps that simulated surgical error during implantation did not appear to cause any major changes in terms of magnitude or distribution of micromotion compared to the perfect proximal fit ABG during walking. In stair-climbing, on the other hand, the existence of a lateral-proximal gap increased the micromotion around this region significantly. There was also a considerable increase in micromotion between a perfect fit model and the distally overreamed model in stair-climbing compared to walking. The results also showed that the introduction of an interference fit of $100\mu\text{m}$ caused a considerable reduction in micromotion in all cases.

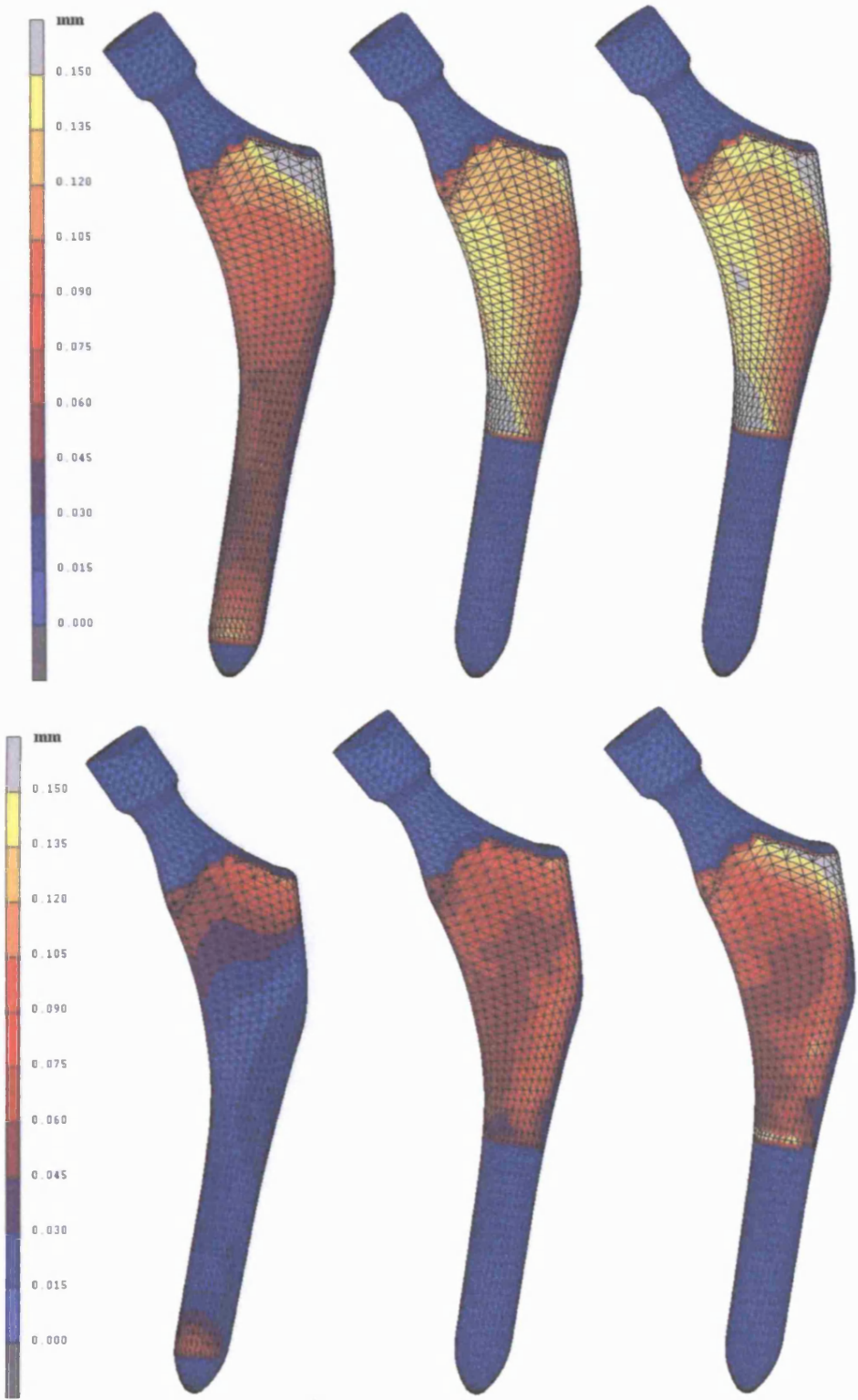


Figure 6.108: Micromotion results using Fisher's gait cycle forces for the ABG stem with distal gap (middle) and distal + lateral proximal gap (right) compared with a perfect fit model (left). Top pictures are results without interference fit, bottom pictures are results with an interference fit of 0.1mm.

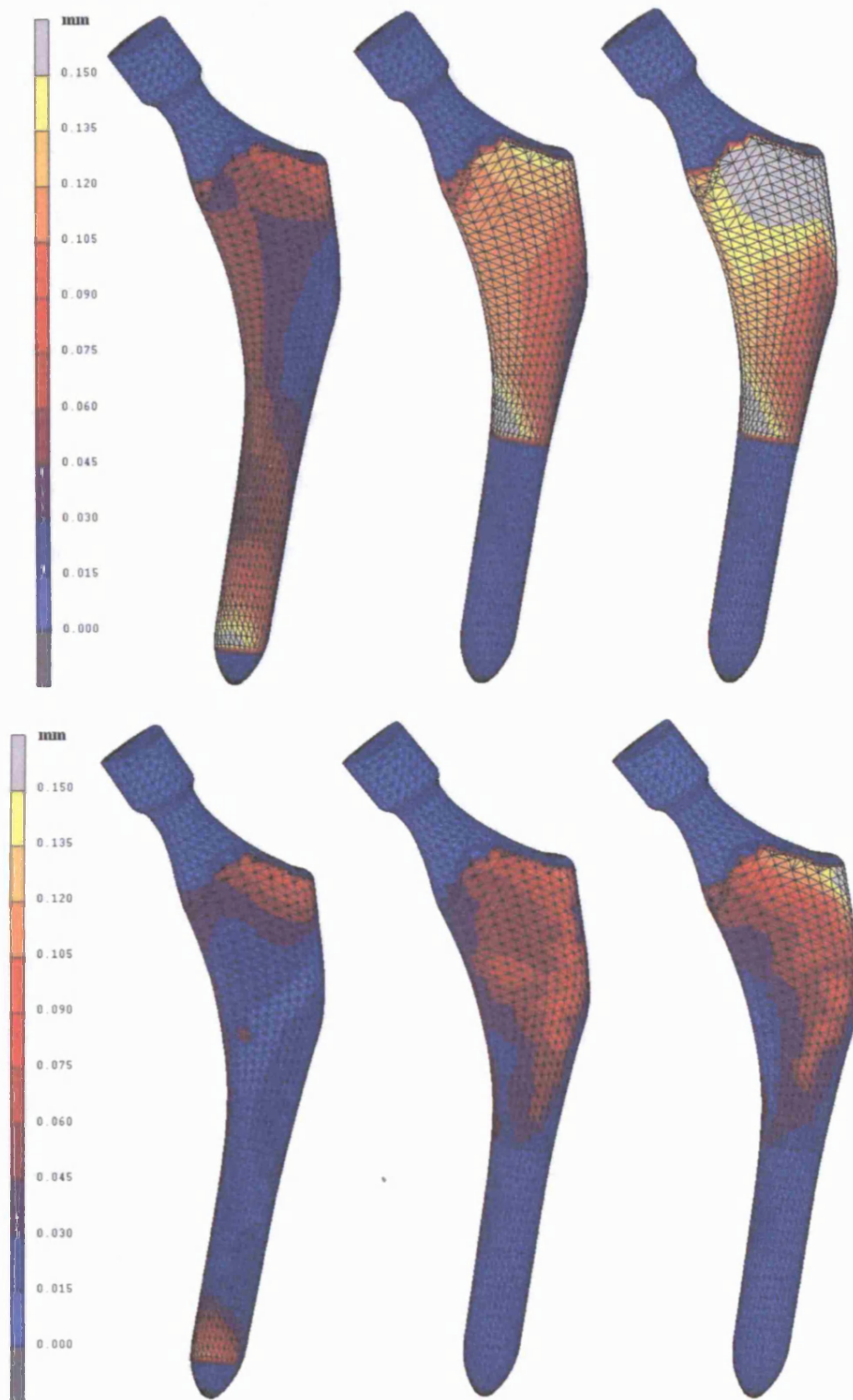


Figure 6.109: Micromotion results using Duda's stair-climbing forces for the ABG stem with distal gap (middle) and distal + lateral proximal gap (right) compared with a perfect fit model (left). Top pictures are results without interference fit, bottom pictures are results with an interference fit of 0.1 mm.

Figure 6.110 shows the results for the AML hip stems under physiological walking and stair-climbing loads. In both physiological loadings, the increase in micromotion was found to be localised in the region around the gaps. *Figure 6.111* shows the surface area with micromotion in excess of the threshold limit of 50 μ m for the two AML modelled with proximal gaps. The contour plots show that the surface area unfeasible for bone ingrowth in the AML modelled with gaps in the proximal $\frac{1}{2}$ did not exceed beyond the region of the gaps, and the distribution and magnitudes of micromotion in the distal $\frac{1}{2}$ of the stem were found to be unchanged. Similar results were obtained for the AML modelled with $\frac{1}{3}$ proximal gaps.

6.1.5 Discussion

Primary stability is important because it is an indicator of bone osseointegration and improved long-term fixation (Pilliar, Lee & Maniopoulos 1986). Poor initial stability might lead to bone resorption and encourage the formation of fibrous tissue at the interface (Soballe et al. 1999). It has been suggested that maximising the contact area of the implant surface with the host bone could improve the initial stability of the implant (Healy 2002). Since the shape of the prosthesis is exactly known, the opening of the femoral canal can be accurately milled with the use of surgical robots to create a precise cavity for the implant used. If this hypothesis is true, the primary stability of an implant in a robotically prepared cavity should be superior to that of a traditionally broached cavity.

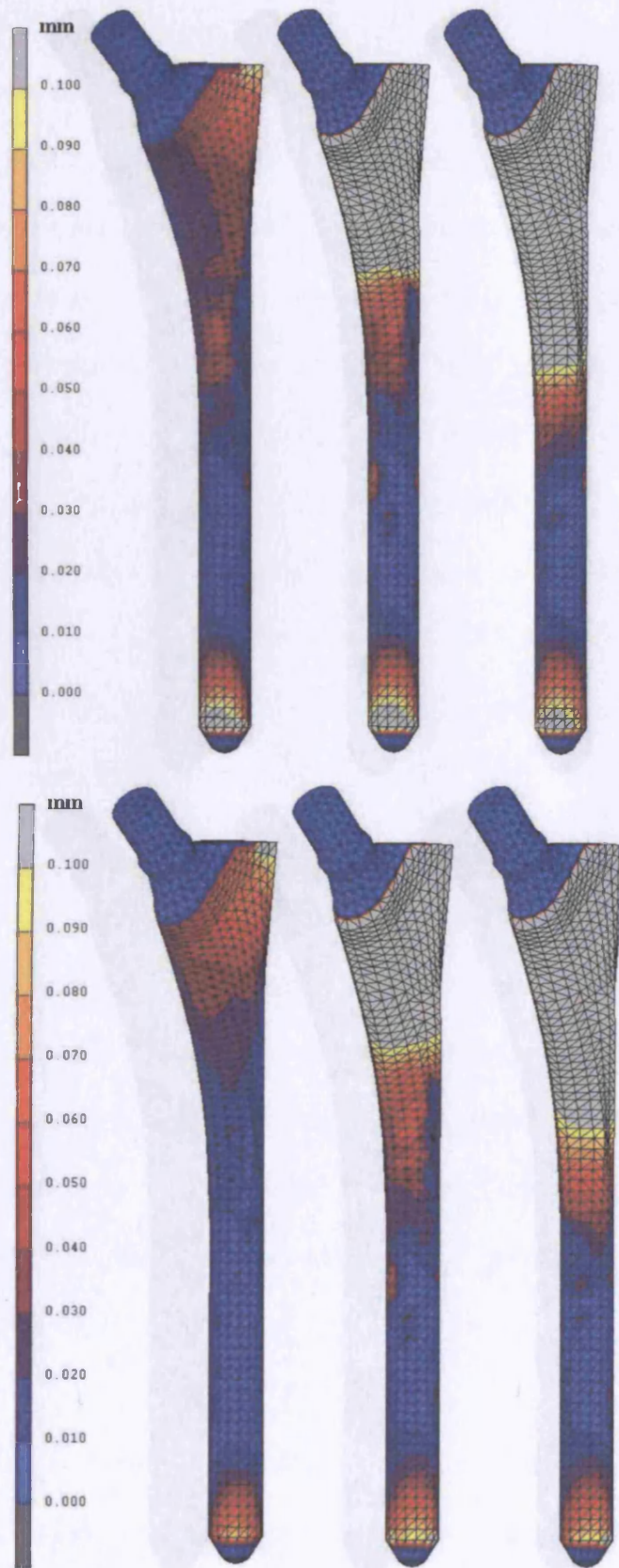


Figure 6.110: Micromotion results using Duda's stair-climbing forces (top set) and Fisher's gait cycle forces (bottom set) for the AML stem with gaps in the proximal $\frac{1}{3}$ (middle) and gaps in the proximal $\frac{1}{2}$ (right), compared to a perfect fit model (left).

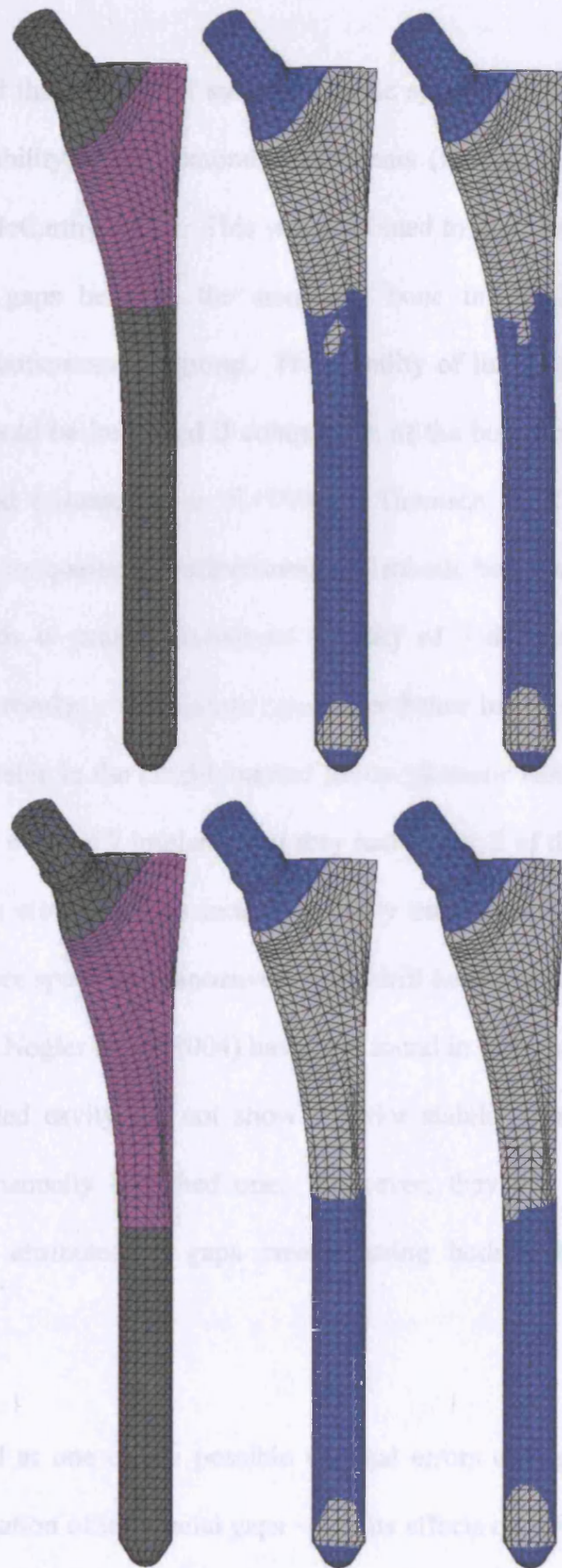


Figure 6.111: Surface area (grey colour) unfeasible for bone ingrowth for the AML modelled with $\frac{1}{3}$ proximal gap (top set) and $\frac{1}{2}$ proximal gap (bottom set). Results using Fisher's walking forces (middle) and Duda's stair-climbing forces (right).

It has been reported that the use of surgical robotic systems improves the initial fit as well as primary stability of the femoral components (Bargar, Bauer & Borner 1998; Paravic, Noble & McCarthy 1999). This was attributed to their findings that there were significantly more gaps between the stem and bone in the hand-broached group compared to the robotic-reaming group. The stability of implants in the traditionally-broached femora could be improved if compaction of the bone bed and critical contact areas were achieved (Alexander et al. 1999). Thomsen et al. (2002) reported an experimental study comparing the effectiveness of robotic bone milling with traditional broaching as regards to primary rotational stability of 7 different cementless stems. They found mixed results – some stem types were better in the robotic groups whilst others were more stable in the hand-broached group. Robotic canal preparation did not improve stability in 4 of the 7 implants that they had tested; 2 of these were anatomic in design. They have attributed this lack of stability on the gaps created by the robot because it needs more space for manoeuvring the drill head around the curved shoulder of anatomic stems. Nogler et al. (2004) have also found in their experimental study that the robotically milled cavity did not show superior stability for an anatomical stem compared to the manually broached one. However, they did not mention if their findings could be attributed to gaps created using both techniques during bone preparation.

This section looked at one of the possible surgical errors during implantation of hip prostheses – the creation of interfacial gaps – and its effects on primary stability. Three models were analysed – the rectangularly tapered Alloclassic, the anatomically shaped ABG and the straight cylindrical AML. The interfacial gaps in the Alloclassic were

identified using a unique multiple CT scanning technique. For the ABG and the AML, only discussions with experienced surgeons could be conducted. Based on these discussions, the location of gaps for the ABG was assumed to be most probable in the lateral-proximal region, and in the proximal area for the AML.

The existence of gaps due to surgical error did not affect the stability of the Alloclassic stem during common physiological activities of walking and stair-climbing. This is because the stability was achieved by wedging into the bone using the corners of the rectangular stem. The Alloclassic is designed to fit the femoral canal in the frontal plane but does not fill in the lateral plane. As long as press-fit is achieved by way of the four cortical corners along the stem, gaps at the non-critical areas such as the anterior and posterior surface of the stem do not endanger its stability.

For the ABG however, the stability seemed to be compromised in stair-climbing if there were gaps in the lateral-proximal region. Since the distal endosteal bone is over-reamed, the ABG relied mostly on a perfect fit of the ellipsoidal shape of the proximal part. This shape did not seem to be very stable under torsional load; slight surgical errors that introduce gaps could endanger the stability of the ABG hip stem. The Alloclassic, on the other hand, was better in sustaining torsional load because the four corners of the rectangularly-tapered design strongly anchored the stem to the endosteal bone.

This section also analysed the fixation of a distally fixed anatomical design such as the PCA and a distally over-reamed anatomical design such as the ABG. The PCA is the early cementless anatomic design where perfect surface to surface contact is used. Later

anatomic designs such as the IPS (DePuy) and the ABG rely on the proximal fixation concept where gaps were intentionally created to avoid cortical contact distally. Our FE results showed that the perfect bone-implant contact design such as the one used in the PCA was more stable than the distally-over-reamed ABG. This is in accordance with the study by Dujardin et al. (1996) who reported that well-fitted stems and a high percentage of canal fill reduced micromotion. This has also been analysed in the previous chapter when comparing between proximal versus distal fixation designs, where the distal fixation was found to be more stable than proximal fixation. However, if an interference fit of at least 100µm could be achieved, a drastic improvement in terms of primary stability was predicted. It showed the importance of an interference fit especially in stems where there are gaps distally or otherwise.

Our FE results were in accordance with follow up studies reported in the literature for both the PCA and the ABG stems. A couple of follow-up studies of the PCA showed signs of adverse bone remodelling (Jacobsson et al. 1993; Jansson & Refior 1992). Due to the distally fixed design of the PCA, bone hypertrophy was found distally and bone atrophy proximally. A 2-year follow-up study of the ABG showed that no mechanical complications such as loosening and migration can be found (Tonino et al. 1995). Distal hypertrophy, however, was identified but the extent was not as great as that found in the PCA.

The results of the AML hip stem showed that proximal gaps did not compromise the stability of the stem. In both physiological loadings, the surface area in excess of the threshold limit did not exceed beyond the region of the gaps, and the distribution and

magnitude of micromotion in the distal ½ of the stem was found to be unchanged. The stability of the stem was therefore maintained by the distal half of the stem.

As discussed in the previous chapter, the AML femoral component performed well in hip arthroplasty. The results are well published, and good clinical results at 15 years could be obtained. The FE results in this study showed that one of the reasons to the success of the AML could be due to the stability of the stem in the presence of interfacial proximal gaps. As long as press-fit is achieved distally, the stem should be stable.

6.2 The effect of undersizing and malalignment on micromotion

Another type of common surgical error is implant undersizing. Engh & Massin (1989) for example, reported that out of 343 AML stems they had implanted, 42% of them were found to be significantly undersized. They reported that these undersized stems statistically showed more late migration than correctly sized stems. Undersizing of stems occurred normally due to the cautiousness of surgeons who did not want to make the implant too tight in the canal as this would fracture or split the bone (Kim & Kim 1994). Undersized stems also have a tendency to shift into varus position – a malaligned situation (Ries et al. 1996).

Varus (medial tilt) or valgus (lateral tilt) malalignment is determined by measuring the angle made by the intersection of a line through the mid-stem of the prosthesis and a line through the midshaft of the femur as seen on the anteroposterior radiograph (*Figure 6.112*) (Khalily & Whiteside 1998; Rökkum & Reigstad 1999).

Malalignment is not necessarily caused by shifting of the once-aligned undersized stem. It could also happen during bone preparation for implantation. If the reamer used is not properly aligned to the femoral canal, the tip of the reamer will touch the distal cortex sooner than it should. This will not only cause implant undersizing but also implant malalignment in a valgus or varus position.

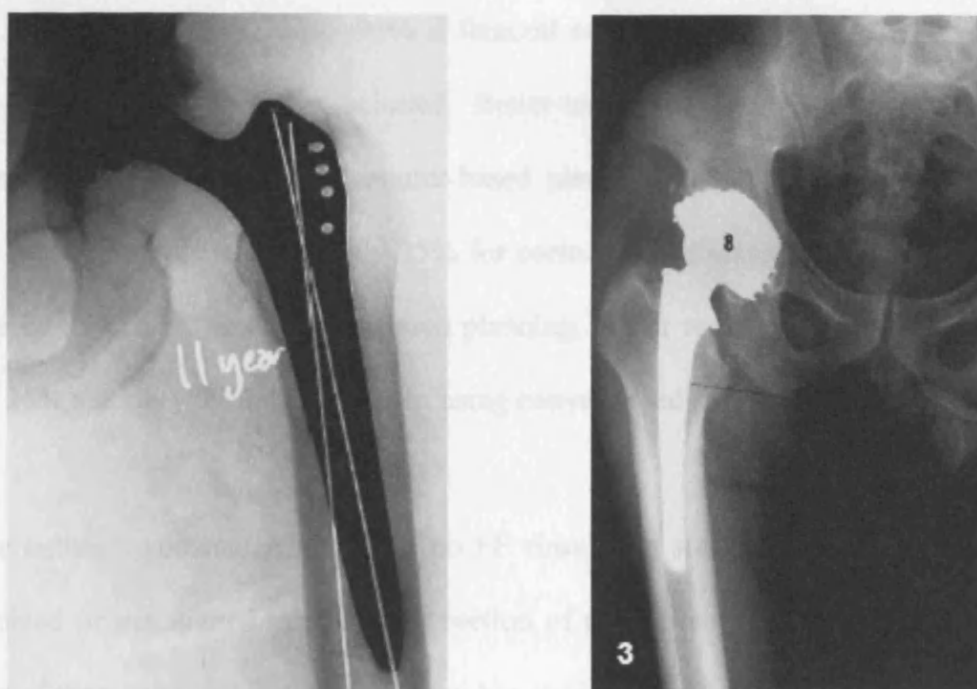


Figure 6.112: AP radiographs showing varus malalignment of the Alloclassic hip stem (left – picture taken from Khalily & Whiteside 1998) and the Roy-Camille hip stem (right – picture taken from Chen et al. 1998).

The conventional way of planning for the correct implant size is by the use of template planning – a procedure where templates are placed over X-Ray images to help the

surgeon decide the proper size for the patient. However, this procedure is not entirely reliable – the accuracy of templating improved as the level of training and experience increased, but even the most experienced surgeon could not achieve 100% accuracy using the traditional 2D templating method. There are various published papers that evaluate planned-versus-achieved (PVA) accuracy or the repeatability of conventional template planning. A study carried out on the PCA cementless stems showed that the planned stem size was used in only 42% of cases, the other 58% had either undersized or oversized stems (Knight & Atwater 1992). Similar results were reported by Carter et al. (1995) who studied 74 cases of primary total hip arthroplasty with cementless femoral components, independently planned with templates by three surgeons. The templated size corresponded to the actual femoral component used in only 50% of cases. The accuracy rose to 88-95% if femoral components within one size below or above the templated size were included. Better templating in THA is possible through the use of three-dimensional computer-based planning (Viceconti et al. 2003). The paper reported an accuracy of only 35% for correct sizing using traditional templating compared to 52% using computer-based planning. Their results also showed that there was a 25% tendency to undersize when using conventional templating.

To the author's knowledge, there are no FE simulation studies analysing the effect of undersized or malaligned stems. This section of the chapter will therefore look at the effects of these surgical errors on primary hip stability. And since a malaligned implant is also most likely to be undersized, the analyses on malaligned stems will only be conducted on and compared to undersized stems.

6.2.1 Methods

Two types of hip stems were used in this study – the straight cylindrical AML and the rectangularly tapered Alloclassic. The bone model used in this study was the normal healthy bone taken from the VHP dataset. In chapter 5, a suitable size that fits the VHP bone model was identified to be size 5 for the Alloclassic, and size 135 for the AML was found to fit and fill the medullary canal. For the undersized stems of the Alloclassic, the original surface mesh of size 5 was scaled down into size 4 and size 3 using the actual size 5 as the template. For the undersized stems of the AML, since they are different in shape particularly in the proximal area, the two smaller sizes were created from the original CAD drawings obtained from the manufacturer. The two step sizes smaller than size 135 are the AML size 120 and size 105. These numbers represent the diameter of the stem's shaft – for example, size 135 represents a shaft diameter of 13.5mm. These two undersized AMLs and the two undersized Alloclassics will be analysed and compared with their corresponding correct implant size that fits the femur model created from the VHP dataset.

For the malaligned implants, the smallest size from the above models of the Alloclassic (size 3) and the AML (size 105) were used. These implants were angulated in Amira software from their aligned position to represent $\sim 5^{\circ}$ varus malalignment (*Figure 6.113*). There were problems however, involving the FE analyses with malaligned stems. The FE software (MARC.Mentat) could not solve the analyses when an interference fit was included. A solution could only be obtained if the interference fit was switched off. This could be because the distal region of the malaligned stems was not entirely in contact with solid bone. Bone marrow in the distal region of the canal

caused problems in the FE software when an interference fit was included. The interference fit was therefore excluded in all analyses in this section in order to make a proper comparison.

All other parameters were set to be the same as described in chapter 2 and the models were loaded using both Duda's and Fisher's physiological loading conditions. The results for the undersized stems are shown first, followed by the results for the malaligned stems.

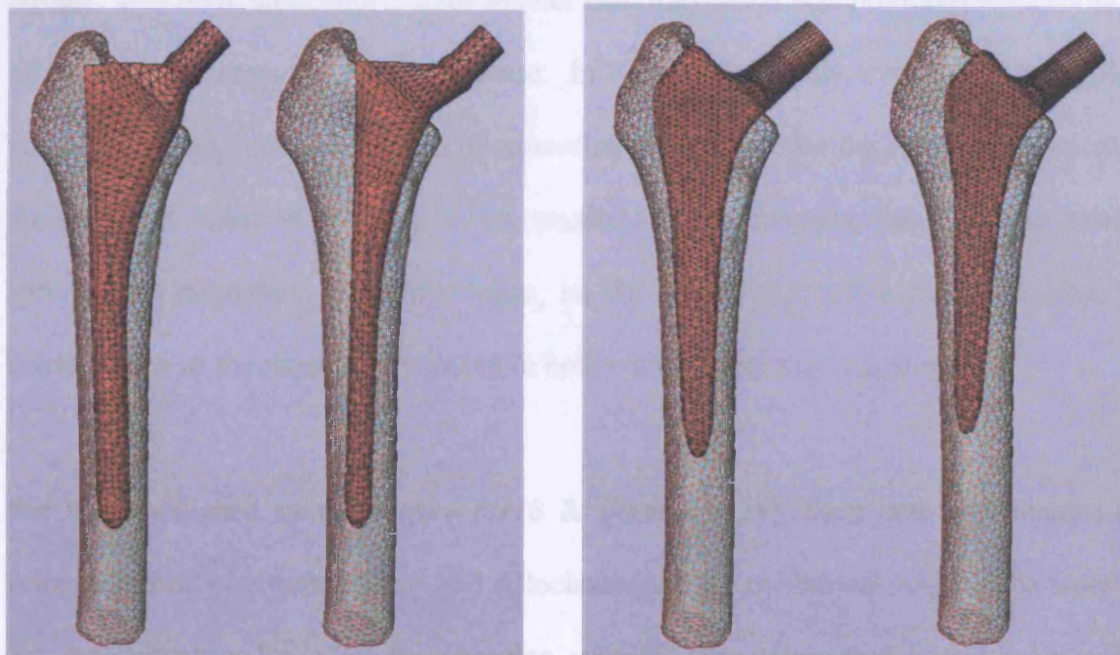


Figure 6.113: Pictures showing the correct size implants and their undersized + malaligned counterparts (AML on left; Alloclassic on right).

6.2.2 Results

The results for the undersized stems (*Figure 6.114, Figure 6.115, Figure 6.116 & Figure 6.117*) showed that micromotion increased as the stem sizes were reduced for both implants and in both walking and stair-climbing. The results also showed that the undersized tapered design was better in terms of stability than an undersized cylindrical design. The AML stem with 2 sizes smaller than the correct size produced micromotion up to 10 times larger in Duda's loadcase. In Fisher's gait cycle, even one size smaller can cause a significant increase in micromotion. The result for the AML with two step sizes smaller failed to solve up to the maximum load, meaning that the stem would suffer gross migration. The Alloclassic, on the other hand, had a steady increase in micromotion as the sizes were reduced in both walking and stair-climbing.

For the malaligned stems (*Figure 6.118 & Figure 6.119*), there was a difference in primary stability between the tapered Alloclassic and the cylindrical AML. The tapered design seemed to be better in achieving stability even when malaligned in a varus position. In contrast, a varus malaligned cylindrical design produced between 2-3 times more micromotion than a perfectly aligned implant.

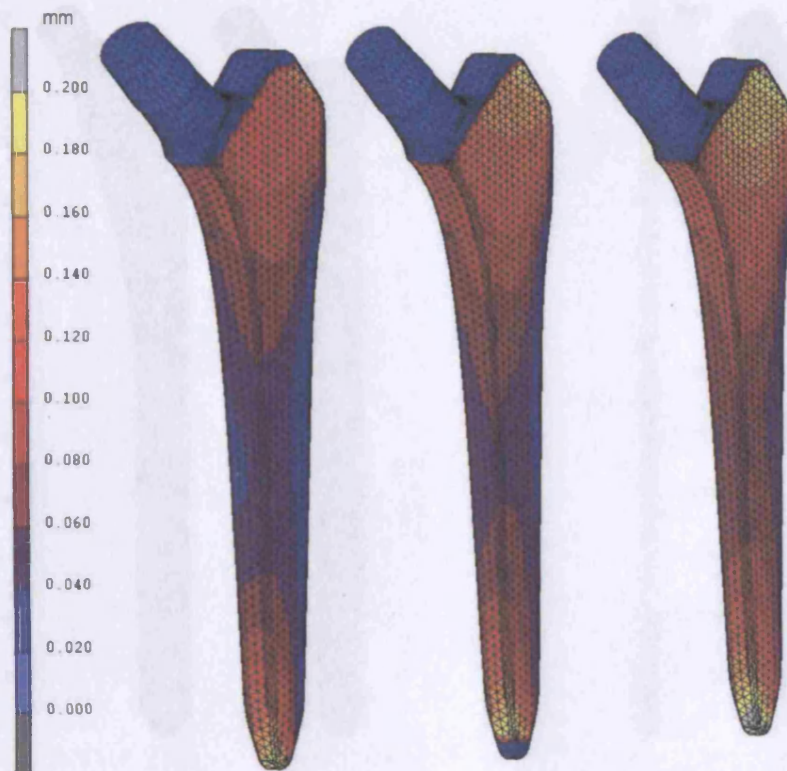


Figure 6.114: Micromotion results for the Alloclassic size 5 (left), 4(centre) and 3 (right) using Duda's stair-climbing loads.

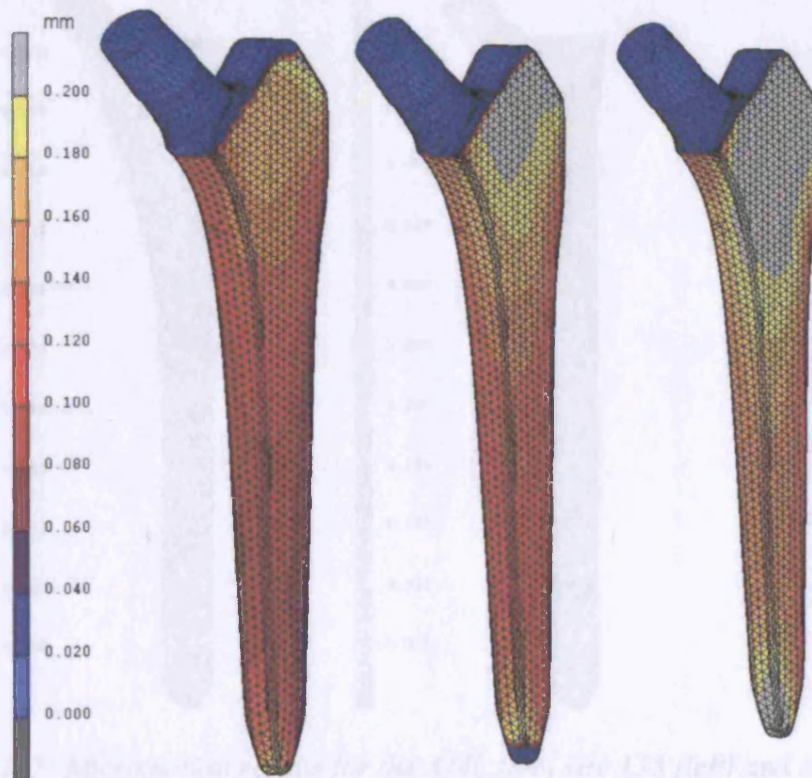


Figure 6.115: Micromotion results for the Alloclassic size 5 (left), 4(centre) and 3 (right) using Fisher's gait cycle loads.

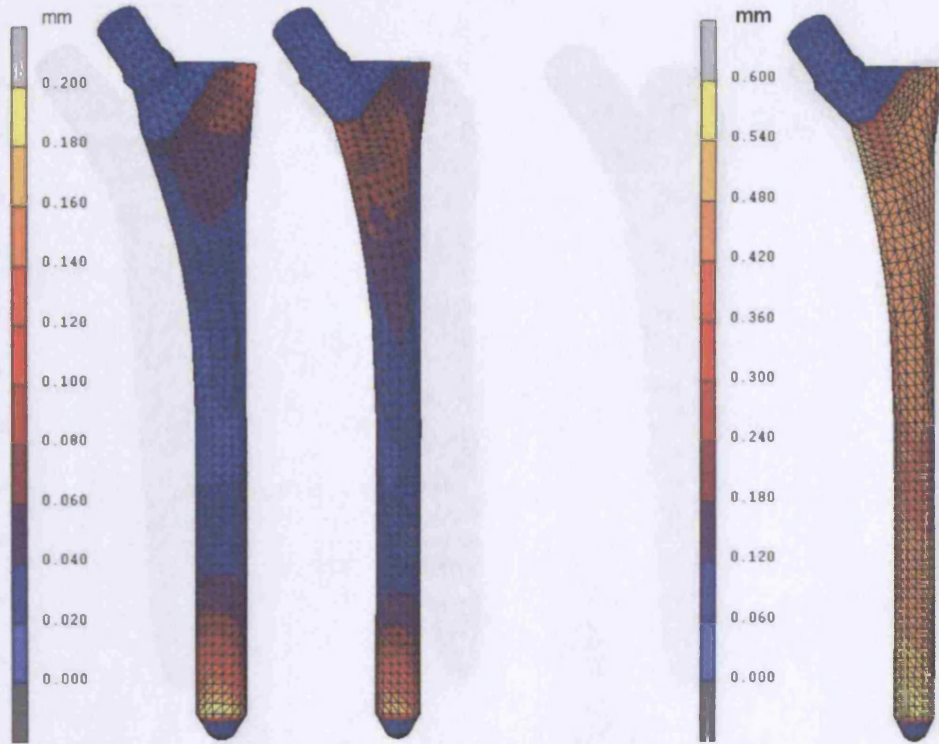


Figure 6.116: Micromotion results for the AML stem size 135 (left), size 120 and with a different scale, size 105 (right) in stair-climbing.

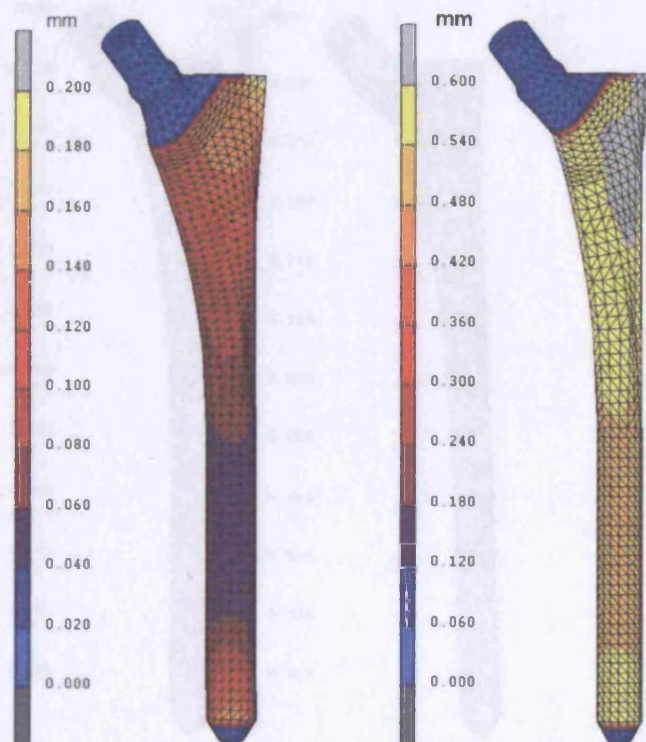


Figure 6.117: Micromotion results for the AML stem size 135 (left) and size 120 (right) in Fisher's gait cycle. Result for the AML size 105 was not included as the analysis failed before maximum load was achieved.

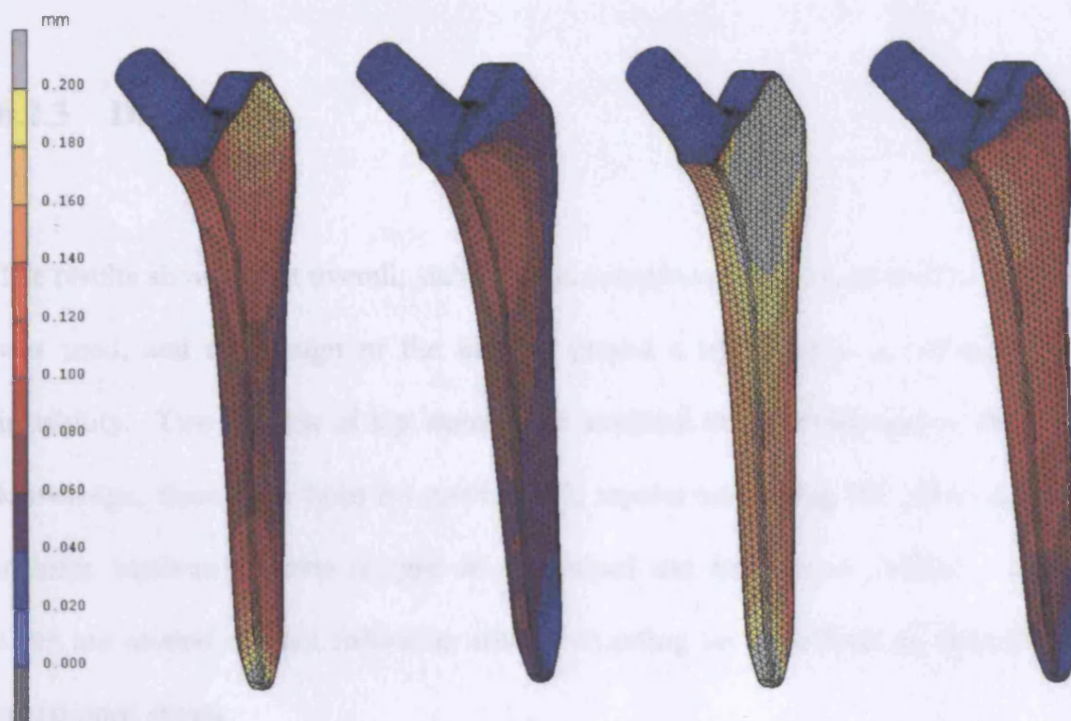


Figure 6.118: Micromotion results for the Alloclassic size 3 in proper alignment and in varus malalignment. First set on the left using Duda's stair-climbing, and the second set on the right using Fisher's gait cycle.

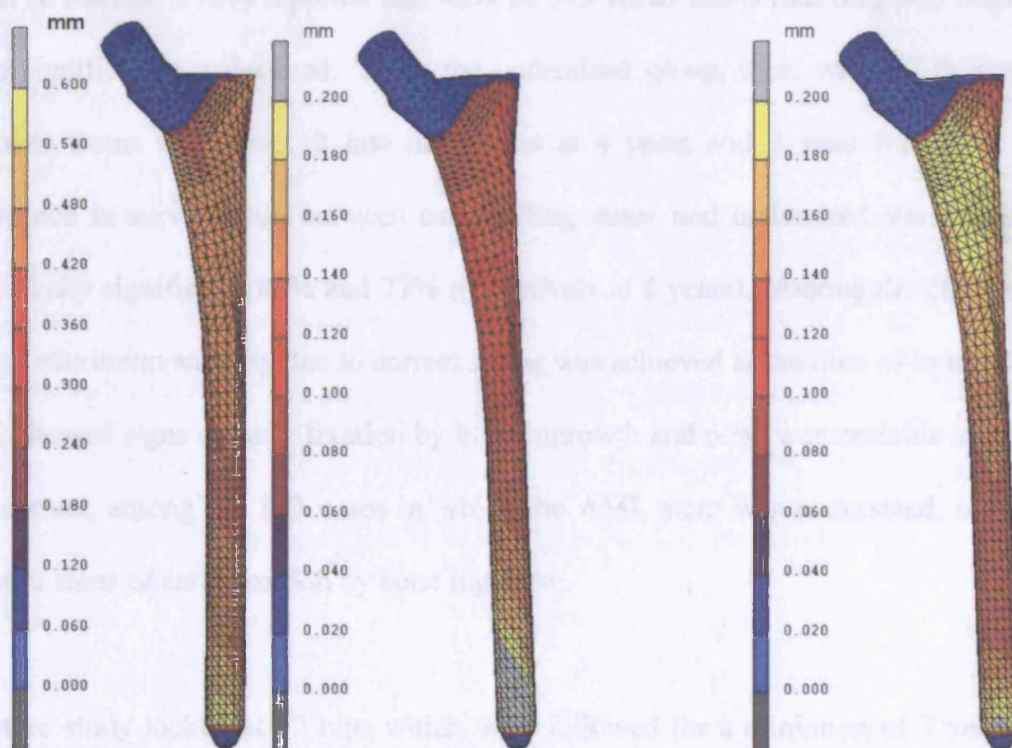


Figure 6.119: Micromotion results for the AML stem size 105 in proper alignment and in varus malalignment using Duda's stair-climbing loads (first two pictures). The last picture on the right showed micromotion results using Fisher's gait cycle for malaligned AML size 105. Analysis for properly aligned AML size 105 failed before maximum load was achieved.

6.2.3 Discussion

The results showed that overall, stability was compromised when an undersized implant was used, and the design of the implant played a crucial role in the extent of its instability. Two designs of hip stems were analysed in this study and to the author's knowledge, there have been no previous FE reports comparing the effect on primary stability between the two designs in undersized and malaligned position. However, there are several clinical follow-up studies reporting on the effects of undersized and malaligned stems.

Engh & Massin (1989) reported that 42% of 343 AML stems that they had implanted were significantly undersized. From the undersized group, there were 19 failures (15 unstable stems at 2 years, 2 late migrations at 4 years and 2 stem fractures). The difference in survivorship between canal-filling stems and undersized stems was also statistically significant (88% and 77% respectively at 8 years). Among the 200 cases in which maximum stability due to correct sizing was achieved at the time of implantation, 94% showed signs of early fixation by bone ingrowth and none was unstable at 2 years. In contrast, among the 143 cases in which the AML stem was undersized, only 60% showed signs of early fixation by bone ingrowth.

Another study looked at 52 hips which were followed for a minimum of 7 years after they had primary total hip arthroplasty with the AML hip system (Kim & Kim 1994). Three hips (6%) which were undersized showed stable fibrous tissue ingrowth and another three undersized stems were found to be unstable. This can be compared with

the 41 hips where the correct stem size was achieved, when 70% had bone ingrowth and 30% had stable fibrous tissue ingrowth. Another study (Haddad, Cook & Brinker 1990) showed that undersized stems were more likely to have excessive subsidence ($\geq 3\text{mm}$) than correctly sized stems. Three different stems were compared – the AML, the PCA and the LSF – and those stems that were undersized were found to be 19-25% more likely to subside.

Giannikas et al. (2002) also reported similar observations in their follow-up study of the ABG, a hip stem which has similar cylindrical feature of the AML. They also reported that revision surgery was performed on an undersized stem, because it caused persistent thigh pain due to significant subsidence of the prosthesis.

The FE results also showed that the micromotion was greater for the undersized implants than undersized + malaligned implants. The micromotion was smaller for the latter because the stem engaged the medial calcar proximally and the lateral endosteal cortex distally. This can be confirmed by a study on canine femoral prostheses, where the authors found that subsidence was significantly greater for the undersized implant in a neutral position than the undersized implant in varus malalignment (Pernell et al. 1994). They also reported that there was no significant difference in subsidence between the correctly sized implant in neutral position and the varus group.

For the Alloclassic hip stems, our FE analyses showed that this design is stable even if positioned in a varus alignment. This is in accordance with a follow-up study by Khalily & Lester (2002). No adverse effects were found on the Alloclassic hip stems with at least 5° of varus angulation at 5 years. They were all found to be clinically and

radiographically stable. Another follow-up study also showed that 30% of the Alloclassic hip stems had been implanted in slight varus position with no adverse clinical effect (Delaunay, Cazeau & Kapandji 1998). The report also showed that 16% of the stems subsided more than 2mm within the first 2 years after operation, but no progressive subsidence was detected after the second year. However, the author did not explain the cause of the subsidence. Based on our FE results, it could be that these stems were implanted undersized.

The FE results showed that undersized Alloclassic stems seemed to be better than undersized AML stems. This could be due to the differing geometrical design between the two stems. The taper in the Alloclassic provides a self-locking mechanism where a tighter fit is achieved under load, and the four corners of its rectangular shape provide the anchoring effect that is particularly effective in torsion. The undersized Alloclassic stem will therefore sink steadily under load until a stable position is achieved. This explanation is in agreement with a follow-up study on the Alloclassic stem reported by Delaunay et al. (2001). In their study, 4 stems were found to have subsided – 3 stems between 2 to 5mm and 1 stem subsided 5 to 10mm within the first year. However, no progressive subsidence could be detected beyond this period – a condition which is usually termed late stabilisation. The AML stem, on the other hand, has a straight cylindrical shape which is much more unstable when implanted undersize because bone-anchoring can not be achieved until it has sunk to the point where it rests on its proximal taper.

6.3 The effect of bone diseases on micromotion

Another important parameter that could affect primary stability is the pathological condition of the bone. Skeletal diseases such as osteoporosis and osteoarthritis affect the bone's material properties. Osteoarthritic changes are mainly concentrated around the articulating surface of the joint where the cartilage covering the bone ends deteriorates due to age or injury. The properties of bone further away from the articulating joint may or may not change. Osteoporosis, on the other hand, is a skeletal disorder characterised by a significant loss of bone stock and structural deterioration of bone tissue. The bone becomes weak and fragile, and more likely to fracture under a sudden strain or fall.

Osteoarthritis is the most common cause of hip disease leading to primary hip replacement because it causes pain and severely reduced mobility. However, patients requiring hip arthroplasty also sometimes suffer from osteoporosis (Haddad, Cook & Brinker 1990). As osteoporotic bone is significantly weaker than normal healthy bone, it affects the decision made by the surgeon in terms of selection of suitable hip stems. It has been suggested that patients with osteoporosis would be better off having cemented hip stems to ensure strong primary fixation (Dorr, Wan & Gruen 1997; Haber & Goodman 1998). However, Healy (2002) reported that cementless stems were also reliable for elderly patients with poor bone stock.

Bone quality has been found to influence the extent of stress-shielding; severe bone loss was noted in poorer quality bones than in healthy ones (Kerner et al. 1998; Ohsawa et

al. 1998). However, in terms of primary stability, it is unknown if weaker bone stock causes more micromotion and instability of the replaced hip. In general, stronger bone is preferred for stability, even though no conclusive evidence is available to support this hypothesis (Healy 2002). This is why cementless stems are still not widely used in patients with osteoporosis.

In chapter 4, the effect of bone material properties on micromotion was analysed by reducing its stiffness values gradually to simulate weaker bone mass. This was done by reducing the constant value in the density-stiffness relationship proposed by Carter and Hayes (1977). In this section of the chapter, actual femoral CT datasets from patients suffering from osteoporosis and osteoarthritis will be used. The study will compare the interface micromotion and the stability of a cementless stem inside the two bone models (osteoarthritic and osteoporotic) with a healthy bone under physiological loadings. It is hoped that this study will give some qualitative data on the use of cementless stems on patients with weaker bone mass.

6.3.1 Methods

Data from patients about to undergo hip replacement surgery were obtained from the hospital. These data were originally being used by another researcher to study bone remodelling. All the patients were suffering from osteoarthritis of the hip joint, and the patients' femurs were CT scanned before the surgery. Out of 13 patients, only 1 femur was found to be osteoporotic as well. The Young Adult T-score of the patient, which is

the World Health Organisation (WHO) criterion for osteoporosis, showed marked osteoporosis in all regions of the femur. The CT dataset of this patient as well as one other osteoarthritic bone were obtained, and segmented in Amira software. The CT dataset for the osteoporotic bone, however, was scanned separately for the proximal and middle parts with different voxel sizes. The models, therefore, had to be created separately because datasets from different voxel sizes cannot combine into a single dataset. The separate models were then joined together using Magics software as shown in *Figure 6.120* below. Material properties also need to be assigned separately for the proximal and middle part of the femur. A short computer code (see Appendix) was written to help combine the large number of scattered material properties data from the two separate models. For the osteoarthritic bone, a single CT dataset was obtained. The construction of the bone model and the material properties assignment were therefore followed the procedure as described in chapter 2.

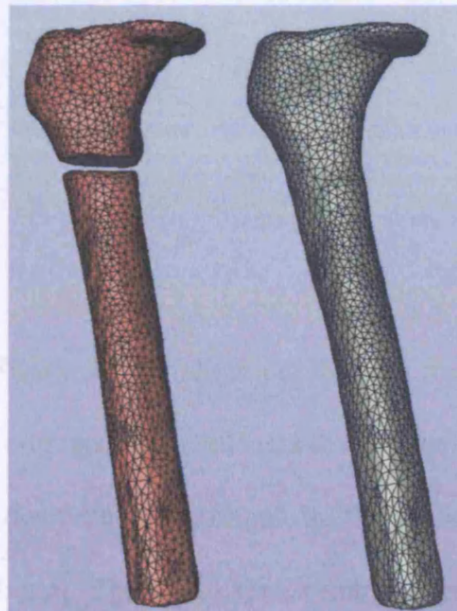


Figure 6.120: The femur model created separately from two CT datasets and the combined model.

Once the bone models had been created, the size of a suitable AML stem needed to be identified for each bone model. Four available sizes of the AML were manually positioned using Amira software, by orientating them until the stem was found to fit and fill the canal whilst maintaining the anteversion angle of the neck as described in Chapter 2. The best size to fit and fill the canal of the osteoporotic femur was found to be the largest size, AML-size150, and the suitable size for the osteoarthritic bone was found to be AML-size120. The stem size used for the normal bone was AML-size135, and the only difference between this and the other two sizes was the stem diameter; changed from 13.5mm to 15mm for the osteoporotic and 12mm for the osteoarthritic cases. The meshes of the two sizes of the AML stems were refined from their original 3D models and turned into solid tetrahedrals as described previously in Chapter 2. The models were then loaded as though in physiological stair-climbing using Duda's loadcase and walking using Fisher's loadcase. The micromotion results obtained were then compared with the micromotion for the implant in the normal bone from the VHP dataset (from chapter 5).

6.3.2 Results

The first set of results (*Figure 6.121*) show cut-through models of the three different bones, together with their corresponding stiffness distribution. The contour plot showed that there was a large decrease in stiffness in the patient suffering osteoporosis compared to the healthy bone. There was also a marked reduction in thickness of the cortex on the anterior and posterior side of the osteoporotic femur. The contour plot of the osteoarthritic bone, however, showed slightly larger stiffness than the normal bone. Osteoarthritis is a joint disease that is concentrated on the area surrounding the joint.

However, a comparative study made by Li and Aspden (1997) showed that there appeared to be a small increase in mineralization and about 70% increase in the volume of trabecular bone in the osteoarthritic group compared to a normal group. They also found that increased apparent density of the OA trabecular bone resulted in a greater stiffness, yield strength and energy absorbed to yield.

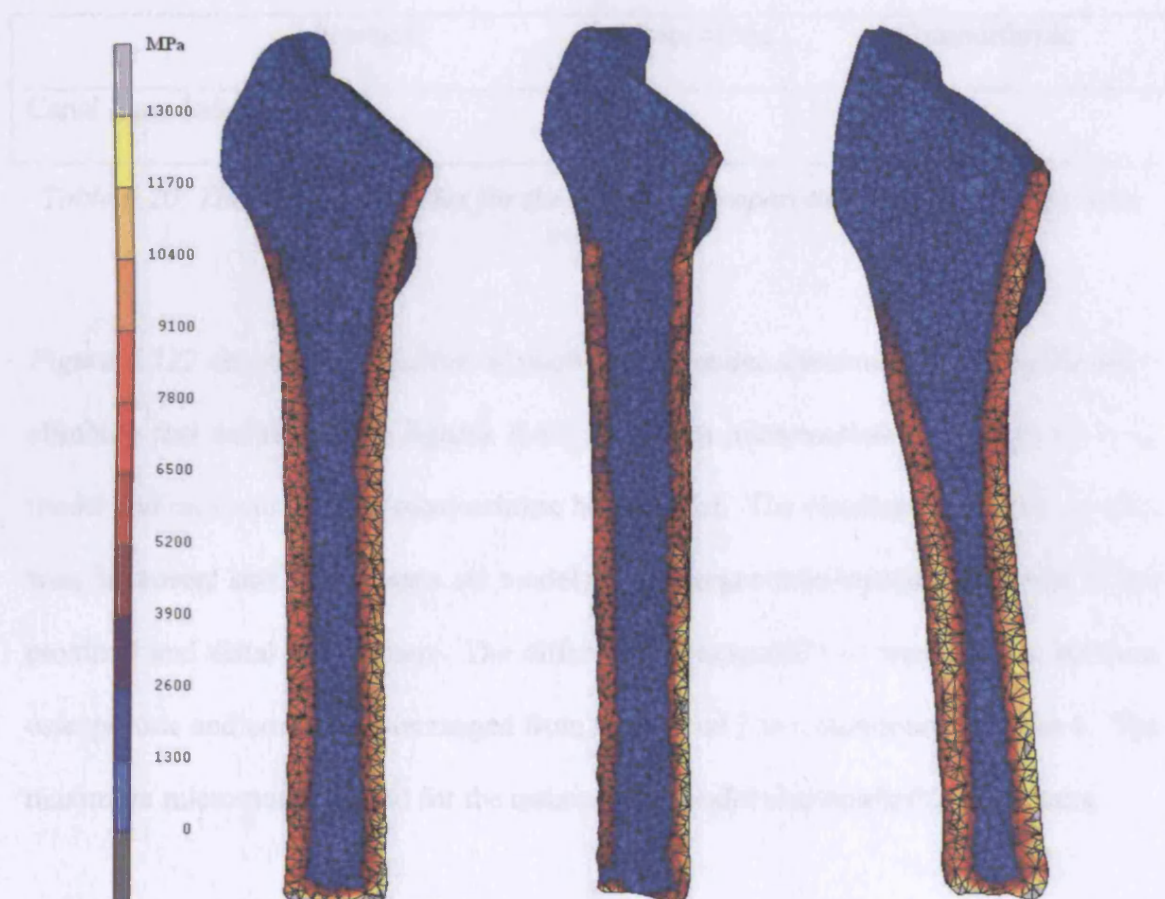


Figure 6.121: The Young's modulus of bones from the normal VHP dataset (left), from a patient suffering from osteoporosis (middle) and osteoarthritis (right) (Pictures were scaled to fit).

The canal flare index was calculated for the three bone models using the technique proposed by Noble et al. (1988). The ratio of the canal diameter at two locations – 20mm above the lesser trochanter and the isthmus – was calculated from the antero-posterior view. The measurement was made from the FE software and the results are shown in Table 6.20. In their paper, Noble et al. reported that canal flare indices of less

than 3.0 described stovepipe canals (type C), 3.0-4.7 normal canals (type B), and 4.7-6.5, canals with a champagne-fluted appearance (type A). *Table 6.20* below shows that the normal bone used in this study is of type B, the osteoarthritic bone is of type A and the osteoporotic bone is of type C.

	Normal	Osteoporotic	Osteoarthritic
Canal Flare Index	3.6	2.3	6.2

Table 6.20: The canal flare index for the normal, osteoporotic and osteoarthritic bone models.

Figure 6.122 shows contour plots of micromotion under simulated physiological stair-climbing and walking. The figures show maximum micromotion for the osteoporotic model and minimum for the osteoarthritic bone model. The distribution of micromotion was, however, similar between all models, with larger micromotion observed at the proximal and distal of the stem. The difference in magnitude of micromotion between osteoporotic and normal bones ranged from a factor of 3 to a maximum of about 4. The maximum micromotion found for the osteoporotic model also reached 250 microns.

Table 6.21 shows the surface area with micromotion of 50 μ m or larger for all three models. Overall, stair-climbing had more surface area beyond the threshold limit than walking. The osteoarthritic model was the most stable in both physiological loadings as it showed the least area. For the normal bone and the osteoporotic model, the surface area with micromotion larger than 50 μ m depended on the type of activity. In walking, there was not much difference in the size of the area. In Duda's stair-climbing, however, there was almost twice as much surface area with micromotion $\geq 50\mu$ m in the osteoporotic than in the normal bone.

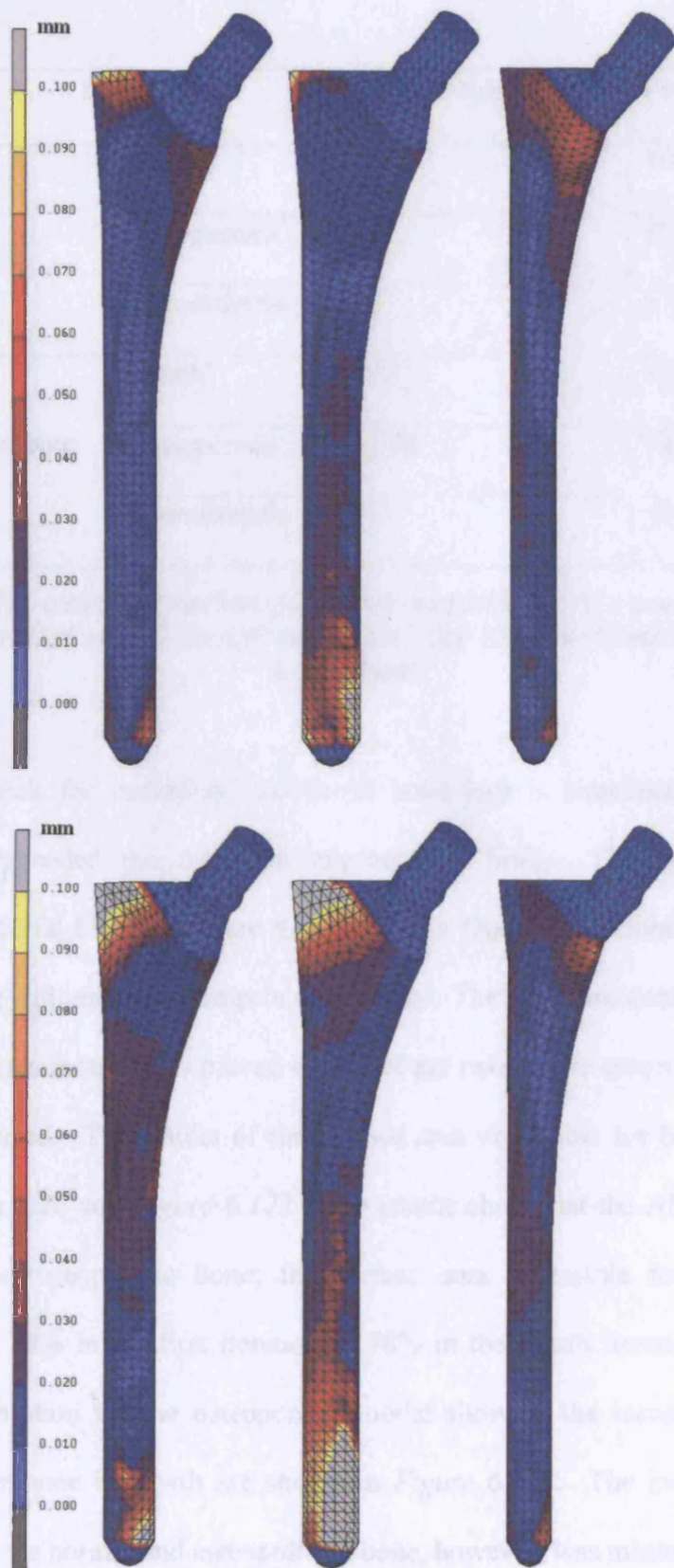


Figure 6.122: The micromotion result from the normal VHP dataset (left), the osteoporotic bone (middle) and osteoarthritic bone (right) using Fishers's gait (top) and Duda's stair-climbing forces (bottom).

		<i>Area > 50μm (mm²)</i>	<i>Percentage (%)</i>
Fishers' gait	Normal	769	9%
	Osteoporosis	754	8%
	Osteoarthritis	44	1%
Duda's stair-climbing	Normal	890	10%
	Osteoporosis	1,776	18%
	Osteoarthritis	78	1%

Table 6.21: The amount of surface area more than 50 μ m of micromotion. The total surface area for AML size 135 is 8,976mm², AML size 150 is 9,902mm² & AML size 120 is 7,858mm².

In order to check for instability, interfacial bone loss is simulated in areas where micromotion exceeded the threshold micromotion limit. The new models with simulated interfacial bone loss were then loaded in Duda's stairclimbing mode as this was the loading with maximum impact on stability. The iterations continued until either a stable state micromotion is achieved or one of the two failure criteria, as described in chapter 2, occurred. The results of the surface area unfeasible for bone ingrowth are shown in *Table 6.22* and *Figure 6.123*. The results show that the AML hip stem was unstable in the osteoporotic bone; the surface area unfeasible for bone ingrowth increased from 18% in the first iteration to 78% in the fourth iteration. The contour plots of micromotion for the osteoporotic model showing the increase in unfeasible surface area for bone ingrowth are shown in *Figure 6.124*. The increase of the 'no growth' area in the normal and osteoarthritic bone, however, was minimal.

	1 st iteration		2 nd iteration		3 rd iteration		4 th iteration	
	Area >50 μm (mm ²)	%	Area >50 μm (mm ²)	%	Area >50 μm (mm ²)	%	Area >50 μm (mm ²)	%
Normal	769	9%	890	10%	933	10%	-	-
OP	1,776	18%	3,159	32%	4,975	50%	7,730	78%
OA	78	1%	154	2%	188	2%	-	-

Table 6.22: The increase in surface area with more than 50 μm of micromotion for the normal, osteoarthritic and osteoporotic models.

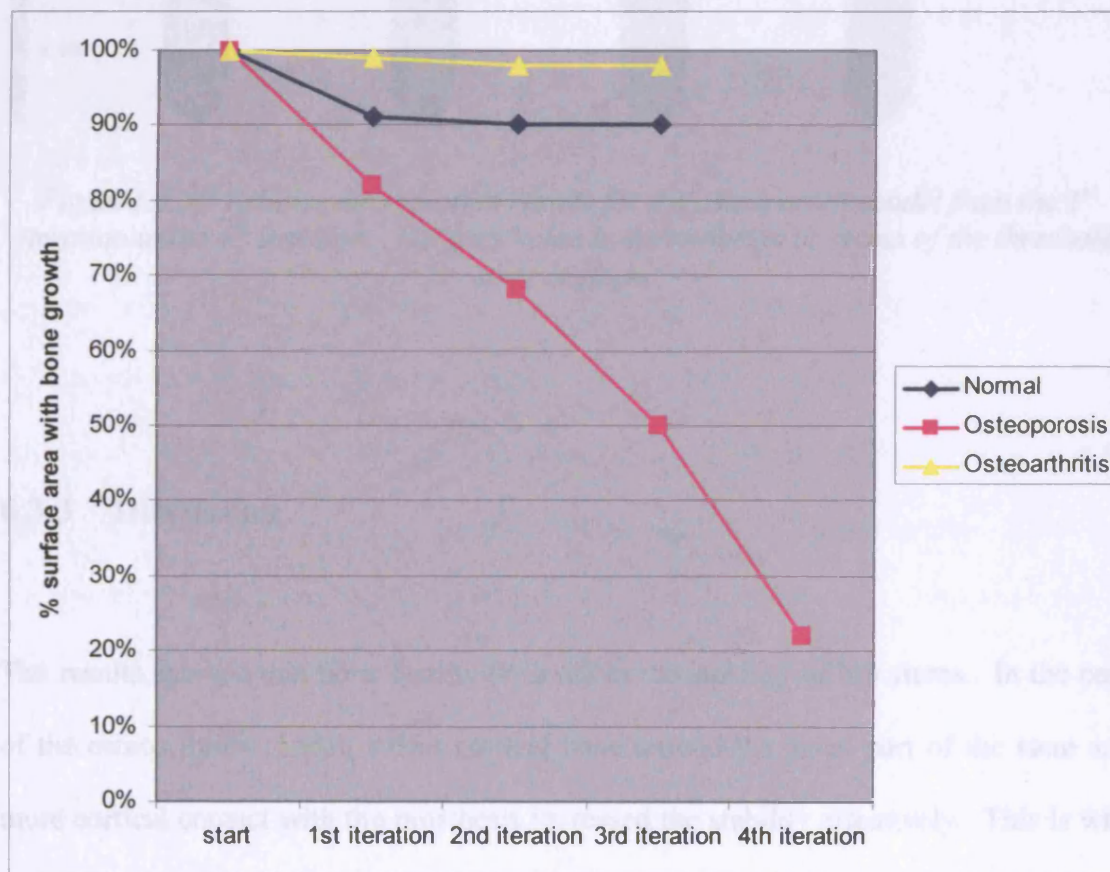


Figure 6.123: The reduction in surface area feasible for bone ingrowth.

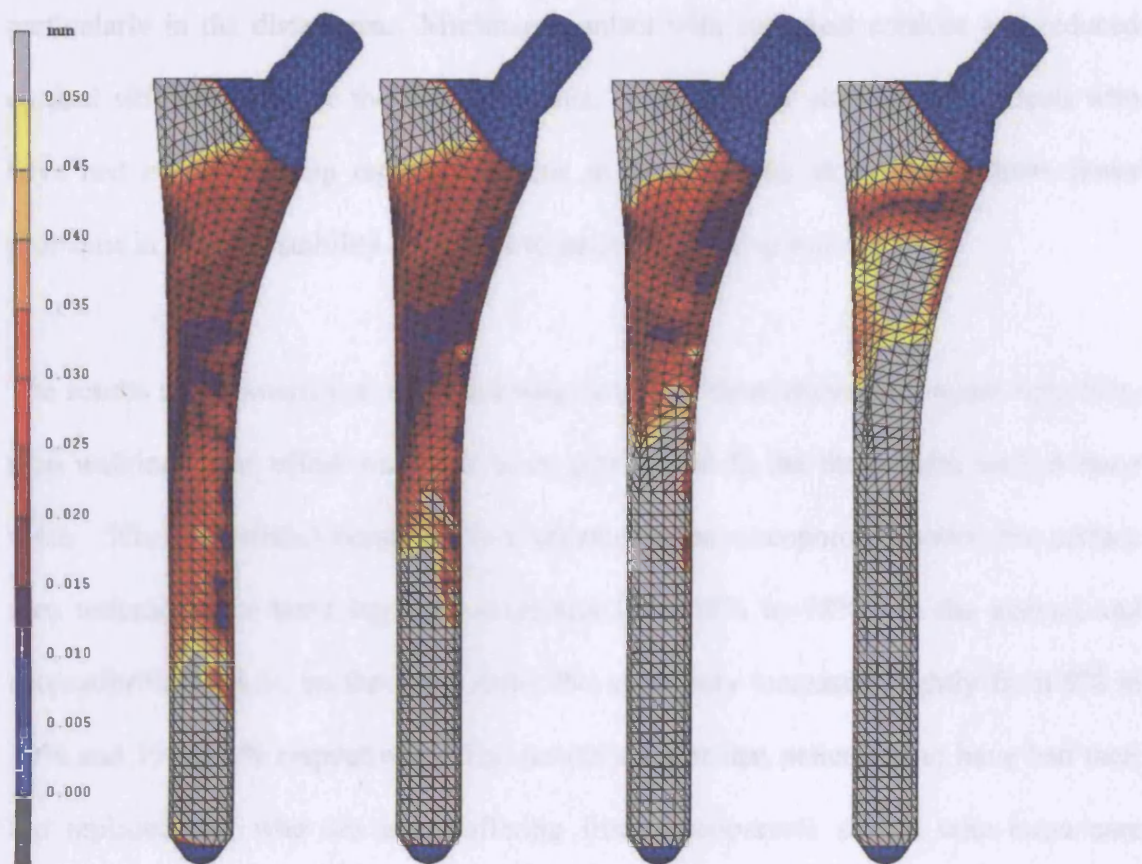


Figure 6.124: Relative micromotion results for the osteoporotic model from the 1st iteration to the 4th iteration. The grey value is micromotion in excess of the threshold limit of 50 μm .

6.3.3 Discussion

The results showed that bone quality does affect the stability of hip stems. In the case of the osteoarthritic model, stiffer cortical bone around the distal part of the stem and more cortical contact with the prosthesis increased the stability effectively. This is why the osteoarthritic model was found to be the most stable in both walking and stair-climbing. The osteoporotic bone, which had reduced bone stiffness and thinning of the cortex on the anterior and posterior sides showed significantly larger micromotion

particularly in the distal area. Minimum contact with endosteal cortices and reduced cortical stiffness could be the reason for this. The FE study showed that patients who have had cementless hip replacement due to osteoarthritis alone should have fewer problems in terms of stability compared to patients suffering osteoporosis.

The results also showed that stair-climbing produced more micromotion and instability than walking. The effect was even more detrimental in the femur with weaker bone mass. When interfacial bone loss is simulated in the osteoporotic model, the surface area unfeasible for bone ingrowth increased from 18% to 78%. In the normal and osteoarthritic models, on the other hand, the areas only increased slightly from 9% to 10% and 1% to 2% respectively. The results suggest that patients who have had their hip replaced and who are also suffering from osteoporosis should take extra care especially during stair-climbing.

To the author's knowledge, there are no published reports comparing the primary stability of prostheses inside normal bone and bone with skeletal diseases. However, there are several reports showing that good bone quality is preferable to poor bone stock. Kim & Kim (1994) for example showed that the AML stems used in younger patients had much lower frequency of loosening and revision rates compared to older patients. They have attributed this success to good bone quality, among other things. Krischak et al. (2003) reported that femoral prosthesis loosening after seven years could be predicted by bone quality at the time of implantation – with loosening more likely if the bone quality was poor. A retrieval study by Maloney et al. (1996) on various types of cemented and cementless stems showed that the extent of bone loss depended on the density of the bone; the less dense the bone was pre-operatively, the greater the extent

of bone loss. This trend was also found by the study of Kerner et al. (1998) when studying the AML stem.

The FE results in this section have been obtained from different AML sizes – the normal bone had size 135, the osteoporotic had size 150 and the osteoarthritic had size 120 – due to the characteristics of the femoral canals. It could be that the FE results were affected not just by the material properties of the bone, but also by the different implant sizes used. However, in chapter 4 the effect of weaker bone mass on micromotion was simulated by reducing the stiffness of the bone gradually from the Carter & Hayes relationship. The results from chapter 4 were obtained using the VHP femoral dataset and size 135 of the AML, and they showed that micromotion increased as bone material properties get weaker. In conjunction with the results from Chapter 4, it is concluded that the stability of a cementless femoral prosthesis is compromised in weaker bone mass (such as in osteoporosis).

6.4 Conclusion

This chapter looked at various surgical and pathological parameters that could affect the stability of cementless hip stems. In the first section, the effect of interfacial gaps on three types of cementless hip prostheses was examined. In hip stems where the standard surgical procedure involved distal over-reaming of the endosteal bone, micromotion was found to be larger than in a design where perfect bone-implant contact was achieved. In this proximally fixed hip stem, achieving interference fit was crucial to the

stability of the stem. In a design where canal filling was not a criterion, such as the Alloclassic hip stem, gaps in certain locations may not necessarily endanger its stability. The stability of the AML hip stem was also not compromised by the presence of proximal interfacial gaps as long as interference fit is achieved distally.

The second section looked at the effect of implant undersizing and malalignment. Varus angulation of the prosthesis was looked at since this is the most common type of malalignment. Undersizing and malalignment were analysed together in this section because varus malalignment is mostly connected to implant undersizing. In general, undersizing should always be prevented if possible because it increases micromotion and implant instability. The design of the implant determines the magnitude of instability: the FE results showed that an undersized straight cylindrical stem was more unstable than an undersized tapered rectangular stem. This was also true in the varus position, where the tapered rectangular stem was found to be more stable than a cylindrical stem.

The last section of the chapter looked at the pathological aspect of hip arthroplasty. Two CT datasets of bones with skeletal diseases of osteoarthritis and osteoporosis were obtained and used in the analyses to compare their stability with the results from a normal healthy bone. The FE results showed that micromotion does depend on the quality of the bone - the weaker the bone mass, the more unstable the implant is. The results also showed that stair-climbing activity had a detrimental effect on the stability of a straight cylindrical femoral component implanted in an osteoporotic bone.

Chapter 7 Summary, conclusions and Further Work.

Cementless hip stems are gaining popularity in hip joint arthroplasty but the issues related to their stability are a major concern. This research uses Finite Element Analyses to study various factors that affect the stability of cementless hip stems. A micromotion algorithm was written in Compaq Visual Fortran to calculate and display interface micromotion - a parameter that describes the stability of hip stems. The computer code was checked for accuracy using published data of a simplified cylindrical bone-implant model. The model was also used to study the effect of location for measurement of relative micromotion; FE studies calculate micromotion at the interface, whereas in-vitro experiments measure micromotion of the implant relative to the outer surface of the cortex. With a bending moment of 20Nm, a difference of up to 20 μ m was found between in-vitro measurements and interface micromotion.

In this study, two types of micromotion results were presented. The first was simply the contour plots of implant micromotion relative to the bone as used previously by other researchers. However, this method alone could not answer whether the stem was stable or unstable. A novel technique was proposed, where bone loss was simulated at the interface where micromotion exceeded the threshold limit for bone ingrowth. The analysis was repeated until either a stable-state micromotion was achieved or the implant failed – either by exceeding the interfacial shear strength or the implant surface was encapsulated with the threshold micromotion limit, i.e. encapsulated with fibrous tissue. This technique was used in this project to analyse various factors that could affect the stability of cementless hip stems.

The FE micromotion code was validated via a simple in-vitro experiment. Four cadaveric femurs were implanted with an Alloclassic hip stem each and loaded axially at the shoulder of the implant on a testing machine. The implants were cyclically loaded and the micromotions were measured at each loading cycle using a linear displacement transducer. One of the femurs was CT scanned whilst intact and after implantation to create an exact FE model of the experiment. A parallel virtual experiment simulating the physical experiment was carried out and the results were compared with the experiment. The FE results correlated well with the experimental findings.

Several parameters affecting the FE predictions were also analysed. The values of the coefficient of friction used in the literature varied between 0.1 and 1.73. A study was therefore conducted to analyse the effect of coefficient of friction on interface micromotion. Using an AML hip stem model, micromotion was found to reduce as the

friction coefficient was increased. Significant reduction in micromotion occurred between $\mu=0.01$ and $\mu=0.2$ with an average micromotion calculated along a particular line on the anterior surface dropped from 1.556mm to 0.162mm. However, as the values of friction coefficient were increased further, the reduction in micromotion became less abrupt. The average micromotion for $\mu=0.8$ and $\mu=1.0$ was 0.037mm and 0.031mm respectively.

The effect of interference fit was also analysed. Most FE work on micromotion did not include interference fit, maybe due to the fact that it would be difficult if not impossible to measure exactly how much press-fit has been achieved and the actual distribution of the fit post-surgery. However, to ignore the interference fit altogether would be inappropriate as cementless stems are designed with press-fit. In this study, the maximum amount of interference fit was estimated using a simplified cylindrical bone-implant model. A value of 113 μm was found from this calculation. A comparative study was then conducted, using three types of radial interference fit values – 0, 50 μm and 100 μm . The relative micromotion was found to reduce by up to 15 times in areas of cortical contact when maximum interference fit of 100 μm was included, and up to 3 times in the proximal area of cancellous contact, compared to the model without an interference fit. However, there was not much difference in magnitude and distribution of micromotion between an interference fit of 50 μm and 100 μm . The results showed the importance of modelling the interference fit in micromotion FEA and the importance of achieving press-fit in cementless hip arthroplasty.

The study also looked at the effect of cyclic loading on micromotion. The results showed that cyclic loading produced similar types of micromotion found in in-vitro

experiments – permanent, reversible and total micromotion. However, the magnitudes of micromotion were affected by the inclusion of an interference fit. When an interference fit was not included, the magnitudes of the total, permanent and reversible micromotions were different in the first few cycles. Longer cycles were therefore required before these values stabilised. When a maximum interference fit was included, the stem stabilised immediately and permanent micromotion was found to be negligible. The total micromotion from the first loading curve could therefore be used as a reasonable estimate to the reversible micromotion.

The effect of muscle forces on interface micromotion was also analysed. Muscle forces should be included in all FE analyses because ignoring them will underestimate the magnitude of micromotion and the surface area unfeasible for bone ingrowth. Another FE parameter studied was the bone material properties. The bone's elastic modulus was reduced to simulate weaker bone mass using the Carter & Hayes relationship. The results showed that as the modulus was reduced, interface micromotion increased.

The major part of this project looked at the effect of hip stem designs on interface micromotion and stability. A search was conducted gathering as much information as possible on cementless hip stem designs. These stems were categorised into three basic types based on the overall geometry – straight cylindrical, tapered, and anatomical designs. A member of each group was modelled and analysed in physiological loading conditions. The results showed that all three models representing the three groups had similar magnitude and distribution of micromotion. When interfacial bone loss was simulated, all of them were found to be stable, with the anatomical design the most stable in both simulated walking and stair climbing.

The study continued with the effect of implant material stiffness on micromotion and stability. Three elastic moduli representing cobalt chromium, titanium alloy and a composite material were analysed under physiological loading. The contour plots of micromotion confirmed the results from other published reports - the more flexible the implant, the larger the micromotion. However, with the proposed technique of measuring instability, all three implants were predicted to be stable. The composite stem was still the worst, with predicted fibrous tissue formation covering the proximal half of the stem. However, the results showed that the stem should still be stable if tight fit was achieved distally.

The effect of stem length on stability was also studied. This is important because if a shorter stem could be used in hip arthroplasty, fewer problems would be encountered if a revision surgery is required because the distal cortex would still be available for fixation. Four hip stems with a decreasing stem length were modelled, with the shortest one having minimal cortical bone contact. The results showed that micromotion increased as the length was shortened, with the shortest stem having micromotion in excess of the threshold limit covering almost the whole surface. When bone loss was simulated, the first three stems were found to be stable. The results predicted that as long as cortical contact was achieved with press-fit, stability was not compromised. When sufficient cortical contact was not achieved, instability occurred as proved by the shortest stem model.

There are two design philosophies regarding the fixation of cementless hip stems – proximal fixation and distal fixation. An FEA study was conducted to compare the

micromotion and stability of these two design fixation philosophies. The comparative micromotion results showed that the distribution of micromotion was different between the two designs. Less micromotion was found in the lateral area of the proximal design, which could be attributed to the effectiveness of the lateral flare feature. However, more micromotion was found in the medial area of the proximal design than the distal design. When bone loss was simulated, the proximal design was found to be unstable compared to the distal design. The total loss of fixation was due to the loss of bone contact in the medial region.

The study continued with analyses on proximal macrofeatures. Most stems with proximal fixation design have macrofeatures in the proximal area to improve stability. However, the effectiveness of these macrofeatures has never been measured. Several major types of proximal macrofeatures were analysed in this study; they were the ridges, the grooves at various angles, the fins and the indentation features. The fins, the ridges and the grooves were analysed using the CLS hip stem model whilst the indentation macrofeature was analysed using the ABG hip stem model. The results showed that the original tapered fins macrofeature of the CLS performed the best in both physiological loadings. The effectiveness of grooves depended on the angles of the grooves. Grooves that aligned to the joint load had the largest micromotion and grooves opposing the direction of loading had the lowest micromotion. The medial ridge macrofeature was also found to reduce micromotion, but was not enough to maintain stability when bone loss was simulated. The indentation macrofeature of the ABG was found to contribute significantly to the stability of a proximally fixed cementless hip stem. Overall, proximal macrofeatures are beneficial in terms of

providing stability, with the magnitude of improvement depending on the types of macrofeatures.

The last chapter of the thesis looked into the effect of surgical and pathological parameters on micromotion. During bone preparation, broaching and reaming could create gaps at the interface. A technique of identifying the location of interfacial gaps using multiple CT datasets was proposed, and implemented on the Alloclassic hip stem. The micromotion result showed that the gaps created during bone preparation did not affect the stability of the stem as long as press-fit was achieved by way of the four corners along the stem. Apart from the Alloclassic hip stem, two other hip stem designs were also analysed – the straight cylindrical AML and the anatomical ABG. However, the technique of identifying interfacial gaps could not be used because of the unavailability of specimens. The possible locations of interfacial gaps created due to surgical error on the AML and the ABG hip systems were discussed with a senior orthopaedic surgeon. For the ABG, the most likely place for the gap to occur is in the proximal lateral region due to the shape of the stem and the surgical technique involved. For the AML, fixation is usually achieved through press-fit in the distal area, causing a possible gap in the proximal area. The results showed that micromotion was larger in hip stems with distal bone over-reaming compared to a design with a perfect bone-implant contact. Achieving interference fit in a proximally-fixed cementless hip stem is also important as it reduces the effect of interfacial gaps on stability. The stability of a distally fixed straight cylindrical hip stem was not compromised by the presence of proximal interfacial gaps as long as interference fit was achieved distally.

The effect of hip stems malalignment and undersizing due to surgical error was also carried out. Two types of hip stems were analysed – the straight cylindrical AML and the tapered Alloclassic. The results showed that undersizing should always be prevented if possible because it increased micromotion and implant instability. The design of the implant determined the magnitude of instability - the straight cylindrical design was found to be more susceptible to instability when undersized components were used compared to the tapered design. For hip stems in varus malalignment, both designs were found to be relatively more stable than undersized normally aligned stems, because the varus stems rested on the medial calcar proximally and the lateral cortex distally. In varus malalignment, the tapered design was more stable than the straight cylindrical design.

For the effect of pathological condition on stability, two femoral models were constructed from two CT datasets of patients suffering from osteoarthritis and osteoporosis respectively. The canal flare indices for the two bones, as well as the normal healthy bone from the VHP dataset were calculated. The osteoarthritic bone model was found to be of type A (champagne-fluted characteristic), whereas the osteoporotic bone had a stovepipe characteristic (type C). The normal VHP femur was of bone type B. The sizes of the AML stem used in the study were found to increase from type A to type C. The three models were analysed under physiological loading conditions and the micromotion results were compared with each other. The FE results showed that the quality of bone did affect the stability of cementless hip stems. The normal and osteoarthritic bones had relatively small micromotion and were found to be stable when bone loss was simulated. Osteoporotic bone, however, had the largest area

of interface micromotion in excess of the threshold limit especially during stair-climbing, and was found to be unstable when bone loss was simulated.

One of the limitations of this study was the inability of the micromotion code to separate the interface micromotion into axial and rotational components. The micromotion code was written to measure the interface micromotion, which was the criteria for bone ingrowth, and to check for instability when interface micromotion exceeded the threshold value. As such the components of the resultant micromotion vector were not required. However, the rotational and axial components of micromotion could be useful when analysing different design features of cementless hip stems. Certain hip stem designs could be better in sustaining torsional load than others.

The proposed technique of predicting hip stems instability could be improved. In this project, the process of manually creating interfacial gaps was very time consuming. An automated procedure that creates gaps automatically at each iteration and stops when failure conditions are met would make the technique more time-effective. Apart from interface micromotion, bone remodelling due to stress-shielding could also be included in the algorithm for better prediction of hip stems stability.

For the effect of interfacial gaps due to surgical error, the proposed technique of identifying gaps could only be used on the Alloclassic hip stem, due to the availability of the stem and femoral cadavers. The effect of interfacial gaps on micromotion for the AML and the ABG could not be implemented using the above technique due to the unavailability of these stems. Proper comparison between the three hip stem designs

could only be made if the AML and the ABG hip stems, as well as more specimens, were available.

In the study of the effect of bone's pathological condition on micromotion and stability, only the AML stem was analysed. Further studies using other cementless hip stem designs, such as the tapered or the anatomical, would be useful as these designs could perform better in osteoporotic condition or bone with type C characteristics.

Appendix 1

```

c *****
c Program to search for nodes at the bone-implant interface.
c Author      : M R Abdul Kadir
c Date started : 26 February 2001
c Last altered : 30 August 2002
c *****
c NB : Copy the nodal co-ordinate values from .mfd and save in a
c      .txt file. The coordinate values need to be +ve. Set "nref"
c      to the total number of nodes. Make sure to renumber all
c      nodes. The total number of common nodes is displayed at
c      the end of the result file. Cut and place it at the top
c      before using the data file in the micromotion subroutine.
c *****
c Program Find_required_nodes_2

integer ibone1,iimplant1,nref,i,j,k
integer inum1(100000)
real set_x(100000),set_y(100000),set_z(100000)
integer nil1(100000),nil2(100000),nil3(100000)
real lim

character*150 nodal_cood

c The program asks for the input file name.

write(*,*) 'Enter nodal coordinates file name:'
read(*,*) nodal_cood

call read_coords(nodal_cood,nref,inum1,set_x,set_y,set_z,
.nil1,nil2,nil3,k,lim)

stop
end
c *****
c subroutine read_coords(nodal_cood,nref,inum1,set_x,set_y,set_z,
.nil1,nil2,nil3,k,lim)

integer ibone1,iimplant1,nref,i,j,k
integer inum1(100000)
real set_x(100000),set_y(100000),set_z(100000)
integer nil1(100000),nil2(100000),nil3(100000)
real lim

character*150 nodal_cood

open(unit=20,file=nodal_cood,status='unknown')

```

```

c
c CHANGE FILE NAME !!!!!
c OTHERWISE YOU'LL OVERWRITE IMPORTANT DATA!!!!
c
  open(unit=22,file='d:\1rafiq\0_fit\02_ABG\1_feature\
&DATA_1nodes_CLSfeat2D.txt',status='unknown')

c The program starts searching for the 'common' nodes.

  nref=16440
  do i=1,nref
    read(20,*) inum1(i),set_x(i),set_y(i),set_z(i),
.nil1(i),nil2(i),nil3(i)
  enddo

  k=0
  lim=0.05

  do i=1,nref-1
    do j=i+1,nref
      if (abs(set_x(i)-set_x(j)).lt.lim.and.abs(set_y(i)-set_y(j)).lt.lim) then
        if (abs(set_z(i)-set_z(j)).lt.lim) then
          write(*,*) inum1(i),inum1(j)
          ibone1=inum1(i)
          iimplant1=inum1(j)
          k=k+1
          write(22,*) ibone1,iimplant1
        goto 25
      endif
    endif
  enddo
25  enddo

  write(22,100) k
100 format(t1,1x,i10)

c
  return
  end
c*****

```

Appendix 2

```

c *****
c User subroutine to calculate & display interface relative motion.
c *****
c
c Author      : M R Abdul Kadir
c
c DATE started : 05 September 2002
c
c DATE altered : 18 June 2003
c
c *****
c SUBROUTINE upstno(nqcode,nodeid,verno,nqncomp,nqtype,
  * nqaver,nqcomptype,nqdatatype,
  * nqcompname)
  implicit real*8 (a-h,o-z)
c *****
c
  dimension verno(*)
  dimension verno1(3),verno2(3)
  dimension raften(3),raftwenty(3)
  dimension inode(8,50000)
  character*24 nqcompname(*)
  include "../common/space"
  include "../common/arrays"
  include "../common/array2"
  include "../common/develp"
  include "../common/concom"
  common /iref1/iref1(50000)
  common /iref2/iref2(50000)
  common /inode1/inode1(50000)
  common /inode2/inode2(50000)
  common /icount/icount
  common /iflag/iflag
  common /nnodes1/nnodes1

c      Data files on the calculated interface micromotion

c      open(unit=101,file='d:\check1.txt',status='unknown')
c      open(unit=102,file='d:\1Rafiq\0_fit\01_AML\
.AML-stair2nd-inc01.txt',status='unknown')
c      open(unit=103,file='d:\1Rafiq\0_fit\01_AML\
.AML-stair2nd-inc10.txt',status='unknown')
c      open(unit=104,file='d:\1Rafiq\5_AML2\
.AML-stair-inc40.txt',status='unknown')
c      open(unit=105,file='d:\1Rafiq\5_AML2\
.AML-stair-inc50.txt',status='unknown')
c      open(unit=106,file='d:\1Rafiq\5_AML2\
.AML-stair-inc60.txt',status='unknown')

```

```

c      open(unit=107,file='d:\1Rafiq\5_AML2\
c      .AML-stair-inc70.txt',status='unknown')
c      open(unit=108,file='d:\1Rafiq\5_AML2\
c      .AML-stair-inc80.txt',status='unknown')
c      open(unit=109,file='d:\1Rafiq\5_AML2\
c      .AML-stair-inc90.txt',status='unknown')
c      open(unit=110,file='d:\1Rafiq\5_AML2\
c      .AML-stair-inc100.txt',status='unknown')

c
c      Read a list of the 'common' nodes from an external file
c      nnodes1 = total no. of nodes
c      iref1 = "common nodes" of the bone
c      iref2 = "common nodes" of the implant
c
c      if (iflag.eq.0) then
c          open(unit=98,file='d:\1Rafiq\2b_meshcon\DATA\
c      .DATA_1nodes_Dtet.txt',status='unknown')
c          read(98,*) nnodes1
c          do i=1,nnodes1
c              read(98,*) iref1(i),iref2(i)
c          enddo

c          iflag=iflag+1
c      endif

c      MAIN CODE FOR MEASURING MICROMOTION & ITS COMPONENTS

c      Call nodal coordinate's values (displaying purposes)

c      call nodvar(1,nodeid,valno,nqncomp,nqndatatype)
c      write(101,*) nodeid,valno(1),valno(2),valno(3)

c      Reset the value of micromotion

c          valno1=0.0
c          valno2=0.0

c      Find implant's "common nodes" from the elements' connectivity list

c      do i=1,nnodes1

c          if (nodeid.eq.iref2(i)) then

c              call nodvar(1,iref2(i),valno1,nqncomp,nqndatatype)
c              write(101,*) nodeid,iref1(i),valno1
c              call nodvar(1,iref1(i),valno2,nqncomp,nqndatatype)
c              write(102,*) nodeid,iref2(i),valno2

```

```
    if (inc.eq.1) then
      do j=1,nqncomp
        raften(j)=valno1(j)-valno2(j)
        write(102,*) nodeid,raften(j)
      enddo
    endif

    if (inc.eq.10) then
      do j=1,nqncomp
        raftwenty(j)=valno1(j)-valno2(j)
        write(103,*) nodeid,raftwenty(j)
      enddo
    endif

c    if (inc.eq.40) then
c      do j=1,nqncomp
c        raften(j)=valno1(j)-valno2(j)
c        write(104,*) nodeid,raften(j)
c      enddo
c    endif

c
c    if (inc.eq.50) then
c      do j=1,nqncomp
c        raftwenty(j)=valno1(j)-valno2(j)
c        write(105,*) nodeid,raftwenty(j)
c      enddo
c    endif

c
c    if (inc.eq.60) then
c      do j=1,nqncomp
c        raften(j)=valno1(j)-valno2(j)
c        write(106,*) nodeid,raften(j)
c      enddo
c    endif

c
c    if (inc.eq.70) then
c      do j=1,nqncomp
c        raftwenty(j)=valno1(j)-valno2(j)
c        write(107,*) nodeid,raftwenty(j)
c      enddo
c    endif

c
c    if (inc.eq.80) then
c      do j=1,nqncomp
c        raften(j)=valno1(j)-valno2(j)
c        write(108,*) nodeid,raften(j)
c      enddo
c    endif

c
c    if (inc.eq.90) then
c      do j=1,nqncomp
c        raftwenty(j)=valno1(j)-valno2(j)
c        write(109,*) nodeid,raftwenty(j)
c      enddo
```

```
c      endif
c
c      if (inc.eq.100) then
c          do j=1,nqncomp
c              raftwenty(j)=valno1(j)-valno2(j)
c              write(110,*) nodeid,raftwenty(j)
c          enddo
c      endif
c
c
c      Calculate relative motion
c
c          do j=1,nqncomp
c              rel(j)=valno1(j)-valno2(j)
c          enddo
c      endif
c
c      enddo
c
c      *****
c      DISPLAY RESULTS
c      *****
c
c      Resultant micromotion
c      -----
c
c      if (nqcode.eq.-1) then
c          do j=1,nqncomp
c              valno(j)=valno1(j)-valno2(j)
c          enddo
c
c          nqtype=1
c
c      endif
c
c      return
c  end
c*****
```


Appendix 3

```

c *****
c Program to interchange data from 2 CT datasets.
c Author       : M R Abdul Kadir
c Date started  : 07 June 2003
c Last altered  : 18 February 2004
c *****
c Program Interchange

integer ibone1,iimplant1,nref,i,j,k
integer inum1(100000)
real set_x(100000),set_y(100000),set_z(100000)
integer nil1(100000),nil2(100000),nil3(100000)
real lim

character*150 nodal_cood1
character*150 nodal_cood2

c The program asks for 2 input files (from 2 CT datasets).

write(*,*) 'Enter file name 1:'
read(*,*) nodal_cood1

write(*,*) 'Enter file name 2:'
read(*,*) nodal_cood2

call read_coords(nodal_cood1,nodal_cood2,nref,inum1,set_x,set_y,
.set_z,nil1,nil2,nil3,k,lim)

stop
end
c *****
c subroutine read_coords(nodal_cood1,nodal_cood2,nref,inum1,set_x,
.set_y,set_z,nil1,nil2,nil3,k,lim)

integer ibone1,iimplant1,nref,i,j,k
integer inum1(100000)
real set_x(100000),set_y(100000),set_z(100000)
integer nil1(100000),nil2(100000),nil3(100000)
real lim

character*150 nodal_cood1
character*150 nodal_cood2

open(unit=20,file=nodal_cood1,status='unknown')
open(unit=21,file=nodal_cood2,status='unknown')
c

```

```
c CHANGE FILE NAME !!!!!  
c OTHERWISE YOU'LL OVERWRITE IMPORTANT DATA!!!!  
c
```

```
open(unit=22,file='c:\1rafiq\2e_matprop\DATA\  
&DATA_1matprop_OPcombine3.txt',status='unknown')
```

```
c nref is the total number of nodes
```

```
nref=24903
```

```
c set_x is the proximal part
```

```
c set_y is the distal part
```

```
do i=1,nref  
    read(20,*) inum1(i),set_x(i)  
    read(21,*) inum1(i),set_y(i)  
enddo
```

```
c lim is taken from the values obtained from the 1st CT dataset.
```

```
k=0
```

```
lim=22103.28
```

```
do i=1,nref  
    if (set_x(i).eq.lim) then  
        set_z(i)=set_y(i)  
    else  
        set_z(i)=set_x(i)  
    endif  
    write(22,*) i,set_z(i)
```

```
enddo
```

```
c  
return  
end
```

```
c*****
```

Appendix 4

```

c *****
c Program to find nodes on the periosteal surface normal to the
c surface of the stem.
c Author : M R Abdul Kadir
c Date : 21 March 2003
c *****
c NB : Copy the nodal co-ordinates values from .mfd and save in a
c .txt file. The coordinate values need to be +ve. Set "nref"
c to the total number of nodes. Make sure you have renumber
c all nodes. The total number of "required"
c common nodes is at the end of the result file.
c Don't forget to replace it to the top.
c *****
c Program Outer_Cortex

integer ibone1,iimplant1,nref,i,j,k
integer inum1(10000),inum2(10000)
real set_x(10000),set_y(10000),set_z(10000)
real set_x2(10000),set_y2(10000),set_z2(10000)
integer nil1(10000),nil2(10000),nil3(10000)
integer nil4(10000),nil5(10000),nil6(10000)
real lim

character*150 nodal_cood1
character*150 nodal_cood2

c The program asks for 2 input files (from the stem and the bone)

write(*,*) 'Enter file name 1:'
read(*,*) nodal_cood1

write(*,*) 'Enter file name 2:'
read(*,*) nodal_cood2

call read_coords(nodal_cood1,nodal_cood2,nref,inum1,inum2,
.set_x,set_y,set_z,set_x2,set_y2,set_z2,nil1,nil2,nil3,
.nil4,nil5,nil6,k,lim)

stop
end
c*****
c subroutine read_coords(nodal_cood1,nodal_cood2,nref,inum1,
.inum2,set_x,set_y,set_z,set_x2,set_y2,set_z2,nil1,nil2,nil3,
.nil4,nil5,nil6,k,lim)

integer ibone1,iimplant1,nref,i,j,k
integer inum1(10000),inum2(10000)

```

```

real set_x(10000),set_y(10000),set_z(10000)
real set_x2(10000),set_y2(10000),set_z2(10000)
integer nil1(10000),nil2(10000),nil3(10000)
integer nil4(10000),nil5(10000),nil6(10000)
real lim

```

```

character*150 nodal_cood1
character*150 nodal_cood2

```

```

open(unit=20,file=nodal_cood1,status='unknown')
open(unit=21,file=nodal_cood2,status='unknown')

```

```

c
c CHANGE FILE NAME !!!!!
c OTHERWISE YOU'LL OVERWRITE IMPORTANT DATA!!!!
c

```

```

open(unit=22,file='d:\1rafiq\A1b_Rohlmann\
&DATA_outercortex.txt',status='unknown')

```

```

c nref is the total number of nodes

```

```

nref=1170

```

```

c The program stores information from the two data files.

```

```

do i=1,nref
  read(20,*) inum1(i),set_x(i),set_y(i),set_z(i),
.nil1(i),nil2(i),nil3(i)
enddo

do i=1,nref
  read(21,*) inum2(i),set_x2(i),set_y2(i),set_z2(i),
.nil4(i),nil5(i),nil6(i)
enddo

```

```

c lim is taken from the cylindrical model
c it is the distance between the outer surface of the stem and the outer cortex.

```

```

k=0
lim=5.1

```

```

c The program search for the nodes.

```

```

do i=1,nref
  do j=1,nref
    if (abs(sqrt(((set_x(i)-set_x2(j))*(set_x(i)-set_x2(j)))+
.((set_y(i)-set_y2(j))*(set_y(i)-set_y2(j)))+
.((set_z(i)-set_z2(j))*(set_z(i)-set_z2(j))))).lt.lim) then
      write(*,*) inum1(i),inum2(j)
      ibone1=inum1(i)
      iimplant1=inum2(j)
      k=k+1
      write(22,*) ibone1,iimplant1
    end if
  end do
end do

```

```
c          goto 25
          endif
        enddo
25    enddo

    write(22,100) k
100  format(t1,1x,i10)

c
    return
    end
c*****
```

References

Adam, F., Hammer, D. S., Pfautsch, S., & Westermann, K. 2002, "Early failure of a press-fit carbon fiber hip prosthesis with a smooth surface", *Journal of Arthroplasty*, vol. 17, no. 2, pp. 217-223.

Alexander, J. W., Kamaric, E., Noble, P. C., & McCarthy, J. C. "The effect of robotic machining on the micromotion of cementless femoral stems.", 45th edn, Orthopaedic Research Society.

Amstutz, H. C. 2000, "Innovations in design and technology - The story of hip arthroplasty", *Clinical Orthopaedics and Related Research* no. 378, pp. 23-30.

Ando, M., Imura, S., Omori, H., Okumura, Y., Bo, A., & Baba, H. 1999, "Nonlinear three-dimensional finite element analysis of newly designed cementless total hip stems", *Artificial Organs*, vol. 23, no. 4, pp. 339-346.

Ang, K. C., De, S. D., Goh, J. C. H., Low, S. L., & Bose, K. 1997, "Periprosthetic bone remodelling after cementless total hip replacement - A prospective comparison of two different implant designs", *Journal of Bone and Joint Surgery-British Volume*, vol. 79B, no. 4, pp. 675-679.

Araujo, C. G., Gonzalez, J. F., & Tonino, A. 1998, "Rheumatoid arthritis and hydroxyapatite-coated hip prostheses - Five-year results", *Journal of Arthroplasty*, vol. 13, no. 6, pp. 660-667.

Bachus, K. N., Bloebaum, R. D., & Jones, R. E. 1999, "Comparative micromotion of fully and proximally cemented femoral stems", *Clinical Orthopaedics and Related Research* no. 366, pp. 248-257.

Badhe, N. P., Quinnell, R. C., & Howard, P. W. 2002, "The uncemented Bi-Contact total hip arthroplasty", *The Journal of Arthroplasty*, vol. 17, no. 7, pp. 896-901.

Baleani, M., Cristofolini, L., & Toni, A. 2000, "Initial stability of a new hybrid fixation hip stem: Experimental measurement of implant-bone micromotion under torsional load in comparison with cemented and cementless stems", *Journal of Biomedical Materials Research*, vol. 50, no. 4, pp. 605-615.

Bargar, W. L., Bauer, A., & Borner, M. 1998, "Primary and revision total hip replacement using the Robodoc (R) system", *Clinical Orthopaedics and Related Research* no. 354, pp. 82-91.

Barrack, R. L., Castro, F., & Guinn, S. 1996, "Cost of implanting a cemented versus cementless femoral stem", *Journal of Arthroplasty*, vol. 11, no. 4, pp. 373-376.

Barrack, R. L. 1998, "Pre-Operative Planning," in *The Adult Hip*, 1st edn, J. J. Callaghan, A. G. Rosenberg, & H. E. Rubash, eds., Lippincott-Raven, pp. 925-950.

Bauer, T. W. & Schils, J. 1999, "The pathology of total joint arthroplasty - II. Mechanisms of implant failure.", *Skeletal Radiology*, vol. 28, no. 9, pp. 483-497.

Berend, K. R., Lombardi, A. V., Mallory, T. H., Dodds, K. L., & Adams, J. B. 2004, "Cementless double-tapered total hip arthroplasty in patients 75 years of age and older", *The Journal of Arthroplasty*, vol. 19, no. 3, pp. 288-295.

Bernakiewicz, M., Viceconti, M., & Toni, A. 2001, "Investigation of the influence of periprosthetic fibrous tissue on the primary stability of uncemented hip prosthesis", *Computer Methods in Biomechanics and Biomedical Engineering*, vol. 3, pp. 21-26.

Berzins, A., Sumner, D. R., Andriacchi, T. P., & Galante, J. O. 1993, "Stem Curvature and Load Angle Influence the Initial Relative Bone-Implant Motion of Cementless Femoral Stems", *Journal of Orthopaedic Research*, vol. 11, no. 5, pp. 758-769.

- Biegler, F. B., Reuben, J. D., Harrigan, T. P., Hou, F. J., & Akin, J. E. 1995, "Effect of porous coating and loading conditions on total hip femoral stem stability", *Journal of Arthroplasty*, vol. 10, no. 6, pp. 839-847.
- Boss, J. H., Shajrawi, I., Soudry, M., & Mendes, D. G. 1990, "Histological Features of the Interface Membrane of Failed Isoelastic Cementless Prostheses", *International Orthopaedics*, vol. 14, no. 4, pp. 399-403.
- Bourne, R. B. & Rorabeck, C. H. 1998, "A critical look at cementless stems - Taper designs and when to use alternatives", *Clinical Orthopaedics and Related Research* no. 355, pp. 212-223.
- Brand, R., Pederson, D., & Friederich, J. 1986, "The sensitivity of muscle force predictions to changes in physiologic cross-sectional area.", *Journal of Biomechanics*, vol. 19, no. 8, pp. 589-596.
- Brand, R., Pederson, D., Davy, D., Kotzar, G., Heiple, K., & Goldberg, V. 1994, "Comparison of hip force calculations and measurements in the same patient.", *Journal of Arthroplasty*, vol. 9, no. 1, pp. 45-51.
- Bronzino, J. D. 1995, *The Biomedical Engineering Handbook*, 1st edn, CRC Press.
- Buhler, D. W., Oxland, T. R., & Nolte, L. P. 1997, "Design and evaluation of a device for measuring three- dimensional micromotions of press-fit femoral stem prostheses", *Medical Engineering & Physics*, vol. 19, no. 2, pp. 187-199.
- Buhler, D. W., Berlemann, U., Lippuner, K., Jaeger, P., & Nolte, L. P. 1997, "Three-dimensional primary stability of cementless femoral stems", *Clinical Biomechanics*, vol. 12, no. 2, pp. 75-86.
- Buma, P., van Loon, P. J. M., Versleyen, H., Weinans, H., Slooff, T. J. J. H., de Groot, K., & Huiskes, R. 1997, "Histological and biomechanical analysis of bone and interface

reactions around hydroxyapatite-coated intramedullary implants of different stiffness: a pilot study on the goat", *Biomaterials*, vol. 18, no. 18, pp. 1251-1260.

Burke, D. W., Oconnor, D. O., Zalenski, E. B., Jasty, M., & Harris, W. H. 1991, "Micromotion of Cemented and Uncemented Femoral Components", *Journal of Bone and Joint Surgery-British Volume*, vol. 73, no. 1, pp. 33-37.

Callaghan, J. J., Fulghum, C. S., Glisson, R. R., & Stranne, S. K. 1992, "The Effect of Femoral Stem Geometry on Interface Motion in Uncemented Porous-Coated Total Hip Prostheses - Comparison of Straight-Stem and Curved-Stem Designs", *Journal of Bone and Joint Surgery-American Volume*, vol. 74A, no. 6, pp. 839-848.

Cann, C. & Genant, H. 1980, "Precise measurement of vertebral mineral content using computed tomography", *Journal of Computer Assisted Tomography*, vol. 4, no. 4, pp. 493-500.

Capello, W. N., 'A, D., Manley, M. T., & Feinberg, J. R. 1998, "Hydroxyapatite in total hip arthroplasty - Clinical results and critical issues", *Clinical Orthopaedics and Related Research* no. 355, pp. 200-211.

Carter, D. & Hayes, W. 1977, "The compressive behaviour of bone as a two-phase porous structure", *Journal of Bone and Joint Surgery-American Volume*, vol. 59, no. 7, pp. 954-962.

Carter, L. W., Stovall, D. O., & Young, T. R. 1995, "Determination of Accuracy of Preoperative Templating of Noncemented Femoral Prostheses", *Journal of Arthroplasty*, vol. 10, no. 4, pp. 507-513.

Chan, Y. K., Chiu, K. Y., Yip, D. K. H., Ng, T. P., & Tang, W. M. 2003, "Full weight bearing after non-cemented total hip replacement is compatible with satisfactory results", *International Orthopaedics*, vol. 27, no. 2, pp. 94-97.

- Chang, C. K., Wu, J. S., Mao, D. L., & Ding, C. X. 2001, "Mechanical and histological evaluations of hydroxyapatite- coated and noncoated Ti6Al4V implants in tibia bone", *Journal of Biomedical Materials Research*, vol. 56, no. 1, pp. 17-23.
- Cheal, E. J., Spector, M., & Hayes, W. C. 1992, "Role of Loads and Prosthesis Material Properties on the Mechanics of the Proximal Femur After Total Hip-Arthroplasty", *Journal of Orthopaedic Research*, vol. 10, no. 3, pp. 405-422.
- Chen, C. H., Shih, C. H., Lin, C. C., & Cheng, C. K. 1998, "Cementless Roy-Camille femoral component", *Archives of Orthopaedic and Trauma Surgery*, vol. 118, no. 1-2, pp. 85-88.
- Chess, D. G., Grainger, R. W., Phillips, T., Zarzour, Z. D., & Sheppard, B. R. 1996, "The cementless anatomic medullary locking femoral component: An independent clinical and radiographic assessment", *Canadian Journal of Surgery*, vol. 39, no. 5, pp. 389-392.
- Ciccotti, M. G., Rothman, R. H., Hozack, W. J., & Moriarty, L. 1994, "Clinical and roentgenographic evaluation of hydroxyapatite-augmented and nonaugmented porous total hip arthroplasty", *The Journal of Arthroplasty*, vol. 9, no. 6, pp. 631-639.
- Clohisy, J. C. & Harris, W. H. 1999, "The Harris-Galante uncemented femoral component in primary total hip replacement at 10 years", *The Journal of Arthroplasty*, vol. 14, no. 8, pp. 915-917.
- Cruz-Pardos, A. & Garcia-Cimbrelo, E. 2001, "The Harris-Galante total hip arthroplasty - A minimum 8-year follow-up study", *Journal of Arthroplasty*, vol. 16, no. 5, pp. 586-597.
- Dammak, M., Shiraziadl, A., & Zukor, D. J. 1997, "Analysis of cementless implants using interface nonlinear friction - Experimental and finite element studies", *Journal of Biomechanics*, vol. 30, no. 2, pp. 121-129.

- Davies, M. S., Parker, B. C., Ward, D. A., Hua, J., & Walker, P. S. 1999, "Migration of the uncemented CLS femoral component", *Orthopedics*, vol. 22, no. 2, pp. 225-228.
- Delaunay, C., Cazeau, C., & Kapandji, A. I. 1998, "Cementless primary total hip replacement - Four to eight year results with the Zweymuller-Alloclassic (R) prosthesis", *International Orthopaedics*, vol. 22, no. 1, pp. 1-5.
- Delaunay, C., Bonomet, F., North, J., Jobard, D., Cazeau, C., & Kempf, J. F. 2001, "Grit-blasted titanium femoral stem in cementless primary total hip arthroplasty - A 5-to 10-year multicenter study", *Journal of Arthroplasty*, vol. 16, no. 1, pp. 47-54.
- deNies, F. & Fidler, M. W. 1996, "The Harris-Galante cementless femoral component - Poor results in 57 hips followed for 3 years", *Acta Orthopaedica Scandinavica*, vol. 67, no. 2, pp. 122-124.
- Dhert, W. J. A. & Jansen, J. A. 2000, "The validity of a single pushout test," in *Mechanical testing of bone and the bone-implant interface*, 1st edn, Y. H. An & R. A. Draughn, eds., CRC Press, pp. 477-488.
- Dickob, M. & Martini, T. 1996, "The cementless PM hip arthroplasty - Four-to-seven-year results", *Journal of Bone and Joint Surgery-British Volume*, vol. 78B, no. 2, pp. 195-199.
- Doehring, T. C., Rubash, H. E., & Dore, D. E. 1999, "Micromotion measurements with hip center and modular neck length alterations", *Clinical Orthopaedics and Related Research* no. 362, pp. 230-239.
- Donnelly, W. J., Kobayashi, A., Freeman, M. A. R., Chin, T. W., Yeo, H., West, M., & Scott, G. 1997, "Radiological and survival comparison of four methods of fixation of a proximal femoral stem", *Journal of Bone and Joint Surgery-British Volume*, vol. 79B, no. 3, pp. 351-360.

Dorr, L. D., Faugere, M. C., Mackel, A. M., Gruen, T. A., Bogner, B., & Malluche, H. H. 1993, "Structural and Cellular Assessment of Bone Quality of Proximal Femur", *Bone*, vol. 14, no. 3, pp. 231-242.

Dorr, L. D. & Wan, Z. N. 1996, "Comparative results of a distal modular sleeve, circumferential coating, and stiffness relief using the Anatomic Porous Replacement II", *Journal of Arthroplasty*, vol. 11, no. 4, pp. 419-428.

Dorr, L. D., Wan, Z. N., & Gruen, T. 1997, "Functional results in total hip replacement in patients 65 years and older", *Clinical Orthopaedics and Related Research* no. 336, pp. 143-151.

Dorr, L. D., Lewonowski, K., Lucero, M., Harris, M., & Wan, Z. N. 1997, "Failure mechanisms of anatomic porous replacement I cementless total hip replacement", *Clinical Orthopaedics and Related Research* no. 334, pp. 157-167.

Dowson, D. & Wright, V. 1981, *Introduction to the Biomechanics of Joints and Joint Replacement*, 1st edn, Mechanical Engineering Publication Ltd..

Duda, G. 1996, *Influence of muscle forces on the internal loads in the femur during gait*, Ph.D. thesis, Technische Universität Hamburg.

Duda, G., Heller, M., Bergmann, G., Graichen, F., & Rohlmann, A. Hip 98. 1998. Free University Berlin; Humboldt University Berlin.

Ref Type: Computer Program

Duda, G. N., Heller, M., Albinger, J., Schulz, O., Schneider, E., & Claes, L. 1998, "Influence of muscle forces on femoral strain distribution", *Journal of Biomechanics*, vol. 31, no. 9, pp. 841-846.

Duffy, G. P., Muratoglu, O. K., Biggs, S. A., Larson, S. L., Lozynsky, A. J., & Harris, W. H. 2001, "A critical assessment of proximal macrotexturing on cemented femoral components", *Journal of Arthroplasty*, vol. 16, no. 8, pp. 42-48.

Duffy, G. P., Berry, D. J., Rowland, C., & Cabanela, M. E. 2001, "Primary uncemented total hip arthroplasty in patients [It]40 years old: 10- to 14-year results using first-generation proximally porous-coated implants", *The Journal of Arthroplasty*, vol. 16, no. 8, Supplement 1, pp. 140-144.

Dujardin, F. H., Mollard, R., Toupin, J. M., Coblenz, A., & Thomine, J. M. 1996, "Micromotion, fit, and fill of custom made femoral stems designed with an automated process", *Clinical Orthopaedics and Related Research* no. 325, pp. 276-289.

Duparc, J. & Massin, P. 1992, "Results of 203 Total Hip Replacements Using A Smooth, Cementless Femoral Component", *Journal of Bone and Joint Surgery-British Volume*, vol. 74, no. 2, pp. 251-256.

Eckardt, A., Aberman, H. M., Cantwell, H. D., & Heine, J. 2003, "Biological fixation of hydroxyapatite-coated versus grit- blasted titanium hip stems: a canine study", *Archives of Orthopaedic and Trauma Surgery*, vol. 123, no. 1, pp. 28-35.

Effenberger, H., Heiland, A., Ramsauer, T., Plitz, W., & Dorn, U. 2001, "A model for assessing the rotational stability of uncemented femoral implants", *Archives of Orthopaedic and Trauma Surgery*, vol. 121, no. 1-2, pp. 60-64.

Effenberger, H., Ramsauer, T., Bohm, G., Hilzensauer, G., Dorn, U., & Lintner, F. 2002, "Successful hip arthroplasty using cementless titanium implants in rheumatoid arthritis", *Archives of Orthopaedic and Trauma Surgery*, vol. 122, no. 2, pp. 80-87.

Eingartner, C., Volkmann, R., Winter, E., Maurer, F., Sauer, G., Weller, S., & Weise, K. 2000, "Results of an uncemented straight femoral shaft prosthesis after 9 years of follow-up", *The Journal of Arthroplasty*, vol. 15, no. 4, pp. 440-447.

- Ek, E. T. & Choong, P. F. M. 2005, "Comparison between triple-tapered and double-tapered cemented femoral stems in total hip arthroplasty - A prospective study comparing the C-Stem versus the Exeter Universal early results after 5 years of clinical experience", *Journal of Arthroplasty*, vol. 20, no. 1, pp. 94-100.
- El Warrak, A. O., Olmstead, M. L., von Rechenberg, B., & Auer, J. A. 2001, "A review of aseptic loosening in total hip arthroplasty", *Veterinary and Comparative Orthopaedics and Traumatology*, vol. 14, no. 3, pp. 115-124.
- Emery, D., Britton, A., Clarke, H., & Grover, M. 1997, "The Stanmore total hip arthroplasty - A 15- to 20-year follow-up study", *Journal of Arthroplasty*, vol. 12, no. 7, pp. 728-735.
- Engh, C. A., Bobyn, J. D., & Glassman, A. H. 1987, "Porous-Coated Hip-Replacement - the Factors Governing Bone Ingrowth, Stress Shielding, and Clinical-Results", *Journal of Bone and Joint Surgery-British Volume*, vol. 69, no. 1, pp. 45-55.
- Engh, C. A. & Massin, P. 1989, "Cementless Total Hip-Arthroplasty Using the Anatomic Medullary Locking Stem - Results Using A Survivorship Analysis", *Clinical Orthopaedics and Related Research* no. 249, pp. 141-158.
- Engh, C. A., Oconnor, D., Jasty, M., MCGovern, T. F., Bobyn, J. D., & Harris, W. H. 1992, "Quantification of Implant Micromotion, Strain Shielding, and Bone-Resorption with Porous-Coated Anatomic Medullary Locking Femoral Prostheses", *Clinical Orthopaedics and Related Research* no. 285, pp. 13-29.
- Engh, C. A., Hooten, J. P., Zettschaffer, K. F., Ghaffarpour, M., MCGovern, T. F., Macalino, G. E., & Zicat, B. A. 1994, "Porous-Coated Total Hip-Replacement", *Clinical Orthopaedics and Related Research* no. 298, pp. 89-96.
- Engh, C. A. 1998, "Mini-symposium: Total hip replacement - (ii) Distal porous coating yields optimal fixation", *Current Orthopaedics*, vol. 12, no. 4, pp. 232-238.

- Engh, C. A., Sychterz, C., & Engh, C. 1999, "Factors affecting femoral bone remodeling after cementless total hip arthroplasty", *Journal of Arthroplasty*, vol. 14, no. 5, pp. 637-644.
- Fisher, I. A. 2000, *A mathematical investigation of the influence of skeletal geometry on the mechanics of a prosthetic human hip joint.*, Imperial College London.
- Gerritsma-Bleeker, C. L. E., Deutman, R., Mulder, T. J., & Steinberg, J. D. J. 2000, "The Stanmore total hip replacement - A 22-year follow-up", *Journal of Bone and Joint Surgery-British Volume*, vol. 82B, no. 1, pp. 97-102.
- Giannikas, K. A., Din, R., Sadiq, S., & Dunningham, T. H. 2002, "Medium-term results of the ABG total hip arthroplasty in young patients", *Journal of Arthroplasty*, vol. 17, no. 2, pp. 184-188.
- Gong, W. L., Abdelouas, A., & Lutze, W. 2001, "Porous bioactive glass and glass-ceramics made by reaction sintering under pressure", *Journal of Biomedical Materials Research*, vol. 54, no. 3, pp. 320-327.
- Gortz, W., Nagerl, U. V., Nagerl, H., & Thomsen, M. 2002, "Spatial micromovements of uncemented femoral components after torsional loads", *Journal of Biomechanical Engineering-Transactions of the Asme*, vol. 124, no. 6, pp. 706-713.
- Gotze, C., Steens, W., Vieth, V., Poremba, C., Claes, L., & Steinbeck, J. 2002, "Primary stability in cementless femoral stems: custom-made versus conventional femoral prosthesis", *Clinical Biomechanics*, vol. 17, no. 4, pp. 267-273.
- Grant, P., Groggaard, B., & Nordsletten, L. 2004, "Ultralok uncemented femoral prostheses: 12 to 15 year follow-up evaluation", *The Journal of Arthroplasty*, vol. 19, no. 3, pp. 274-280.

- Gustilo, R. B., Bechtold, J. E., Giacchetto, J., & Kyle, R. F. 1989, "Rationale, Experience, and Results of Long-Stem Femoral Prosthesis", *Clinical Orthopaedics and Related Research* no. 249, pp. 159-168.
- Haber, D. & Goodman, S. B. 1998, "Total hip arthroplasty in juvenile chronic arthritis - A consecutive series", *Journal of Arthroplasty*, vol. 13, no. 3, pp. 259-265.
- Hacking, S. A., Bobyn, J. D., Tanzer, M., & Krygier, J. J. 1999, "The osseous response to corundum blasted implant surfaces in a canine hip model", *Clinical Orthopaedics and Related Research* no. 364, pp. 240-253.
- Hacking, S. A., Bobyn, J. D., Toh, K. K., Tanzer, M., & Krygier, J. J. 2000, "Fibrous tissue ingrowth and attachment to porous tantalum", *Journal of Biomedical Materials Research*, vol. 52, no. 4, pp. 631-638.
- Haddad, R. J., Cook, S. D., & Brinker, M. R. 1990, "A Comparison of 3 Varieties of Noncemented Porous-Coated Hip- Replacement", *Journal of Bone and Joint Surgery-British Volume*, vol. 72, no. 1, pp. 2-8.
- Hamadouche, M., Witvoet, J., Porcher, R., Meunier, A., Sedel, L., & Nizard, R. 2001, "Hydroxyapatite-coated versus grit-blasted femoral stems - A prospective, randomised study using EBRA-FCA", *Journal of Bone and Joint Surgery-British Volume*, vol. 83B, no. 7, pp. 979-987.
- Harris, W. H. 1997, "Options for primary femoral fixation in total hip arthroplasty - Cemented stems for all", *Clinical Orthopaedics and Related Research* no. 344, pp. 118-123.
- Hayashi, K., Mashima, T., & Uenoyama, K. 1999, "The effect of hydroxyapatite coating on bony ingrowth into grooved titanium implants", *Biomaterials*, vol. 20, no. 2, pp. 111-119.

Healy, W. L. 2002, "Hip implant selection for total hip arthroplasty in elderly patients", *Clinical Orthopaedics and Related Research* no. 405, pp. 54-64.

Hefzy, M. S. & Singh, S. P. 1997, "Comparison between two techniques for modeling interface conditions in a porous coated hip endoprosthesis", *Medical Engineering & Physics*, vol. 19, no. 1, pp. 50-62.

Herrera, A., Canales, V., Anderson, J., Garcia-Araujo, C., Murcia-Mazon, A., & Tonino, A. J. 2004, "Seven to 10 years followup of an anatomic hip prosthesis - An international study", *Clinical Orthopaedics and Related Research* no. 423, pp. 129-137.

Hildebrand, T., Laib, A., Muller, R., Dequeker, J., & Ruegsegger, P. 1999, "Direct three-dimensional bone morphometric analysis of human cancellous bone : microstructural data from spine, femur, iliac crest and calcaneus", *Journal of Bone and Mineral Research*, vol. 14, pp. 1167-1174.

Hofmann, A. A., Feign, M. E., Klauser, W., VanGorp, C. C., & Camargo, M. P. 2000, "Cementless primary total hip arthroplasty with a tapered, proximally porous-coated titanium prosthesis", *The Journal of Arthroplasty*, vol. 15, no. 7, pp. 833-839.

Hopkins, A. R. 2005, *Total Shoulder Arthroplasty Simulation using Finite Element Analysis*, Imperial College London.

Horikoshi, M., Macaulay, W., Booth, R. E., Crossett, L. S., & Rubash, H. E. 1994, "Comparison of Interface Membranes Obtained from Failed Cemented and Cementless Hip and Knee Prostheses", *Clinical Orthopaedics and Related Research* no. 309, pp. 69-87.

Howard, J. L., Hui, A. J., Bourne, R. B., McCalden, R. W., MacDonald, S. J., & Rorabeck, C. H. 2004, "A quantitative analysis of bone support comparing cementless tapered and distal fixation total hip replacements", *Journal of Arthroplasty*, vol. 19, no. 3, pp. 266-273.

- Hozack, W. J., Rothmann, R. H., Eng, K., & Mesa, J. 1996, "Primary cementless hip arthroplasty with a titanium plasma sprayed prosthesis", *Clinical Orthopaedics and Related Research* no. 333, pp. 217-225.
- Hozack, W., Gardiner, R., Hearn, S., Eng, K., & Rothman, R. 1994, "Taperloc femoral component : A 2-6-year study of the first 100 consecutive cases", *The Journal of Arthroplasty*, vol. 9, no. 5, pp. 489-493.
- Hua, J. & Walker, P. S. 1994, "Relative Motion of Hip Stems Under Load - An In-Vitro Study of Symmetrical, Asymmetrical, and Custom Asymmetrical Designs", *Journal of Bone and Joint Surgery-American Volume* , vol. 76A, no. 1, pp. 95-103.
- Huiskes, R., Verdonschot, N., & Nivbrant, B. 1998, "Migration, stem shape, and surface finish in cemented total hip arthroplasty", *Clinical Orthopaedics and Related Research* no. 355, pp. 103-112.
- Huo, M. H., Martin, R. P., Zatorski, L. E., & Keggi, K. J. 1995, "Total hip arthroplasty using the Zweymuller stem implanted without cement - A prospective study of consecutive patients with minimum 3-year follow-up period", *Journal of Arthroplasty*, vol. 10, no. 6, pp. 793-799.
- Incavo, S. J., Havener, T., Benson, E., McGrory, B. J., Coughlin, K. M., & Beynonn, B. D. 2004, "Efforts to improve cementless femoral stems in THR - 2- to 5- year follow-up of a high-offset femoral stem with distal stem modification (secur-fit plus)", *Journal of Arthroplasty*, vol. 19, no. 1, pp. 61-67.
- Jacobsen, S., Jensen, F. K., Poulsen, K., Sturup, J., & Retpen, J. B. 2003, "Good performance of a titanium femoral component in cementless hip arthroplasty in younger patients - 97 arthroplasties followed for 5-11 years", *Acta Orthopaedica Scandinavica*, vol. 74, no. 3, pp. 248-252.

Jacobsson, S. A., Djerf, K., Gillquist, J., Hammerby, S., & Ivarsson, I. 1993, "A Prospective Comparison of Butel and PCA Hip-Arthroplasty", *Journal of Bone and Joint Surgery-British Volume*, vol. 75, no. 4, pp. 624-629.

Jakim, I., Barlin, C., & Sweet, M. B. E. 1988, "RM Isoelastic Total Hip Arthroplasty", *Journal of Arthroplasty*, vol. 3, no. 3, pp. 191-199.

Jansson, V. & Refior, H. J. 1992, "Clinical-Results and Radiologic Findings After Cementless Implantation of PCA Stems in Total Hip-Replacement", *Archives of Orthopaedic and Trauma Surgery*, vol. 111, no. 6, pp. 305-308.

Jinno, T., Kirk, S. K., Morita, S., & Goldberg, V. M. 2004, "Effects of calcium ion implantation on osseointegration of surface-blasted titanium alloy femoral implants in a canine total hip arthroplasty model", *The Journal of Arthroplasty*, vol. 19, no. 1, pp. 102-109.

Johnston, D. W. C., Davies, D. M., Beaupre, L. A., & Lavoie, G. 2001, "Standard anatomical medullary locking (AML) versus tricalcium phosphate-coated AML femoral prostheses", *Canadian Journal of Surgery*, vol. 44, no. 6, pp. 421-427.

Kang, J. S., Dorr, L. D., & Wan, Z. N. 2000, "The effect of diaphyseal biologic fixation on clinical results and fixation of the APR-II stem", *Journal of Arthroplasty*, vol. 15, no. 6, pp. 730-735.

Kapandji, I. A. 1987, *The physiology of the joints*, 5th edn, Churchill Livingstone.

Karrholm, J., Anderberg, C., Snorrason, F., Thanner, J., Langeland, N., Malchau, H., & Herberts, P. 2002, "Evaluation of a femoral stem with reduced stiffness - A randomized study with use of radiostereometry and bone densitometry", *Journal of Bone and Joint Surgery-American Volume*, vol. 84A, no. 9, pp. 1651-1658.

- Kato, H., Neo, M., Tamura, J., & Nakamura, T. 2001, "Bone bonding in bioactive glass ceramics combined with a new synthesized agent TAK-778", *Journal of Biomedical Materials Research*, vol. 57, no. 2, pp. 291-299.
- Kato, H., Nishiguchi, S., Furukawa, T., Neo, M., Kawanabe, K., Saito, K., & Nakamura, T. 2001, "Bone bonding in sintered hydroxyapatite combined with a new synthesized agent, TAK-778", *Journal of Biomedical Materials Research*, vol. 54, no. 4, pp. 619-629.
- Keaveny, T. M. & Bartel, D. L. 1993, "Effects of Porous Coating, with and Without Collar Support, on Early Relative Motion for A Cementless Hip-Prosthesis", *Journal of Biomechanics*, vol. 26, no. 12, pp. 1355-1368.
- Keisu, K. S., Orozco, F., McCallum, I. I. I., Bissett, G., Hozack, W. J., Sharkey, P. F., & Rothman, R. H. 2001, "Cementless femoral fixation in the rheumatoid patient undergoing total hip arthroplasty: Minimum 5-year results", *The Journal of Arthroplasty*, vol. 16, no. 4, pp. 415-421.
- Kendrick, J. B., Noble, P. C., & Tullos, H. S. 1995, "Distal Stem Design and the Torsional Stability of Cementless Femoral Stems", *Journal of Arthroplasty*, vol. 10, no. 4, pp. 463-469.
- Kerner, J. 1999, *Patient specific computer modelling of bone changes around orthopaedic implants*, Imperial College London.
- Kerner, J., Huiskes, R., van Lenthe, G. H., Weinans, H., van Rietbergen, B., Engh, C. A., & Amis, A. A. 1999, "Correlation between pre-operative periprosthetic bone density and post-operative bone loss in THA can be explained by strain- adaptive remodelling", *Journal of Biomechanics*, vol. 32, no. 7, pp. 695-703.
- Khalily, C. & Lester, D. K. 2002, "Results of a tapered cementless femoral stem implanted in varus", *Journal of Arthroplasty*, vol. 17, no. 4, pp. 463-466.

Khalily, C. & Whiteside, L. A. 1998, "Predictive value of early radiographic findings in cementless total hip arthroplasty femoral components : An 8- to 12-Year Follow-up", *The Journal of Arthroplasty*, vol. 13, no. 7, pp. 768-773.

Kienapfel, H., Sprey, C., Wilke, A., & Griss, P. 1999, "Implant fixation by bone ingrowth", *The Journal of Arthroplasty*, vol. 14, no. 3, pp. 355-368.

Kim, Y. H., Oh, S. H., & Kim, J. S. 2003, "Primary total hip arthroplasty with a second-generation cementless total hip prosthesis in patients younger than fifty years of age", *Journal of Bone and Joint Surgery-American Volume*, vol. 85A, no. 1, pp. 109-114.

Kim, Y. H., Kim, J. S., Oh, S. H., & Kim, J. M. 2003, "Comparison of porous-coated titanium femoral stems with and without hydroxyapatite coating", *Journal of Bone and Joint Surgery-American Volume*, vol. 85A, no. 9, pp. 1682-1688.

Kim, Y. H. & Kim, V. E. M. 1994, "Cementless porous-coated anatomic medullary locking total hip prostheses", *The Journal of Arthroplasty*, vol. 9, no. 3, pp. 243-252.

Kim, Y. H. 2002, "Bilateral cemented and cementless total hip arthroplasty", *The Journal of Arthroplasty*, vol. 17, no. 4, pp. 434-440.

Kitamura, S., Hasegawa, Y., Iwasada, S., Yamauchi, K. i., Kawamoto, K., Kanamono, T., & Iwata, H. 1999, "Catastrophic failure of cementless total hip arthroplasty using a femoral component without surface coating", *The Journal of Arthroplasty*, vol. 14, no. 8, pp. 918-924.

Knight, J. L. & Atwater, R. D. 1992, "Preoperative planning for total hip arthroplasty - Quantitating its utility and precision", *Journal of Arthroplasty*, vol. 7, no. Supplement, pp. 403-409.

Knight, J. L., Atwater, R. D., & Guo, J. 1998, "Clinical results of the midstem porous-coated anatomic uncemented femoral stem in primary total hip arthroplasty : A five- to nine-year prospective study", *The Journal of Arthroplasty*, vol. 13, no. 5, pp. 535-545.

Kobayashi, A., Donnelly, W. J., Scott, G., & Freeman, M. A. R. 1997, "Early radiological observations may predict the long-term survival of femoral hip prostheses", *Journal of Bone and Joint Surgery-British Volume*, vol. 79B, no. 4, pp. 583-589.

Kotzar, G. M., Davy, D. T., Berilla, J., & Goldberg, V. M. 1995, "Torsional loads in the early postoperative period following total hip replacement", *Journal of Orthopaedic Research*, vol. 13, no. 6, pp. 945-955.

Krischak, G. D., Wachter, N. J., Zabel, T., Suger, G., Beck, A., Kinzl, L., Claes, L. E., & Augat, P. 2003, "Influence of preoperative mechanical bone quality and bone mineral density on aseptic loosening of total hip arthroplasty after seven years", *Clinical Biomechanics*, vol. 18, no. 10, pp. 916-923.

Kronick, J. L., Barba, M. L., & Paprosky, W. G. 1997, "Extensively coated femoral components in young patients", *Clinical Orthopaedics and Related Research* no. 344, pp. 263-274.

Kuiper, J. H. & Huiskes, R. 1996, "Friction and stem stiffness affect dynamic interface in total hip replacement", *Journal of Orthopaedic Research*, vol. 14, no. 1, pp. 36-43.

Kusakabe, H., Sakamaki, T., Nihei, K., Oyama, Y., Yanagimoto, S., Ichimiya, M., Kimura, J., & Toyama, Y. 2004, "Osseointegration of a hydroxyapatite-coated multilayered mesh stem", *Biomaterials*, vol. 25, no. 15, pp. 2957-2969.

Kwong, K. S. C. 1990, "The Biomechanical Role of the Collar of the Femoral Component of A Hip-Replacement", *Journal of Bone and Joint Surgery-British Volume*, vol. 72, no. 4, pp. 664-665.

Laine, H. J., Poulakka, T. J. S., Moilanen, T., Pajamaki, K. J., Wirta, J., & Lehto, M. U. K. 2000, "The effects of cementless femoral stem shape and proximal surface texture on 'fit-and-fill' characteristics and on bone remodeling", *International Orthopaedics*, vol. 24, no. 4, pp. 184-190.

Lautiainen, I. A., Joukainen, J., & Makela, E. A. 1994, "Clinical and roentgenographic results of cementless total hip arthroplasty", *The Journal of Arthroplasty*, vol. 9, no. 6, pp. 653-660.

Leali, A., Fetto, J., Insler, H., & Elfenbein, D. 2002, "The effect of a lateral flare feature on implant stability", *International Orthopaedics*, vol. 26, no. 3, pp. 166-169.

Lester, D. K. 1997, "Cross-section radiographic analysis of 10 retrieved titanium alloy press-fit femoral endoprostheses", *The Journal of Arthroplasty*, vol. 12, no. 8, pp. 930-937.

Li, B. & Aspden, R. M. 1997, "Material properties of bone from the femoral neck and calcar femorale of patients with osteoporosis or osteoarthritis", *Osteoporosis International*, vol. 7, no. 5, pp. 450-456.

Longjohn, D. B. & Dorr, L. D. 1998, "Mini-symposium: Total hip replacement - (iii) Proximal fixation stems yield optimal fixation", *Current Orthopaedics*, vol. 12, no. 4, pp. 239-243.

Macdonald, D. A. 1998, "Mini Symposium: Total hip replacement - (i) Risks versus rewards of total hip replacement", *Current Orthopaedics*, vol. 12, no. 4, pp. 229-231.

Maistrelli, G. L., Fornasier, V., Binnington, A., Mckenzie, K., Sessa, V., & Harrington, I. 1991, "Effect of Stem Modulus in A Total Hip-Arthroplasty Model", *Journal of Bone and Joint Surgery-British Volume*, vol. 73, no. 1, pp. 43-46.

Mallory, T. H., Lombardi, A. V., Leith, J. R., Fujita, H., Hartman, J. F., Capps, S. G., Kefauver, C. A., Adams, J. B., & Vorys, G. C. 2001, "Minimal 10-year results of a tapered cementless femoral component in total hip arthroplasty", *Journal of Arthroplasty*, vol. 16, no. 8, pp. 49-54.

Mallory, T. H., Lombardi, A. V., Leith, J. R., Fujita, H., Hartman, J. F., Capps, S. G., Kefauver, C. A., Adams, J. B., & Vorys, G. C. 2002, "Why a taper?", *Journal of Bone and Joint Surgery-American Volume*, vol. 84A, pp. 81-89.

Maloney, W. J., Jasty, M., Burke, D. W., Oconnor, D. O., Zalenski, E. B., Bragdon, C., & Harris, W. H. 1989, "Biomechanical and Histologic Investigation of Cemented Total Hip Arthroplasties - A Study of Autopsy-Retrieved Femurs After Invivo Cycling", *Clinical Orthopaedics and Related Research* no. 249, pp. 129-140.

Maloney, W. J. & Woolson, S. T. 1996, "Increasing incidence of femoral osteolysis in association with uncemented Harris-Galante total hip arthroplasty - A follow-up report", *Journal of Arthroplasty*, vol. 11, no. 2, pp. 130-134.

Maloney, W. J., Sychterz, C., Bragdon, C., McGovern, T., Jasty, M., Engh, C. A., & Harris, W. H. 1996, "Skeletal response to well fixed femoral components inserted with and without cement", *Clinical Orthopaedics and Related Research* no. 333, pp. 15-26.

Mann, K. A., Bartel, D. L., Wright, T. M., & Burstein, A. H. 1995, "Coulomb Frictional Interfaces in Modeling Cemented Total Hip Replacements - A More Realistic Model", *Journal of Biomechanics*, vol. 28, no. 9, pp. 1067-1078.

Mann, K. A., Ayers, D. C., & Damron, T. A. 1997, "Effects of stem length on mechanics of the femoral hip component after cemented revision", *Journal of Orthopaedic Research*, vol. 15, no. 1, pp. 62-68.

- Matsuzaka, K., Walboomers, X. F., Yoshinari, M., Inoue, T., & Jansen, J. A. 2003, "The attachment and growth behavior of osteoblast-like cells on microtextured surfaces", *Biomaterials*, vol. 24, no. 16, pp. 2711-2719.
- Matsuzaka, K., Yoshinari, M., Shimono, M., & Inoue, T. 2004, "Effects of multigrooved surfaces on osteoblast-like cells in vitro: Scanning electron microscopic observation and mRNA expression of osteopontin and osteocalcin", *Journal of Biomedical Materials Research Part A*, vol. 68A, no. 2, pp. 227-234.
- McAuley, J. P., Culpepper, W. J., & Engh, C. A. 1998, "Total hip arthroplasty - Concerns with extensively porous coated femoral components", *Clinical Orthopaedics and Related Research* no. 355, pp. 182-188.
- McBroom, R. J., Hayes, W. C., Edwards, W. T., Goldberg, R. P., & White, A. A. 1985, "Prediction of Vertebral Body Compressive Fracture Using Quantitative Computed-Tomography", *Journal of Bone and Joint Surgery-American Volume*, vol. 67A, no. 8, pp. 1206-1214.
- McMinn, R. M. H. & Hutchings, R. T. 1990, *A colour atlas of Human Anatomy*, 2nd edn, Wolfe Medical Publications Ltd..
- McNamara, B. P., Cristofolini, L., Toni, A., & Taylor, D. 1997, "Relationship between bone-prosthesis bonding and load transfer in total hip reconstruction", *Journal of Biomechanics*, vol. 30, no. 6, pp. 621-630.
- Meding, J. B., Ritter, M. A., Keating, E. M., & Faris, P. M. 1997, "Comparison of collared and collarless femoral components in primary uncemented total hip arthroplasty", *The Journal of Arthroplasty*, vol. 12, no. 3, pp. 273-280.
- Menon, D. K. & McCreath, S. W. 1999, "5- to 8-Year results of the freeman press-fit hip arthroplasty without HA coating : A clinicoradiologic study", *The Journal of Arthroplasty*, vol. 14, no. 5, pp. 581-588.

- Mont, M. A. & Hungerford, D. S. 1997, "Proximally coated ingrowth prostheses - A review", *Clinical Orthopaedics and Related Research* no. 344, pp. 139-149.
- Monti, L., Cristofolini, L., & Viceconti, M. 2001, "Interface biomechanics of the Anca Dual Fit hip stem: an in vitro experimental study", *Proceedings of the Institution of Mechanical Engineers Part H- Journal of Engineering in Medicine*, vol. 215, no. H6, pp. 555-564.
- Morrey, B. F. 1989, "Short-Stemmed Uncemented Femoral Component for Primary Hip-Arthroplasty", *Clinical Orthopaedics and Related Research* no. 249, pp. 169-175.
- Morscher, E., Bombelli, R., Schenk, R., & Mathys, R. 1981, "The Treatment of Femoral-Neck Fractures with An Isoelastic Endoprosthesis Implanted Without Bone-Cement", *Archives of Orthopaedic and Trauma Surgery*, vol. 98, no. 2, pp. 93-100.
- Morscher, E. W. & Dick, W. 1983, "Cementless Fixation of Isoelastic Hip Endoprostheses Manufactured from Plastic Materials", *Clinical Orthopaedics and Related Research* no. 176, pp. 77-87.
- Mouzin, O., Soballe, K., & Bechtold, J. E. 2001, "Loading improves anchorage of hydroxyapatite implants more than titanium implants", *Journal of Biomedical Materials Research*, vol. 58, no. 1, pp. 61-68.
- Mulliken, B. D., Nayak, N., Bourne, R. B., Rorabeck, C. H., & Bullas, R. 1996, "Early radiographic results comparing cemented and cementless total hip arthroplasty", *Journal of Arthroplasty*, vol. 11, no. 1, pp. 24-33.
- Nercessian, O. A., Wu, W. H., & Sarkissian, H. 2001, "Clinical and radiographic results of cementless AML total hip arthroplasty in young patients", *The Journal of Arthroplasty*, vol. 16, no. 3, pp. 312-316.

Niinimäki, T., Puranen, J., & Jalovaara, P. 1994, "Total Hip-Arthroplasty Using Isoelastic Femoral Stems - A 7- Year to 9-Year Follow-Up in 108 Patients", *Journal of Bone and Joint Surgery-British Volume*, vol. 76B, no. 3, pp. 413-418.

Niki, M., Ito, G., Matsuda, T., & Ogino, M. 1991, "Comparative push-out data of bioactive and non-bioactive materials of similar rugosity," in *The Bone-Biomaterial Interface*, J. E. Davies, ed., University of Toronto Press, pp. 350-356.

Noble, P. C., Alexander, J. W., Lindahl, L. J., Yew, D. T., Granberry, W. M., & Tullos, H. S. 1988, "The Anatomic Basis of Femoral Component Design", *Clinical Orthopaedics and Related Research* no. 235, pp. 148-165.

Nogler, M., Polikeit, A., Wimmer, C., Bruckner, A., Ferguson, S. J., & Krismer, M. 2004, "Primary stability of a ROBODOC (R) implanted anatomical stem versus manual implantation", *Clinical Biomechanics*, vol. 19, no. 2, pp. 123-129.

Nordin, M. & Frankel, V. H. 1980, *Basic biomechanics of the musculoskeletal system*, 2nd edn, Lea & Febiger.

Nourbash, P. S. & Paprosky, W. G. 1998, "Cementless femoral design concerns - Rationale for extensive porous coating", *Clinical Orthopaedics and Related Research* no. 355, pp. 189-199.

O'Toole, I. I. I., Jaramaz, B., DiGioia, I. I. I., Visnic, C. D., & Reid, R. H. 1995, "Biomechanics for preoperative planning and surgical simulations in orthopaedics", *Computers in Biology and Medicine*, vol. 25, no. 2, pp. 183-191.

Ohsawa, S., Fukuda, K., Matsushita, S., Mori, S., Norimatsu, H., & Ueno, R. 1998, "Middle-term results of anatomic medullary locking total hip arthroplasty", *Archives of Orthopaedic and Trauma Surgery*, vol. 118, no. 1-2, pp. 14-20.

Oonishi, H. 1991, "Interfacial reactions to bioactive and non-bioactive bone cements," in *The Bone-Biomaterial Interface*, J. E. Davies, ed., University of Toronto Press, pp. 321-333.

Otani, T., Whiteside, L. A., White, S. E., & McCarthy, D. S. 1993, "Effects of femoral component material properties on cementless fixation in total hip arthroplasty", *Journal of Arthroplasty*, vol. 8, no. 1, pp. 67-74.

Pancanti, A., Bernakiewicz, M., & Viceconti, M. 2003, "The primary stability of a cementless stem varies between subjects as much as between activities", *Journal of Biomechanics*, vol. 36, no. 6, pp. 777-785.

Paravic, V., Noble, P. C., & McCarthy, J. C. "The impact of robotic surgery on the fit of cementless femoral prostheses.", 45th edn, Orthopaedic Research Society.

Park, M. S., Choi, B. W., Kim, S. J., & Park, J. H. 2003, "Plasma spray-coated Ti femoral component for cementless total hip arthroplasty", *Journal of Arthroplasty*, vol. 18, no. 5, pp. 626-630.

Parvizi, J., Keisu, K. S., Hozack, W. J., Sharkey, P. F., & Rothman, R. H. 2004, "Primary total hip arthroplasty with an uncemented femoral component: a long-term study of the taperloc stem", *The Journal of Arthroplasty*, vol. 19, no. 2, pp. 151-156.

Paul, H. A., Bargar, W. L., Mittlestadt, B., Musits, B., Taylor, R. H., Kazanzides, P., Zuhars, J., Williamson, B., & Hanson, W. 1992, "Development of A Surgical Robot for Cementless Total Hip- Arthroplasty", *Clinical Orthopaedics and Related Research* no. 285, pp. 57-66.

Pazzaglia, U. E., Brossa, F., Zatti, G., Chiesa, R., & Andriani, L. 1998, "The relevance of hydroxyapatite and spongy titanium coatings in fixation of cementless stems - An experimental comparative study in rat femur employing histological and

microangiographic techniques", *Archives of Orthopaedic and Trauma Surgery*, vol. 117, no. 4-5, pp. 279-285.

Perizzolo, D., Lacefield, W. R., & Brunette, D. M. 2001, "Interaction between topography and coating in the formation of bone nodules in culture for hydroxyapatite- and titanium-coated micromachined surfaces", *Journal of Biomedical Materials Research*, vol. 56, no. 4, pp. 494-503.

Pernell, R. T., Gross, R. S., Milton, J. L., Montgomery, R. D., Wenzel, J. G. W., Savory, C. G., & Aberman, H. M. 1994, "Femoral Strain Distribution and Subsidence After Physiological Loading of A Cementless Canine Femoral Prosthesis - the Effects of Implant Orientation, Canal Fill, and Implant Fit", *Veterinary Surgery*, vol. 23, no. 6, pp. 503-518.

Petersilge, W. J., Dlima, D. D., Walker, R. H., & Colwell, C. W. 1997, "Prospective study of 100 consecutive Harris-Galante porous total hip arthroplasties - 4- to 8-year follow-up study", *Journal of Arthroplasty*, vol. 12, no. 2, pp. 185-193.

Phillips, T. W. & Messieh, S. S. 1988, "Cementless Hip-Replacement for Arthritis - Problems with A Smooth Surface Moore Stem", *Journal of Bone and Joint Surgery-British Volume*, vol. 70, no. 5, pp. 750-755.

Phillips, T. W., Messieh, S. S., & McDonald, P. D. 1990, "Femoral Stem Fixation in Hip-Replacement - A Biomechanical Comparison of Cementless and Cemented Prostheses", *Journal of Bone and Joint Surgery-British Volume*, vol. 72, no. 3, pp. 431-434.

Pieringer, H., Auersperg, V., Griessler, W., & Bohler, N. 2003, "Long-term results with the cementless alloclassic brand hip arthroplasty system", *Journal of Arthroplasty*, vol. 18, no. 3, pp. 321-328.

- Pieringer, H., Labek, G., Auersperg, V., & Bohler, N. 2003, "Cementless total hip arthroplasty in patients older than 80 years of age", *Journal of Bone and Joint Surgery-British Volume*, vol. 85B, no. 5, pp. 641-645.
- Pilliar, R. M., Lee, J. M., & Maniopoulos, C. 1986, "Observations on the Effect of Movement on Bone Ingrowth Into Porous-Surfaced Implants", *Clinical Orthopaedics and Related Research* no. 208, pp. 108-113.
- Pilliar, R. M. 1991, "Quantitative evaluation of the effect of movement at a porous coated implant-bone interface," in *The Bone-Biomaterial Interface*, 1st edn, J. E. Davies, ed., University of Toronto Press, pp. 380-387.
- Prendergast, P. J. 1997, "Finite element models in tissue mechanics and orthopaedic implant design", *Clinical Biomechanics*, vol. 12, no. 6, pp. 343-366.
- Purves, W. K., Orians, G. H., Heller, H. C., & Sadava, D. 2001, *Life: The Science of Biology*, 6th edn, Sinauer Associates.
- Ramamurti, B. S., Orr, T. E., Bragdon, C. R., Lowenstein, J. D., Jasty, M., & Harris, W. H. 1997, "Factors influencing stability at the interface between a porous surface and cancellous bone: a finite element analysis of a canine in vivo micromotion experiment", *Journal of Biomedical Materials Research*, vol. 36, no. 2, pp. 274-280.
- Rancourt, D., Shiraziadl, A., Drouin, G., & Paiement, G. 1990, "Friction Properties of the Interface Between Porous-Surfaced Metals and Tibial Cancellous Bone", *Journal of Biomedical Materials Research*, vol. 24, no. 11, pp. 1503-1519.
- Rasquinha, V. J., Dua, V., Rodriguez, J. A., & Ranawat, C. S. 2003, "Fifteen-year survivorship of a collarless, cemented, normalized femoral stem in primary hybrid total hip arthroplasty with a modified third-generation cement technique", *Journal of Arthroplasty*, vol. 18, no. 7, pp. 86-94.

- Reitman, R. D., Emerson, R., Higgins, L., & Head, W. 2003, "Thirteen year results of total hip arthroplasty using a tapered titanium femoral component inserted without cement in patients with type C bone", *Journal of Arthroplasty*, vol. 18, no. 7, pp. 116-121.
- Ricci, J. L., Spivak, J. M., Blumenthal, N. C., & Alexander, H. 1991, "Modulation of bone ingrowth by surface chemistry and roughness," in *The Bone-Biomaterial Interface*, J. E. Davies, ed., University of Toronto Press, pp. 334-349.
- Ries, M. D., Lynch, F., Jenkins, P., Mick, C., & Richman, J. 1996, "Varus migration of PCA stems", *Orthopedics*, vol. 19, no. 7, pp. 581-585.
- Robinson, R. P., Lovell, T. P., & Green, T. M. 1994, "Hip arthroplasty using the cementless CLS stem : A 2-4-year experience", *The Journal of Arthroplasty*, vol. 9, no. 2, pp. 177-192.
- Rogers, A., Kulkarni, R., & Downes, E. M. 2003, "The ABG hydroxyapatite-coated hip prosthesis: One hundred consecutive operations with average 6-year follow-up", *The Journal of Arthroplasty*, vol. 18, no. 5, pp. 619-625.
- Rohlmann, A., Cheal, E. J., Hayes, W. C., & Bergmann, G. 1988, "A nonlinear finite element analysis of interface conditions in porous coated hip endoprosthesis", *Journal of Biomechanics*, vol. 21, no. 7, pp. 605-611.
- Rokkum, M. & Reigstad, A. 1999, "Total hip replacement with an entirely hydroxyapatite-coated prosthesis - 5 years' follow-up of 94 consecutive hips", *Journal of Arthroplasty*, vol. 14, no. 6, pp. 689-700.
- Rossi, P., Sibelli, P., Fumero, S., & Crua, E. 1995, "Short-Term Results of Hydroxyapatite-Coated Primary Total Hip- Arthroplasty", *Clinical Orthopaedics and Related Research* no. 310, pp. 98-102.

- Rothman, R. H., Hozack, W. J., Ranawat, A., & Moriarty, L. 1996, "Hydroxyapatite-coated femoral stems - A matched-pair analysis of coated and uncoated implants", *Journal of Bone and Joint Surgery-American Volume*, vol. 78A, no. 3, pp. 319-324.
- Rubin, P. J., Rakotomanana, R. L., Leyvraz, P. F., Zysset, P. K., Curnier, A., & Heegaard, J. H. 1993, "Frictional interface micromotions and anisotropic stress distribution in a femoral total hip component", *Journal of Biomechanics*, vol. 26, no. 6, pp. 725-739.
- Sakai, T., Sugano, N., Nishii, T., Haraguchi, K., Ochi, T., & Ohzono, K. 1999, "Stem length and canal filling in uncemented custom-made total hip arthroplasty", *International Orthopaedics*, vol. 23, no. 4, pp. 219-223.
- Sanghera, B., Naique, S., Papaharilaou, Y., & Amis, A. 2001, "Preliminary study of rapid prototype medical models", *Rapid Prototyping Journal*, vol. 7, no. 5, pp. 275-284.
- Schneider, E., Eulenberger, J., Steiner, W., Wyder, D., Friedman, R. J., & Perren, S. M. 1989, "Experimental-Method for the Invitro Testing of the Initial Stability of Cementless Hip Prostheses", *Journal of Biomechanics*, vol. 22, no. 6-7, pp. 735-744.
- Schneider, E., Kinast, C., Eulenberger, J., Wyder, D., Eskilsson, G., & Perren, S. M. 1989, "A Comparative-Study of the Initial Stability of Cementless Hip Prostheses", *Clinical Orthopaedics and Related Research* no. 248, pp. 200-209.
- Schreiner, U., Scheller, G., Herbig, J., & Jani, L. 2001, "Mid-term results of the cementless CLS stem - A 7-to 11-year follow-up study", *Archives of Orthopaedic and Trauma Surgery*, vol. 121, no. 6, pp. 321-324.
- Simmons, C. A., Valiquette, N., & Pilliar, R. M. 1999, "Osseointegration of sintered porous-surfaced and plasma spray-coated implants: An animal model study of early postimplantation healing response and mechanical stability", *Journal of Biomedical Materials Research*, vol. 47, no. 2, pp. 127-138.

Smith, E. & Harris, W. H. 1995, "Increasing Prevalence of Femoral Lysis in Cementless Total Hip- Arthroplasty", *Journal of Arthroplasty*, vol. 10, no. 4, pp. 407-412.

Soballe, K., Overgaard, S., Hansen, E. S., Brokstedt-Rasmussen, H., Lind, M., & Bunger, C. 1999, "A review of ceramic coatings for implant fixation", *Journal of Long-Term Effects of Medical Implants*, vol. 9, no. 1-2, pp. 131-151.

Stauffer, R. N. 1982, "10-Year Follow-Up-Study of Total Hip-Replacement - with Particular Reference to Roentgenographic Loosening of the Components", *Journal of Bone and Joint Surgery-American Volume*, vol. 64, no. 7, pp. 983-990.

Stolk, J., Verdonschot, N., & Huiskes, R. 2001, "Hip-joint and abductor-muscle forces adequately represent in vivo loading of a cemented total hip reconstruction", *Journal of Biomechanics*, vol. 34, no. 7, pp. 917-926.

Stolk, J., Maher, S. A., Verdonschot, N., Prendergast, P. J., & Huiskes, R. 2003, "Can finite element models detect clinically inferior cemented hip implants?", *Clinical Orthopaedics and Related Research* no. 409, pp. 138-150.

Sugiyama, H., Whiteside, L. A., & Engh, C. A. 1992, "Torsional Fixation of the Femoral Component in Total Hip- Arthroplasty - the Effect of Surgical Press-Fit Technique", *Clinical Orthopaedics and Related Research* no. 275, pp. 187-193.

Sugiyama, H., Whiteside, L. A., Engh, C. A., & Otani, T. 1994, "Late Mechanical Stability of the Proximal Coated Aml Prosthesis", *Orthopedics*, vol. 17, no. 7, pp. 583-588.

Sumner, D. R., Turner, T. M., Urban, R. M., & Galante, J. O. 1991, "Bone ingrowth into porous coatings attached to prosthesis of differing stiffness," in *The Bone-Biomaterial Interface*, J. E. Davies, ed., University of Toronto Press, pp. 388-390.

- Sumner, D. R., Turner, T. M., Igloria, R., Urban, R. M., & Galante, J. O. 1998, "Functional adaptation and ingrowth of bone vary as a function of hip implant stiffness", *Journal of Biomechanics*, vol. 31, no. 10, pp. 909-917.
- Sutherland, C. J., Wilde, A. H., Borden, L. S., & Marks, K. E. 1982, "A 10-Year Follow-Up of 100 Consecutive Muller Curved-Stem Total Hip-Replacement Arthroplasties", *Journal of Bone and Joint Surgery-American Volume*, vol. 64, no. 7, pp. 970-982.
- Suzuki, K., Aoki, K., & Ohya, K. 1997, "Effects of surface roughness of titanium implants on bone remodeling activity of femur in rabbits", *Bone*, vol. 21, no. 6, pp. 507-514.
- Szmukler-Moncler, S., Salama, H., Reingewirtz, Y., & Dubruille, J. H. 1998, "Timing of loading and effect of micromotion on bone-dental implant interface: Review of experimental literature", *Journal of Biomedical Materials Research*, vol. 43, no. 2, pp. 192-203.
- Tanner, K. E., Yettram, A. L., Loeffler, M., Goodier, W. D., Freeman, M. A. R., & Bonfield, W. 1995, "Is stem length important in uncemented endoprostheses?", *Medical Engineering & Physics*, vol. 17, no. 4, pp. 291-296.
- Tennent, T. D. & Goddard, N. J. 2000, "Current attitudes to total hip replacement in the younger patient: results of a national survey", *Annals of the Royal College of Surgeons of England*, vol. 82, no. 1, pp. 33-38.
- Testi, D., Simeoni, M., Zannoni, C., & Viceconti, M. 2004, "Validation of two algorithms to evaluate the interface between bone and orthopaedic implants", *Computer Methods and Programs in Biomedicine*, vol. 74, no. 2, pp. 143-150.
- Thomason, I. I. I. & Lachiewicz, P. F. 2001, "The influence of technique on fixation of primary total hip arthroplasty in patients with rheumatoid arthritis", *The Journal of Arthroplasty*, vol. 16, no. 5, pp. 628-634.

Thomsen, M. N., Breusch, S. J., Aldinger, P. R., Gortz, W., Lahmer, A., Honl, M., Birke, A., & Nagerl, H. 2002, "Robotically-milled bone cavities - A comparison with hand-broaching in different types of cementless hip stems", *Acta Orthopaedica Scandinavica*, vol. 73, no. 4, pp. 379-385.

Tissakht, M., Eskandari, H., & Ahmed, A. M. 1995, "Micromotion analysis of the fixation of total knee tibial component", *Computers and Structures*, vol. 56, pp. 365-375.

Toni, A., McNamara, B., Viceconti, M., Sudanese, A., Baruffaldi, F., & Giunti, A. 1996, "Bone remodelling after total hip arthroplasty", *Journal of Materials Science-Materials in Medicine*, vol. 7, no. 3, pp. 149-152.

Tonino, A. J., Romanini, L., Rossi, P., Borroni, M., Greco, F., Garciaaraujo, C., Garciadihinx, L., Murciamazon, A., Hein, W., & Anderson, J. 1995, "Hydroxyapatite-Coated Hip Prostheses - Early Results from An International Study", *Clinical Orthopaedics and Related Research* no. 312, pp. 211-225.

Uchida, A., Nade, S. M. L., McCartney, E. R., & Ching, W. 1984, "The Use of Ceramics for Bone-Replacement - A Comparative-Study of 3 Different Porous Ceramics", *Journal of Bone and Joint Surgery-British Volume*, vol. 66, no. 2, pp. 269-275.

van Rietbergen, B. & Huiskes, R. 2001, "Load transfer and stress shielding of the hydroxyapatite-ABG hip - A study of stem length and proximal fixation", *Journal of Arthroplasty*, vol. 16, no. 8, pp. 55-63.

Viceconti, A., Lattanzi, R., Antonietti, B., Paderni, S., Olmi, R., Sudanese, A., & Toni, A. 2003, "CT-based surgical planning software improves the accuracy of total hip replacement preoperative planning", *Medical Engineering & Physics*, vol. 25, no. 5, pp. 371-377.

- Viceconti, M., Muccini, R., Bernakiewicz, M., Baleani, M., & Cristofolini, L. 2000, "Large-sliding contact elements accurately predict levels of bone-implant micromotion relevant to osseointegration", *Journal of Biomechanics*, vol. 33, no. 12, pp. 1611-1618.
- Viceconti, M., Monti, L., Muccini, R., Bernakiewicz, M., & Toni, A. 2001, "Even a thin layer of soft tissue may compromise the primary stability of cementless hip stems", *Clinical Biomechanics*, vol. 16, no. 9, pp. 765-775.
- von Knoch, M., Engh, C. A., Sychterz, C. J., Engh, C. A., & Willert, H. G. 2000, "Migration of polyethylene wear debris in one type of uncemented femoral component with circumferential porous coating - An autopsy study of 5 femurs", *Journal of Arthroplasty*, vol. 15, no. 1, pp. 72-78.
- Vresilovic, E. J., Hozack, W. J., & Rothman, R. H. 1994, "Radiographic assessment of cementless femoral components : Correlation with intraoperative mechanical stability", *The Journal of Arthroplasty*, vol. 9, no. 2, pp. 137-141.
- Walker, P. S., Culligan, S. G., Hua, J., Muirhead-Allwood, S. K., & Bentley, G. 1999, "The effect of a lateral flare feature on uncemented hip stems.", *Hip International*, vol. 9, no. 2, pp. 71-80.
- Weidenhielm, L. R. A., Mikhail, W. E. M., Nelissen, R. G. H. H., & Bauer, T. W. 1995, "Cemented Collarless (Exeter-Cpt) Versus Cementless Collarless (Pca) Femoral Components - A 2- to 14-Year Follow-Up Evaluation", *Journal of Arthroplasty*, vol. 10, no. 5, pp. 592-597.
- Weinans, H., Huiskes, R., & Grootenboer, H. J. 1993, "Quantitative-Analysis of Bone Reactions to Relative Motions at Implant Bone Interfaces", *Journal of Biomechanics*, vol. 26, no. 11, pp. 1271-1281.

- Whiteside, L. A., Amador, D., & Russell, K. 1988, "The Effects of the Collar on Total Hip Femoral Component Subsidence", *Clinical Orthopaedics and Related Research* no. 231, pp. 120-126.
- Whiteside, L. A. 1989, "The Effect of Stem Fit on Bone Hypertrophy and Pain Relief in Cementless Total Hip-Arthroplasty", *Clinical Orthopaedics and Related Research* no. 247, pp. 138-147.
- Whiteside, L. A. & Easley, J. C. 1989, "The Effect of Collar and Distal Stem Fixation on Micromotion of the Femoral Stem in Uncemented Total Hip-Arthroplasty", *Clinical Orthopaedics and Related Research* no. 239, pp. 145-153.
- Whiteside, L. A., White, S. E., Engh, C. A., & Head, W. 1993, "Mechanical evaluation of cadaver retrieval specimens of cementless bone-ingrown total hip arthroplasty femoral components.", *Journal of Arthroplasty*, vol. 8, no. 2, pp. 147-155.
- Whiteside, L. A., Arima, J., White, S. E., Branam, L., & McCarthy, D. S. 1994, "Fixation of the Modular Total Hip Femoral Component in Cementless Total Hip-Arthroplasty", *Clinical Orthopaedics and Related Research* no. 298, pp. 184-190.
- Williams, P. L., Warwick, R., Dyson, M., & Bannister, L. H. 1989, *Gray's Anatomy*, 37th edn, Churchill Livingstone.
- Woolson, S. T. & Comstock, C. G. 1996, "Porous pad separation and loosening of Harris-Galante femoral hip components", *Journal of Arthroplasty*, vol. 11, no. 4, pp. 474-477.
- Woolson, S. T. & Adler, N. S. 2002, "The effect of partial or full weight bearing ambulation after cementless total hip arthroplasty", *The Journal of Arthroplasty*, vol. 17, no. 7, pp. 820-825.

- Yamamuro, T. & Takagi, H. 1991, "Bone bonding behaviour of biomaterials with different surface characteristics under load-bearing conditions," in *The Bone-Biomaterial Interface*, J. E. Davies, ed., University of Toronto Press, pp. 406-414.
- Yee, A. J. M., Kreder, H. K., Bookman, I., & Davey, J. R. 1999, "A randomized trial of hydroxyapatite coated prostheses in total hip arthroplasty", *Clinical Orthopaedics and Related Research* no. 366, pp. 120-132.
- Yildiz, H., Chang, F. K., & Goodman, S. 1998, "Composite hip prosthesis design. II. Simulation", *Journal of Biomedical Materials Research*, vol. 39, no. 1, pp. 102-119.
- Yildiz, H., Ha, S. K., & Chang, F. K. 1998, "Composite hip prosthesis design. I. Analysis", *Journal of Biomedical Materials Research*, vol. 39, no. 1, pp. 92-101.
- Yoshinari, M., Matsuzaka, K., Inoue, T., Oda, Y., & Shimono, M. 2003, "Effects of multigrooved surfaces on fibroblast behavior", *Journal of Biomedical Materials Research Part A*, vol. 65A, no. 3, pp. 359-368.
- Zachariah, S. G. & Sanders, J. E. 2000, "Finite element estimates of interface stress in the trans-tibial prosthesis using gap elements are different from those using automated contact", *Journal of Biomechanics*, vol. 33, no. 7, pp. 895-899.
- Zimmerman, S., Hawkes, W. G., Hudson, J. I., Magaziner, J., Richard Hebel, J., Towheed, T., Gardner, J., Provenzano, G., & Kenzora, J. E. 2002, "Outcomes of surgical management of total HIP replacement in patients aged 65 years and older: cemented versus cementless femoral components and lateral or anterolateral versus posterior anatomical approach", *Journal of Orthopaedic Research*, vol. 20, no. 2, pp. 182-191.